MINISTÉRIO DA CIÊNCIA, TECNOLOGIA, INOVAÇÕES E COMUNICAÇÕES
INSTITUTO NACIONAL DE PESQUISAS ESPACIAIS

INFLUENCE OF PERTURBATIVE FORCES IN THE MOTION OF SPACECRAFT: AROUND ARTIFICIAL EQUILIBRIUM POINTS AND IN MEASUREMENTS OF INDICES

Allan Kardec de Almeida Junior

Doctorate Thesis of the Graduate Course in Space Engineering and Technology/Space Mechanics and Control, guided by Drs. Diogo Merguizo Sanchez, Tadashi Yokoyama, and Antonio Fernando Bertachini de Almeida Prado, approved in September 14, 2018.

URL of the original document:
<http://urlib.net/8JMKD3MGP3W34R/3RLBNPL>

INPE

São José dos Campos

2018

INFLUENCE OF PERTURBATIVE FORCES IN THE MOTION OF SPACECRAFT: AROUND ARTIFICIAL EQUILIBRIUM POINTS AND IN MEASUREMENTS OF INDICES

Allan Kardec de Almeida Junior

Doctorate Thesis of the Graduate Course in Space Engineering and Technology/Space Mechanics and Control, guided by Drs. Diogo Merguizo Sanchez, Tadashi Yokoyama, and Antonio Fernando Bertachini de Almeida Prado, approved in September 14, 2018.

URL of the original document:
<http://urlib.net/8JMKD3MGP3W34R/3RLBNPL>

INPE

São José dos Campos

2018

Aluno (a): *Allan Kardec de Almeida Junior*

Título: "INFLUENCE OF PERTURBATIVE FORCES IN THE MOTION OF SPACECRAFT: AROUND ARTIFICIAL EQUILIBRIUM POINTS AND IN MEASUREMENTS OF INDICES"

Aprovado (a) pela Banca Examinadora em cumprimento ao requisito exigido para obtenção do Título de *Doutor(a)* em *Engenharia e Tecnologia Espaciais/Mecânica Espacial e Controle*

Dr.   Rodolpho Vilhena de Moraes

Presidente / INPE / São José dos Campos - SP

( ) *Participação por Video - Conferência*

(x) *Aprovado*   ( ) *Reprovado*

Dr.   Diogo Merguizo Sanchez

Orientador(a) / INPE / São José dos Campos - SP

( ) *Participação por Video - Conferência*

(x) *Aprovado*   ( ) *Reprovado*

Dr.   Tadashi Yokoyama

Orientador(a) / UNESP / Rio Claro - SP

(x) *Participação por Video - Conferência*

(x) *Aprovado*   ( ) *Reprovado*

Dra.   Vivian Martins Gomes

Convidado(a) / UNESP/FEG / Guaratinguetá - SP

( ) *Participação por Video - Conferência*

(x) *Aprovado*   ( ) *Reprovado*

Este trabalho foi aprovado por:

( ) *maioria simples*

(x) *unanimidade*

São José dos Campos, 14 de setembro de 2018

Aprovado (a) pela Banca Examinadora em cumprimento ao requisito exigido para obtenção do Título de *Doutor(a)* em

Engenharia e Tecnologia Espaciais/Mecânica Espacial e Controle

Dra. Rita de Cássia Domingos

Convidado(a) / UNESP / São João da Boa Vista - SP

( ) Participação por Video - Conferência

(X) Aprovado ( ) Reprovado

Este trabalho foi aprovado por:

( ) maioria simples

(X) unanimidade

São José dos Campos, 14 de setembro de 2018

"Só quem já esteve, por alguns momentos sequer, entre os muros tenebrosos de uma enxovia, sabe resolver esses problemas em que os números são parcelas terríveis da desgraça humana."

<div align="right">

MALBA TAHAN
em *"O Homem que Calculava"*, de Bagdá, 19 da Lua de Ramadã de 1321.

</div>

To the past, to the cosmo, and to the reader.

ACKNOWLEDGEMENTS

ABSTRACT

This thesis describes a research about the effects of perturbative forces over the motion of a spacecraft around artificial equilibrium points and over measurements of "integral indices". In order to accomplish the task, an initial investigation about how the artificial equilibrium points are located in the space is done, whose results are applied to the Sun-Earth system and to a planar solar sail. Using this concept, solutions are proposed for a communication problem between a spacecraft located near the classical lagrangean point L_3 and the Earth, due to the presence of the Sun. Moreover, analytical solutions are proposed to describe the motion of a spacecraft around artificial equilibrium points, whose results are applied to a spacecraft located near L_3 in the Sun-Earth system perturbed by the gravity of Jupiter and Venus, to be compared with numerical integrations of the equations of motion. Such kind of analytical solutions are extended to a spacecraft located above/below a massive body that rotates with another massive body around their barycenter, perturbed by a general moon. This last kind of solution involves periodic corrections of the thrust applied over the spacecraft. The results show that the analytical solution comes closer to the numerical integration of the equations of motion when the frequency of the corrections is higher. The influence of perturbative forces over "integral indices" is also investigated in this thesis. Initially, they are defined analogously to the ones known in the literature and they are evaluated using the driven harmonic, Duffing, and Van der Pol oscillators, which may represent perturbative models of the simple harmonic oscillator. Thus, this research is extended to a more realistic astrodynamic case of a spacecraft moving around a massive body (the Earth) subjected to a thrust in the tangential and radial directions. New indices are defined and evaluated using a perturbative solution for a low, constant and radial thrust. Thus, an index is identified as capable of describe interesting perturbative effects over the motion.

Keywords: artificial equilibrium points. analytical solutions. perturbative solutions. integral indices. solar sail.

INFLUÊNCIA DE FORÇAS PERTURBATIVAS NO MOVIMENTO DE UMA ESPAÇONAVE: EM TORNO DE PONTOS DE EQUILÍBRIO ARTIFICIAIS E EM MEDIDAS DE ÍNDICES

RESUMO

Nesta tese, são estudados os efeitos de forças perturbativas sobre o movimento de um veículo espacial em torno de pontos de equilíbrio artificiais e sobre medições de "índices de integrais". Para tanto, uma investigação inicial sobre a relação de pontos de equilíbrio artificiais no espaço é realizada, cujos resultados são aplicados para o sistema Sol-Terra, incluindo aplicações para uma vela solar plana. Usando tal conceito, soluções são propostas para um problema de comunicação entre um veículo espacial localizado próxima ao ponto lagrangeano L_3 e a Terra. Na sequência, soluções analíticas são propostas para descrever o movimento de um veículo espacial em torno de pontos de equilíbrio artificiais, cujos resultados são aplicados para um veículo espacial localizado próxima ao L_3 no sistema Sol-Terra perturbada pela gravidade de Júpiter e Vênus, para serem comparadas com integrações numéricas das equações de movimento. Tais tipos de soluções analíticas são estendidas para um veículo espacial localizado acima/abaixo de um corpo massivo que gira com outro corpo massivo em torno de um centro de massa comum perturbada por uma lua genérica. Este último tipo de solução envolve correções periódicas do propulsor do veículo espacial e os resultados mostram que a solução analítica se aproxima da integração numérica das equações do movimento quando a frequência das correções é mais alta. A influência das forças perturbativas sobre "índices de integrais" também é investigada nesta tese. Inicialmente, tais índices são definidos de maneira análoga aos conhecidos na literatura e são calculados usando os osciladores forçado, de Duffing e de Van der Pol, que podem representar modelos perturbados do oscilador harmônico simples. Na sequência, tal pesquisa é estendida para um caso mais realístico da astrodinâmica de um veículo espacial movendo-se em torno de um corpo massivo (a Terra) sujeita a propulsão nas direções tangencial e radial. Novos índices são definidos e calculados usando uma solução perturbativa para uma propulsão pequena e constante na direção radial. Em seguida, um índice é identificado como capaz de descrever efeitos perturbativos interessantes sobre o movimento.

Palavras-chave: Pontos de equilíbrio artificiais. Soluções analíticas. Soluções perturbativas. Índices de integral. Vela solar.

LIST OF FIGURES

xx

LIST OF TABLES

LIST OF ABBREVIATIONS

AEP   –   Artificial equilibrium points
PAEP   –   Pseudo artificial equilibrium points

CONTENTS

1 INTRODUCTION

A system may be defined as a small part of the universe. This part is isolated from the rest such that it can be independently investigated, studied, and understood. Mathematical solutions may be found for a system, turning it predictable. The problem is that, in the real world, a system usually cannot be isolated from the rest of the universe, due to the perturbation that the rest of the universe imposes over it. However, a mathematical solution known for a system may be used as an approximation to describe it under the influence of their surroundings in the universe. In this sense, a small perturbation may be interpreted as the influence that only the surroundings of the system exert over it. Then, some of the small perturbations over a system may be taken into account such that the mathematical solution obtained for this perturbed system is a better approximation to mathematically describe it in the real world than the solution obtained for the unperturbed and more isolated system.

In this thesis, the main system to be studied is the circular restricted three body problem, which is constituted of two massive main bodies, e.g. the Sun and the Earth, rotating in a circular trajectory around a point, their common center of mass, and a third body with a comparative very small mass, e.g. the spacecraft. However, other systems will also be studied in this thesis, like a satellite rotating around a massive body (the Earth) or a simple harmonic oscillator. We will take the advantage of the fact that there are known solutions in the literature for the systems described above. In order to take this advantage, these systems will be perturbed by a force (usually a small one), which we call as a perturbative force, and the solutions of the perturbed system will be found if they do not exist in the literature or will be used to solve further problems in the case they already exist in the literature.

In this scenario, using a spacecraft under the system described by the circular restricted three body problem, some regions of the space will be considered as observation spots, e.g. the momentary opposite side of the Sun, or particular and uncommon locations relative to other objects, e.g. poles of asteroids, satellites or planets. The study of these points is not a trivial task, it requires the integration of many strategies, from the geometry and dynamic of the involved bodies, the estimative of a stability parameter to, finally, the fuel cost involved in a spatial mission.

A fundamental condition to achieve success in this type of observation of particular regions or hidden side is that the spacecraft must be positioned and stabilized in strategic points such that the costs are minimized. It will be shown that these points

can be dynamically "created" in an artificial way through the use of external forces, via thrusts that may be provided using propellant or not, like the ones generated by the solar radiation pressure. These are the so called Artificial Equilibrium Points (AEP) and once they are created, the problem of to stabilize the spacecraft around them using a thrust arises. This stabilization generates cost, which is related to the fuel consumption of the spacecraft. Thus, a previous analyze of these costs must be done. In order to accomplish this task, an important tool is analyzed, developed, and improved - the "integral indices" - to allow to establish regions of low costs to create the AEP.

Several important topics are involved in this thesis and it will be seen at the end of the process that they are fully integrated. In order to facilitate the comprehension of this integration, three objectives are established. Hence, the perturbative forces are used in the investigations on three main objectives of this thesis:

a) **"Integral indices"**: to analyze the influence of the perturbative forces over the trajectory and velocity of a spacecraft through the use of "integral indices";

b) **Artificial equilibrium points**: to use perturbative forces as thrusts to generate AEP that can be useful for many missions and different purposes;

c) **Spacecraft motion around artificial equilibrium points**: to investigate the influence of the perturbative forces on the motion of a spacecraft around an AEP.

These three objectives are respectively related to three subjects, which are categorized as "Integral indices", "Artificial equilibrium points", and "Spacecraft motion around artificial equilibrium points". Each of these subjects is divided into two chapters, which has been investigated separately. As a result, each chapter is self-sufficient in the sense that it contains its own notation and description of the mathematical models used during the respective stage of the research. Introductions that relate the subject with previous work available in the literature and results are also shown independently in every respective chapter, as well as brief conclusions in its last section. The description of each subject is detailed below, including links to the chapters related to the respective stage of the research.

1.1 "Integral indices"

In order to study regions with low costs, i.e. low fuel consumption, to place and maintain a spacecraft, an efficient estimator can be used, which requires low computational cost. This estimator is called "integral index" and its investigation is the first objective of the thesis, where its presentation, definition, and development are exhaustively discussed. In general, such kind of index can be used to differentiate regular and smooth regions from others highly perturbed and unpredictable. This differentiation becomes important, since it allows us to determine regions that demand low fuel consumption.

Thus, in order to reach the first of the three main objectives, "integral indices" available in the literature will be investigated using several systems and some other new "integral indices" will be defined and investigated too. As said before, these indices should help to describe the behavior of a perturbed system, but in order to evaluate them analytically, the investigation requires that an analytical solution of the system under consideration must be known. In general, analytical solutions of the satellite problem are scarce. Hence, the first stage of the research on this subject is to analyze the indices considering well known systems, which solutions are already known in the literature. They will be evaluated using the simple harmonic oscillator perturbed by several forms of perturbations, which becomes the driven harmonic, Duffing, and Van der Pol oscillators. This first stage is written in chapter 2 and already published (DE ALMEIDA JUNIOR et al., 2017b). Once the results of the first stage of the research are analyzed, we should be able to discard "bad indices", to create new ones, and to evaluate them in a more realistic system, a satellite problem. This will be done in the second stage of the research. The chosen system is a spacecraft orbiting a massive body under the influence of a thrust applied in the tangential and a radial directions. This system is known as the Tsien problem (TSIEN, 1953). Although it has solutions available in the literature, they are written in terms of elliptic integrals. Hence, we will find several alternatives analytical solutions to this problem, including one that requires the use of perturbative methods. Several "Integral indices" will then be defined, evaluated, and analyzed. This will be done in the second stage of the research, written in chapter 3. Introductory details about each of these two stages are written in the initial part of the respective chapter, in sections 2.1 and 3.1, respectively.

1.2 Artificial equilibrium points

The second of the three main objectives is to use a perturbative force as a thrust to generate AEP that can be useful for many missions and purposes. By restricting our system to the circular restricted three body problem, a spacecraft can be parked at five possible location from the point of view of the rotating frame of reference, i.e. if its initial velocity is null, then it will be find in a stationary condition. They are the well known lagrangian points. On the other hand, in the case this spacecraft can be thrusted, then it can be parked anywhere in the whole space. The only requirement is that its thrust balances the gravitational forces plus the centrifugal force. In that case, the spacecraft will be parked in the rotating frame of reference, i.e. it will rotate with the same angular velocity of the two massive bodies around their barycenter. Note that from the point of view of the Earth, fixed spots relative to its translational motion around the Sun may be useful for many missions. Some advantages of these points are the predictability of the location and the fixed distance relative to the Earth and to the Sun, that could be used to permanent monitor the Sun or the Earth, but also taking the advantage of the trip through the travel space to observe other bodies during this motion. The thrust may be generated by several kinds of sources, like electric, solar, or magnetic sails, as will be explained later, ionic thrusts, or even by a source that uses propellant. In any case, it generates costs, like the fuel consumption, the size of the sail or its capacity to carry mass, the technology available, etc. By lowering these costs, a mission may become feasible or even affordable, or its duration can be extended. Thus, investigations on these costs are useful in order to offer essential information to a mission designer. Moreover, sometimes, depending on the kind of the mission and the spacecraft, the thrust may be constrained in some directions of the motion, like in the case of a spherical spacecraft subjected to the force generated by the solar rays. Given this constraint, the equilibrium points where the spacecraft can be parked in the space is not anymore unlimited, quite on contrary, they are restricted to some specific regions of the space. Thus, the first stage to reach the second main objective is to find the places in the space where a spacecraft can be parked in the case the thrust is restricted to a single or two directions. These places will be determined by the solutions of the equations generated by balancing the thrust, gravitational, and centrifugal forces in the rotating frame of reference. This process will be done for several directions of the thrust. Note that some specific kinds of solutions already exist in the literature, like solutions in the x-y or x-z planes (MCINNES, 2004), however, the approach used in this thesis is a new one. The second stage to reach the second main objective is to use the AEP to solve a problem. A satellite near the lagrangean L_3 is able

to permanent contact the instantaneous hidden side of the Sun from the point of view of the Earth. Given the period of the rotation of the Sun, which is about 25 days in the equator, the observation of its hidden side may offer us the opportunity to predict coronal mass ejection weeks in advance. One of the problems to place a spacecraft in such a position is that the Sun is placed between the lagrangean L_3 and the Earth, hence there can be no direct communication between the spacecraft and the Earth. This problem will be solved by displacing the equilibrium position of one or two spacecraft equipped with a planar solar sail using three types of different strategies. This is the subject of the second stage of the research, which is already published (DE ALMEIDA JUNIOR et al., 2017a). These first and second stages are written in chapters 4 and 5, respectively. Detailed introductory information on both stages connected with previous works available in the literature is given in subsections 4.1 and 5.1.

1.3 Spacecraft motion around artificial equilibrium points

The first model used to reach the second main objective (Artificial equilibrium points) in the research done in chapters 4 and 5 is a simplified one, since other external perturbations are not taken into consideration. In the real world, a spacecraft parked in the AEP is always perturbed by its surroundings, that is, the gravitational effects of other planets, moons or asteroids, the solar rays, albedo, solar wind, etc. Due to these perturbations, the spacecraft will be displaced from its equilibrium point, and this displacement will generate an extra force[1] that will be combined with the perturbation to define its motion. Thus, the third of the three main objectives of this thesis is to investigate the influence of external perturbative forces on the motion of a spacecraft around an AEP. In order to accomplish this task, several considerations that do not exist so far in the literature will be done. Note that it is important to know to where the spacecraft is initially going, e.g. this information can be used to adapt some kind of control to turn it back. Moreover, once the solution for the motion is analytically developed, the thrust or even the perturbation can used to maintain the spacecraft around the AEP for long periods of time. A method will be created to use the thrust combined with the perturbation to maintain the spacecraft around the AEP, independently of its linearly stability. Note that only specific and small regions in the space are linearly stable, thus this kind of motion is very useful for a mission designer.

---

[1]A force is defined in an inertial frame of reference, not a rotating one, but an analogous concept can be used taken into account extra terms (pseudo-forces).

In the first stage of the research, the thrust will be assumed to balance the gravitational and the centrifugal forces, but not the perturbation force. This is an important assumption, since it simplifies the equations of motion. Then, some general types of perturbative forces will be proposed and the equations of motion in the rotating frame will be analytically solved for these given perturbations. Then, analyses on the validity of the model will be made by comparing the proposed and developed new analytical solutions for several forms of the perturbation with a solution of the coupled and linearized equations of motion and with a numerical solution obtained via a Runge Kutta method. This first stage of the research is written in chapter 6 and already available in the literature (DE ALMEIDA JUNIOR et al., 2018). Introductory information about this research is given in section 6.1.

The second stage to reach the third main objective (Spacecraft motion around artificial equilibrium points) is to apply this idea using a perturbation force directly related with some astrodynamic case. At this moment, we can investigate more complex problems with more elaborated geometry, like to observe the poles of asteroids, planets or natural satellites, in dynamically very rich scenario, full of details. Thus, we will assume a moon in a circular orbit around one of the primaries in the circular restricted three body problem. The gravitational effect generated by this moon over the spacecraft will be considered as the perturbing force. The equations of motion will be solved analytically. The validity of the solution obtained in the first stage (in chapter 6) is restricted for short periods of time. This happens mainly due to the assumption that the thrust balances the gravitational and the centrifugal forces, which is true at the AEP, but not far from it. The main innovation in this stage is that the thrust will be updated each period of time such that the analytical solution will be valid again for the next period. In order to check the results, a comparison of the analytical solutions with a numerical one will show that the higher is the frequency of the updating of the thrust, the closer the analytical solution is to the numerical one and vice-versa, since the numerical solution is also a function of this frequency. This second stage is written in chapter 7, with introductory information written in section 7.1.

1.4 Considerations

The final conclusions of the thesis are shown in chapter 8, which describes how the main objectives are reached by the collections of the results obtained in the several stages of the research.

As can be noted by the perusal so far, the subject *integral indices* is self-sufficient,

studied in chapters 2 and 3, which present their own introductory definitions, mathematical models, results and considerations of their researches. Otherwise, although chapters 4-7 are also written to be self-sufficient in an isolated form, the subjects *artificial equilibrium points* (chapters 4 and 5) and *spacecraft motion around artificial equilibrium points* (chapters 6 and 7) are complementary in the sense of a hierarchy of knowledge - the second subject cannot be completely understood without the understanding of the first one. The complementarity between the first and the other two subjects is not explicit in this thesis, but it is included in the conclusions (chapter 8), where the respective crossing is left as idea for an open new subject to be studied in further investigations.

Summarizing this introduction, the chapters of this thesis are organized as follows:

a) First main objective: To analyze the influence of perturbative forces on the trajectory and velocity of a spacecraft through the use of "integral indices".

- First stage - chapter 2: Analyses over "integral indices" are made based on small perturbations of the driven harmonic, Duffing, and Van der Pol oscillators.
- Second stage - chapter 3: Analyses of several kinds of "integral indices" are made using astrodynamics systems.

b) Second main objective: To use perturbative forces as thrusts to generate AEP that can be useful for many missions and purposes.

- First stage - chapter 4: The AEP are defined and the regions in the space where they can or cannot be generated are investigated as function of several types of thrusts. Additionally, the results are applied to a planar solar sail.
- Second stage - chapter 5: Three different solutions are proposed to a problem of communication between a spacecraft located near the traditional Lagrangian point L_3 and the Earth using the concept of the AEP.

c) Third main objective: To investigate the influence of perturbative forces on the motion of a spacecraft around AEP.

- First stage - chapter 6: Analytical solutions to the motion of a spacecraft around AEP are proposed for general and specific forms of the perturbations.

– Second stage - chapter 7: An extended form of the analytical solution obtained in chapter 6 is used to maintain a spacecraft for long time above or below the poles of a massive body that rotates around a common center of mass of another massive body using the perturbative gravitational force of a moon.

d) A final conclusion is made in chapter 8 explaining how the three main objectives are reached and the contributions of this thesis to the knowledge.

2   ANALYZING "INTEGRAL INDICES" TO QUANTIFY THE EF-FECTS OF A PERTURBING FORCE IN THE DRIVEN HARMONIC, DUFFING, AND VAN DER POL OSCILLATORS

The goal in the present chapter is to study the use of "integral indices" to quantify the effects of a perturbing force in the driven harmonic, Duffing, and Van der Pol oscillators. The main idea is to define a scalar index that can represent the cumulative effects over time that a perturbing force causes in a dynamical system. An index of this type can help to prepare "perturbation maps", which can identify situations of larger or smaller effects. This idea appeared in the astrodynamics literature with the goal of finding less perturbed orbits for a spacecraft, but it is applied here to the driven harmonic and Duffing oscillators. The reason for those applications is that those problems have analytical solutions, which allows a better comparison of the indices. In particular, the effects of calculating this index using a perturbed and a non-perturbed trajectory are evaluated with the goal of better understanding these effects. The results show that the difference between both indices depends on the frequency and amplitude of the perturbing force.

2.1   Introduction

A good choice for the orbit of a spacecraft is a major step for the success of the mission, usually allowing a reduction in the costs of the orbital maneuvers and/or increasing the duration of the mission (QIAN et al., 2016).

The study of the effects of perturbation forces acting in a spacecraft is a very important problem in orbital dynamics. They modify the trajectory of the spacecraft in the short, medium and long timescales. In some cases, the perturbations are forces that need to be avoided or compensated with the use of propulsion systems but, sometimes, they are forces that can help the spacecraft to complete the desired mission (MORTARI et al., 2014). In any case, it is necessary to know the relation between perturbation, trajectory and velocity with some degree of accuracy to perform the mission analysis phase of the project.

In that sense, maps that can show the perturbation level of orbits can help to choose the best location to place a spacecraft. To elaborate this type of map it is necessary to find an adequate definition for the "perturbation level" of a particular orbit, which means to define a scalar number that can quantify the strength of the perturbations affecting the orbit. After that, it is possible to build "perturbation maps" (using the denomination given by Sanchez et al. (2016)), which are plots that

show the perturbation level of a given region in a grid of initial conditions to the orbit. Those maps can be used to find orbits with minimum perturbations, which can be used for practical applications. Such orbits are important because they may have less oscillations with respect to the Keplerian equivalent orbits and because they are good candidates to have a smaller number of station-keeping maneuvers, so reducing the costs involved in keeping the spacecraft near the desired orbit.

This type of problem has been under consideration for a long time. In particular, in recent years, the astrodynamics literature show some different forms to define the "perturbation level" of an orbit. The main point of those researches is to find a scalar number that can represent the perturbation received by a spacecraft along one orbital period, to allow the construction of the "perturbation maps".

Having this goal in mind, it is natural to consider integrals to generate this scalar quantity, because the integration is a process that relates effects occurring during one given time, like a full orbital period of a spacecraft, in one scalar number.

A first definition of this type of "integral index" is shown by Prado (2013), where orbits around the Earth perturbed by the Sun and the Moon are mapped based in "integrals". The index is defined as the integral of the magnitude of the perturbing forces acting on the spacecraft during one orbital period. The reason of using the magnitude of the forces is to take into account perturbations that modify the orbit of the spacecraft during one orbital period, but has a zero or near-zero net result after a full revolution. The goal of using this index is to find orbits with smaller oscillations with respect to a Keplerian (non-perturbed) orbit over short time scale of the order of one orbital period. To obtain this index it is assumed that the trajectory of the spacecraft is Keplerian, not taking into account the real trajectory the spacecraft describes under the effects of the perturbing forces. The consequences of this assumption depends on the deviation of the real trajectory of the spacecraft with respect to the Keplerian one, which depends on the magnitude of the disturbing forces and other factors. It means that this assumption may limit the accuracy and applicability of this index in the form proposed. In particular, terms coming from the difference between the Keplerian term of the gravity field of the Earth applied to the real trajectory and to the Keplerian one are not included in the integral. Then, a next step in the search for an index that can represent better the level of perturbation of an orbit is to remove this assumption, so measuring the integral of the perturbing forces over the real trajectory of the spacecraft and considering this difference in the Keplerian term of the gravity field.

This same index was used in some other applications, like mapping orbits around a triple asteroid (PRADO, 2014), with the goal of comparing the levels of the different perturbations acting in trajectories in that system. Another study verified the possibility of using solar radiation pressure to control the effects of the other perturbations (OLIVEIRA et al., 2014). The application of those maps for constellations of satellites was also considered by Oliveira and Prado (2014). The search for less perturbed orbits in the Pluto-Charon (SANCHEZ et al., 2014) and Haumea system (SANCHEZ et al., 2016) was also made using this index. Frozen orbits around Europa were also searched with the help of this integral, by Carvalho et al. (2014) and Santos et al. (2015). "Perturbation maps" were made for orbits around cubes (VENDITTI; PRADO, 2014). This same definition of the "integral index" was used to measure the effects of each term of the gravity field of the Earth in the trajectory of a spacecraft (SANCHEZ et al., 2014). These indices are summarized by Sanchez and Prado (2018) and studied for a spacecraft around the near-Earth asteroid (153591) 2001 SN$_{263}$. The indices to be defined and studied in this thesis will be different from these ones described above in the sense that the real trajectory will be taken into account in their evaluation, obtained by considering the effects of the perturbing terms in the dynamics.

In the simpler case of the J_2 problem - a conservative model in which the Geopotential is truncated to the second zonal harmonic - it has been recently shown that mapping the dynamics by means of the integral of the perturbing acceleration alone may be representative of the perturbation problem only with respect to the dynamics in the orbital plane (LARA, 2016).

To get a deeper insight in the integral of the perturbing acceleration and the utility of integral indices based on this approach, the present research has the goal of studying the importance of considering the perturbed trajectories in the definition of integral indices. Although these indices appeared in the literature related to applications to spacecraft trajectories, a different problem is used here. Indeed, the driven harmonic oscillator and the Duffing and Van der Pol equations are taken as perturbations of the simple harmonic oscillator. The reason to choose these systems is that they are integrable problems for small perturbations and their analytical solutions can be used for a better understanding of the integral indices. In that sense, it is crucial to show the situations in which different integral indices provide analogous or divergent results. This study will not answer this question for other systems, like the ones related to spacecraft trajectories. To understand those problems, it is necessary to perform specific studies for each case, which is a required step for all the researches

published up to now. Therefore, the scope of the investigation in the initial stage of the thesis is limited to make a first study that reveals the differences in the perturbation level that is obtained when using different integral indices when dealing with perturbed motion. The method and the results of this research are shown in this chapter, including a brief discussion in section 2.6.

2.2 Preliminary definitions

In Newtonian mechanics, the motion of a particle of mass m is described by its position $\vec{r}$ and velocity $\vec{v} = \mathrm{d}\vec{r}/\mathrm{d}t$ vectors, where t is time. Then, the equations of motion are

$$m\frac{\mathrm{d}^2\vec{r}}{\mathrm{d}t^2} = \vec{F} \tag{2.1}$$

where, in general, the force $\vec{F}$ depends on position, velocity, and time, viz. $\vec{F} \equiv \vec{F}(\vec{r}, \vec{v}; t)$. The impulse per unit of mass exerted by $\vec{F}$ between the initial time $t = t_1$ and the final time $t = t_2$ is

$$\vec{J} = \int_{t_1}^{t_2} \frac{\vec{F}}{m} \, \mathrm{d}t = \int_{t_1}^{t_2} \frac{\mathrm{d}^2\vec{r}}{\mathrm{d}t^2} \, \mathrm{d}t = \vec{v}(t_2) - \vec{v}(t_1). \tag{2.2}$$

Let a force $\vec{\alpha}$ be defined such that its magnitude is much smaller than the magnitude of $\vec{F}$, that is, $\|\vec{\alpha}\| \ll \|\vec{F}\|$, and a force $\vec{f}$ be defined as the difference between $\vec{F}$ and $\vec{\alpha}$. Hence, the resultant force can be decomposed into two forces, as follows: $\vec{F} = \vec{f} + \vec{\alpha}$. In this case, when

$$m\frac{\mathrm{d}^2\vec{r}}{\mathrm{d}t^2} = \vec{f}, \tag{2.3}$$

is integrable, that is

$$\vec{r} = \vec{\xi}(t; \vec{r}_0, \vec{v}_0),$$

then, Eq. (2.1) is called a *perturbation problem* (NAYFEH, 2004). It is commonly written as

$$m\frac{\mathrm{d}^2\vec{r}}{\mathrm{d}t^2} = \vec{f} + \epsilon\,\vec{\alpha}, \tag{2.4}$$

where ϵ is a *small parameter*, either physical or formal, which is used to unambiguously manifest the perturbative nature of the problem. Hence,

$$\vec{J} = \frac{1}{m} \int_{t_1}^{t_2} (\vec{f} + \epsilon\,\vec{\alpha}) \, \mathrm{d}t. \tag{2.5}$$

To compute the impulse $\vec{J}$, the solution $\vec{r} = \vec{r}(t)$ of Eq. (2.4) must be known, so that $\vec{f} = \vec{f}(\vec{r}, \vec{v}, t)$ and $\vec{\alpha} = \vec{\alpha}(\vec{r}, \vec{v}, t)$ can be expressed as functions of time. In general,

Eq. (2.4) will be non-integrable. However, perturbation solutions of the form

$$\vec{r} = \vec{\xi}(t; \vec{r}_0, \vec{v}_0) + \sum_{i \geq 1} \epsilon^i \vec{R}_i(t; \vec{r}_0, \vec{v}_0), \tag{2.6}$$

can be obtained in some cases, like the ones studied in this chapter, i.e. the driven harmonic, Duffing and Van der Pol oscillators up to the first order ($i = 1$). Correspondingly,

$$\vec{v} = \vec{\eta}(t; \vec{r}_0, \vec{v}_0) + \sum_{i \geq 1} \epsilon^i \vec{V}_i(t; \vec{r}_0, \vec{v}_0), \tag{2.7}$$

where $\vec{\eta} = \mathrm{d}\vec{\xi}/\mathrm{d}t$.

Using Eqs. (2.6) and (2.7), $\vec{f} = \vec{f}(\vec{r}, \vec{v}, t)$ becomes

$$\vec{f} = \vec{f}(\vec{\xi}(t; \vec{r}_0, \vec{v}_0) + \sum_{i \geq 1} \epsilon^i \vec{R}_i(t; \vec{r}_0, \vec{v}_0), \vec{\eta}(t; \vec{r}_0, \vec{v}_0) + \sum_{i \geq 1} \epsilon^i \vec{V}_i(t; \vec{r}_0, \vec{v}_0), t). \tag{2.8}$$

Expanding Eq. (2.8) about $\epsilon = 0$, it becomes

$$\vec{f} = \vec{f}(\vec{\xi}, \vec{\eta}, t) + \epsilon \left[\vec{R}_1 \frac{\partial \vec{f}}{\partial \vec{r}}\bigg|_{\epsilon=0} + \vec{V}_1 \frac{\partial \vec{f}}{\partial \vec{v}}\bigg|_{\epsilon=0} \right] + \mathcal{O}(\epsilon^2). \tag{2.9}$$

Analogously, expanding $\vec{\alpha} = \vec{\alpha}(\vec{r}, \vec{v}, t)$ about $\epsilon = 0$, it becomes

$$\epsilon \vec{\alpha}(\vec{r}, \vec{v}, t) = \epsilon \vec{\alpha}(\vec{\xi}, \vec{\eta}, t) + \mathcal{O}(\epsilon^2). \tag{2.10}$$

Using Eqs. (2.9) and (2.10), Eq. (2.4) becomes

$$m \frac{\mathrm{d}^2 \vec{r}}{\mathrm{d}t^2} = \vec{f}(\vec{\xi}, \vec{\eta}, t) + \epsilon \left[\vec{\alpha}(\vec{\xi}, \vec{\eta}, t) + \vec{R}_1 \frac{\partial \vec{f}}{\partial \vec{r}} + \vec{V}_1 \frac{\partial \vec{f}}{\partial \vec{v}} \right] + \mathcal{O}(\epsilon^2), \tag{2.11}$$

where the partial derivatives of $\vec{f}$ must be evaluated at $\vec{r} = \vec{\xi}$ and $\vec{v} = \vec{\eta}$. Due to the perturbative nature of the problem, terms of second or higher orders in the small parameter ϵ can be neglected. Using Eq. (2.11), the specific impulse given by Eq. (2.2) as

$$\vec{J} = \int_{t_1}^{t_2} \frac{\mathrm{d}^2 \vec{r}}{\mathrm{d}t^2} \, \mathrm{d}t$$

can be written in the form

$$\vec{J} = \vec{J}_0 + \vec{\Pi} + \vec{\Delta},$$

where

$$\vec{J_0} = \vec{\eta}(t_2) - \vec{\eta}(t_1),\tag{2.12}$$

is the specific impulse of the unperturbed problem in Eq. (2.3), which may be zero for periodic solutions (ESMAILZADEH et al., 1996) if $t_2 - t_1 =$ period multiple,

$$\vec{\Pi} = \frac{\epsilon}{m} \int_{t_1}^{t_2} \vec{\alpha}(\vec{\xi}, \vec{\eta}, t)\, \mathrm{d}t,\tag{2.13}$$

is the integral of the disturbing acceleration measured along the unperturbed path, which is called the "perturbation integral", and

$$\vec{\Delta} = \vec{J} - (\vec{\Pi} + \vec{J_0}) = \frac{\epsilon}{m} \int_{t_1}^{t_2} \left(\vec{R_1} \frac{\partial \vec{f}}{\partial \vec{r}} + \vec{V_1} \frac{\partial \vec{f}}{\partial \vec{v}} \right) \mathrm{d}t + \mathcal{O}(\epsilon^2).\tag{2.14}$$

Note that $\vec{J_0}$ and $\vec{\Pi}$ can always be computed, either analytically or numerically, from the solution of Eq. (2.3) — the integrable part of the perturbation problem. On the contrary, to compute $\vec{\Delta}$ one must know, at least, a first order approximation to the solution of Eq. (2.4). Disregarding $\vec{\Delta}$ may be valid in some particular instances (LARA, 2016), but this is not a general result: quite on the contrary, the contributions of $\vec{\Delta}$ and $\vec{\Pi}$ to the total impulse are of the same order.

The importance of $\vec{\Delta}$ is explored in three particular problems: the driven harmonic, the Duffing, and the Van der Pol oscillators. These problems are integrable at least for small values of the perturbation, yet, for particular values of the problem parameters they can be viewed as perturbations of a simpler integrable problem: the simple harmonic oscillator

$$\frac{\mathrm{d}^2 x}{\mathrm{d}t^2} + x = 0 \quad \Rightarrow \quad x = A\sin(t + \phi)\tag{2.15}$$

where A and ϕ are arbitrary integration constants, the amplitude of the oscillations and the initial phase. Note that mass and time units are chosen such that both the mass and the oscillation frequency are equal to one. Then, advantage of the integrability of the "perturbed" problems is taken to compute $\vec{\Delta}$ analytically.

The three perturbed oscillators are systems of one degree of freedom. Therefore, the total impulse and associated quantities are scalars and can take the role of integral indices.

2.3 The Driven Harmonic Oscillator

The driven harmonic oscillator can be described by the ordinary differential equation (LANDAU; LIFSHITZ, 1976)

$$\frac{\mathrm{d}^2 x}{\mathrm{d}t^2} + x = \epsilon(1 - \omega^2)\cos\omega t, \tag{2.16}$$

where, in our time units, ω is the non-dimensional frequency and $\epsilon(1 - \omega^2)$ is the amplitude of the forcing term, respectively. The driven harmonic oscillator is an integrable problem whose solution is obtained by adding a particular solution of Eq. (2.16) to the general solution of the homogeneous part, Eq. (2.15). Hence, the general solution to the driven harmonic oscillator is

$$x = A\sin(t + \phi) + \epsilon\cos\omega t \tag{2.17}$$

If ϵ is small, it can be assumed that Eq. (2.17) is a perturbation solution of the form of Eq. (2.6) in which terms $\mathcal{O}(\epsilon^2)$ and higher are neglected. Then,

$$x = \xi(t) + \epsilon X_1(t) + \mathcal{O}(\epsilon^2)$$

with $\xi = A\sin(t + \phi)$, and $X_1 = \cos\omega t$,

$$v = \frac{\mathrm{d}x}{\mathrm{d}t} = \eta(t) + \epsilon V_1(t) + \mathcal{O}(\epsilon^2),$$

with $\eta = A\cos(t + \phi)$, and $Y_1 = -\omega\sin\omega t$, and

$$\frac{\mathrm{d}^2 x}{\mathrm{d}t^2} = f + \epsilon\alpha. \tag{2.18}$$

Comparing Eq. (2.18) with Eq. (2.16), we get $f = -x$, $\alpha = (1 - \omega^2)\cos\omega t$. Hence, from Eq. (2.12), we get

$$J_0 = \eta(t_2) - \eta(t_1) = A\left[\cos(t_2 + \phi) - \cos(t_1 + \phi)\right]; \tag{2.19}$$

from Eq. (2.13), we get

$$\Pi = \epsilon\int_{t_1}^{t_2}(1 - \omega^2)\cos\omega t\,\mathrm{d}t = \epsilon\frac{1 - \omega^2}{\omega}(\sin\omega t_2 - \sin\omega t_1); \tag{2.20}$$

15

and from Eq. (2.5), we get

$$J = \int_{t_1}^{t_2} \left[-x(t) + \epsilon \left(1 - \omega^2 \right) \cos \omega t \right] \mathrm{d}t, \qquad (2.21)$$

where $x(t)$ must be replaced by the solution in Eq. (2.17). Hence,

$$J = J_0 - \epsilon \omega (\sin \omega t_2 - \sin \omega t_1). \qquad (2.22)$$

Finally, Δ is computed from Eq. (2.14), either by subtracting J and $J_0 + \Pi$, or by direct solution of the quadrature. We get

$$\Delta = -\frac{\epsilon}{\omega} (\sin \omega \, t_2 - \sin \omega \, t_1), \qquad (2.23)$$

which allows, for the driven harmonic oscillator, to establish the relations

$$\Pi = (\omega^2 - 1)\Delta = \frac{\omega^2 - 1}{\omega^2} (J - J_0). \qquad (2.24)$$

Equation (2.24) clearly disclose the physics of the problem. Indeed, $\Pi \to 0$ when $\omega \to 1$, a case in which the problem converts into the simple harmonic oscillator, cf. Eq. (2.16). On the other hand, high values of ω make Δ less relevant and $J \approx J_0 + \Pi$, but in this case the amplitude of the forcing term $\epsilon(1 - \omega^2)$ will be high and the driven harmonic oscillator can no longer being considered a perturbation problem. As a consequence, talking about perturbation integrals does not seem to make much sense. Finally, for small values of ω, and assuming that $t_2 - t_1$ is not too big, the impulse in Eq. (2.22) can be expanded in power series of ω. Thus, $J = J_0 - \epsilon(t_2 - t_1)\omega^2 \left[1 + \mathcal{O}(\omega^2) \right]$, which, after replaced in Eq. (2.24) leads to $\Pi = -\Delta = \epsilon (t_2 - t_1)$. Therefore, in the case of the driven harmonic oscillator, the integral Δ keeps an important part of the dynamics and cannot be neglected.

Let three new functions R_1, R_2, and R_3 be defined as

$$
\begin{aligned}
R_1 &= \frac{\Delta}{\Pi} = \frac{1}{\omega^2 - 1}, \\
R_2 &= \frac{\Pi}{(J - J_0)} = 1 - \frac{1}{\omega^2}, \\
R_3 &= \frac{\Delta}{(J - J_0)} = \frac{1}{\omega^2}.
\end{aligned}
$$

Thus, the behavior of the indices is illustrated in Fig. 2.1, where the relative importance of each integral - when compared to the difference between the perturbed and

unperturbed problems - as well as the ratio Δ/Π are presented. In particular, we note that the curve Δ/Π has a vertical asymptote in $\omega = 1$. Some relevant values of the ratios are shown in Table 2.1, which highlights some values of ω^2 showed in the vertical gridlines of Fig. 2.1 and the respective values of R_1, R_2 and R_3 as functions of ω^2 in the horizontal gridlines of Fig. 2.1. For the first value of ω^2 showed in Table 2.1, the curves R_1 and R_2 of Fig. 2.1 are coincident. For the second value of ω^2, R_1 and R_3 are symmetrically opposite. For the third value of ω^2, R_1 equals $\pm$infinity, R_2 equals zero and R_3 equals unity. For the fourth value of ω^2, R_1 equals unity and R_2 and R_3 are coincident. For the fifth value of ω^2, R_1 and R_2 are also coincident.

Figure 2.1 - The curve R_1 in gray is the ratio Δ/Π, the dashed curve R_2 is the ratio $\Pi/(J - J_0)$ and the curve R_3 in black is the ratio $\Delta/(J - J_0)$, in Eqs. (2.22-2.24). The gridlines highlight the particular values in Table 2.1.
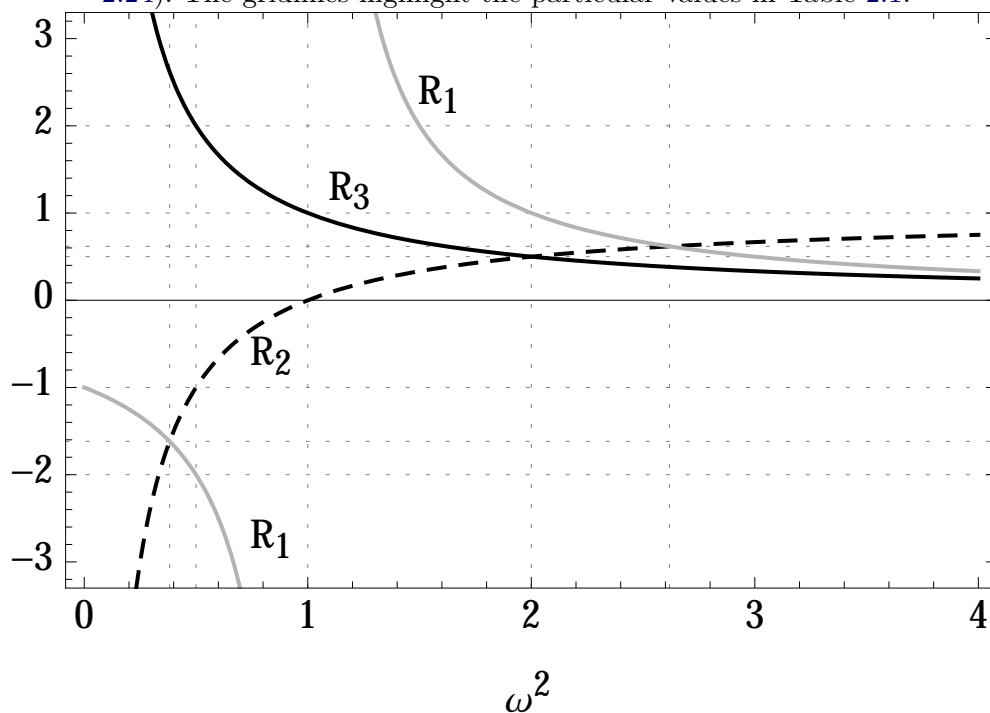
SOURCE: Author's production.

Table 2.1 - Relevant particular values in Fig. 2.1, where $R_1 = \frac{1}{\omega^2-1}$, $R_2 = 1 - \frac{1}{\omega^2}$ and $R_3 = \frac{1}{\omega^2}$

ω^2	R_1	R_2	R_3
$\frac{1}{2}(3-\sqrt{5})$	$-\frac{1}{2}(\sqrt{5}+1)$	$-\frac{1}{2}(\sqrt{5}+1)$	$\frac{1}{2}(3+\sqrt{5})$
$\frac{1}{2}$	-2	-1	2
1	$\pm\infty$	0	1
2	1	$\frac{1}{2}$	$\frac{1}{2}$
$\frac{1}{2}(3+\sqrt{5})$	$\frac{1}{2}(\sqrt{5}-1)$	$\frac{1}{2}(\sqrt{5}-1)$	$\frac{1}{2}(3-\sqrt{5})$

In the specific case in which the impulse is measured in the interval $t_2 - t_1 = 2\pi$, which is the period of the simple harmonic oscillator (the unperturbed problem), J_0 vanishes. Then $J = \Delta + \Pi$ and Eq. (2.24) is rewritten as

$$\Pi = (\omega^2 - 1)\Delta = \frac{\omega^2 - 1}{\omega^2}J. \tag{2.25}$$

In the particular case where $t_1 = 0$ and $t_2 = 2\pi$, a comparative plot of the ratios $\frac{\Delta}{\epsilon}$ and $\frac{\Pi}{\epsilon}$ is shown in Fig. 2.2. This figure exhibits, for any given ϵ, that the absolute values of Δ and Π are of the same order of magnitude for the most relevant values of ω in which Eq. (2.16) represents a perturbation problem - *i.e.*, the value of ω is not too large. Thus, both their contributions to J are equally significant and Δ cannot be neglected.

Of course other similar forms to the perturbation of the driven harmonic oscillator could be used instead of the one shown in Eq. (2.16). For example, if the perturbation of this equation is given by $\epsilon \cos \omega t$ instead of $\epsilon(1 - \omega^2) \cos \omega t$, similar results can be obtained, but the second option offers a better analytical solution that is more compatible to the preliminary definitions given in Section 2.2.

2.4 Duffing equation

Another case of integrable forced oscillators is the Duffing equation, which we write

$$\frac{d^2x}{dt^2} + x = -\varepsilon \, x^3. \tag{2.26}$$

For ε small, a perturbation solution to Eq. (2.26) can be written as (NAYFEH, 2004)

$$x = x_0 \cos t + \frac{1}{32}\varepsilon \, x_0^3 \left[-12t \sin t + \cos 3t - \cos t\right], \tag{2.27}$$

Figure 2.2 - Comparative plot of the ratios $\frac{\Delta}{\epsilon}$ and $\frac{\Pi}{\epsilon}$ as functions of ω in the particular case where $t_1 = 0$ and $t_2 = 2\pi$.
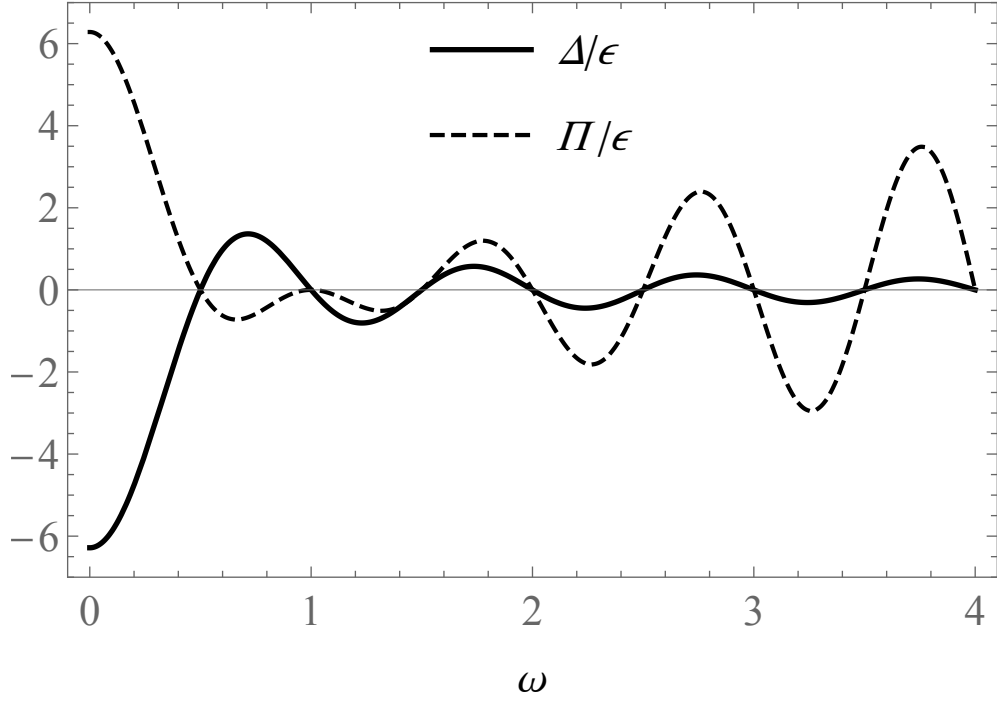
SOURCE: Author's production.

where $x_0 = x(0)$.

Proceeding as before, $f \equiv -x$, $\alpha \equiv -x^3$, $\xi \equiv x_0 \cos t$, $\eta \equiv -x_0 \sin t$, and

$$X_1 \equiv \frac{1}{32} x_0^3 \left[-12t \sin t + \cos 3t - \cos t \right].$$

Then

$$J_0 = -x_0 \left(\sin t_2 - \sin t_1 \right)$$

and, for a small enough interval $t_2 - t_1$ in which the quadratures are evaluated,

$$
\begin{aligned}
\Pi &= -\varepsilon \int_{t_1}^{t_2} x^3(t)\,\mathrm{d}t = -\frac{3x_0^3}{12}\varepsilon \left[\frac{1}{3}(\sin 3t_2 - \sin 3t_1) + 3(\sin t_2 - \sin t_1) \right] + \mathcal{O}(\varepsilon^2), \\
\Delta &= -\varepsilon \int_{t_1}^{t_2} X_1(t)\,\mathrm{d}t + \mathcal{O}(\varepsilon^2) \\
&= \frac{x_0^3}{32}\varepsilon \left[\frac{1}{3}(\sin 3t_2 - \sin 3t_1) + 13(\sin t_2 - \sin t_1) + 12(t_2 \cos t_2 - t_1 \cos t_1) \right] + \mathcal{O}(\varepsilon^2), \\
J &= J_0 + \Pi + \Delta
\end{aligned}
$$

19

When the impulse and related integrals are evaluated along the interval $t_2 = t_1 + 2\pi$, we find $J_0 = 0$, $\Pi = \mathcal{O}(\varepsilon^2)$, and

$$J = \Delta = \frac{3}{4}\epsilon x_0^3 \pi \cos t_1 + \mathcal{O}(\varepsilon^2),$$

which clearly shows that, for the Duffing equation, the perturbation integral Π is irrelevant in the study of the perturbed dynamics.

If now we compute the integrals in a slightly different interval $t_2 - t_1 = 2\pi + \delta$, both Π and Δ remain unaltered up to the order of ϵ, but J_0 no longer vanishes. Indeed, assuming that δ and ε are of the same order,

$$J_0 = -\delta\, x_0 \cos t_1 + \mathcal{O}(\varepsilon^2).$$

Hence,

$$J = J_0 + \Delta = \varepsilon\left(\frac{3}{4}x_0^2\pi - \frac{\delta}{\varepsilon}\right)x_0 \cos t_1 + \mathcal{O}(\varepsilon^2),$$

and the total impulse along the perturbed trajectory will vanish when the evaluation interval is varied a small quantity

$$\delta = \frac{3}{4}\varepsilon x_0^2 \pi.$$

In the specific case where $t_1 = 0$ and $x_0 = 1$, the values of J as a function of δ and ε are shown in a gray scale in Fig. 2.3, from where it is possible to observe the contributions of J_0 and Δ to J. Either if δ equals zero or not, Δ has a linear dependence on ε, which means that its contribution to J cannot not be neglected.

The solution of Eq. (2.26) given by Eq. (2.27) is valid for the initial condition $v(0) = 0$, where $v(t) = \frac{dx(t)}{dt}$ and it is not valid for too large values of time, because of the secular term $t\sin(t)$. Despite these restrictions, this solution is written in a good manipulable form, which allowed us to calculate J, J_0, Π and Δ analytically.

2.5 Van der Pol equation

The Van der Pol equation can be written as

$$\frac{d^2x}{dt^2} = -x + \epsilon(1 - x^2)\frac{dx}{dt}. \tag{2.28}$$

20

Figure 2.3 - Gray scale exhibits the value of J as a function of δ and ε for $t_1 = 0$ and $x_0 = 1$. J equals zero over the black straight line, which means $\varepsilon = \frac{4\delta}{3\pi}$.
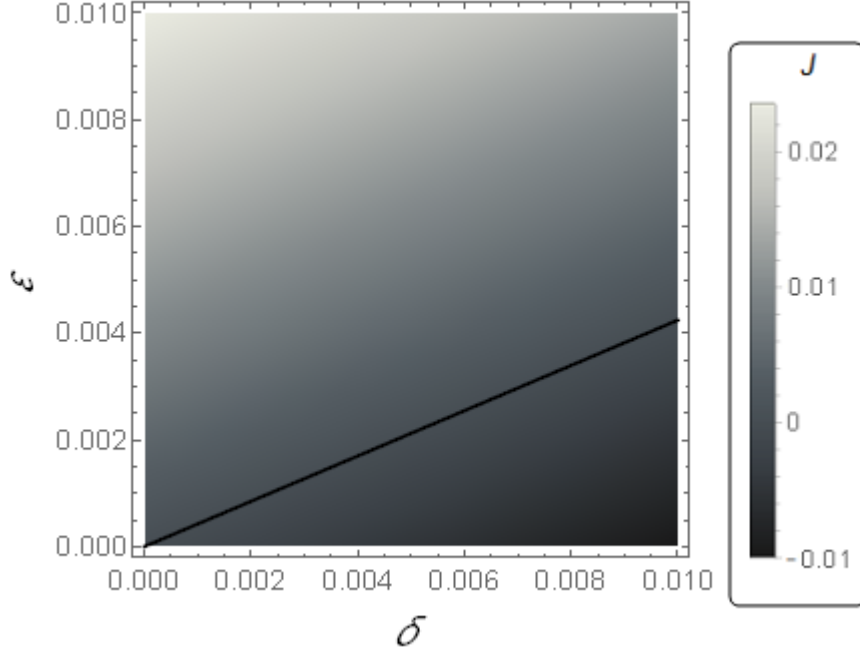
A solution for the above equation in the case where ϵ is a small parameter and t is not too large is (ABBASI, 2017)

$$x(t) = -\frac{1}{32}x_0\epsilon\sin(t)\left(5v_0^2 - 7x_0^2 + 16\right) + \frac{1}{2}tv_0\epsilon\sin(t)\left(\frac{1}{4}\left(x_0^2 - v_0^2\right) + 1\right)$$

$$+\frac{1}{32}x_0\epsilon\sin(3t)\left(3v_0^2 - x_0^2\right) + \epsilon\cos(t)\left(\frac{1}{32}v_0x_0^2 - \frac{v_0^3}{32} + \frac{v_0}{8}\right)$$

$$+\frac{1}{2}tx_0\epsilon\cos(t)\left(\frac{1}{4}\left(-v_0^2 - x_0^2\right) + 1\right) + \frac{1}{8}v_0\epsilon\cos(3t)\left(\frac{1}{4}\left(v_0^2 - x_0^2\right) - 1\right)$$

$$+v_0\sin(t) + x_0\cos(t), \quad (2.29)$$

where $x_0 = x(0)$, $v_0 = v(0)$ and $v(t) = \frac{dx}{dt}$.

Using the solution of the Simple Harmonic Oscillator, we can write

$$\xi(t, x_0, v_0) = v_0\sin t + x_0\cos t \quad (2.30)$$

and

$$\eta(t, x_0, v_0) = v_0\cos t - x_0\sin t. \quad (2.31)$$

21

We will assume the first period of the Simple Harmonic Oscillator plus a small time δ, thus $t_1 = 0$ and $t_2 = 2\pi + \delta$. According to Eq. (2.12), J_0 is evaluated as

$$J_0 = \eta(2\pi + \delta) - \eta(0) = v_0 \cos \delta - x_0 \sin \delta - v_0. \tag{2.32}$$

Using Eq. (2.28) and the definition of $\vec{\alpha}(\vec{\xi}, \vec{\eta}, t)$ given in Eq. (2.4), we can find that

$$\alpha(\xi, \eta, t) = (1 - \xi^2)\eta. \tag{2.33}$$

Hence, using Eq. (2.13), the function Π can be written as

$$\Pi = \frac{\epsilon}{12}\bigg(-3v_0 \sin(\delta) \left(v_0^2 + x_0^2 - 4 \right) + v_0 \sin(3\delta) \left(v_0^2 - 3x_0^2 \right)$$

$$-3x_0 \cos(\delta) \left(v_0^2 + x_0^2 - 4 \right) - x_0 \cos(3\delta) \left(x_0^2 - 3v_0^2 \right) + 4 \left(x_0^2 - 3 \right) x_0 \bigg). \tag{2.34}$$

Using Eq. (2.2), the total impulse per unit of mass can be written as

$$J = \int_0^{2\pi + \delta} \frac{d^2 x}{dt^2} \, dt = v(2\pi + \delta) - v(0), \tag{2.35}$$

where x is the solution of the Van der Pol equation and $v = \frac{dx}{dt}$. Hence, for the Van der Pol equation, the total impulse is written as

$$
\begin{aligned}
J = \ & \frac{1}{32}\bigg(3v_0\epsilon \sin(3\delta) \left(-v_0^2 + x_0^2 + 4 \right) \\
& + \sin(\delta) \left(\epsilon \left(4(\delta + 2\pi)v_0^2 x_0 + 3v_0 \left(x_0^2 + 4 \right) - 3v_0^3 + 4(\delta + 2\pi) \left(x_0^2 - 4 \right) x_0 \right) - 32x_0 \right) \\
& + \cos(\delta) \left(-4(\delta + 2\pi)v_0^3 \epsilon + 4v_0 \left((\delta + 2\pi) \left(x_0^2 + 4 \right) \epsilon + 8 \right) - 9v_0^2 x_0 \epsilon + 3x_0^3 \epsilon \right) \\
& - 3x_0 \epsilon \cos(3\delta) \left(x_0^2 - 3v_0^2 \right) - 32v_0 \bigg).
\end{aligned}
\tag{2.36}
$$

Now we are able to evaluate the Δ function. According to Eq. (2.14), this evaluation

gives

$$
\begin{aligned}
\Delta \;=\; & \frac{1}{96}\epsilon\Bigg(v_0 \sin(3\delta)\left(-17v_0^2 + 33x_0^2 + 36\right) \\
& + 3\sin(\delta)\left(4(\delta + 2\pi)\left(v_0^2 - 4\right)x_0 + 11v_0 x_0^2 + 5\left(v_0^2 - 4\right)v_0 + 4(\delta + 2\pi)x_0^3\right) \\
& - x_0 \cos(3\delta)\left(x_0^2 - 3v_0^2\right) \\
& - 3\cos(\delta)\left(4(\delta + 2\pi)\left(v_0^2 - 4\right)v_0 - 4(\delta + 2\pi)v_0 x_0^2 + \left(v_0^2 + 32\right)x_0 - 11x_0^3\right) \\
& - 32x_0\left(x_0^2 - 3\right)\Bigg).
\end{aligned}
\tag{2.37}
$$

One can note directly from Eq. (2.37) that the Δ function has a linear relation with ϵ. Either if δ equals zero or not, Δ has a linear dependence on ϵ, as well as Π, which means that both their contribution to J are of the same order in ϵ. Thus, Δ cannot be neglected, which is the same result as it was obtained before for the Duffing Oscillator in the section 2.4.

Supposing a specific case where $\epsilon = 0.01$, $x_0 = 1$, and $v_0 = 1$, the Δ can be ploted as a function of δ. This plot can be seen in Fig. 2.4. Note from this figure that Δ has an approximate linear relation with δ too.

Figure 2.4 - Δ as a function of δ (given by Eq. (2.37)) in the specific case where $\epsilon = 0.01$, $x_0 = 1$, and $v_0 = 1$. The absolute value of Π (given by Eq. (2.34)) is less than 10^{-6} in this specific case for the same interval of δ.
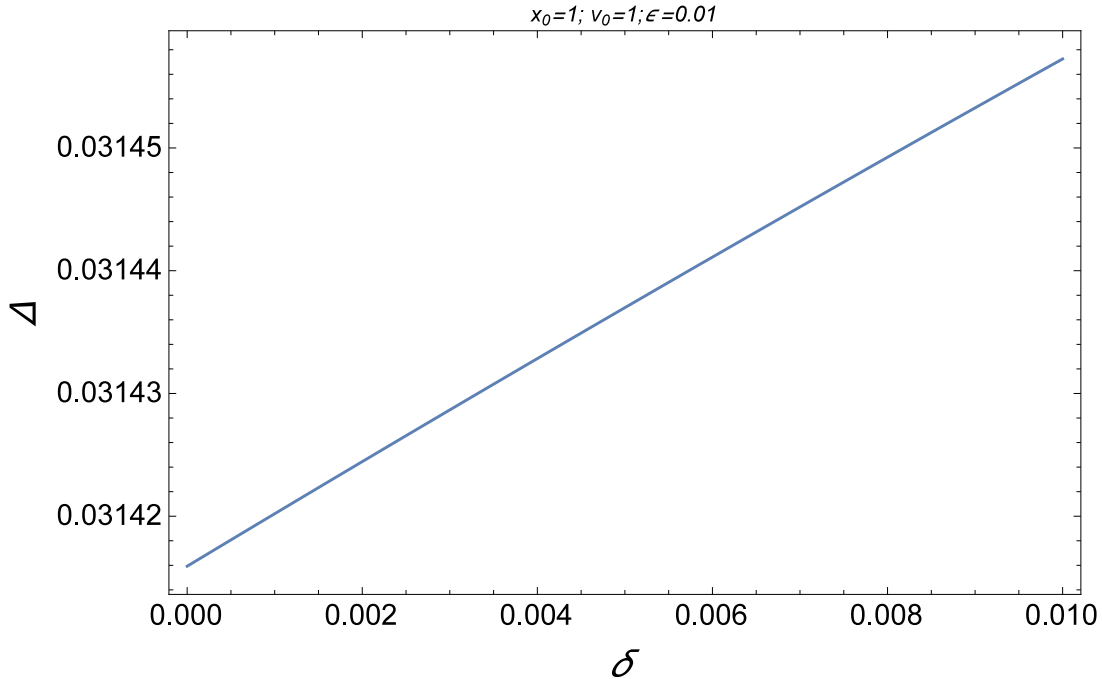
SOURCE: Author's production.

2.6 Considerations

The present chapter developed an analytical study of the application of "integral indices" to quantify the effects of a perturbing force in the harmonic, Duffing, and Van der Pol oscillators. Two scalar indices were defined with the goal of measuring the cumulative effects over the time that a perturbing force causes in those three dynamical systems. The main difference between the indices used is that one of them is calculated using a trajectory obtained from the non-perturbed system, so assuming that the perturbation is not large enough to make larger modifications in the trajectory during the integration time. The second index does not make that assumption, and, therefore, uses a more realistic approach.

The results showed that the differences between both indices may depend on some specific parameters of the dynamical system under study, which for the driven harmonic oscillator is the frequency of the disturbing force. Therefore, a similar study to the one presented here should be made before applying some specific integral index in the search for less perturbed orbits by means of perturbation maps. In particu-

lar, the construction of such perturbation maps in the case of perturbed Keplerian motion would require to know a first order, approximate solution to evaluate the quadratures that define the integral index. This research is done in the next chapter.

3 ANALYZING "INTEGRAL INDICES" TO QUANTIFY THE EFFECTS OF A PERTURBING FORCE OVER SATELLITES

Integral indices are useful tools that can be used to identify intrinsic characteristics of an orbit. Using analytical solutions for a perturbative (low, constant, and radial thrust) version of the Tsien problem, several indices are defined and evaluated. The utility of the indices is discussed. Based on the influence of the perturbation over the relative displacement between the trajectory and the Keplerian orbit, the results showed that an index is able to reveal some perturbative characteristics of the orbit. Using this index, it is possible to make a complete map of the orbits disturbed by the radial thrust, not only indicating the less perturbed ones, but also quantifying the level of perturbations of those orbits. The index found in this thesis can be used as useful tool in several other more practical problems in astrodynamics, including systems of asteroids, small bodies, or to guide the choice of an orbit for a mission such that the fuel consumption for station-keeping is minimized.

3.1 Introduction

The associated errors of the indices were studied in chapter 2, but only for one dimensional oscillators, not yet for astrodynamics cases. Thus, the second stage of this research is to make similar investigations in more practical and applied astrodynamics cases, which is also done in this thesis. A primary investigation (LARA, 2016) and the results of the research presented in chapter 2 and published in the literature (DE ALMEIDA JUNIOR et al., 2017b) show that the index could carry intrinsic errors that would inhibit it to be representative in order to map the effects of the perturbation in orbits in the most general cases. Although the index could be representative in some particular cases (LARA, 2016), these results suggest that more investigations should be done.

In general, the lack of analytical solutions of the satellite problem is an obstacle to identify the utility of general indices that could allow to produce perturbation maps and to evaluate the delta-v per orbit. On the other hand, there are few particular cases in which the satellite problem accepts an exact solution (TSIEN, 1953; JEZEWSKI, 1983). We deal with the Tsien problem where the gravitational attraction exerted over a satellite is disturbed by a constant thrust in the radial direction (TSIEN, 1953). Different approaches provide the solution to the Tsien problem in terms of elliptic integrals (AKELLA; BROUCKE, 2002; SAN-JUAN et al., 2012), but, alternatively, approximate analytical solutions have also been proposed that avoid the use of special functions and may be of practical application (QUARTA; MENGALI,

2012; BATTIN, 1999). In this stage, in order to continue the analyses and the search for indices, we assume that the constant thrust acting in the opposite direction of the central gravitational attraction is low, equivalent to a small fraction of the radial acceleration due to the gravity of the central body, and develop a perturbation solution to the Tsien problem in terms of trigonometric functions. This solution is used in the analyses and the search for indices that could quantify the effects of the perturbation in the delta-v impulse equivalent index.

Then, the goal in this stage of the research is to search for an adequate integral index that can be used to map orbits, trying to identify which ones are the more and the less perturbed by the assumed radial thrust. It is also developed an index that has the goal of measuring how much an orbit is deviated from the Keplerian equivalent one due to this thrust introduced. In this way, it is possible to compare the two different indices: an index that measures the element that generates a perturbation with an index that measures the consequence of this perturbation, which is the deviation of the real orbit compared to the Keplerian equivalent orbit. Thus, it is possible to validate the index based on the integral of the accelerations in terms of selecting orbits that are less perturbed.

After those calculations, the final goal is to find an index that indicates which orbit is less perturbed just by applying an integral index based in one orbital period of the spacecraft, without the need of longer numerical integrations. These types of indices can be used in a large variety of problems and, in some cases, depending on the type of the perturbation, they can be obtained analytically. This research is written in this chapter. The frame of reference and the Tsien problem are defined in section 3.2, together with some results of the evaluations of some previously defined indices. A thrust purely given in the tangential direction of the frame of reference is proposed in section 3.3, which analytical solutions are obtained, but not used. A low and constant thrust given in the radial direction is proposed in section 3.4. Several kinds of solutions are obtained, but the chosen one is the perturbation solution, which is analyzed in detail in subsection 3.4.4. Four different indices are defined and evaluated in section 3.5 using the solution obtained in subsection 3.4.4, which results are briefly discussed in section 3.6.

3.2   Introductory definitions

A polar reference inertial system (r, θ) can be defined from the standard rectangular reference system (x, y), according to Fig. 3.1, both with the Earth in their centers.

The position vector is written in the rectangular coordinate system as

$$\vec{r} = x\vec{i} + y\vec{j}. \tag{3.1}$$

Figure 3.1 - Polar coordinates (r, θ).
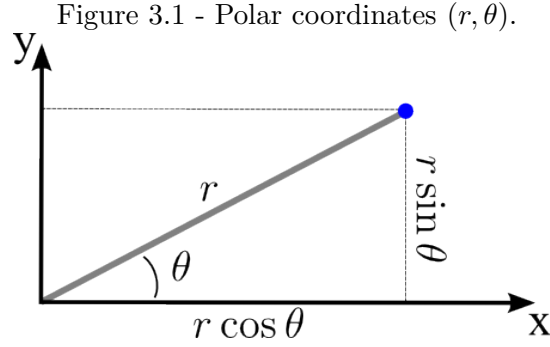
Using the polar frame of reference, two unit vectors are defined as

$$\hat{\vec{r}} = \cos\theta\vec{i} + \sin\theta\vec{j} \tag{3.2}$$

$$\hat{\vec{\theta}} = -\sin\theta\vec{i} + \cos\theta\vec{j}. \tag{3.3}$$

Hence, the position is
$$\vec{r} = r\hat{\vec{r}}, \tag{3.4}$$

the velocity is
$$\dot{\vec{r}} = \dot{r}\hat{\vec{r}} + r\dot{\theta}\hat{\vec{\theta}}, \tag{3.5}$$

and the acceleration is

$$\ddot{\vec{r}} = \left(\ddot{r} - r\dot{\theta}^2\right)\hat{\vec{r}} + \left(\frac{1}{r}\frac{\mathrm{d}}{\mathrm{d}t}\left(r^2\dot{\theta}\right)\right)\hat{\vec{\theta}}, \tag{3.6}$$

where the dots represent the derivative with respect to time.

3.2.1 Unperturbed (Keplerian) system

Suppose a spacecraft traveling under the gravitational influence of a planet. In an inertial frame of reference which center is coincident with the center of the planet,

29

the equations of motion of such a spacecraft are

$$\ddot{R} - R\dot{\theta}^2 = -\frac{\mu}{R^2},$$
(3.7)

where μ is the gravitational parameter, and

$$\frac{1}{R}\frac{\mathrm{d}}{\mathrm{d}t}\left(R^2\dot{\theta}\right) = 0.$$
(3.8)

3.2.2 Earlier definitions of integral indices

In the case where the system given by Eqs. (3.7) and (3.8) is perturbed by an acceleration $\vec{\alpha}$, the total impulse per unit of mass of the motion evolved from the time $t = t_1$ to $t = t_2$ is defined as

$$\vec{J} = \int_{t_1}^{t_2} \ddot{\vec{r}}\,\mathrm{d}t = \dot{\vec{r}}\Big|_{t_1}^{t_2}.$$
(3.9)

In order to evaluate $\vec{J}$ the solution of $\dot{\vec{r}}$ must be known. The "perturbation integral" $\vec{\Pi}$ has been defined in the chapter 2 as

$$\vec{\Pi} = \int_{t_1}^{t_2} \vec{\alpha}\,\mathrm{d}t.$$
(3.10)

This perturbation is written as function of its components in the radial and tangential directions as $\vec{\alpha} = \alpha_r\hat{\vec{r}} + \alpha_\theta\hat{\vec{\theta}}$, according to Fig. 3.2.

Figure 3.2 - The components of the perturbation.
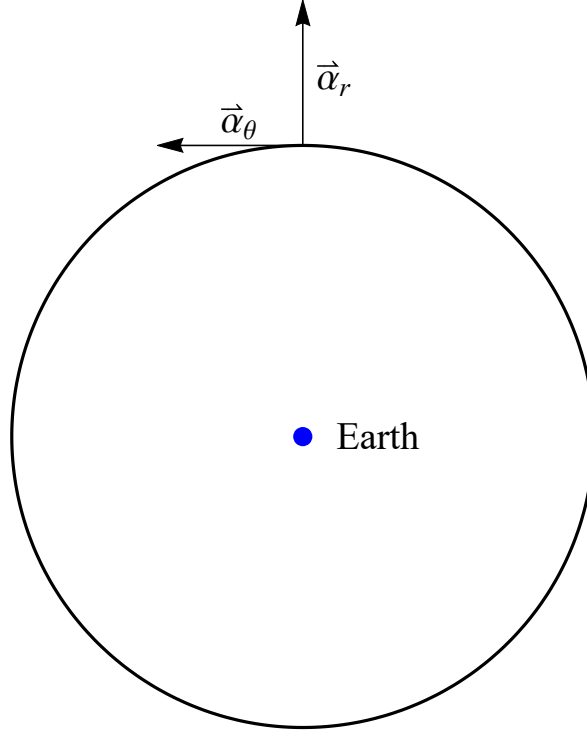
Hence, Eq. (3.10) becomes

$$\vec{\Pi} = \int_{t_1}^{t_2} \alpha_r \hat{\vec{r}} \, \mathrm{d}t + \int_{t_1}^{t_2} \alpha_\theta \hat{\vec{\theta}} \, \mathrm{d}t, \tag{3.11}$$

Using Eqs. (3.2) and (3.3), Eq. (3.11) becomes

$$\vec{\Pi} = \int_{t_1}^{t_2} \left(\alpha_r \cos\theta - \alpha_\theta \sin\theta \right) \mathrm{d}t \vec{i} + \int_{t_1}^{t_2} \left(\alpha_r \sin\theta + \alpha_\theta \cos\theta \right) \mathrm{d}t \vec{j}, \tag{3.12}$$

For unperturbed circular motion, the period of the motion is $P = 2\pi \sqrt{R_0^3/\mu}$, where R_0 is the radius of the orbit. Hence, the angular solution is $\theta = 2\pi t/P$ and Eq. (3.12) becomes

$$\vec{\Pi} = \int_{t_1}^{t_2} \left(\alpha_r \cos\left(\frac{2\pi t}{P}\right) - \alpha_\theta \sin\left(\frac{2\pi t}{P}\right) \right) \mathrm{d}t \vec{i} + \int_{t_1}^{t_2} \left(\alpha_r \sin\left(\frac{2\pi t}{P}\right) + \alpha_\theta \cos\left(\frac{2\pi t}{P}\right) \right) \mathrm{d}t \vec{j}. \tag{3.13}$$

Other definitions of indexes may involve the integral along one period of the unper-

turbed motion of the modulus of the perturbing acceleration $\|\vec{\alpha}\|$, or each component of it, or the variation $\vec{\alpha} \cdot \vec{v}$ or the kinetic energy. Namely, Π_1 (PRADO, 2014; OLIVEIRA; PRADO, 2014; SANCHEZ et al., 2014; VENDITTI; PRADO, 2014; SHORT et al., 2017), Π_2 (SANCHEZ et al., 2014; SHORT et al., 2017), and Π_3 (SANCHEZ; PRADO, 2018):

$$\Pi_1 = \frac{1}{P} \int_{t_1}^{t_2} \|\vec{\alpha}\| \, \mathrm{d}t, \tag{3.14}$$

$$\Pi_2 = \frac{1}{P} \int_{t_1}^{t_2} \vec{\alpha} \cdot \vec{v} \, \mathrm{d}t, \tag{3.15}$$

$$\Pi_3 = \frac{1}{P} \left(\left(\int_{t_1}^{t_2} \alpha_x \, \mathrm{d}t \right)^2 + \left(\int_{t_1}^{t_2} \alpha_y \, \mathrm{d}t \right)^2 + \left(\int_{t_1}^{t_2} \alpha_z \, \mathrm{d}t \right)^2 \right)^{\frac{1}{2}}, \tag{3.16}$$

where $\vec{v}$ is the velocity vector of the spacecraft and α_x, α_y, and α_z are the components of $\vec{\alpha}$ in the x, y, and z directions. In the case where the perturbation is a constant on time and the integration is taken over a period ($t_2 = t_1 + P$), the evaluation of Eqs. (3.13)-(3.16) are shown in Table 3.1. The solution of the perturbed problem $\vec{r}(t)$ is unknown yet, so as the specific impulse $\vec{J}$. Hence, the comparisons between $\vec{J}$ or $\|\vec{J}\|$ and the other indices ($\vec{\Pi}$, Π_1, Π_2, and Π_3) cannot be done yet. On the other hand, an analysis of the evaluation of them shown in Table 3.1 can lead to the following comments:

a) $\vec{\Pi}$ clearly leads to the conclusion that the spacecraft is not perturbed.

b) Π_1 depends only on the intensity of the perturbation.

c) Π_2 neglects the radial component of the perturbation.

d) Π_3 also leads to the conclusion that the spacecraft is not perturbed.

The conclusion that any constant perturbation is not capable of change the trajectory and velocity of the spacecraft at all is obviously wrong. It will be shown later in this chapter that even non-eccentric orbits clearly may be perturbed. We see in Table 3.1 that $\vec{\Pi}$ and Π_3 may lead to wrong conclusions, hence they do not seem good "indices".

Note that the magnitude of the gravitational force decays with R_0, since it is proportional to the inverse of R_0^2. If the perturbation is fixed, the ratio ($\frac{|perturbation|}{|gravitational force|}$) becomes stronger when R_0 is increased. This relative perturbation (this ratio) is stronger for larger values of R_0, thus it is reasonable to expect that the orbit should be affected in the same way. We also expect that a good "index" must represent the

Table 3.1 - The evaluation of indices. $\vec{0}$ is the null vector.

Perturbation	$\vec{\Pi}$	Π_1	Π_2	Π_3
$\vec{\alpha} = \alpha_r \hat{\vec{r}} + \alpha_\theta \hat{\vec{\theta}}$	$\vec{0}$	$\sqrt{\alpha_r^2 + \alpha_\theta^2}$	$\sqrt{\frac{\mu}{R_0}}\alpha_\theta$	0
$\vec{\alpha} = \alpha_r \hat{\vec{r}}$	$\vec{0}$	α_r	0	0
$\vec{\alpha} = \alpha_\theta \hat{\vec{\theta}}$	$\vec{0}$	α_θ	$\sqrt{\frac{\mu}{R_0}}\alpha_\theta$	0

influence of this relative perturbation over the orbit. This aspect can be seen later in Fig. 3.17, which shows that the orbit is more perturbed for larger values of the semi-major axis.

Table 3.1 shows that the "index" Π_1 does not depend on the radius of the orbit or any other parameter, except the intensity of the perturbation. Hence, Π_1 also does not seem a good "index".

The evaluation of Π_2 shown in Table 3.1 indicates that there is no influence of the radial component of the perturbation, as expected by its definition. Moreover, Π_2 is proportional to the inverse of the square root of R_0, which means that if R_0 increases, the "index" Π_2 decreases. Thus, beside the fact that this "index" neglects the influence of the radial component of the perturbation, it also does not represent our expectation to increase as R_0 increases, according to the relative perturbation. Therefore, Π_2 is not a good "index" too.

In conclusion, all of the "indices" described above are meaningless, at least in this case, and they cannot be used to describe orbits that are less perturbed. Thus, our effort will be now spent to find "indices" that are able to describe the influence of the perturbation over the orbit, but taking into account the real trajectory of the perturbed system over the integration required to obtain them.

3.3 Tangential Thrust

Suppose that the spacecraft under a thrust α_θ in the tangential direction of its motion. The equations of motion become

$$\ddot{r} - r\dot{\theta}^2 = -\frac{\mu}{r^2} \tag{3.17}$$

and

$$\frac{d}{dt}\left(r^2\dot{\theta}\right) = r\alpha_\theta \tag{3.18}$$

3.3.1 Constant perturbation

For very small values of the constant perturbation α_θ, the radial acceleration is small enough so that the centripetal acceleration is approximately balanced by gravity (BATTIN, 1999). Hence, Eq. (3.17) becomes

$$\dot{\theta} = \pm\sqrt{\frac{\mu}{r^3}}. \tag{3.19}$$

The option with the negative signal of the above equation is disregarded because the initial condition is such that the motion is counterclockwise. Substituting the option with positive signal of Eq. (3.19) into Eq. (3.18), this last one is rewritten as

$$r^{-\frac{3}{2}}\dot{r} = \frac{2\alpha_\theta}{\sqrt{\mu}}. \tag{3.20}$$

The integration of Eq. (3.20) in dt gives the solution expressed as

$$r(t) = \frac{\mu}{v_0^2 \left(1 - \frac{(t-t_1)\alpha_\theta}{v_0}\right)^2}, \tag{3.21}$$

where $v_0 = \|\dot{\vec{r}}(t_1)\|$ is the absolute value of the initial velocity. The derivative of Eq. (3.21) is

$$\dot{r}(t) = \frac{2\mu\alpha_\theta}{v_0^3 \left(1 - \frac{(t-t_1)\alpha_\theta}{v_0}\right)^3}. \tag{3.22}$$

Using Eq. (3.21), Eq. (3.19) becomes

$$\dot{\theta}(t) = \frac{v_0^3 \sqrt{\left(1 - \frac{(t-t_1)\alpha_\theta}{v_0}\right)^6}}{\mu}. \tag{3.23}$$

The quadrature of Eq. (3.23) yields

$$
\begin{aligned}
\theta(t) \;=\; & \frac{1}{4\mu\alpha_\theta}\Bigg[\alpha_\theta\Bigg(4\theta_0\mu + v_0^3\Bigg(t\sqrt{\frac{(-t\alpha_\theta + t_1\alpha_\theta + v_0)^6}{v_0^6}} - \\
& t_1\sqrt{\frac{(-t\alpha_\theta + t_1\alpha_\theta + v_0)^6}{v_0^6}} + t_1\sqrt{\frac{(t_1\alpha_\theta + v_0)^6}{v_0^6}}\Bigg)\Bigg) + \\
& v_0^4\Bigg(\sqrt{\frac{(t_1\alpha_\theta + v_0)^6}{v_0^6}} - \sqrt{\frac{(-t\alpha_\theta + t_1\alpha_\theta + v_0)^6}{v_0^6}}\Bigg)\Bigg],
\end{aligned}
\tag{3.24}
$$

where $\theta_0 = \theta(0)$ is the initial value of θ.

According Eq. (3.9), the specific impulse is

$$\vec{J} = \dot{\vec{r}}\Big|_{t_1}^{t_2} = \left(\dot{r}\hat{r} + r\dot{\theta}\hat{\theta}\right)\Big|_{t_1}^{t_2}. \tag{3.25}$$

Equations (3.21) - (3.24) can provide the solutions for $r(t)$, $\dot{r}(t)$, $\dot{\theta}(t)$, and $\theta(t)$ required to evaluate $\vec{J}$. Note that the solution of the differential Eqs. (3.17) and (3.18) of second order should provide 4 constants, to be defined by the initial conditions of the motion. A problem is that Eq. (3.20) represents a constraint and all the obtained solutions $r(t)$, $\dot{r}(t)$, and $\dot{\theta}(t)$ depend only on a single constant v_0. Due to this problem, this solution will not be chosen to express the results.

3.4 The low, constant, radial thrust problem

Suppose a spacecraft perturbed by a thrust in the radial direction of its motion ($\vec{\alpha} = \alpha_r\hat{r}$). The equations of motion become

$$\ddot{r} - r\dot{\theta}^2 = -\frac{\mu}{r^2} + \alpha_r \tag{3.26}$$

and

$$\frac{d}{dt}\left(r^2\dot{\theta}\right) = 0, \tag{3.27}$$

which can be integrated to give the following constant of motion:

$$r^2\dot{\theta} = \sqrt{\mu r_0}. \tag{3.28}$$

The constant radial thrust problem is obtained from the potential energy

$$V = -\frac{\mu}{r} - \alpha_r r, \tag{3.29}$$

where $r = \|\vec{r}\|$ is the distance from the central body's center of mass, and α_r is a constant acceleration. Because Eq. (3.29) is a central potential, the constant, radial thrust problem

$$\ddot{\vec{r}} = \left(-\frac{\mu}{r^2} + \alpha_r\right)\hat{r}. \tag{3.30}$$

is integrable, yet it requires the use of special functions (BROUCKE, 1980; TSIEN, 1953). Alternatively, for small thrust values, useful approximate solutions can be expressed in trigonometric functions (QUARTA; MENGALI, 2012). We will find several different analytical solutions for this problem in the next subsections. Then, we will

choose the perturbation solution - to be obtained in subsection 3.4.4 - to evaluate the "indices". This choice is mainly due to the possibility of obtain similar solutions (using perturbation methods) for other astrodynamics systems.

3.4.1   Quarta and Mengali solution for a constant perturbation

For a small perturbation a_r, an approximated solution for r as a function of θ is given by (QUARTA; MENGALI, 2012)

$$r = \frac{r_0/(1-\eta)}{1 + (\eta/(1-\eta))\cos(\theta)}, \tag{3.31}$$

where $\eta = a_r r_0^2/\mu$. Note that this equation represents the polar equation of an ellipse with one of the focuses in the center of the coordinate system. The trajectory is approximated by an ellipse through this solution.

Using Eq. (3.28) $\dot\theta$ is

$$\dot\theta = \frac{\sqrt{\mu r_0}}{r^2} = \left(\frac{(1-\eta)^2\sqrt{\mu r_0}\left(\frac{\eta\cos(\theta)}{1-\eta}+1\right)^2}{r_0^2}\right). \tag{3.32}$$

Using Eqs. (3.31) and (3.32), the derivative of r with respect to time is

$$\dot r = \left(\frac{\partial r}{\partial \theta}\right)(\dot\theta) = \frac{\eta\sin(\theta)\sqrt{\mu r_0}}{r_0} \tag{3.33}$$

According Eq. (3.9), the specific impulse is $\vec J = \dot{\vec r}\Big|_{t_1}^{t_2} = \left(\dot r\hat r + r\dot\theta\hat\theta\right)\Big|_{t_1}^{t_2}$, which requires the solution $\theta(t)$. The evaluation of $t(\theta)$ can be obtained analytically by solving the integration of Eq. (3.32) in time. The problem is that its respective inverse function $\theta(t)$ could not be obtained.

3.4.2   First order series solution in $r - r_0$ for a constant perturbation

Using Eq. (3.28), Eq. (3.26) becomes

$$\ddot r = \frac{\mu r_0}{r^3} - \frac{\mu}{r^2} + \alpha_r \tag{3.34}$$

Defining a new variable $s = r - r_0$, supposing that r varies in a small quantity around r_0, and using the first order Taylor expansion of r around r_0, Eq. (3.34) can

be written as

$$\ddot{s} = -\frac{\mu}{r_0^3}s + \alpha_r, \tag{3.35}$$

which solution is

$$s = A\sin(\omega_0 t) + B\cos(\omega_0 t) + \frac{\alpha_r}{\omega_0^2}, \tag{3.36}$$

where $\omega_0 = \sqrt{\mu/r_0^3}$.

Using the boundary conditions $s(0) = 0$ and $\dot{s}(0) = 0$, the solution becomes

$$s = -\frac{\alpha_r}{\omega_0^2}\cos(\omega_0 t) + \frac{\alpha_r}{\omega_0^2}. \tag{3.37}$$

Hence, the solution $r(t)$ is

$$r = r_0 - \frac{\alpha_r}{\omega_0^2}\cos(\omega_0 t) + \frac{\alpha_r}{\omega_0^2}, \tag{3.38}$$

which derivative with respect to time is

$$\dot{r} = \frac{\alpha_r}{\omega_0}\sin(\omega_0 t), \tag{3.39}$$

Using Eq. (3.38), Eq. (3.28) can be written as

$$\dot{\theta} = \frac{\sqrt{\mu r_0}}{\left(r_0 - \frac{\alpha_r}{\omega_0^2}\cos(\omega_0 t) + \frac{\alpha_r}{\omega_0^2}\right)^2}. \tag{3.40}$$

which integration yields

$$
\begin{aligned}
\theta \;=\;& \frac{1}{r_0^{3/2}\omega_0\left(\frac{2\alpha_r}{\omega_0^2}+r_0\right)^{3/2}\left(\frac{\alpha_r}{\omega_0^2}-\frac{\alpha_r\cos(t\omega_0)}{\omega_0^2}+r_0\right)} \\
& \left[\sqrt{r_0}\sqrt{\frac{2\alpha_r}{\omega_0^2}+r_0}\left(\theta_0 r_0\omega_0\left(\frac{\alpha_r}{\omega_0^2}+r_0\right)\left(\frac{2\alpha_r}{\omega_0^2}+r_0\right)-\right.\right.\\
& \left.\frac{\theta_0 r_0\alpha_r\left(\frac{2\alpha_r}{\omega_0^2}+r_0\right)\cos\left(t\omega_0\right)}{\omega_0}+\frac{\alpha_r\sqrt{\mu r_0}\sin\left(t\omega_0\right)}{\omega_0^2}\right)+\\
& 2\sqrt{\mu r_0}\left(\frac{\alpha_r}{\omega_0^2}+r_0\right)\left(\frac{\alpha_r}{\omega_0^2}-\frac{\alpha_r\cos\left(t\omega_0\right)}{\omega_0^2}+r_0\right)\\
& \left.\tan^{-1}\left(\frac{\sqrt{\frac{2\alpha_r}{\omega_0^2}+r_0}\tan\left(\frac{t\omega_0}{2}\right)}{\sqrt{r_0}}\right)\right]
\end{aligned}
\tag{3.41}
$$

The solution of $\theta(t)$ has been obtained, however comparisons with numerical solutions for some values of the parameters shown that further studies on its range of validity is required with special attention to the term related to the inverse of the trigonometric function ($\tan^{-1}$).

3.4.3 Radial thrust proportional to $\dot\theta$

Suppose a thrust acting in the radial direction of motion of a spacecraft given by $\vec\alpha = kf(\theta)\dot\theta\hat r$, where k is a constant and $f(\theta)$ is a general function of θ. The vectorial form of the equations of motion is

$$
\left(\ddot r - r\dot\theta^2\right)\hat r + \left(\frac{1}{r}\frac{d}{dt}\left(r^2\dot\theta\right)\right)\hat\theta = \left(-\frac{\mu}{r^2}+kf(\theta)\dot\theta\right)\hat r
\tag{3.42}
$$

The θ component of this equation is

$$
\frac{1}{r}\frac{d}{dt}\left(r^2\dot\theta\right) = 0,
\tag{3.43}
$$

which may be integrated to give the following constant of motion:

$$
r^2\dot\theta = \sqrt{\mu r_0}.
\tag{3.44}
$$

Equation (3.6) can be integrated on time to give

$$
\dot{\vec r} = \int\left(\ddot r - r\dot\theta^2\right)\hat r\,dt + \int\left(\frac{1}{r}\frac{d}{dt}\left(r^2\frac{d\theta}{dt}\right)\right)\hat\theta\,dt.
\tag{3.45}
$$

Equation (3.42) can be integrated in dt. The result is

$$\int \left(\ddot{r} - r\dot{\theta}^2 \right) \hat{r} \, dt + \int \frac{1}{r} \frac{d}{dt} \left(r^2 \frac{d\theta}{dt} \right) \hat{\theta} \, dt = -\int \frac{\mu}{r^2} \hat{r} \, dt + \int k f(\theta) \dot{\theta} \hat{r} \, dt. \qquad (3.46)$$

Using Eq. (3.46), Eq. (3.45) can be rewritten as

$$\dot{\vec{r}} = -\int \frac{\mu}{r^2} \hat{r} \, dt + \int k f(\theta) \dot{\theta} \hat{r} \, dt. \qquad (3.47)$$

Using Eq. (3.44), Eq. (3.47) becomes

$$\dot{\vec{r}} = -\sqrt{\frac{\mu}{r_0}} \int \dot{\theta} \hat{r} \, dt + k \int f(\theta) \dot{\theta} \hat{r} \, dt. \qquad (3.48)$$

Using Eq. (3.2), Eq. (3.48) becomes

$$\dot{\vec{r}} = \sqrt{\frac{\mu}{r_0}} \left(\int \cos\theta \, d\theta \vec{i} + \int \sin\theta \, d\theta \vec{j} \right) + k \left(\int f(\theta) \cos\theta \, d\theta \vec{i} + \int f(\theta) \sin\theta \, d\theta \vec{j} \right). \qquad (3.49)$$

or

$$\dot{\vec{r}} = \sqrt{\frac{\mu}{r_0}} \left(\sin\theta \vec{i} - \cos\theta \vec{j} \right) + k \left(\int f(\theta) \cos\theta \, d\theta \vec{i} + \int f(\theta) \sin\theta \, d\theta \vec{j} \right). \qquad (3.50)$$

Using Eq. (3.3), Eq. (3.50) becomes

$$\dot{\vec{r}} = \sqrt{\frac{\mu}{r_0}} \hat{\theta} + k \left(\int f(\theta) \cos\theta \, d\theta \vec{i} + \int f(\theta) \sin\theta \, d\theta \vec{j} \right). \qquad (3.51)$$

Note that the first member of the right side of Eq. (3.51) is a constant vector in de direction of $\hat{\theta}$, which means that its contribution to $\vec{J}$ is always zero. Hence, $\vec{J}$ can be evaluated using Eq. (3.9), which gives

$$\vec{J} = k \left(\int_{\theta(0)}^{\theta(T)} f(\theta) \cos\theta \, d\theta \vec{i} + \int_{\theta(0)}^{\theta(T)} f(\theta) \sin\theta \, d\theta \vec{j} \right). \qquad (3.52)$$

According Eq. (3.12), the evaluation of $\vec{\Pi}$ for this kind of thrust is

39

$$\vec{\Pi} = \int_{t_1}^{t_2} k f(\theta) \dot{\theta} \cos \theta \, \mathrm{d}t \vec{i} + \int_{t_1}^{t_2} \left(k f(\theta) \dot{\theta} \sin \theta \right) \mathrm{d}t \vec{j}, \tag{3.53}$$

which can be written as

$$\vec{\Pi} = k \left(\int_0^{2\pi} f(\theta) \cos \theta \, \mathrm{d}\theta \vec{i} + \int_0^{2\pi} f(\theta) \sin \theta \, \mathrm{d}\theta \vec{j} \right) \tag{3.54}$$

The period of the unperturbed system given by Eqs. (3.7) and (3.8) is $T = 2\pi \sqrt{r_0^3/\mu}$, which means a complete evolution of the system. $\theta(t_1)$ and $\theta(t_2)$ represents the integration limits of the perturbed system. In the case where the integration interval of the perturbed system is also taken from 0 to 2π, then Eq. (3.52) and (3.54) can be used to show that $\vec{\Pi} = \vec{J}$. Equation (3.52) shows that $\vec{J}$ (or $\vec{\Pi}$) has a linear relation with k. Table 3.2 shows the values of $\vec{J}$ (or $\vec{\Pi}$) for some values of $f(\theta)$ in which Eq. (3.52) is integrable.

Table 3.2 - Values of $\vec{\Pi}$ or $\vec{J}$ for some values of $f(\theta)$

$f(\theta)$	$\vec{\Pi}$ or $\vec{J}$
1	$0\vec{i} + 0\vec{j}$
θ	$0\vec{i} - 2\pi k \vec{j}$
θ^2	$4\pi k \vec{i} - 4\pi^2 k \vec{j}$
θ^3	$12\pi^2 k \vec{i} + (12\pi - 8\pi^3) k \vec{j}$
$\sin \theta$	$0\vec{i} + \pi k \vec{j}$
$\cos \theta$	$\pi k \vec{i} + 0\vec{j}$
e^θ	$e^\pi \sinh(\pi) k \vec{i} - e^\pi \sinh(\pi) k \vec{j}$

3.4.4 Perturbation solution

The constant radial thrust problem admits Hamiltonian formulation $\mathcal{K} = T + V$ where T is the kinetic energy. Furthermore, for values of the thrust acceleration α_r much smaller than the central Keplerian acceleration $\alpha_K = an^2$, where a is the orbit semi-major axis and n the mean motion, the problem can be viewed as a perturbation of the Keplerian motion

$$\mathcal{K} = -\frac{\mu}{2a} \left(1 + \beta \frac{r}{a} \right), \qquad \beta = 2 \frac{\alpha_r}{\alpha_K} \ll 1. \tag{3.55}$$

Then, using the relation valid of an ellipse $r = a(1 - e \cos u)$, where u is the eccentric anomaly, we make the perturbative arrangement $\mathcal{K} = K_0 + K_1$, with

$$K_0 = -\frac{\mu}{2a} = -\frac{1}{2}n^2a^2, \qquad K_1 = \beta K_0(1 - e \cos u).$$

The eccentric anomaly can be written in terms of the mean anomaly M using standard expansions of the elliptic motion (BROUWER; CLEMENCE, 1961). In the case of low eccentric orbits, terms of the order of e^4 and higher can be neglected, yielding

$$K_1 = \beta K_0 \left[1 + \frac{1}{2}e^2 - \left(1 - \frac{3}{8}e^2 \right) e \cos M - \frac{1}{2}e^2 \cos 2M - \frac{3}{8}e^3 \cos 3M \right] \qquad (3.56)$$

Up to the first order of β, a perturbation solution (NAYFEH, 2004) is obtained by a change of variables $(M, \omega, a, e) \to (M', \omega', a', e')$ given by

$$M = M' + \beta'\delta M, \quad \omega = \omega' + \beta'\delta\omega, \quad a = a' + \beta'\delta a, \quad e = e' + \beta'\delta e, \qquad (3.57)$$

with $\beta' = 2\alpha_r/(n'^2 a')$, $n' = \sqrt{\mu/a'^3}$,

$$\delta M = \left(\frac{1}{2e} + \frac{23}{16}e - \frac{3}{8}e^3 \right) \sin M + \frac{1}{8}(2 + 3e^2) \sin 2M \qquad (3.58)$$
$$+ \frac{1}{16}e(3 + 2e^2) \sin 3M,$$
$$\delta\omega = -\left(\frac{1}{2e} - \frac{13}{16}e + \frac{7}{32}e^3 \right) \sin M - \frac{1}{8}(2 - e^2) \sin 2M \qquad (3.59)$$
$$- \frac{3}{32}e(2 - e^2) \sin 3M,$$
$$\delta a = -a \left[\left(1 - \frac{3}{8}e^2 \right) e \cos M + \frac{1}{2}e^2 \cos 2M + \frac{3}{8}e^3 \cos 3M \right], \qquad (3.60)$$
$$\delta e = -\frac{1}{16}(8 - 11e^2) \cos M - \frac{1}{4}(1 - e^2)e \cos 2M - \frac{3}{16}e^2 \cos 3M, \qquad (3.61)$$

where the right members must be evaluated in prime variables, e', a', n' and, therefore, β' are constant, and

$$M' = M'_0 + n' \left(1 - \frac{3}{2}\beta' \right) t, \qquad \omega' = \omega'_0 + \frac{1}{4}\beta'n'(2 - e'^2)t. \qquad (3.62)$$

Without loose of generality, we assume $M'_0 = M'(0) = 0$. Hence,

$$t = \frac{M'}{n'(1 - \frac{3}{2}\beta')}, \qquad (3.63)$$

and

$$\omega' = \omega_0' + \frac{1}{4}\beta'\ (2 - e'^2)M' + \mathcal{O}(\beta'^2). \tag{3.64}$$

The inverse transformation $(M', \omega', a', e') \to (M, \omega, a, e)$ is

$$M' = M - \beta\,\delta M, \quad \omega' = \omega - \beta\delta\omega, \quad a' = a - \beta\delta a, \quad e' = e - \beta\delta e, \tag{3.65}$$

where Eqs. (3.58)–(3.61) are used again, but now with the right sides in original variables.

Note that Eqs. (3.58) and (3.59) are singular for circular orbits. If needed, the perturbation solution can be reformulated in non-singular variables (DEPRIT; ROM, 1970; LARA, 2008).

3.4.4.1 Acceleration

The acceleration given in Eq. (3.30) can be written using

$$\frac{\mu}{r^2} = \frac{\mu}{a^2}\left[1 + \frac{1}{2}e^2 + (2 + \frac{3}{4}e^2)e\cos M + \frac{5}{2}e^2\cos 2M + \frac{13}{4}e^3\cos 3M\right], \tag{3.66}$$

and the components of the unit vector $\hat{\vec{r}}$, which are expressed in orbital elements as

$$\begin{aligned} \cos\theta &= -\frac{1}{12}e^3\cos(\omega - 2M) - \frac{1}{8}e^2\cos(\omega - M) - e\cos\omega \\ &\quad +(1 - e^2)\cos(\omega + M) + (e - \frac{5}{4}e^3)\cos(\omega + 2M) \\ &\quad +\frac{9}{8}e^2\cos(\omega + 3M) + \frac{4}{3}e^3\cos(\omega + 4M)\ , \end{aligned} \tag{3.67}$$

$$\begin{aligned} \sin\theta &= -\frac{1}{12}e^3\sin(\omega - 2M) - \frac{1}{8}e^2\sin(\omega - M) - e\sin\omega \\ &\quad +(1 - e^2)\sin(\omega + M) + (e - \frac{5}{4}e^3)\sin(\omega + 2M) \\ &\quad +\frac{9}{8}e^2\sin(\omega + 3M) + \frac{4}{3}e^3\sin(\omega + 4M)\ . \end{aligned} \tag{3.68}$$

In order to compute the indices based on this solution, the acceleration must be expressed as an explicit function of time. That is, first, the original variables must be replaced by the prime ones, as given by Eq. (3.57). Then, the integrand is expanded in power series of β' and terms of $\mathcal{O}(\beta'^2)$ are neglected, which is consistent with our perturbation assumption that β is small. Finally, Eq. (3.62) can be used to show the

explicit time dependence, which will allow to solve the quadrature analytically.

3.4.4.2 Range of validity of the perturbation solution

The validity of the perturbation solution could be stated by a direct comparison with a Taylor series expansion of the exact solution. However, in view of the fact that the exact solution depends on special functions and, besides that, it is given in implicit forms, these kinds of expansions can be rather unwieldy (LARA; FERRER, 2015a) (see also the expanded version in (LARA; FERRER, 2015b)).

Alternatively, the range of the variables where the solution obtained is valid can be investigated by comparing the analytical solution with a numerical integration of the equations of motion. This is the approach taken here where the numerical solution has been integrated with a Runge-Kutta method, and the comparisons have been made as follows. An analytical solution $r_A(M')$ is obtained by isolating r in Eq. (3.66), after the proper indicated transformation of variables to the prime ones. The analytical solutions $\cos\theta_A(M')$ and $\sin\theta_A(M')$ can be obtained in a similar way using Eqs. (3.67) and (3.68), where θ represents the angle between the vector pointing from the origin of the frame of reference to the spacecraft and the x axis. The analytical solution $\theta_A(M')$ can be obtained using the trigonometric inverse of the solutions $\cos\theta_A(M')$ and $\sin\theta_A(M')$. Finally, using the transformation from M' to t given in Eq. (3.62), the complete vector solution $\vec{r}_A(t)$ can be found.

The analytical solutions $r_A(M')$, $\cos\theta_A(M')$ and $\sin\theta_A(M')$ obtained using Eqs. (3.66) - (3.68) contain singularities in the case where e is too small. These singularities are expected and they come from the term $1/e$ present in Eqs. (3.58) and (3.59). As mentioned before, nonsingular variables such as, for instance, $F = M + \omega$, $C = e\cos\omega$, and $S = e\sin\omega$ could be used to avoid singularities. On the other hand, the following alternative approach is made. The solutions obtained $r_A(M')$, $\cos\theta_A(M')$, and $\sin\theta_A(M')$ are now written in Taylor series for the variable β' around zero. Terms with second or higher orders in β' are neglected. This result is written in Taylor series once again, but now for the variable e' and terms with fourth or higher order in e' are disregarded. The analytical solution neglects $\mathcal{O}(\beta^2)$; on the other hand, the expansions used neglect $\mathcal{O}(e^4)$. So, in order to be consistent, we must assume that $\mathcal{O}(\beta^2) \sim \mathcal{O}(e^4)$. That is, crossed terms of the order of βe^2 and βe^3 are also neglected from the analytical solution. The result of these approximations are the new solutions $\cos\theta_B$, $\sin\theta_B$, and r_B. These new solutions do not contain

singularities and they are given by

$$r_{\rm B} = a' \left\{ 1 + \frac{\beta'}{2} + e' \left[-\frac{3}{4}\beta' \cos\left(M'\right) - \cos\left(M'\right) \right] + \right. \tag{3.69}$$

$$\left. (e')^2 \left[\sin^2\left(M'\right) \right] + (e')^3 \left[\frac{3}{2}\sin^2\left(M'\right)\cos\left(M'\right) \right] \right\},$$

$$\cos\theta_B = \cos\left(M' + \omega'\right) + \tag{3.70}$$

$$e' \left[-\frac{1}{2}3\beta' \sin\left(M'\right)\sin\left(M' + \omega'\right) - 2\sin\left(M'\right)\sin\left(M' + \omega'\right) \right] -$$

$$(e')^2 \left[\frac{1}{4}\sin\left(M'\right)\left(9\sin\left(2M' + \omega'\right) + \sin\left(\omega'\right)\right) \right] -$$

$$(e')^3 \left[\frac{1}{6}\sin\left(M'\right)\left(-\sin\left(M' - \omega'\right) + \sin\left(M' + \omega'\right) + 16\sin\left(3M' + \omega'\right)\right) \right],$$

$$\sin\theta_B = \sin\left(M' + \omega'\right) + \tag{3.71}$$

$$e' \left[\frac{3}{2}\beta' \sin\left(M'\right)\cos\left(M' + \omega'\right) + 2\sin\left(M'\right)\cos\left(M' + \omega'\right) \right] +$$

$$(e')^2 \left[\frac{1}{4}\sin\left(M'\right)\left(9\cos\left(2M' + \omega'\right) + \cos\left(\omega'\right)\right) \right] +$$

$$(e')^3 \left[\frac{1}{6}\sin\left(M'\right)\left(\cos\left(M' - \omega'\right) + \cos\left(M' + \omega'\right) + 16\cos\left(3M' + \omega'\right)\right) \right],$$

where $M' = n'\left(1 - \frac{3}{2}\beta'\right)t$ and $\omega' = \omega_0' + \frac{1}{2}\beta'n't$.

The Keplerian solution is exact, but it involves the solution of the Kepler equation. On the other hand, for low eccentricity orbits, a time explicit approximation can be obtained by making $\beta' = 0$ in Eqs. (3.69)–(3.71). That is

$$r_{\rm K} = a\left(\frac{3}{2}e^3\sin^2(nt)\cos(nt) + e^2\sin^2(nt) - e\cos(nt) + 1 \right), \tag{3.72}$$

$$\cos\theta_{\rm K} = -2e\sin(nt)\sin\left(nt + \omega_0\right) + \cos\left(nt + \omega_0\right) - \tag{3.73}$$

$$\frac{e^2}{4}\sin(nt)\left[9\sin\left(2nt + \omega_0\right) + \sin\left(\omega_0\right)\right] -$$

$$\frac{e^3}{6}\sin(nt)\left[\sin\left(nt + \omega_0\right) + 16\sin\left(3nt + \omega_0\right) - \sin\left(nt - \omega_0\right)\right],$$

$$\sin\theta_{\rm K} = 2e\sin(nt)\cos\left(nt + \omega_0\right) + \sin\left(nt + \omega_0\right) + \tag{3.74}$$

$$\frac{e^2}{4}\sin(nt)\left[9\cos\left(2nt + \omega_0\right) + \cos\left(\omega_0\right)\right] +$$

$$\frac{e^3}{6}\sin(nt)\left[\cos\left(nt - \omega_0\right) + \cos\left(nt + \omega_0\right) + 16\cos\left(3nt + \omega_0\right)\right].$$

Two new functions Δr and $\Delta \theta$ are defined as

$$\Delta r(t) \quad = \quad \|\vec{r}_N(t) - \vec{r}(t)\|, \tag{3.75}$$

$$\Delta \theta(t) \quad = \quad |\theta_N(t) - \theta(t)|, \tag{3.76}$$

where $\theta_N(t)$ and $\vec{r}_N(t)$ are the numerical solutions for the angle and the position vector, respectively, and $\vec{r}(t)$ and $\theta(t)$ are given by the "A" or "B" analytical solutions. Two more new functions $\max(\Delta r)$ and $\max(\Delta \theta)$ are defined as the maximum absolute value that the functions $\Delta r(t)$ and $\Delta \theta(t)$ reach during the interval of time from 0 to T, where $T = 2\pi/n$. In the case where the "A" analytical solution is used for $\vec{r}(t)$ and $\theta(t)$, the maximum absolute value that the functions $\Delta r(t)$ and $\Delta \theta(t)$ reach are called $\max_A(\Delta r)$ and $\max_A(\Delta \theta)$ and in the case where the "B" analytical solution is used, they are called $\max_B(\Delta r)$ and $\max_B(\Delta \theta)$.

Two new parameters k and r_0 are defined such that they express the magnitude of the perturbation as

$$\alpha_r = k \frac{\mu}{r_0^2}. \tag{3.77}$$

Note that, in the case where r_0 is the initial value of the orbit semi major axis, according Eq. (3.55), $\beta = 2k$.

The length and time units can be defined such that the initial value of the semi-major axis and the gravitational parameter are both units ($a = 1$ and $\mu = 1$). The initial conditions are $r_0 = a$; $\omega(0) = 0$; and $M(0) = 0$. In this case, the evaluation of $\max_A(\Delta r)$ and $\max_B(\Delta r)$ are shown in Fig. 3.3 for a range of the initial eccentricity in the case where the parameter k is set to $k = 0.01$ and in Fig. 3.4 for a range of the parameter k in the case where the initial eccentricity is $e = 0.1$. In a similar way, the evaluation of $\max_A(\Delta \theta)$ and $\max_B(\Delta \theta)$ are shown in Fig. 3.5 for a range of initial eccentricities in the case where the parameter k is set to $k = 0.01$ and in Fig. 3.6 for a range of the parameter k in the case where the initial eccentricity is $e = 0.1$. Both figures (a) and (b) can be compared. Note that the method of the elimination of the singular term through the Taylor expansion could improve the precision of the solution for a considerable range of the eccentricity, which is $0 < e < 0.2$. Figures 3.7 - 3.10 allow us to quantify the dependence of the functions $\max_A(\Delta r)$, $\max_B(\Delta r)$, $\max_A(\Delta \theta)$, and $\max_B(\Delta \theta)$ with both the initial eccentricity and the parameter k. The results shown in these figures for the non-singular case measure the expected behavior that the perturbation increase with both the eccentricity

and with the parameter k. Two different evolutions are observed depending on the values of k. For higher values (above 0.015) there is a nearly linear increase with both parameters eccentricity and k. Below this limit, there is a critical value for the eccentricity where the parameter k dominates the scenario and the impulse has little dependency with the eccentricity. It is visible from the plots, by noting that the border lines between two colors are nearly horizontal. Above this critical value the situation is the opposite, the eccentricity has more effects compared to the parameter k and the border lines between two adjacent colors are nearly vertical. This transition of the evolutions generates the corners in the lines below $k = 0.015$. The range of validity of the eccentricity for this solution can be set to $0 < e < 0.2$. In the solutions for r_B and θ_B, terms of order 4 and higher orders of e' are disregarded, as well as terms with order 2 and higher orders of β'. Neglecting terms of order 4 in the eccentricity means that terms with magnitude larger then $(0.2)^4$ are neglected. Due to the disregarding of terms or order 2 or more in β', the range of validity in this parameter is set to $\beta < 0.04$. Note that $\beta \approx 2k$, which means $k < 0.02$. The nonsingular expanded solution given by Eqs. (3.69)-(3.71) is the best choice. It avoids the unexpected behavior of $\max_A(\Delta r)$ in the range $0 < e < 0.1$, where $\max_A(\Delta r)$ decreases with the eccentricity. This is due to the singularity. Figures 3.3 and 3.4 show the real behavior. Figures 3.5 and 3.6 show the same behavior for the variation in θ, with the same unexpected pattern from $0 < e < 0.1$ when using singular elements. Figures 3.7 - 3.10 study the effects of k and the eccentricity of the orbit. The necessity of using non-singular variables is very clear. Figures 3.8 and 3.10 show the expected behavior of increasing the perturbations with k and with the eccentricity of the orbit. Besides confirming the expected behavior, this figure quantifies the effects in an objective and clear form. This is also important in this problem.

Figure 3.3 - $\max_A(\Delta r)$ and $\max_B(\Delta r)$ as function of e. Maximum values reached by Δr in the interval of time from 0 to $T = 2\pi\sqrt{a_0^3/\mu}$ evaluated for the "A" singular solution given by Eqs. (3.66)-(3.68) in blue and for the "B" non singular solution given by Eqs. (3.69)-(3.71) in red. The units, variables, parameters and initial conditions are such that $r_0 = a = 1$, $\mu = 1$, $\omega(0) = 0$, $M(0) = 0$, and $k = 0.01$
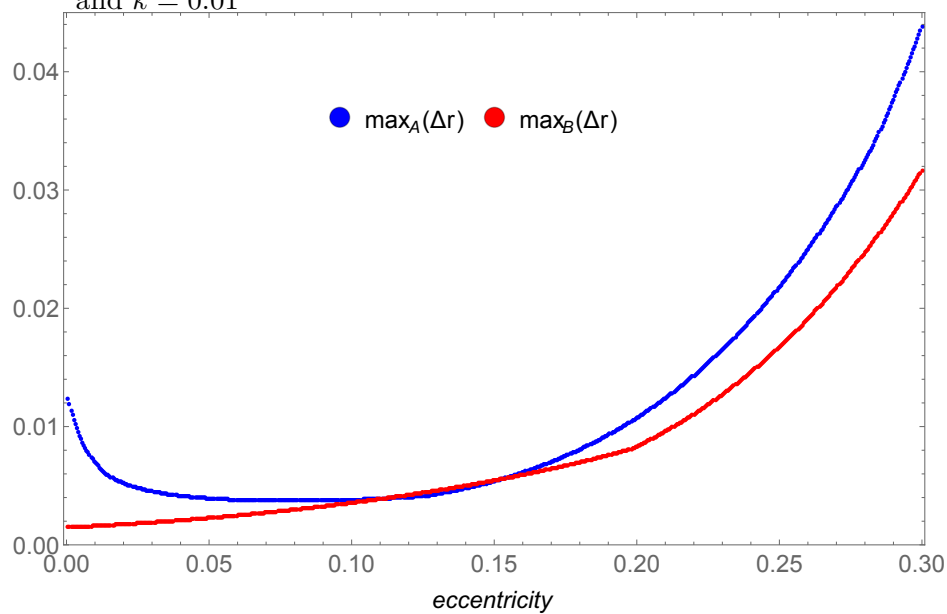
SOURCE: Author's production.

Figure 3.4 - $\max_A(\Delta r)$ and $\max_B(\Delta r)$ as function of k. Maximum values reached by Δr in the interval of time from 0 to $T = 2\pi\sqrt{a_0^3/\mu}$ evaluated for the "A" singular solution given by Eqs. (3.66)-(3.68) in blue and for the "B" non singular solution given by Eqs. (3.69)-(3.71) in red. The units, variables, parameters and initial conditions are such that $r_0 = a = 1$, $\mu = 1$, $\omega(0) = 0$, $M(0) = 0$, and $e = 0.1$.
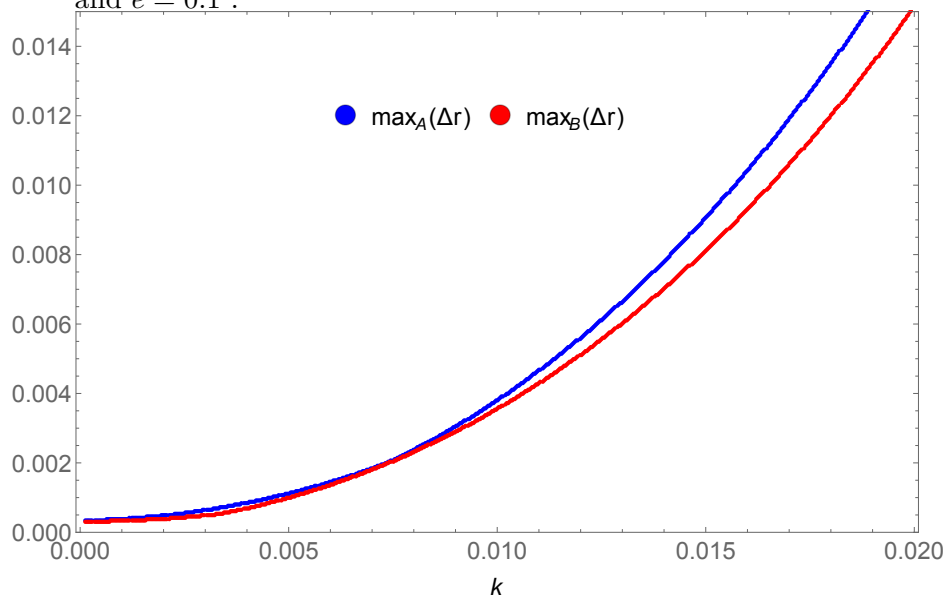
SOURCE: Author's production.

Figure 3.5 - Maximum values reached by $\Delta\theta$ in the interval of time from 0 to $T = 2\pi\sqrt{a_0^3/\mu}$ evaluated for the "A" singular solution given by Eqs. (3.66)-(3.68) in blue and for the "B" nonsingular solution given by Eqs. (3.69)-(3.71) in red. The units, variables, parameters and initial conditions are such that $r_0 = a = 1$, $\mu = 1$, $\omega(0) = 0$, $M(0) = 0$, and $k = 0.01$.
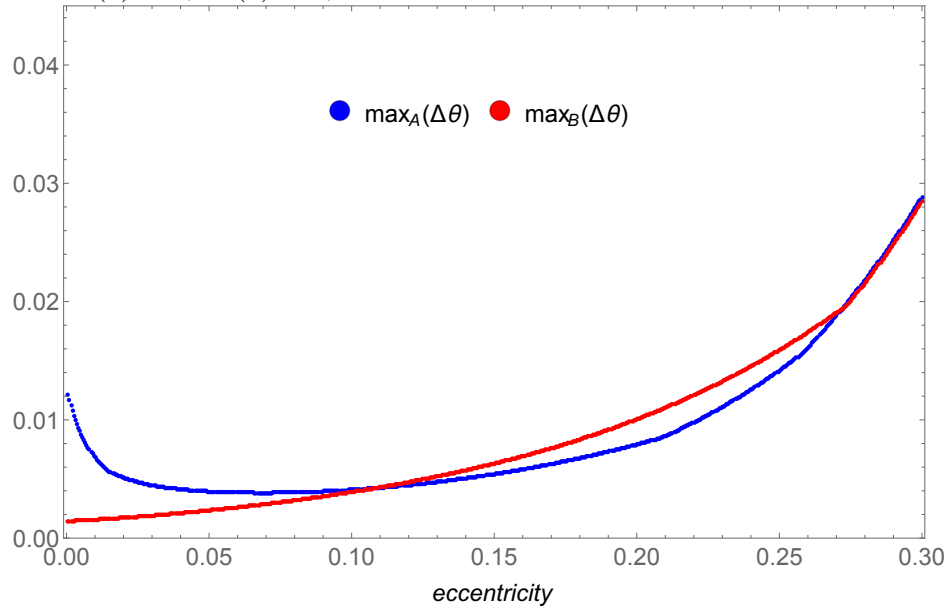
SOURCE: Author's production.

Figure 3.6 - Maximum values reached by $\Delta\theta$ in the interval of time from 0 to $T = 2\pi\sqrt{a_0^3/\mu}$ evaluated for the "A" singular solution given by Eqs. (3.66)-(3.68) in blue and for the "B" nonsingular solution given by Eqs. (3.69)-(3.71) in red. The units, variables, parameters and initial conditions are such that $r_0 = a = 1$, $\mu = 1$, $\omega(0) = 0$, $M(0) = 0$, and $e = 0.1$.
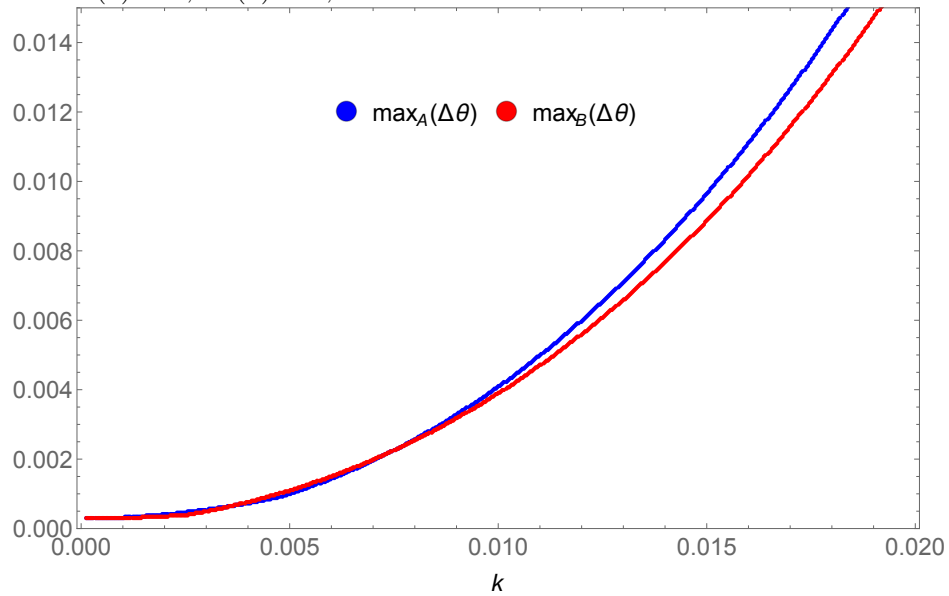
SOURCE: Author's production.

Figure 3.7 - singular solution given by Eqs. (3.66)-(3.68). Maximum values reached by Δr in the interval of time from 0 to $T = 2\pi\sqrt{a_0^3/\mu}$ evaluated for the "A" solution given by Eqs. (3.66)-(3.68). The units, variables, parameters and initial conditions are such that $r_0 = a = 1$, $\mu = 1$, $\omega(0) = 0$, and $M(0) = 0$.
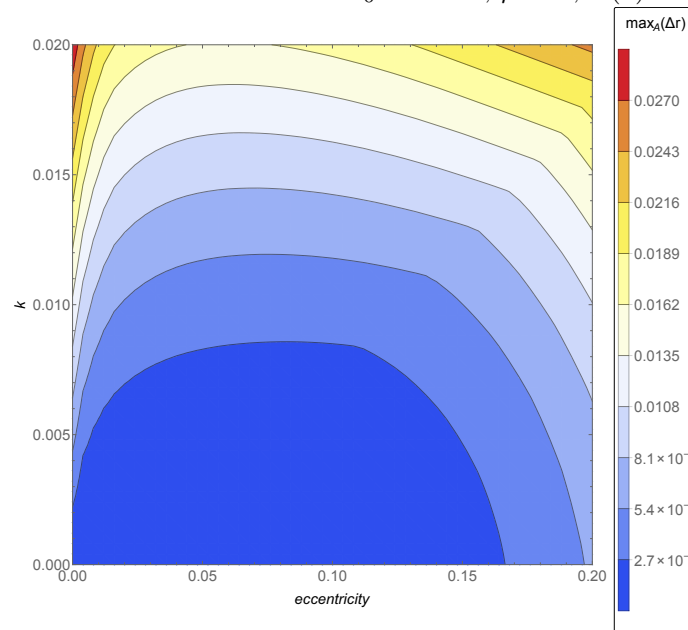
SOURCE: Author's production.

Figure 3.8 - nonsingular solution given by Eqs. (3.69)-(3.71). Maximum values reached by Δr in the interval of time from 0 to $T = 2\pi\sqrt{a_0^3/\mu}$ evaluated for the "B" solution given by Eqs. (3.69)-(3.71). The units, variables, parameters and initial conditions are such that $r_0 = a = 1$, $\mu = 1$, $\omega(0) = 0$, and $M(0) = 0$.
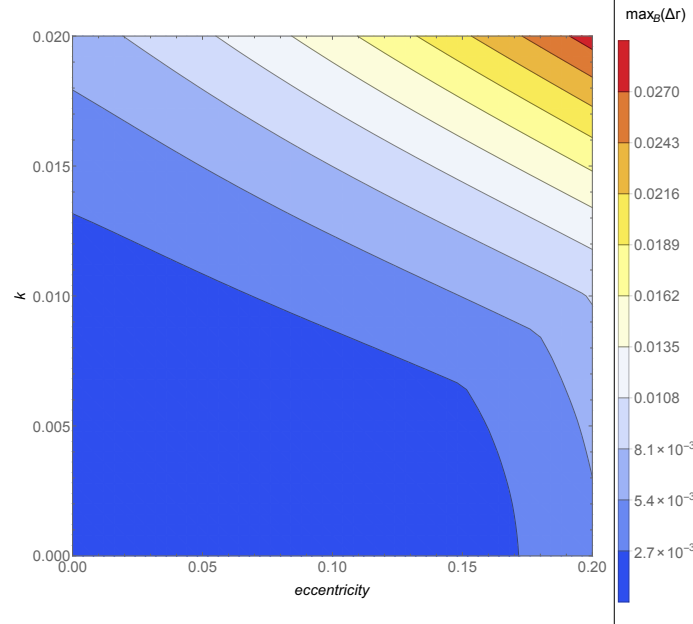
Figure 3.9 - singular solution given by Eqs. (3.66)-(3.68). Maximum values reached by $\Delta\theta$ in the interval of time from 0 to $T = 2\pi\sqrt{a_0^3/\mu}$ evaluated for the "A" solution given by Eqs. (3.66)-(3.68). The units, variables, parameters and initial conditions are such that $r_0 = a = 1$, $\mu = 1$, $\omega(0) = 0$, and $M(0) = 0$.
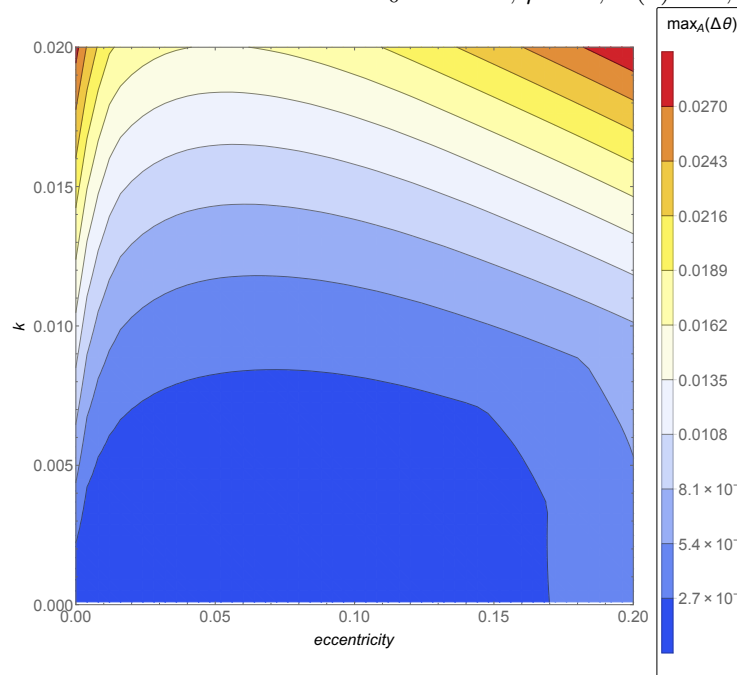
SOURCE: Author's production.

Figure 3.10 - nonsingular solution given by Eqs. (3.69)-(3.71). Maximum values reached by $\Delta\theta$ in the interval of time from 0 to $T = 2\pi\sqrt{a_0^3/\mu}$ evaluated for the "B" solution given by Eqs. (3.69)-(3.71). The units, variables, parameters and initial conditions are such that $r_0 = a = 1$, $\mu = 1$, $\omega(0) = 0$, and $M(0) = 0$.
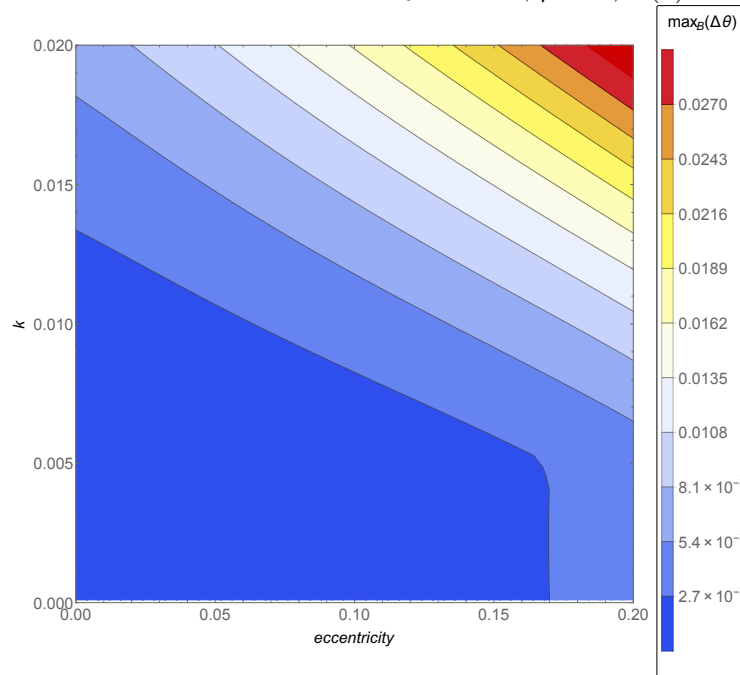
3.5 Results to the perturbation solution

In this section, different indices are defined and calculated based on the solutions obtained in the section 3.4.4, with the goal of finding the most adequate ones to select orbits that are less disturbed. The reason why the perturbation solution is chosen in detriment of the Tsien or Quarta and Mengali solutions, or even in detriment of the one developed in subsection 3.4.2 is that perturbation solutions can also be obtained in cases where other astrodynamics systems are used.

3.5.1 Solution for $\vec{J}$

The specific impulse $\vec{J}$ will be the first index studied. Using Eq. (3.30), the impulse per unit of mass is formulated as

$$\vec{J} = \int_{t_1}^{t_2} \left(-\frac{\mu}{r^2} + \alpha_r \right) \hat{\vec{r}} \mathrm{d}t. \tag{3.78}$$

The solutions given by Eqs. (3.66)-(3.68) are used into Eq. (3.78). The proper changes of variables are made in order to turn all variables to the prime ones. Thus, an expansion in Taylor series with terms up to the first order in β' is made in the integrand. Another expansion in Taylor series keeping terms up to the third order in e' is also made in the integrand. The quadrature is analytically evaluated. In the case where $\omega_0 = 0$, the solutions for J_i and J_j are given by

$$
\begin{aligned}
J_i \;=\; a'n' \Bigg\{ & \frac{1}{2} \left(\beta' - 2 \right) \sin\left(\frac{1}{2} \left(\beta' + 2 \right) M' \right) + e' \left(-\frac{\beta'}{2} - 1 \right) \sin\left(\frac{1}{2} \left(\beta' + 4 \right) M' \right) + \\
& (e')^2 \left[-\frac{1}{8} \sin\left(M' - \frac{\beta' M'}{2} \right) + \frac{1}{2} \sin\left(\frac{1}{2} \left(\beta' + 2 \right) M' \right) - \frac{9}{8} \sin\left(\frac{1}{2} \left(\beta' + 6 \right) M' \right) \right] + \\
& (e')^3 \left[-\frac{17}{32} \sin\left(\frac{\beta' M'}{2} \right) + \frac{1}{12} \sin\left(\frac{1}{2} \left(\beta' - 4 \right) M' \right) + \frac{3}{4} \sin\left(\frac{1}{2} \left(\beta' + 4 \right) M' \right) - \\
& \frac{4}{3} \sin\left(\frac{1}{2} \left(\beta' + 8 \right) M' \right) \right] \Bigg\} \Bigg|_{M'(t_1)}^{M'(t_2)},
\end{aligned}
\tag{3.79}
$$

$$
\begin{aligned}
J_j \;=\; a'n'\Bigg\{ & \left(1-\frac{\beta'}{2}\right)\cos\left(\frac{1}{2}\left(\beta'+2\right)M'\right) + e'\frac{1}{2}\left(\beta'+2\right)\cos\left(\frac{1}{2}\left(\beta'+4\right)M'\right) + \quad (3.80) \\
& (e')^2\left[-\frac{1}{8}\cos\left(M'-\frac{\beta'M'}{2}\right) - \frac{1}{2}\cos\left(\frac{1}{2}\left(\beta'+2\right)M'\right) + \frac{9}{8}\cos\left(\frac{1}{2}\left(\beta'+6\right)M'\right)\right] + \\
& (e')^3\left[\frac{17}{32}\cos\left(\frac{\beta'M'}{2}\right) - \frac{1}{12}\cos\left(\frac{1}{2}\left(\beta'-4\right)M'\right) - \frac{3}{4}\cos\left(\frac{1}{2}\left(\beta'+4\right)M'\right) + \right. \\
& \left.\left. \frac{4}{3}\cos\left(\frac{1}{2}\left(\beta'+8\right)M'\right)\right]\right\}\Bigg|_{M'(t_1)}^{M'(t_2)},
\end{aligned}
$$

where the relation between M' and t is shown in Eq. (3.62).

The length and time units can be defined such that the initial value of the semi-major axis and the gravitational parameter are both units ($a = 1$ and $\mu = 1$). The initial conditions are $e = 0.1$; $\omega(0) = 0$; and $M(0) = 0$ and the parameters relative to the perturbation are set to $k = 0.01$ and $r_0 = 1$. The index $\vec{J}$ is evaluated between two times, which we can call $t_1 = 0$ and $t_2 = t$. The values of the components J_i and J_j of $\vec{J}$ and the absolute value J of $\vec{J}$ as functions of t are shown in Figs. 3.11 and 3.12, for different ranges of t. Note from these figures that neither $\vec{J}$ or its absolute value may be good indices to be related with the perturbation, because their values are oscillatory over time and the net effect of the perturbation over these values is not cumulative, quite on contrary, these effects are canceled in time and the choice of t_2 to evaluate these indices is arbitrary in this sense.

Figure 3.11 - The components J_i (in red) and J_j (in blue) of $\vec{J}$ and its absolute value J (in green) evaluated from $t_1 = 0$ to $t_2 = t$. The vertical black straight line represents $t = 2\pi$ (the period of the respective unperturbed system) and the horizontal black straight line is drawn to guide the eyes. The units, variables, parameters and initial conditions are such that $r_0 = a = 1$; $\mu = 1$; $\omega(0) = 0$; $M(0) = 0$; $k = 0.01$; and $e = 0.1$.
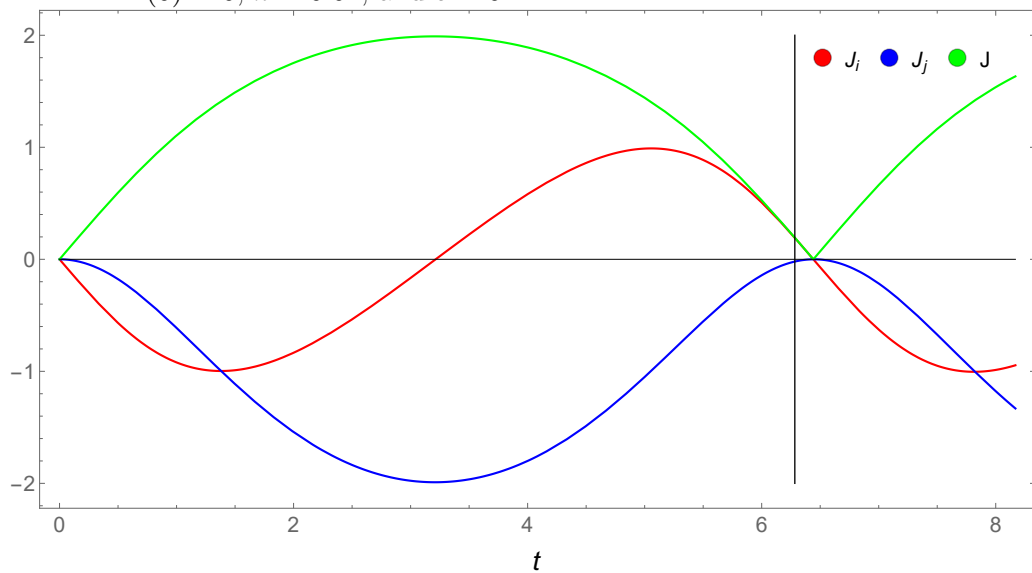
Figure 3.12 - The components J_i (in red) and J_j (in blue) of $\vec{J}$ and its absolute value J (in green) evaluated from $t_1 = 0$ to $t_2 = t$. The vertical black straight lines represent the values of t that are multiples of 2π (the period of the respective unperturbed system) and the horizontal black straight line is drawn to guide the eyes. The units, variables, parameters and initial conditions are such that $r_0 = a = 1$; $\mu = 1$; $\omega(0) = 0$; $M(0) = 0$; $k = 0.01$; and $e = 0.1$.
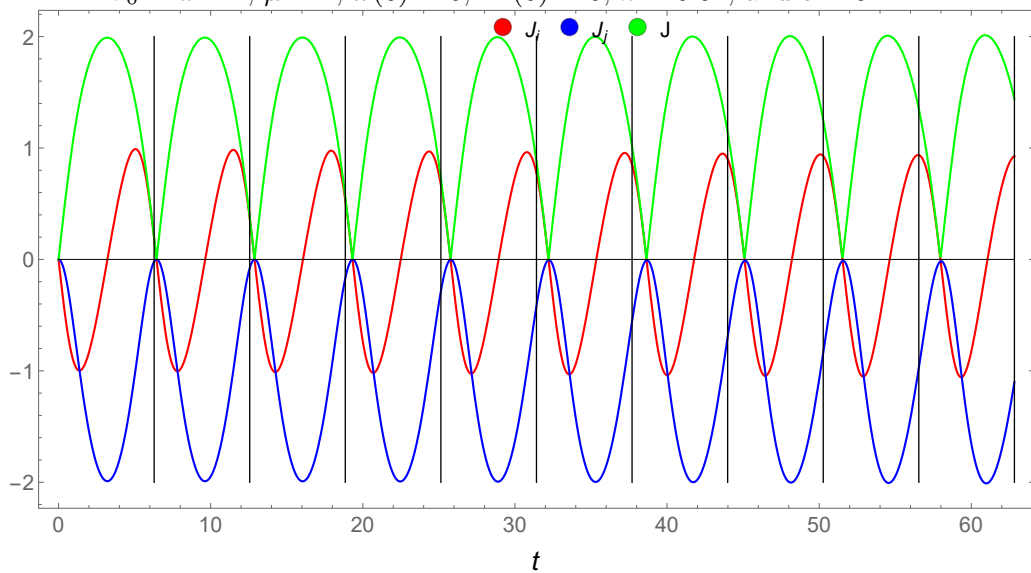
SOURCE: Author's production.

The results show that the impulse makes cycles, always returning to zero. So, the impulse disturbs the orbit and makes it to oscillate around the Keplerian one, but they return to the same point after one period of oscillation. Based in those results, a first conclusion is that the best way to measure the degree of the perturbation received by the spacecraft depends on the goal of the study:

a) In the case of integration times in the order of one orbital period, with small oscillations, it is important to consider the variations during this time. A better index could be the maximum value reached by the magnitude J or, even better, the integral of J with respect to time divided by the integration time. In that way, compensations of the perturbing effects are not computed. Allowing the compensations would give a zero result for the integral for an orbit that is really perturbed. So, for a study in this time range, $\vec{J}$ is not a good choice for an index.

b) In the case of longer times, these compensations should be allowed, or it will give integral indices that are too high. In the long range, indices that allow compensations like $\vec{J}$ are more appropriate.

3.5.2 Integral of the square of the absolute value of the acceleration

A new index J_s is defined as

$$J_s = \frac{1}{(t_2 - t_1)(\mu/a^2)^2} \int_{t_1}^{t_2} \|\ddot{\vec{r}}\|^2 \, dt = \frac{1}{(t_2 - t_1)(\mu/a^2)^2} \int_{t_1}^{t_2} \left\| \left(-\frac{\mu}{r^2} + \alpha_r \right) \hat{\vec{r}} \right\|^2 dt. \tag{3.81}$$

The idea of this index is to avoid compensations of negative and positive contributions to the integral, to create an index that is adequate for short periods of time, in the order of one orbital period. The factor $[(t_2 - t_1)(\mu/a^2)^2]^{-1}$ is used both to make J_s a non-dimensional index and to avoid some cumulative effects of the operations. Using the same procedure used to calculate $\vec{J}$, the solution of Eq. (3.81) is

$$J_s = \frac{(a')^2(n')^3}{(t_2 - t_1)(\mu/a^2)^2} \left\{ \left(1 - \frac{3\beta'}{2} \right) M' + e' \left[(4 - 3\beta') \sin(M') \right] + \right. \tag{3.82}$$

$$\left. (e')^2 \left[3M' + \frac{7}{2} \sin(2M') \right] + (e')^3 \left[\frac{17 \sin(M')}{2} + \frac{23}{6} \sin(3M') \right] \right\} \Bigg|_{M'(t_1)}^{M'(t_2)}.$$

The units of time and distance are defined such that $\mu = 1$ and an arbitrary $a_0 = 1$. The parameters are set to $k = 0.01$; $r_0 = 1$; $t_1 = 0$; and $t_2 = 2\pi\sqrt{a^3/\mu}$, which is the orbital period of the respective unperturbed system. The initial condition is $\omega(0) = 0$ and the initial values of the semi-major axis and the eccentricity are varied according to the range given in Fig. 3.13. In this figure, the evaluation of J_s is shown in the color scale, from blue to red. The same index J_s as a function of k is shown in Fig. 3.14 for the case where the initial eccentricity is fixed in $e = 0.1$, the semi-major axis is $a = 1$, $t_1 = 0$ and $t_2 = 2\pi\sqrt{a^3/\mu}$. The index J_s decreases as k increases for the fixed interval of integration. This happens due to the term α_r associated to the perturbation in the integrand of Eq. (3.81). It decreases the absolute value of the integrand. It happens because perturbation and gravity have opposite directions. This is a very weak point of this index that makes it not useful.

Figure 3.13 - J_s is integrated for different initial conditions of the eccentricity (e) and the semi-major axis (a) over the interval of time from $t_1 = 0$ to $t_2 = 2\pi\sqrt{a^3/\mu}$. The parameters with respect to the intensity of the perturbation are $k = 0.01$ and $r_0 = 1$ and the initial condition is such that $\omega(0) = 0$.
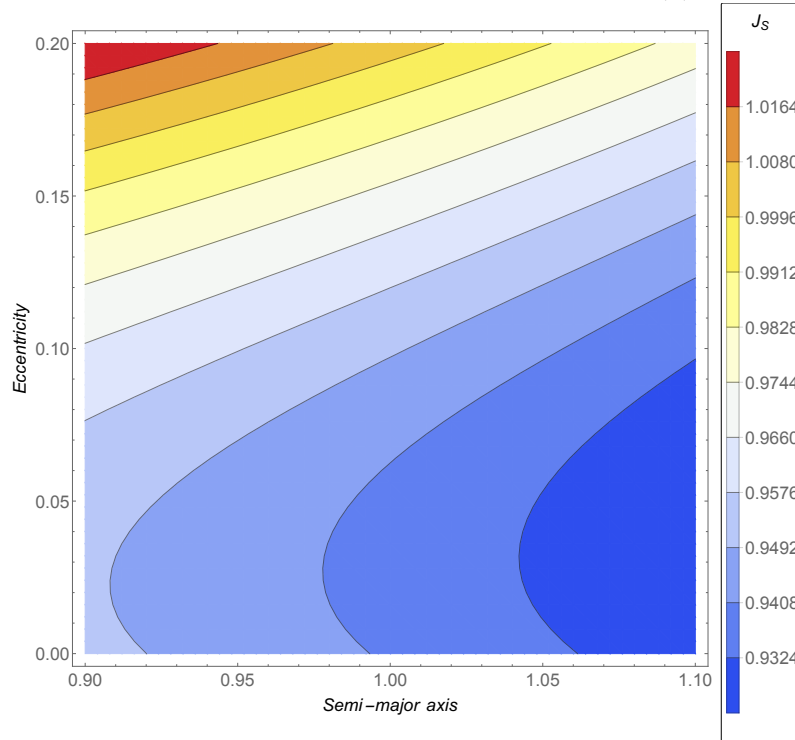
SOURCE: Author's production.

Figure 3.14 - J_s as a function of k evaluated in the interval of time integration from $t_1 = 0$ to $t_2 = 2\pi\sqrt{a^3/\mu}$. The initial conditions and the parameters are $\omega(0) = 0$, $e = 0.1$, $a = 1$, and $r_0 = 1$.
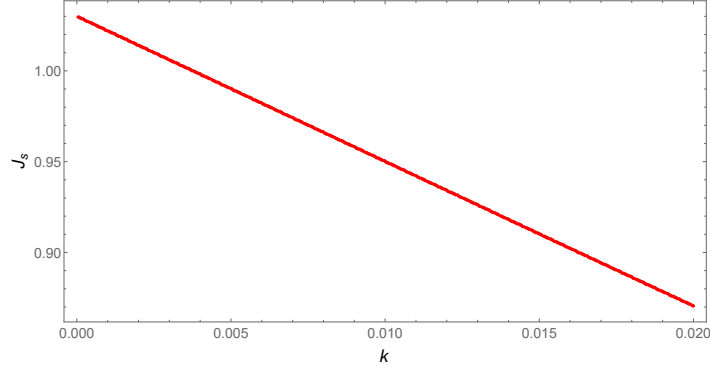
In order to obtain the results, the parameter r_0 was set to $r_0 = 1$. In the case where the parameter r_0 equals the initial value of the semi-major axis ($r_0 = a$), then the index J_s becomes totally independent of the initial value of the semi-major axis a.

3.5.3 Integral of the square of the absolute value of the difference of the accelerations

The differences between the perturbed and the Keplerian accelerations has been used in some variations of the PI index (PRADO, 2013), as attempts to identify more perturbed orbits (SANCHEZ, 2017). Thus, a new index J_a is defined here using the absolute value of the difference between the perturbed and the Keplerian accelerations vectors as

$$
\begin{aligned}
J_a &= \left((t_2 - t_1) \left(\frac{\mu}{a^2} \right)^2 \right)^{-1} \int_{t_1}^{t_2} \|\vec{a}_B - \vec{a}_K\|^2 \, \mathrm{d}t \qquad (3.83) \\
&= \frac{1}{(t_2 - t_1)(\mu/a^2)^2} \int_{t_1}^{t_2} \| \left(-\frac{\mu}{r_B^2} + \alpha_r \right) \hat{\vec{r}}_B - \left(-\frac{\mu}{r_K^2} \right) \hat{\vec{r}}_K \|^2 \, \mathrm{d}t,
\end{aligned}
$$

where a is the initial value of the semi-major axis, $\vec{r}_B$ is the position vector of the perturbed system given by Eqs. (3.69)-(3.71) and $\vec{r}_K$ is the position vector of the unperturbed (Keplerian) system given by Eqs. (3.72)-(3.74).

The idea is to take into account the perturbing acceleration and the indirect effects of disturbing the Keplerian orbit. The factor $[(t_2 - t_1)(\mu/a^2)^2]^{-1}$ is used both to make J_a a non-dimensional index and to avoid some cumulative effects of the operations

61

as to the integration time. The quadrature of Eq. (3.83) is numerically evaluated. The length and time units can be defined such that an arbitrary initial value of the semi-major axis and the gravitational parameter are both units ($a_0 = 1$ and $\mu = 1$). The initial condition is $\omega(0) = 0$ and the parameters relative to the perturbation are set to $k = 0.01$ and $r_0 = 1$. The integration is taken over the interval from $t_1 = 0$ and $t_2 = T$, where $T = 2\pi\sqrt{a^3/\mu}$ is the orbital period of the respective unperturbed system. In this case, the index J_a as a function of the initial conditions a and e is shown in Fig. 3.15. This index increases with the eccentricity and with the semi-major axis. This index is also shown in Fig. 3.16 as a function of k for the same conditions with $e = 0.1$.

Figure 3.15 - J_a calculated in the interval of time integration from $t_1 = 0$ to $t_2 = 2\pi\sqrt{a^3/\mu}$ as a function of the initial variables a and e. The parameters with respect to the intensity of the perturbation are $r_0 = 1$ and $k = 0.01$ and the initial condition is such that $\omega(0) = 0$.
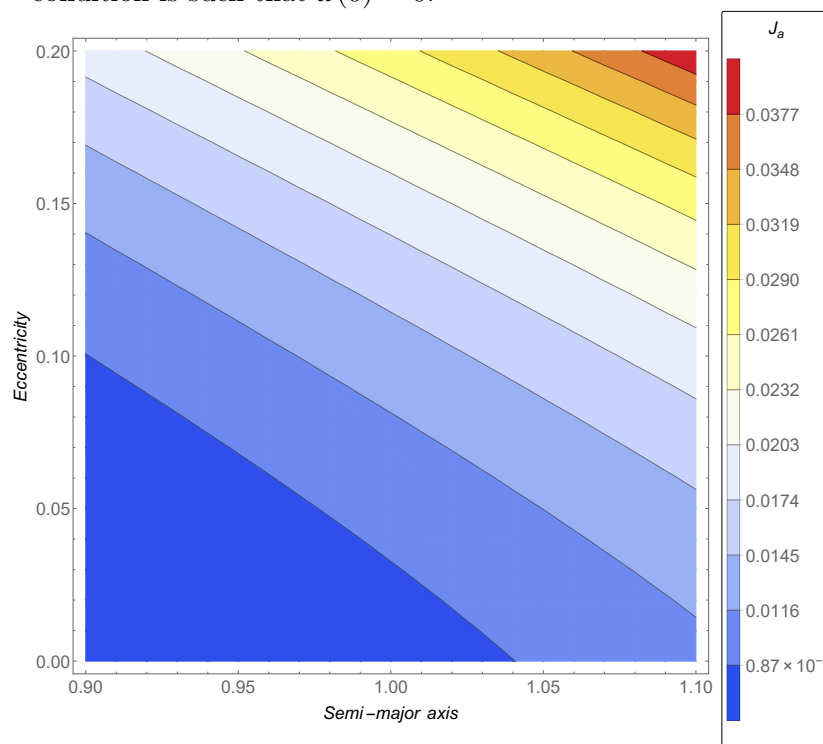
SOURCE: Author's production.

Figure 3.16 - J_a as a function of k evaluated in the interval of time integration from $t_1 = 0$ to $t_2 = 2\pi\sqrt{a^3/\mu}$. The initial conditions and the parameters are $\omega(0) = 0$; $e = 0.1$; $a = 1$; and $r_0 = 1$.
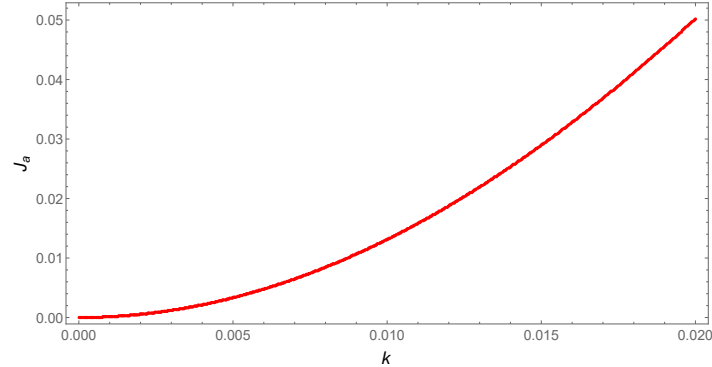
SOURCE: Author's production.

The integration is over the magnitude of the perturbation, so it does not allow compensations that reduces the perturbation level to zero or near zero in situations where the orbit is perturbed. It also addresses the problem of taking into account the perturbations coming from the gravity of the central body due to the fact that the orbit is not Keplerian. The results shown indicate that it is a good index, giving expected results. The index quantifies the increase with the eccentricity, as expected. It also quantifies an increase with the orbit semi-major axis, which is expected, because the gravity field of the central body decreases with the square of the distance, so the perturbation is proportionally higher. It also has an expected result as a function of k, with an increase of the index with k. The trajectories shown in Fig. 3.17 corroborate with the results obtained using the index J_a. It can be checked, from the plots of this figure, that the deviation from the Keplerian orbit is larger for trajectories with higher values for a, e, and k.

Figure 3.17 - Trajectories evolved for the interval of integration time from $t_1 = 0$ to $t_2 = 20T$. In the upper-left figure, the eccentricities are $e = 0.1$ and $e = 0.01$ for the black and red trajectories, respectively. In the upper-right figure, the semi-major axes are $a = 1.3$ and $a = 1$ for the black and red trajectories, respectively. In the down-left figure, the parameters k relative to the intensity of the perturbation are $k = 0.01$ and $k = 0.001$ for the black and red trajectories, respectively. In the down-right figure, the Keplerian orbit is shown ($k = 0$). The blue circle represents the initial position of the motion. The gray and red circles represent the final position of the black and red trajectories, respectively. The initial conditions and the parameters are $\omega(0) = 0$; $k = 0.01$; $e = 0.1$; $a = 1$; and $r_0 = 1$, except the modified parameter for the respective plot.
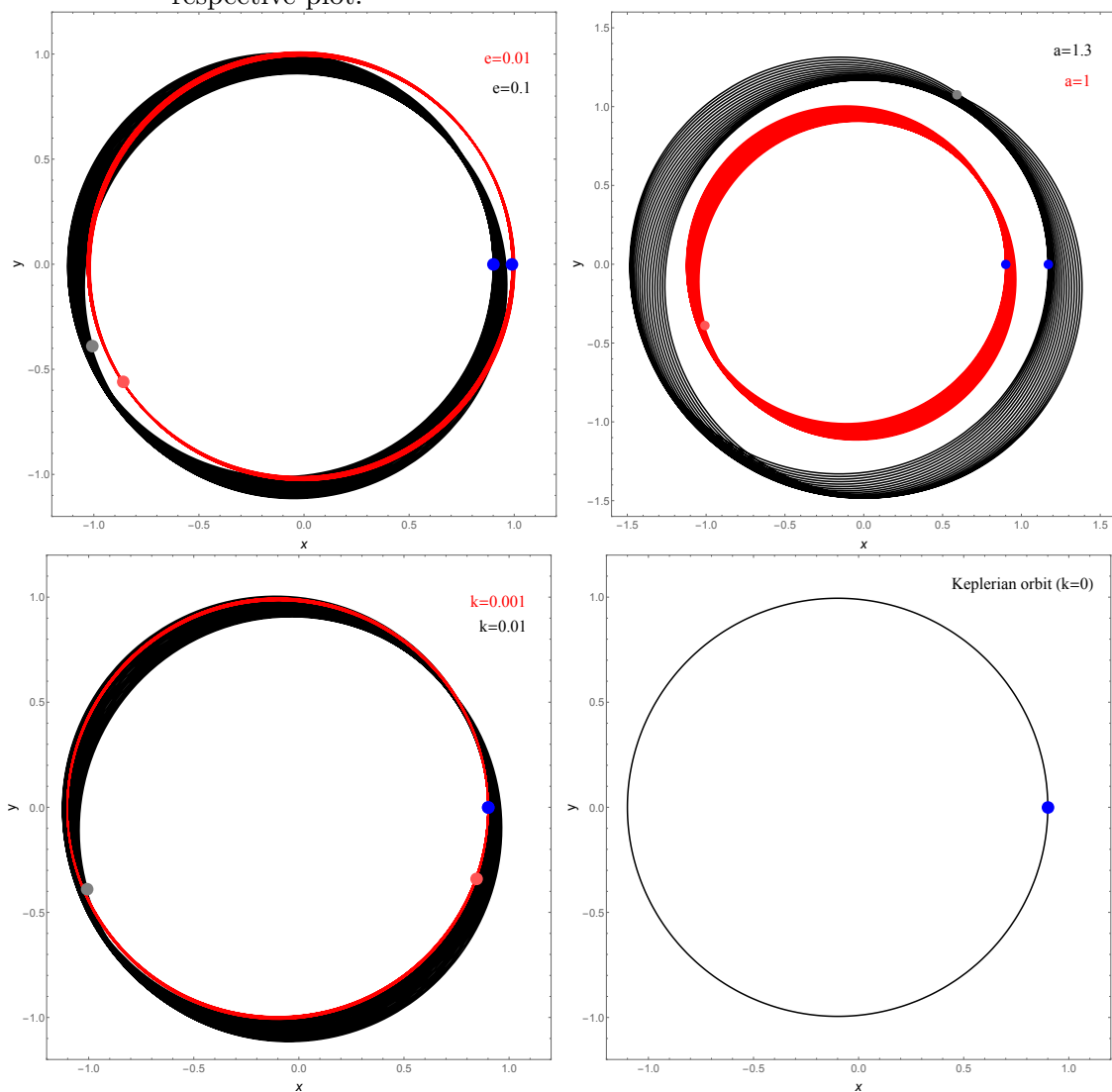
SOURCE: Author's production.

Now, a longer-term analysis is performed. The definition of the mean value of a function $f(t)$ in the interval $[t_1, t_2]$ is $\frac{1}{t_2-t_1} \int_{t_1}^{t_2} f(t)\, \mathrm{d}t$. The index J_a defined in Eq. (3.83) is the mean value of the function $\kappa \|\vec{a}_B - \vec{a}_K\|^2$, where $\kappa = (\mu/a^2)^{-2}$. An integration over small values of the interval time $[t_1, t_2]$ usually offers a good estimate for the value of the index J_a, which in turn can offer valuable information about the influence of the perturbation on the motion of the spacecraft placed in this orbit, due to the form of its definition. In the case where $e = 0.1$ and $k = 0.01$, the function $\kappa \|\vec{a}_B - \vec{a}_K\|^2$ of t is shown in Fig. 3.18 for the interval from $t = 0$ to $t = 250T$. In the case where $t_1 = 0$ and $t_2 = 250T$, the value of the index is $J_a = 1.30$. In the case where the integration is taken over the interval from $t_1 = 0$ to $t_2 = 2500T$, the value of the index is $J_a = 1.28$. Note that, in the case of the Tsien problem, the index J_a (or the mean value of $\kappa \|\vec{a}_B - \vec{a}_K\|^2$) slightly changes for high values of the interval $[t_1, t_2]$. Thus, a short numerical calculation is able to give a result that is an estimate of the behavior of the index J_a, which in turn can predict the influence of the perturbation on the motion of the spacecraft for longer times. This result shows that the perturbation has a constant mean effect over the perturbed motion relative to the keplerian orbit. The fact that this index does not change over large values of time means that the motion is bounded. Moreover, the fact that the mean value over time is constant also means that the perturbed orbit is approximately periodic around the Keplerian one. These conclusions can be checked through the trajectories of the perturbed orbit and the Keplerian one shown in Fig. 3.19 in red and blue, respectively. The argument of perihelion is changed over time, but the orbit is bounded.

Figure 3.18 - $\kappa\|\vec{a}_B - \vec{a}_K\|^2$ as a function of t for the interval $0 < t < 250T$. The initial conditions and the parameters are $\omega(0) = 0$; $e = 0.1$; $k = 0.01$, $a = 1$; and $r_0 = 1$. The horizontal blue line represents the value of $J_a = 1.30$, which is equivalent to the mean value of $\kappa\|\vec{a}_B - \vec{a}_K\|^2$.
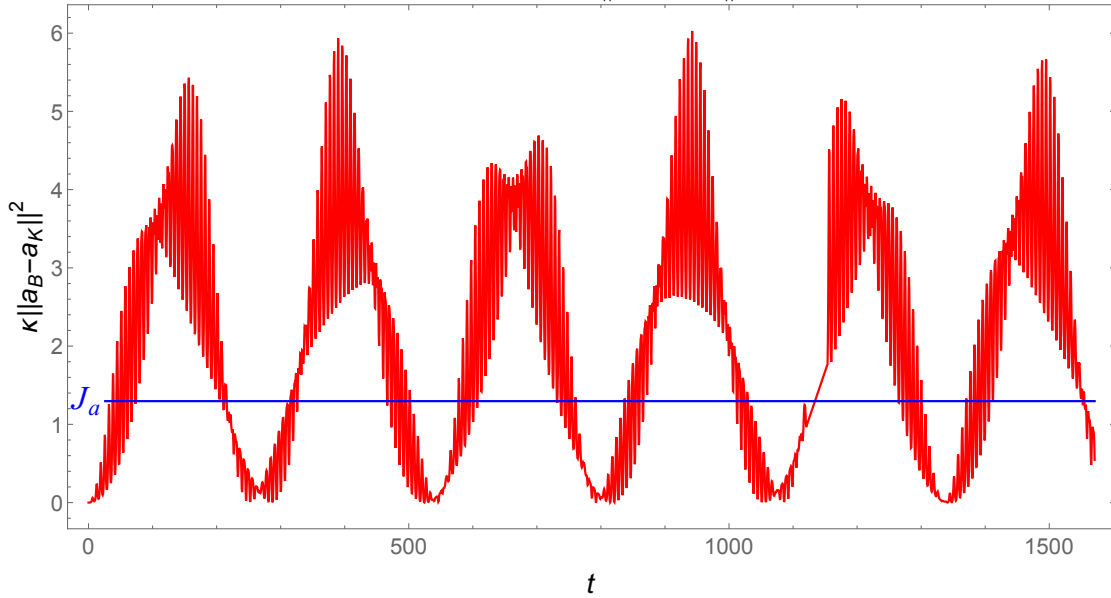
SOURCE: Author's production.

Figure 3.19 - The trajectory of the perturbed orbit is shown in red, evolved from $t_1 = 0$ to $t_2 = 250T$. The keplerian trajectory is shown in blue. The initial conditions and the parameters are $\omega(0) = 0$; $e = 0.1$; $k = 0.01$, $a = 1$; and $r_0 = 1$.
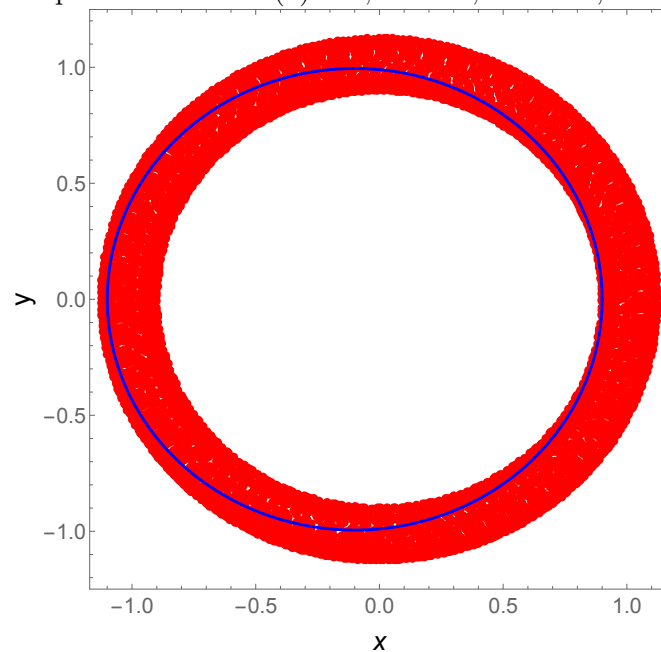
SOURCE: Author's production.

In order to obtain the results, the parameter r_0 was also set to $r_0 = 1$. In the case where the parameter r_0 equals the initial value of the semi-major axis ($r_0 = a$), then the index J_a becomes totally independent of the initial value of the semi-major axis a.

3.5.4 Integral of the square of the absolute value of the difference vector positions

A new index J_r is defined as

$$J_r = \frac{1}{(t_2 - t_1)a^2} \int_{t_1}^{t_2} \|\vec{r}_B - \vec{r}_K\|^2 \, \mathrm{d}t, \tag{3.84}$$

where a is the initial value of the semi-major axis, $\vec{r}_B$ is the position vector of the perturbed system given by Eqs. (3.69)-(3.71) and $\vec{r}_K$ is the position vector of the unperturbed (Keplerian) system given by Eqs. (3.72)-(3.74).

The factor $[(t_2 - t_1)a^2]^{-1}$ is also used both to make J_r a non-dimensional index and to avoid some cumulative effects of the operations due to possible different integration times used for different orbits. The quadrature of Eq. (3.84) is numerically evaluated. The index J_r as a function of the initial conditions a and e is shown in Fig. 3.20 in the case where $\mu = 1$; $t_1 = 0$; $t_2 = 2\pi\sqrt{a^3/\mu}$; $k = 0.01$; $r_0 = 1$; and $\omega(0) = 0$. Note that this index increases with the eccentricity and with the semi-major axis. The index J_r is shown in Fig. 3.21 as a function of k for the same conditions and with $e = 0.1$.

Figure 3.20 - J_r calculated in the interval of time integration from $t_1 = 0$ to $t_2 = 2\pi\sqrt{a^3/\mu}$ as a function of the initial variables a and e. The parameters with respect to the intensity of the perturbation are $k = 0.01$ and $r_0 = 1$ and the initial condition is such that $\omega(0) = 0$.
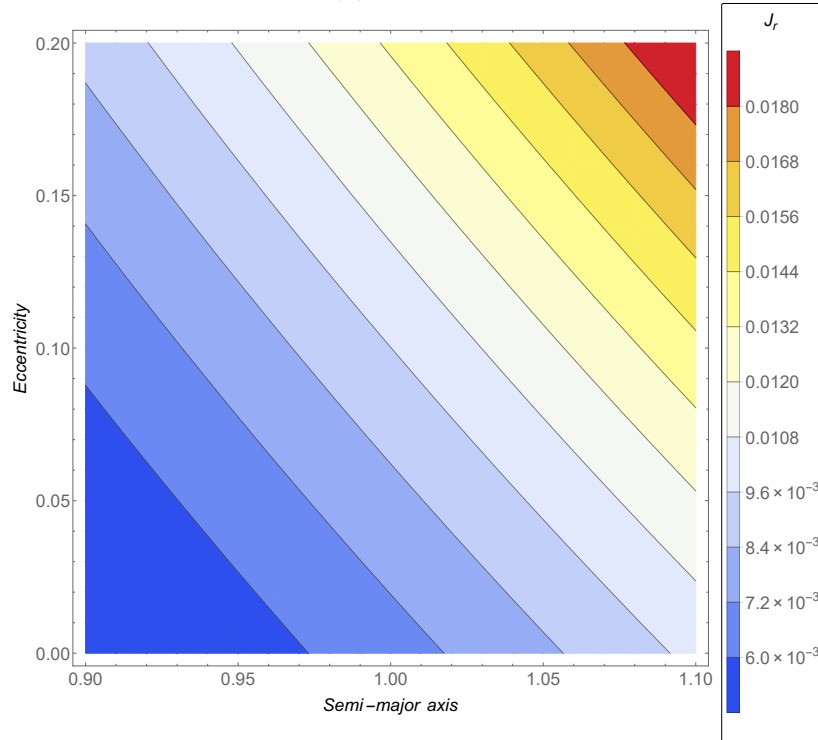
SOURCE: Author's production.

Figure 3.21 - J_r as a function of k evaluated in the interval of time integration from $t_1 = 0$ to $t_2 = 2\pi\sqrt{a^3/\mu}$. The initial conditions and the parameters are $\omega(0) = 0$; $e = 0.1$; $a = 1$; and $r_0 = 1$.
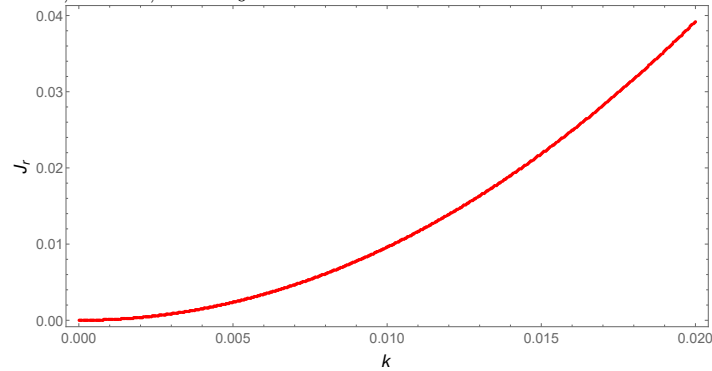
SOURCE: Author's production.

This index complements the integral of the difference of the accelerations J_a as it measures how much an orbit is deviated from a Keplerian one due to the perturbation. The ideal scenario would be to have a correspondence between higher accelerations and higher deviations.

The same initial condition $r_0 = 1$ is used here. If $r_0 = a$, then the index J_r also becomes independent of the initial value of the semi-major axis a.

3.6   Considerations

The main goal of this chapter was to search for indices based in the integral of a perturbing acceleration that is able to predict the level of disturbance in the perturbed trajectory compared with the equivalent Keplerian orbit. In order to reach this goal, we studied three indices based in the integral of the accelerations: $\vec{J}$, given by Eq. (3.78), J_s, given by Eq. (3.81), and J_a, given by Eq. (3.83). A detailed study showed that the indices $\vec{J}$ and J_s have weak points and they are not adequate to measure the perturbation level of an orbit. On the opposite side, J_a showed to be very adequate. This index is able to predict the orbits that are more disturbed.

We also studied indices to measure the consequence of the perturbations. In particular, J_r, given by Eq. (3.84), which results are in agreement with the index J_a. The idea behind the J_r index is that it can measure the deviation of an orbit from a Keplerian one directly from the trajectories.

So, the main conclusion of this chapter is that J_a is the best integral index for astrodynamics problems and can be used for other perturbations. Of course indices Δr, $\Delta \theta$, and J_r can also be used to compare the results, so giving a more detailed verification. This combination of indices can be used to select better orbits in many problems, just by adding more perturbations.

4 DETERMINATION OF THRUSTS TO GENERATE ARTIFICIAL EQUILIBRIUM POINTS IN BINARY SYSTEMS WITH APPLICATIONS TO A PLANAR SOLAR SAIL

It is well known the existence of five equilibrium points in the Circular Restricted Three Body Problem, as well as the fact that they are good options to place a spacecraft to make observations of the surrounding regions. They have several practical applications in astronautics. Following this idea, the literature shows several studies related to artificial equilibrium points, where an extra force is added to the system to give new equilibrium points. In that sense, the idea of the present chapter is to map the space around a binary system to show the magnitude and direction that a continuous thrust needs to have to generate artificial equilibrium points around the binary system. In this way a mission designer can evaluate the cost/benefit for the mission of different locations to place the spacecraft in a stationary position. In particular, applications using a planar solar sail are considered, showing the regions of possible solutions, as well as the area-to-mass ratios involved. The importance of this type of force is that it is a natural component of the dynamics, so requiring low fuel consumption for station-keeping when small extra perturbations are taken into account.

4.1 Introduction

The stationary condition in the rotating frame of reference was firstly referred as an artificial equilibrium point (AEP) in Dusek (1966). Among other possibilities, solar reflectors can take advantage of the solar radiation pressure in order to generate thrust in a spacecraft (TSIOLKOVSKY, 1936; TSANDER, 1967). Using the solar radiation pressure, a spacecraft equipped with a solar sail is able to generate the thrust required to achieve the AEP without the use of propellant. Robert L. Forward patented an idea of a "statite" spacecraft equipped with a solar sail that could maintain permanent contact with both poles of the Earth, above and below the Ecliptic (FORWARD, 1991). Thus, the solar sail becomes an attractive source of thrust to generate AEP in the CRTBP (SIMMONS et al., 1985; MCINNES et al., 1994). Since then, the searching for families of AEP has been the subject of several researches using the CRTBP, including, as particular cases, the use of general thrusts (MCINNES, 1998), AEP around asteroids systems (BROSCHART; SCHEERES, 2005; BU et al., 2017), stability studies using constant thrusts (BOMBARDELLI; PELAEZ, 2011), the study of situations where the primary body is an oblate spheroid (RANJANA; KUMAR, 2013), a thrust purely given in the radial direction (ALIASI et al., 2011), etc. There is also

research considering the elliptical restricted three body problem for a thrust purely given in the radial direction (ALIASI et al., 2012). AEP can be used to solve practical problems where the traditional libration points could not, like to place a stationary spacecraft equipped with a solar sail in a permanent contact with the Earth near the traditional lagrangian point L_3 (DE ALMEIDA JUNIOR et al., 2017a). Regardless of the requirement of a suitable control system to maintain the spacecraft at an unstable AEP, orbits around these points are capable of maintaining the spacecraft near the desired point for the duration of the mission (BAOYING; MCINNES, 2006; WATERS; MCINNES, 2007; BAIG; MCINNES, 2009). Besides Lindstedt-Poincare third order approximation method, a new analytical solution can also be used to describe orbits around AEP (DE ALMEIDA JUNIOR et al., 2018). The solar sail parameters and its dynamics around AEP can also be seen in Farrés and Jorba (2014).

From the point of view of a mission using a spacecraft with limited resources, in particular in the intensity and direction of the thrust, also with constrained objectives relative to its position in space, it is important to know the options available to park such a spacecraft. The conditions that spend too many resources should be avoided in a real mission. These conditions are represented by regions with high values for the magnitude of the thrust required to maintain the equilibrium. Although individual numerical calculations are not being presented, we exhibit several detailed maps from which it is clearly possible to choose the best cost-benefit regions to be considered in a spacecraft mission. Moreover, this is done for several different kinds of thrusts. Nevertheless, the regions where the parking is impossible are also important to be known. The objective in this chapter is then to investigate possible and impossible solutions to place a spacecraft in a stationary condition near a binary system in the rotating frame of reference. The traditional circular restricted three body problem is used to model the system, with an extra force due to the thrust applied to the spacecraft, which can be generated from several sources that requires propellant, like ion engines (GOEBEL; KATZ, 2008), or not, like solar sails (MCINNES, 2004), magnetic sails (UENO et al., 2009; ZUBRIN; ANDREWS, 1991), electric sails (MENGALI; QUARTA, 2009; JANHUNEN, 2004; JANHUNEN; SANDROOS, 2007), or magneto-plasma sails (YAMAKAWA et al., 2006).

The first objective while studying AEP in this thesis is then to investigate possible and non-possible solutions to place a spacecraft in a stationary condition near a binary system in the rotating frame of reference. The traditional circular restricted three body problem is used to model the system, with an extra force due to the thrust applied to the spacecraft. In order to give a good view of the solutions, symmetries

are explored and the equations are solved analytically for a general system of two main bodies. Moreover, the Sun-Earth system is used in the examples. This research is written in this chapter, whose sections are organized as shown in Table 4.1 and described as follows. In section 4.2, the equilibrium condition is investigated through the use of a general thrust in the restricted circular three body problem. In section 4.3, the equilibrium conditions are studied for several directions of the thrusts: thrust in the direction of the $\vec{r}_1$ vector, in subsection 4.3.1; combination of thrusts in the directions of the $\vec{r}_1$ and $\vec{r}_2$ vectors, in subsection 4.3.2; thrust in the direction of the x, y, and z axes, in subsections 4.3.3, 4.3.4, and 4.3.5, respectively; and in the general directions of the x-z and x-y planes, in subsections 4.3.6 and 4.3.7, respectively. In section 4.4, the equilibrium conditions are investigated in the case of the Sun-Earth system with applications to a planar solar sail. Firstly, the regions where the equilibrium is possible and non-possible are identified. Then, these regions are shown combined with the direction and norm of the thrust required to satisfy the equilibrium condition. Finally, instead of the norm of the thrust, these regions are also studied as functions of the ratio area-to-mass in the case where a planar solar sail is used to generate the thrust. These results are shown in subsections 4.4.1 - 4.4.7 for each type of thrust, among the ones investigated in section 4.3. The conclusions are written in section 4.5.

Table 4.1 - The organization of the cases in the paper.

The studied case	System / Subsection General binary	Sun-Earth system
Thrust in the direction of the $\vec{r_1}$ vector	4.3.1	4.4.1
Solution out of the ecliptic	4.3.1.1	
Solution on the x axis	4.3.1.2	
Solution in the ecliptic	4.3.1.3	
Combination of thrusts in the directions of the $\vec{r_1}$ and $\vec{r_2}$ vectors	4.3.2	4.4.2
Solution out of the ecliptic	4.3.2.1	
Solution in the ecliptic	4.3.2.2	
Thrust in the direction of the x axis	4.3.3	4.4.3
Solution in the ecliptic	4.3.3.1	
Solution on the x axis	4.3.3.2	
Thrust in the direction of y axis	4.3.4	4.4.4
Thrust in the direction of z axis	4.3.5	4.4.5
Solution in the x-z plane	4.3.5.1	
Solution out of the x-z plane	4.3.5.2	
Thrust in the x-z plane	4.3.6	4.4.6
Solution out of the x-z plane	4.3.6.1	
Solution in the x-z plane	4.3.6.2	
Thrust in the x-y plane	4.3.7	4.4.7

4.2 Formulation of the problem and description of the mathematical models used

Let two massive primary bodies (M_1 and M_2) moving under their mutual gravitational attraction evolve in circular orbits around the center of mass of the respective system. A rotating frame of reference is defined such that the two primaries are connected along its x axis, which center is located in the barycenter of the primaries. The z axis is oriented as perpendicular to the ecliptic and the y axis arises according to the right hand rule. This frame rotates with constant angular velocity ω along the z axis. The equation of motion of a spacecraft subjected to the gravitational interaction of the two primaries and also subjected to an extra force $\vec{f_p}$ is given by (SYMON, 1971)

$$\frac{d^2\vec{r}}{dt^2} + 2\vec{\omega} \times \frac{d\vec{r}}{dt} + \vec{\omega} \times (\vec{\omega} \times \vec{r}) + \frac{d\vec{\omega}}{dt} \times \vec{r} = -\frac{\mu_1}{r_1^3}\vec{r_1} - \frac{\mu_2}{r_2^3}\vec{r_2} + \frac{1}{m}\vec{f_p}, \qquad (4.1)$$

where: $\vec{r} = (x, y, z)$ denotes the position of the spacecraft; $\vec{\omega}$ is the angular velocity of the rotating frame of reference; $\vec{r_1}$ is the position of the spacecraft with respect

to the body M_1; r_1 is the norm of $\vec{r_1}$; $\vec{r_2}$ locates the spacecraft from the body M_2; r_2 is the norm of $\vec{r_2}$; μ_1 is the gravitational parameter of M_1; μ_2 is the gravitational parameter of M_2; $\vec{f_p}$ is a force acting over the spacecraft; and m is the mass of such spacecraft.

The distances of the bodies M_1 and M_2 from their barycenter are d_1 and d_2, respectively. According to the classic definition of center of mass (SYMON, 1971), these values are given by

$$d_1 = \frac{R\mu_2}{\mu_1 + \mu_2} \quad \text{and} \quad d_2 = \frac{R\mu_1}{\mu_1 + \mu_2}, \tag{4.2}$$

where $R = d_1 + d_2$ is the total distance that separates the two bodies. Using the $\vec{i}$, $\vec{j}$, $\vec{k}$ unitary vectors along the x, y, z axes, respectively, the vectors $\vec{r_1}$ and $\vec{r_2}$ can be written as

$$\vec{r_1} = \vec{r} + d_1\vec{i} \tag{4.3}$$
$$\vec{r_2} = \vec{r} - d_2\vec{i}.$$

Figure 4.1 - The rotating frame of reference
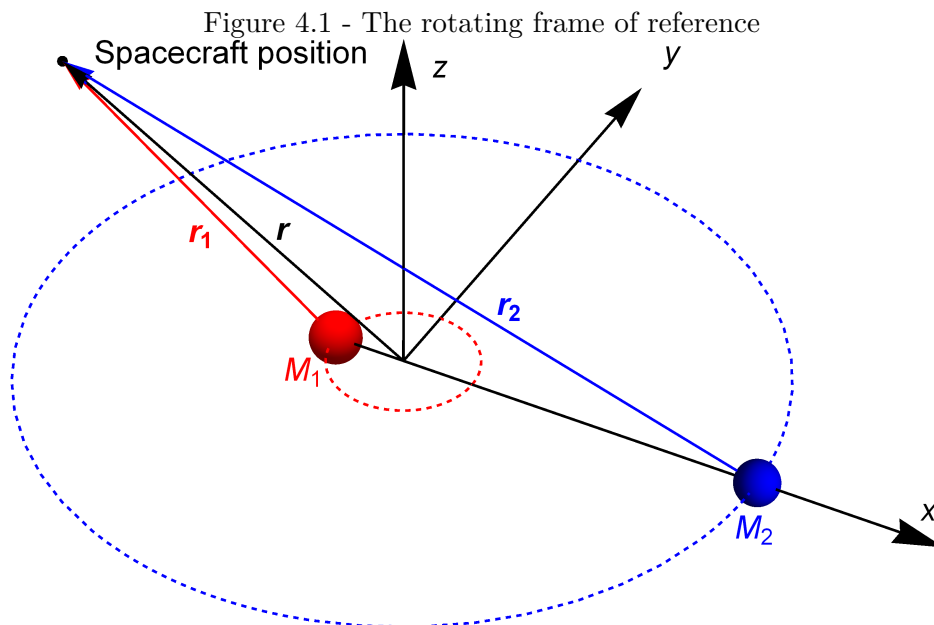
The rotating frame of reference and the relative positions of the bodies involved

are shown in Fig. 4.1. The motion is circular, therefore the $\vec{\omega}$ vector can be written as $\vec{\omega} = \omega\vec{k}$, where ω is a constant given by $\omega = \sqrt{(\mu_1 + \mu_2)/R^3}$. Hence, Eq. (4.1) becomes

$$\frac{d^2\vec{r}}{dt^2} + 2\vec{\omega} \times \frac{d\vec{r}}{dt} - \omega^2\left(\vec{r} - z\vec{k}\right) = -\frac{\mu_1}{r_1^3}\vec{r}_1 - \frac{\mu_2}{r_2^3}\vec{r}_2 + \frac{1}{m}\vec{f}_p. \tag{4.4}$$

The equilibrium condition of Eq. (4.4) is given by

$$\frac{1}{m}\vec{f}_p = -\omega^2\left(\vec{r} - z\vec{k}\right) + \frac{\mu_1}{r_1^3}\vec{r}_1 + \frac{\mu_2}{r_2^3}\vec{r}_2. \tag{4.5}$$

In the case where $\vec{f}_p = 0$, the solutions of Eq. (4.5) are the five lagrangian points, otherwise the solutions of Eq. (4.5) are the so called artificial equilibrium points (AEP). Equation (4.5) can be rewritten as

$$\frac{1}{m}\vec{f}_p = \left(-\omega^2 + \frac{\mu_1}{r_1^3} + \frac{\mu_2}{r_2^3}\right)\vec{r} + \left(\frac{\mu_1 d_1}{r_1^3} - \frac{\mu_2 d_2}{r_2^3}\right)\vec{i} + \omega^2 z\vec{k}. \tag{4.6}$$

Hence, the components of the acceleration $\frac{\vec{f}_p}{m} = f_x\vec{i} + f_y\vec{j} + f_z\vec{k}$ are evaluated using Eq. (4.6).

In order to know the fuel consumed by the spacecraft, an important quantity index to be known is the variation of the velocity given by the extra force applied to the spacecraft Δv, which in this case may be defined by simply the value of the acceleration $\|\frac{1}{m}\vec{f}_p\|$ times the time that the spacecraft is kept in the equilibrium point, that is $\Delta v = \int_{t_i}^{t_f} \|\frac{\vec{f}_p}{m}\|dt$, where t_i and t_f are the initial and final times of integration. Note that, according to Eq. (4.5), the ratio $\frac{\vec{f}_p}{m}$ depends only on the position, not on the time. Hence, we get $\Delta v = \|\vec{f}_p\|T/m$, where $T = t_f - t_i$ is the total time that the spacecraft is subjected to the thrust. Once the period of the mission T is a known parameter, this quantity is easily evaluated, since the magnitude of the ratio $\vec{f}_p/m$ is shown in this paper.

Applications to a planar solar sail: in order to consider the possibility of using a solar sail, it is possible to assume a perfect reflection in its surface. Thus, the force over a planar solar sail is given by (MCINNES, 2004)

$$\vec{f}_s = \frac{kA\cos^2\gamma}{r_1^2}\vec{n}, \tag{4.7}$$

where k is a parameter that depends on the luminosity of the body; r_1 is the vector that locates the sail, measured from the source of photons (the primary M_1); A is the total area of the flat solar sail; $\vec{n}$ is the normal vector to the solar sail; and

γ is the angle between $\vec{n}$ and $\vec{r_1}$, which must be constrained to $|\gamma| < 90°$ (the vector $\vec{n}$ cannot be directed towards the Sun). In the case where M_1 is the Sun, the parameter k is given by $k = 2p_e R^2$, where p_e is the solar radiation pressure at a distance R from the Sun. According to the definition of γ, the term $\cos^2 \gamma$ in Eq. (4.7) is $\cos^2 \gamma = (\vec{r_1} \cdot \vec{n}/r_1)^2$. The components of the thrust required to satisfy the equilibrium condition [Eq. 4.6] are $\vec{f_p} = m\left(f_x \vec{i} + f_y \vec{j} + f_z \vec{k}\right)$. In the case where this equilibrium condition is satisfied by the use of a solar sail, then $\vec{f_p} = \vec{f_s}$, hence the vector normal to the solar sail is written as $\vec{n} = \vec{f_p}/\|\vec{f_p}\|$. Therefore, in this case, the ratio area-to-mass required to maintain the equilibrium condition is given by

$$\frac{A}{m} = \frac{\left(f_x^2 + f_y^2 + f_z^2\right)^{\frac{3}{2}} r_1^4}{k\left((x + d_1)f_x + yf_y + zf_z\right)^2}. \tag{4.8}$$

Note that this model uses a perfect reflective surface for the sail, which is not true for real materials. Gravitational perturbations coming from other planets are also not taken into account. The real low eccentricity of the orbit of the Earth is not considered. In the case of AEP very close to the Sun, other effects should be taken into consideration, like the solar wind. Thus, it is important to note that a mathematical approach to the problem is done in this research, i.e. the results of this paper can be used to decide (or to ignore) an initial strategy for a mission designer, to be used together with station-keeping strategies to compensate extra perturbations.

4.3   Equilibrium conditions

Using the models described in the previous section, the equilibrium conditions are analytically and independently found for several directions of the thrust in this section.

4.3.1   Thrust in the direction of the $\vec{r_1}$ vector

A general study of the artificial equilibrium points is presented in (ALIASI et al., 2011) in the case of a general, continuous, and purely radial thrust using a synodic reference system. In this subsection, we present a different approach to the same problem, which objective is to better visualize the possibilities (locations) and costs (norms of the thrusts) to park a spacecraft in the space, which results are easily applied to the Sun-Earth system and a planar solar sail.

Let a spacecraft be subjected to a force $\vec{f}_p$ given by

$$\vec{f}_p = mf(x, y, z)\vec{r}_1, \tag{4.9}$$

where $f(x, y, z)$ is a scalar function of the coordinates to be found. Hence, the three components of Eq. (4.6) can be separated as

$$\left(-f(x, y, z) - \omega^2 + \frac{\mu_1}{r_1^3} + \frac{\mu_2}{r_2^3}\right)x - f(x, y, z)d_1 + \frac{\mu_1 d_1}{r_1^3} - \frac{\mu_2 d_2}{r_2^3} = 0, \tag{4.10}$$

$$\left(-f(x, y, z) - \omega^2 + \frac{\mu_1}{r_1^3} + \frac{\mu_2}{r_2^3}\right)y = 0, \tag{4.11}$$

$$\left(-f(x, y, z) + \frac{\mu_1}{r_1^3} + \frac{\mu_2}{r_2^3}\right)z = 0. \tag{4.12}$$

4.3.1.1 Solution out of the ecliptic

In the case where $z \neq 0$, Eq. 4.12 becomes

$$f(x, y, z) = \frac{\mu_1}{r_1^3} + \frac{\mu_2}{r_2^3}. \tag{4.13}$$

Using Eq. (4.13), Eq. (4.11) becomes

$$y = 0. \tag{4.14}$$

Using Eq. (4.14) and Eq. (4.13), Eq. (4.10) becomes

$$r_2^3 = -\frac{\mu_2 R^4}{x(\mu_1 + \mu_2)}. \tag{4.15}$$

The x coordinate must be negative in order to satisfy the positive characteristic of r_2 in Eq. (4.15). Thus, Eq. (4.13) constrains the function $f(x, y, z)$, while Eq. (4.14) shows that the solution must lie in the x-z plane. Moreover, the equilibrium points are given by the solution of Eq. (4.15).

4.3.1.2 Solution on the x axis

In the case where $z = 0$, according to Eq. (4.11), there are two options: $y = 0$ or $y \neq 0$. In the case where $y = 0$, the solutions are found at any point along the x

axis. According to Eq. (4.10), the function $f(x, y, z)$ must be given by

$$f(x) = \frac{1}{x + d_1} \left[-\omega^2 x + \frac{\mu_1 (x + d_1)}{|x + d_1|^3} + \frac{\mu_2 (x - d_2)}{|x - d_2|^3} \right]. \tag{4.16}$$

Applications to a planar solar sail: in the case where a planar solar sail is subjected to the photons coming from the primary body M_1, Eq. (4.8) becomes

$$\frac{A}{m} = f(x) \frac{|x + d_1|^3}{k}. \tag{4.17}$$

Thus, the ratio area to mass required to satisfy the equilibrium is given by Eq. (4.17), where $f(x)$ is given by Eq. (4.16). The vector $\vec{n}$ is pointed in the same direction of $\vec{r}_1$. Due to the solar sail constraint, the vector $\vec{n}$ cannot be pointed in a direction opposite to $\vec{r}_1$, hence the solution is allowed where the function $f(x)$ given by Eq. (4.16) is positive.

4.3.1.3 Solution in the ecliptic

In the case where $z = 0$ and $y \neq 0$, Eq. (4.11) becomes

$$f(x, y, z) = -\omega^2 + \frac{\mu_1}{r_1^3} + \frac{\mu_2}{r_2^3}, \tag{4.18}$$

Using Eq. (4.18), Eq. (4.10) becomes $r_2 = R$. Therefore, for a radial thrust, the solutions in the x-y plane are given in a circle of radius R around the secondary body. Using the relation $r_2 = R$, Eq. (4.11) is rewritten as

$$f(x, y, z) = \mu_1 \left(\frac{1}{r_1^3} - \frac{1}{R^3} \right). \tag{4.19}$$

Applications to a planar solar sail: again, in the case of a planar solar sail, if the primary body is the source of the radiation pressure, the vector $\vec{n}$ cannot be pointed in a direction opposite to $\vec{r}_1$, hence the function $f(x, y, z)$ must be positive, which means that, according to Eq. (4.19), only the regions where $r_1 < R$ are available to place such a solar sail. The solution in the x-y plane is then given in the circle $r_2 = R$ combined with the region $r_1 < R$. In this case, the ratio area to mass is given by

$$\frac{A}{m} = \left(\frac{1}{r_1^3} - \frac{1}{R^3} \right) \frac{\mu_1 r_1^3}{k}. \tag{4.20}$$

4.3.2 Combination of thrusts in the directions of the $\vec{r}_1$ and $\vec{r}_2$ vectors

A combination of thrusts in the directions of $\vec{r}_1$ and $\vec{r}_2$ may be a good choice from the point of view of a mission designer, because it can be directly generated by the combination of two sources of photons, one coming from M_1 (e.g. the solar rays) and another one coming from M_2 (e.g. a laser beam) over a symmetrical sail relative to these two sources (e.g. a spherical sail).

Let the extra force over the spacecraft be written as

$$\vec{f}_p = m f_1(x, y, z)\vec{r}_1 + m f_2(x, y, z)\vec{r}_2, \tag{4.21}$$

where $f_1(x, y, z)$ and $f_2(x, y, z)$ are scalar functions of the coordinates to be found. Hence, the three components of Eq. (4.6) are written as

$$(f_1 + f_2)x + f_1 d_1 - f_2 d_2 = \left(-\omega^2 + \frac{\mu_1}{r_1^3} + \frac{\mu_2}{r_2^3}\right)x + \frac{\mu_1 d_1}{r_1^3} - \frac{\mu_2 d_2}{r_2^3}, \tag{4.22}$$

$$(f_1 + f_2)y = \left(-\omega^2 + \frac{\mu_1}{r_1^3} + \frac{\mu_2}{r_2^3}\right)y, \tag{4.23}$$

$$(f_1 + f_2)z = \left(\frac{\mu_1}{r_1^3} + \frac{\mu_2}{r_2^3}\right)z. \tag{4.24}$$

4.3.2.1 Solution out of the ecliptic

In the case where $z \neq 0$, Eq. (4.24) becomes

$$f_1 + f_2 = \left(\frac{\mu_1}{r_1^3} + \frac{\mu_2}{r_2^3}\right). \tag{4.25}$$

Using Eq. (4.25), Eq. (4.23) becomes $y = 0$. Hence, the solutions lie in the x-z plane. Using Eq. (4.25), Eq. (4.22) becomes

$$f_1 d_1 - f_2 d_2 = -\omega^2 x + \frac{\mu_1 d_1}{r_1^3} - \frac{\mu_2 d_2}{r_2^3}, \tag{4.26}$$

Equations (4.25) and (4.26) can be solved for f_1 and f_2, which results are given by

$$f_1 = \frac{\mu_1}{r_1^3} - \frac{\omega^2 x}{R} \tag{4.27}$$

$$f_2 = \frac{\mu_2}{r_2^3} + \frac{\omega^2 x}{R} \tag{4.28}$$

Applications to a planar solar sail: in the case where $mf_1(x, y, z)\vec{r}_1$ (the thrust in the direction of $\vec{r}_1$) is given by a sail which normal vector is pointed in the same direction of $\vec{r}_1$, Eq. (4.7) becomes

$$mf_1(x, y, z)\vec{r}_1 = \frac{kA}{r_1^3}\vec{r}_1. \tag{4.29}$$

Using Eq. (4.27), Eq. (4.29) becomes

$$r_1^3 = \frac{R}{x\omega^2}\left(\mu_1 - \frac{A}{m}k\right). \tag{4.30}$$

Note from the term of the right side of Eq. (4.30) that the solution requires a positive value of x for a ratio area-to-mass less than μ_1/k or a negative value of x otherwise.

4.3.2.2 Solution in the ecliptic

In the case where $z = 0$, there are two cases left: either $y = 0$ or $y \neq 0$. The first case leads to simpler solutions on the x axis. On the other side, in the second case, where $y \neq 0$, Eq. (4.23) becomes

$$f_1 + f_2 = \left(-\omega^2 + \frac{\mu_1}{r_1^3} + \frac{\mu_2}{r_2^3}\right). \tag{4.31}$$

Using Eq. (4.31), Eq. (4.22) becomes

$$f_1 d_1 - f_2 d_2 = \frac{\mu_1 d_1}{r_1^3} - \frac{\mu_2 d_2}{r_2^3}. \tag{4.32}$$

The solutions of Eqs. (4.31) and (4.32) for f_1 and f_2 are given by

$$f_1 = \frac{\mu_1}{r_1^3} - \frac{\omega^2 d_2}{R}, \tag{4.33}$$

$$f_2 = \frac{\mu_2}{r_2^3} - \omega^2\left(1 - \frac{d_2}{R}\right). \tag{4.34}$$

Applications to a planar solar sail: analogously to what was done in subsection 4.3.2.1, in the case where $mf_1(x, y, z)\vec{r}_1$ is given by a solar sail which normal vector is pointed in the direction of $\vec{r}_1$, Eq. (4.7) becomes $f_1(x, y, z)\vec{r}_1 = \frac{A}{m}\frac{k}{r_1^3}\vec{r}_1$. Hence, Eq. (4.33) becomes

$$r_1 = \left[\frac{R}{\omega^2 d_2}\left(\mu_1 - \frac{A}{m}k\right)\right]^{\frac{1}{3}}. \tag{4.35}$$

Therefore, the solutions lie in a circle in the x-y plane centered in the primary M_1, which radius is given by Eq. (4.35). Moreover, due to the positive characteristic of r_1, the solutions only exist for ratios area-to-mass that satisfy $A/m < \mu_1/k$.

4.3.3 Thrust in the direction of the x axis

Equilibrium solutions for a solar sail in the x-z and x-y planes have been shown by McInnes (MCINNES, 2004), encompassing both M_1 and M_2 or close to M_2. Otherwise, in this and the subsequent subsections, the equilibrium solutions are studied as functions of the directions of the thrusts. These solutions reveal the possible and forbidden locations and the magnitude of the thrust required to park a spacecraft in the rotating frame of reference. The first case to be investigated is the thrust in the direction of the x axis.

The extra force over the spacecraft is assumed to be in the form

$$\vec{f_p} = mf(x,y,z)\vec{i}, \tag{4.36}$$

where $f(x,y,z)$ is any scalar function of the coordinates. Using Eq.(4.36), Eq.(4.6) is rewritten as

$$\left(-\omega^2 + \frac{\mu_1}{r_1^3} + \frac{\mu_2}{r_2^3}\right)\vec{r} + \left(-f(x,y,z) + \frac{\mu_1 d_1}{r_1^3} - \frac{\mu_2 d_2}{r_2^3}\right)\vec{i} + \omega^2 z\vec{k} = 0. \tag{4.37}$$

The z component of Eq.(4.37) can be written as

$$\left(\frac{\mu_1}{r_1^3} + \frac{\mu_2}{r_2^3}\right)z = 0, \tag{4.38}$$

which means $z = 0$. The y component of Eq. (4.37) is

$$\left(-\omega^2 + \frac{\mu_1}{r_1^3} + \frac{\mu_2}{r_2^3}\right)y = 0. \tag{4.39}$$

Therefore, there are two situations, either $y = 0$ or $y \neq 0$.

4.3.3.1 Solution in the ecliptic

In the case where $y \neq 0$, Eq. (4.39) becomes

$$\left(-\omega^2 + \frac{\mu_1}{r_1^3} + \frac{\mu_2}{r_2^3}\right) = 0 \tag{4.40}$$

and the $\vec{i}$ component of Eq. (4.37) is given by

$$f(x, y, z) = \frac{\mu_1 d_1}{r_1^3} - \frac{\mu_2 d_2}{r_2^3}. \tag{4.41}$$

Both Eqs. (4.40) and (4.41) satisfy the equilibrium condition. The first one constrains the points in the space where the equilibrium condition is possible, while the last one constrains the function $f(x, y, z)$. The points given by Eq. (4.40) belong to the x-y plane.

4.3.3.2 Solution on the x axis

Using $y = z = 0$, the component of Eq.(4.37) along the x axis can be written as

$$f(x) = -\omega^2 x + \frac{\mu_1(x + d_1)}{|x + d_1|^3} + \frac{\mu_2(x - d_2)}{|x - d_2|^3}. \tag{4.42}$$

The solutions must be along the x axis, and the equilibrium condition is satisfied by the function $f(x, y, z)$ given by Eq.(4.42).

4.3.4 Thrust in the direction of y axis

The extra force over the spacecraft is assumed to be in the form

$$\vec{f_p} = m f(x, y, z)\vec{j}, \tag{4.43}$$

where $f(x, y, z)$ is any scalar function of the coordinates. Using Eq.(4.43), Eq.(4.6) is rewritten as

$$\left(-\omega^2 + \frac{\mu_1}{r_1^3} + \frac{\mu_2}{r_2^3}\right)\vec{r} + \left(\frac{\mu_1 d_1}{r_1^3} - \frac{\mu_2 d_2}{r_2^3}\right)\vec{i} - f(x, y, z)\vec{j} + \omega^2 z\vec{k} = 0. \tag{4.44}$$

The z component of Eq.(4.44) can be written as

$$\left(\frac{\mu_1}{r_1^3} + \frac{\mu_2}{r_2^3}\right)z = 0, \tag{4.45}$$

which means $z = 0$. Hence, the x and y components of Eq. (4.44) are, respectively, given by

$$\left(-\omega^2 + \frac{\mu_1}{r_1^3} + \frac{\mu_2}{r_2^3}\right)x + \left(\frac{\mu_1 d_1}{r_1^3} - \frac{\mu_2 d_2}{r_2^3}\right) = 0 \tag{4.46}$$

$$f(x, y, z) = \left(-\omega^2 + \frac{\mu_1}{r_1^3} + \frac{\mu_2}{r_2^3}\right)y. \tag{4.47}$$

83

Using Eqs. (4.46) and (4.47), the function $f(x, y, z)$ can be rewritten as

$$f(x, y, z) = \left(-\frac{\mu_1 d_1}{r_1^3} + \frac{\mu_2 d_2}{r_2^3}\right)\frac{y}{x}. \tag{4.48}$$

In the case where $y = 0$, Eq. (4.47) becomes $f(x, y, z) = 0$, and the solutions of Eq. (4.46) represent the traditional collinear lagrangian points along the x axis. Otherwise, for a general value of y, the possible equilibrium points are given by the solution of Eq.(4.46), while the norm of the acceleration required to maintain this equilibrium as a function of x and y is given by Eq.(4.48).

4.3.5 Thrust in the direction of z axis

The extra force over the spacecraft is now assumed to be in the form

$$\vec{f_p} = mf(x, y, z)\vec{k}, \tag{4.49}$$

where $f(x, y, z)$ is any scalar function of the coordinates. Using Eq.(4.49), Eq.(4.6) is rewritten as

$$\left(-\omega^2 + \frac{\mu_1}{r_1^3} + \frac{\mu_2}{r_2^3}\right)\vec{r} + \left(\frac{\mu_1 d_1}{r_1^3} - \frac{\mu_2 d_2}{r_2^3}\right)\vec{i} + (\omega^2 z - f(x, y, z))\vec{k} = 0 \tag{4.50}$$

The x component of Eq. (4.50) is given by

$$\left(-\omega^2 + \frac{\mu_1}{r_1^3} + \frac{\mu_2}{r_2^3}\right)x + \left(\frac{\mu_1 d_1}{r_1^3} - \frac{\mu_2 d_2}{r_2^3}\right) = 0. \tag{4.51}$$

The y component of Eq. (4.50) is given by

$$\left(-\omega^2 + \frac{\mu_1}{r_1^3} + \frac{\mu_2}{r_2^3}\right)y = 0. \tag{4.52}$$

The z component of Eq.(4.50) can be written as

$$f(x, y, z) = \left(\frac{\mu_1}{r_1^3} + \frac{\mu_2}{r_2^3}\right)z. \tag{4.53}$$

4.3.5.1 Solution in the x-z plane

In the case where $y = 0$, the value of f is given by Eq. (4.53), while the equilibrium points in the x-z plane is purely given by the solution of Eq. (4.51). In this case,

the form of Eq. (4.51) becomes exactly the same as Eq. (4.46), except for a change of variables from z to y (and vice-versa) inside the variables r_1 and r_2. It means that the set of solutions to Eq. (4.46) for x and y are the same set of solutions of Eq. (4.51) for x and z, just changing y by z.

4.3.5.2 Solution out of the x-z plane

In the case where $y \neq 0$, Eq. (4.52) is rewritten as

$$\left(-\omega^2 + \frac{\mu_1}{r_1^3} + \frac{\mu_2}{r_2^3}\right) = 0. \tag{4.54}$$

Hence, Eq. (4.51) becomes

$$\left(\frac{\mu_1 d_1}{r_1^3} - \frac{\mu_2 d_2}{r_2^3}\right) = 0. \tag{4.55}$$

Using the relations of d_1, d_2, r_1, and r_2 given in Eqs. (4.2) and (4.3), Eq. (4.55) becomes

$$r_1 = r_2, \tag{4.56}$$

which solution is

$$x = \frac{R(\mu_1 - \mu_2)}{2(\mu_1 + \mu_2)}. \tag{4.57}$$

Using Eq. (4.56), Eq. (4.57), and the relation $\omega^2 = (\mu_1 + \mu_2)/R^3$ that comes from the two body problem (M_1 and M_2), Eq. (4.54) can be rewritten as

$$y^2 + z^2 = \frac{3}{4}R^2. \tag{4.58}$$

In the three dimensional space, Eq. (4.58) is a circle of radius $\sqrt{3}R/2$ in the plane given by Eq. (4.57), which center is located at the x axis. Note that this circle passes through the traditional lagrangian points L_4 and L_5 located at the plane $z = 0$. Using Eqs. (4.57) and (4.58), Eq. (4.53) becomes

$$f(x, y, z) = \alpha z, \tag{4.59}$$

where α is a constant defined as $\alpha = \left(\frac{\mu_1}{r_1^3} + \frac{\mu_2}{r_2^3}\right)$. The physics of the problem is disclosed, the solution is the circle shown in Fig. 4.2 and the magnitude of the specific thrust required to maintain the equilibrium has a linear relation with the z coordinate of the spacecraft. In the Sun-Earth system, the α constant has a very

small value around $\alpha \approx 4 \times 10^{-14}/s^2$.

Figure 4.2 - Thrust in the direction of the z axis. The circle is composed by the points where the equilibrium condition is possible. These points satisfy Eqs. (4.57) and (4.58). The two primaries are represented in red and blue. L_4 and L_5 are the traditional triangular lagrangian points at $z = 0$.
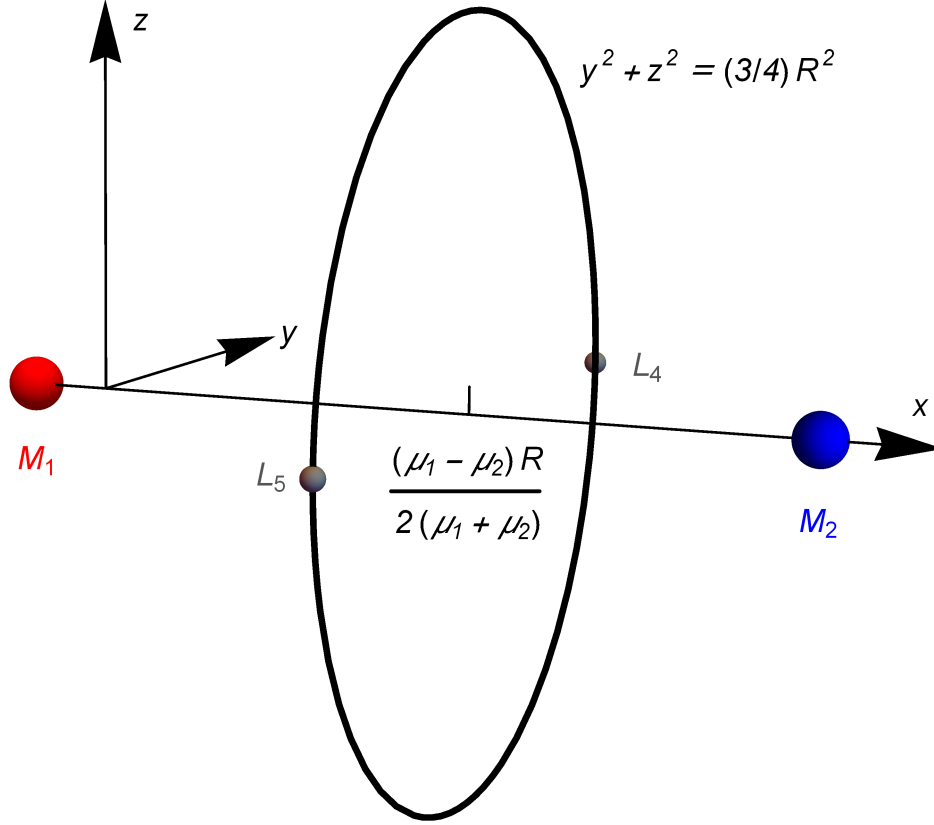
4.3.6 Thrust in the x-z plane

The extra force over the spacecraft is now assumed to be in the form

$$\vec{f_p} = m(f_x \vec{i} + f_z \vec{k}), \tag{4.60}$$

where f_x and f_z are the components of the acceleration in the x and z axis, respectively. Thus, the components of Eq.(4.6) are

$$f_x = \left(-\omega^2 + \frac{\mu_1}{r_1^3} + \frac{\mu_2}{r_2^3}\right)x + \frac{\mu_1 d_1}{r_1^3} - \frac{\mu_2 d_2}{r_2^3}, \tag{4.61}$$

86

$$\left(-\omega^2 + \frac{\mu_1}{r_1^3} + \frac{\mu_2}{r_2^3}\right) y = 0, \tag{4.62}$$

$$f_z = \left(\frac{\mu_1}{r_1^3} + \frac{\mu_2}{r_2^3}\right) z. \tag{4.63}$$

4.3.6.1 Solution out of the x-z plane

In the case where $y \neq 0$, Eq. (4.62) becomes

$$\left(-\omega^2 + \frac{\mu_1}{r_1^3} + \frac{\mu_2}{r_2^3}\right) = 0, \tag{4.64}$$

Hence, Eq. (4.61) becomes

$$f_x = \frac{\mu_1 d_1}{r_1^3} - \frac{\mu_2 d_2}{r_2^3} \tag{4.65}$$

while Eq. (4.63) becomes

$$f_z = \omega^2 z. \tag{4.66}$$

In order to satisfy the equilibrium condition, the values of the parameters f_x and f_z must satisfy Eqs. (4.65) and (4.66), respectively. Moreover, the condition given by Eq. (4.64) must also be satisfied. This condition constrains the region in space where the equilibrium is possible. In the case where $\omega^2 \neq \mu_2/r_2^3$ and $\omega^2 \neq \mu_1/r_1^3$, Eq. (4.64) can be written as

$$r_1 = R\left(1 + \frac{\mu_2}{\mu_1}\left(1 - \frac{R^3}{r_2^3}\right)\right)^{-\frac{1}{3}} \tag{4.67}$$

$$r_2 = R\left(1 + \frac{\mu_1}{\mu_2}\left(1 - \frac{R^3}{r_1^3}\right)\right)^{-\frac{1}{3}} \tag{4.68}$$

respectively. The geometrical configuration of r_1 and r_2 in the space requires that $r_1 < r_2 + R$ and $r_2 < r_1 + R$. The parameters and variables μ_1, μ_2, R, r_1 and r_2 are all positive, hence the right sides of Eqs. (4.67) and (4.68) must be positive. Therefore, the solutions are constrained in the regions of space where

$$\left(\frac{\mu_2}{\mu_1 + \mu_2}\right)^{\frac{1}{3}} R < r_2 < r_1 + R \tag{4.69}$$

$$\left(\frac{\mu_1}{\mu_1 + \mu_2}\right)^{\frac{1}{3}} R < r_1 < r_2 + R. \tag{4.70}$$

In the case where $\mu_2 \ll \mu_1$ (the Sun-Earth system), the first of these two restrictions

forbids solutions in regions very close to M_2, while the second one forbids solutions in regions closer to M_1 than M_2. The analytical solution of Eq. (4.67) is shown in Fig. 4.3.

Figure 4.3 - Analytical solution forms for the situation given in subsection 4.3.6.1. This solution must obey the black curve and must be located between the two orange straight lines.
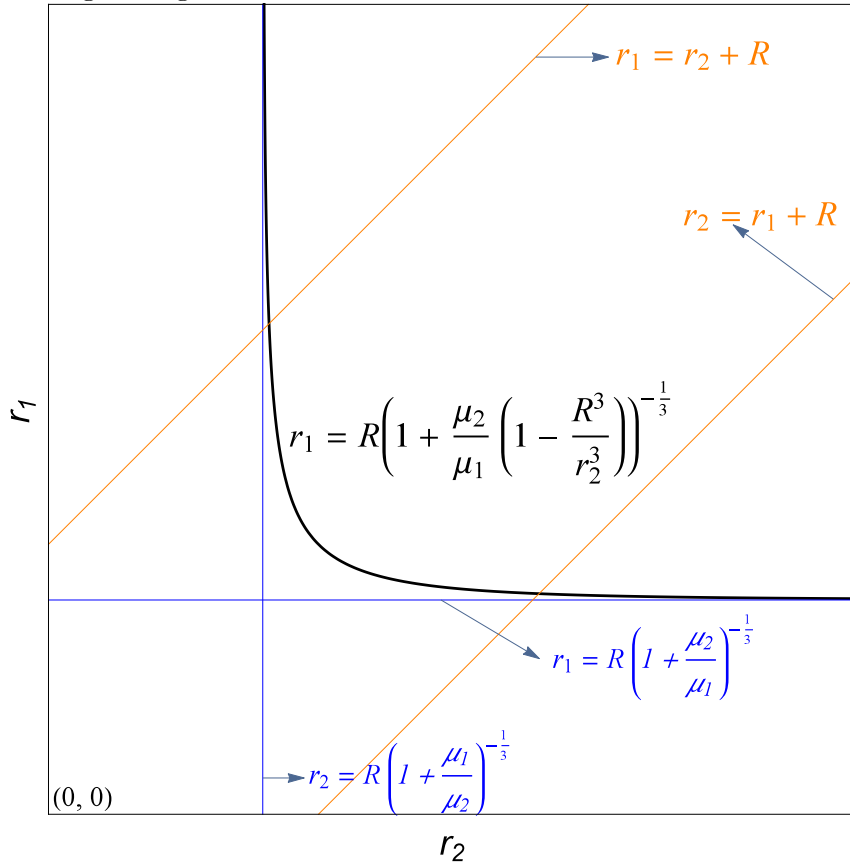
Figure 4.4 - Situation given in subsection 4.3.6.1. Analytical solution forms in the three
dimensional space, which are the circle in black. The angles θ' and α' are also
shown.
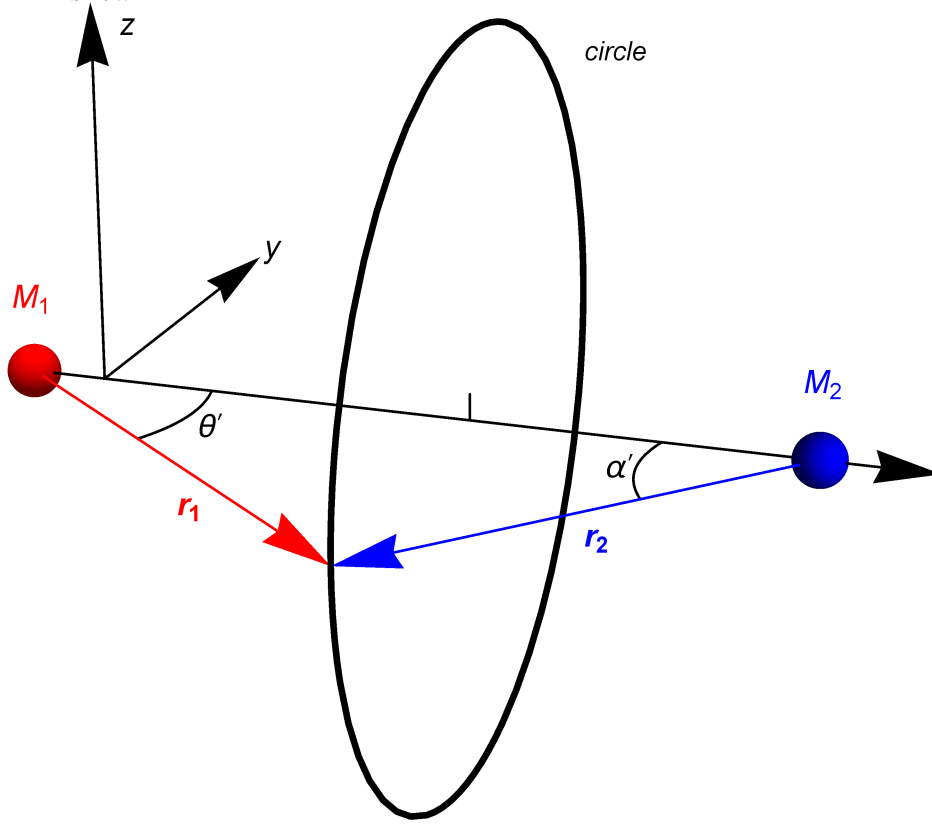
Note that the constraints given by Eqs. (4.69) and (4.70) are shown as the vertical
and the horizontal lines of this figure, respectively. Others two geometrical con-
straints are $r_1 < r_2 + R$ and $r_2 < r_1 + R$. These constraints mean that only the
solutions between the two orange straight lines of Fig. 4.3 are possible. For each
value of r_2, there is a correspondent r_1, hence, this symmetry in the three dimen-
sional space is represented by the black circle of Fig. 4.4, in which the x coordinate
is a constant. In order to find this coordinate, the angles α' and θ' are defined as
the angles between $\vec{r_1}$ and the x axis and between $\vec{r_2}$ and the x axis, respectively,
according to Fig. 4.4. Using these two angles, the following relations can be written:

$$r_1 \sin \theta' = r_2 \sin \alpha' \tag{4.71}$$

$$r_1 \cos \theta' + r_2 \cos \alpha' = R \tag{4.72}$$

Using these angles, the x coordinate of the solution can be written as $x + d_1 =$
$r_1 \cos \theta'$. The square of the radius of the circle shown in Fig. 4.4 is $y^2 + z^2 = (r_1 \sin \theta')^2$.

Hence, using Eqs. (4.71), (4.72), (4.67) and (4.2), the final solution for x, y, z can be parametrized as functions of the variable r_2 as

$$x = \frac{1}{2R}\left[R^2 - r_2^2 + \left[R\left(1 + \frac{\mu_2}{\mu_1}\left(1 - \frac{R^3}{r_2^3}\right)\right)^{-\frac{1}{3}}\right]^2\right] - \frac{R\mu_2}{\mu_1 + \mu_2} \tag{4.73}$$

$$y^2 + z^2 = r_2^2 - \frac{1}{4R^2}\left[R^2 + r_2^2 - \left[R\left(1 + \frac{\mu_2}{\mu_1}\left(1 - \frac{R^3}{r_2^3}\right)\right)^{-\frac{1}{3}}\right]^2\right]^2 \tag{4.74}$$

Note the particular case where $r_2 = r_1 = R$, that satisfies Eq. (4.64), with $f_x = 0$. This is the case given in the subsection 4.3.5.2, which results are shown in Fig. 4.2. Indeed, the whole section 4.3.5 can be seen as a particular case of this one, with $f_x = 0$, as well as section 4.3.3, with $f_z = 0$.

4.3.6.2 Solution in the x-z plane

In this situation, $y = 0$ is the only constraint, hence the solution can be any point in the x-z plane. The f_x and f_z components of the acceleration required to maintain the equilibrium are given by Eqs. (4.61) and (4.63), respectively. Let two new variables f and θ be defined such that the equations $f_x = f\cos\theta$ and $f_z = f\sin\theta$ are simultaneously satisfied. Note that this is the classic polar coordinates, where $f = \sqrt{f_x^2 + f_z^2}$ is the intensity of the total acceleration required to maintain the equilibrium condition, while θ is the angle between the total force $\vec{f_p}$ and the x axis. These two quantities related to polar coordinates disclose the physics of the problem.

4.3.7 Thrust in the x-y plane

The extra force over the spacecraft is assumed to be in the form

$$\vec{f_p} = m(f_x\vec{i} + f_y\vec{j}),, \tag{4.75}$$

where f_x and f_y are the components of the acceleration in the x and y axis, respectively. Thus, the components of Eq.(4.6) are

$$f_x = \left(-\omega^2 + \frac{\mu_1}{r_1^3} + \frac{\mu_2}{r_2^3}\right)x + \frac{\mu_1 d_1}{r_1^3} - \frac{\mu_2 d_2}{r_2^3} \tag{4.76}$$

$$f_y = \left(-\omega^2 + \frac{\mu_1}{r_1^3} + \frac{\mu_2}{r_2^3}\right)y, \tag{4.77}$$

$$0 = \left(\frac{\mu_1}{r_1^3} + \frac{\mu_2}{r_2^3} \right) z. \tag{4.78}$$

The main conclusion of this kind of thrust can be obtained from Eq. (4.78), which is $z = 0$. Hence, Eqs. (4.76)-(4.78) accept solutions at any point of the x-y plane. The components of the acceleration are given by Eqs. (4.76) and (4.77).

4.4 Results for the Sun-Earth system

In this section, the results of the development obtained in section 4.3 are shown for the Sun-Earth system, where M_1 is the Sun and M_2 is the Earth. They are also applied for a planar solar sail, which redirects the photons coming from M_1. The values of the parameters are given in Table 4.2. Note that small variations in these parameters (specially in p_e) from these values may lead to small displacements in the positions of the equilibrium points. The numerical solutions of the respective equations satisfy them with an accuracy of the order of 10^{-10} in optimized units, which means 10^{-13} in the international system of units.

Table 4.2 - Values of the parameters for the Sun-Earth system.

R	$1.495978707 \times 10^{11}$ $m = 1$ au
μ_1	$1.32712440041 \times 10^{20}$ m^3/s^2 (LUZUM et al., 2011)
μ_2	$4.03503235267 \times 10^{14}$ m^3/s^2 (LUZUM et al., 2011)
p_e	4.56×10^{-6} $(ms^2)^{-1}$

4.4.1 Thrust in the direction of the $\vec{r}_1$ vector

According to subsection 4.3.1.1, the equilibrium points out of the ecliptic lie in the x-z plane. In the case of the Sun-Earth system, these points are shown in Fig. 4.5. This figure shows the only possible solutions to place a stationary spacecraft outside the x-y plane for the given z interval. A solution valid for a general system and thrust is presented in (ALIASI et al., 2011), which is in agreement with the one shown in Fig. 4.5 in the case of the Sun-Earth system.

Figure 4.5 - The only possible solutions are drawn in black for the given z interval, out of the Ecliptic and for a thrust in the direction of $\vec{r}_1$.
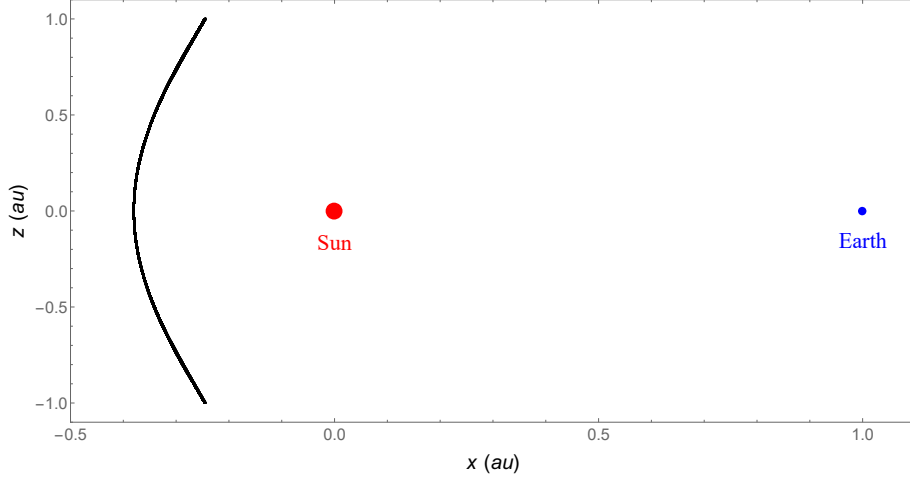
Applications to a planar solar sail: the force given by Eq. (4.9) can model a force due to the solar radiation pressure over a solar planar sail which normal vector to the planar solar sail is parallel to the rays of the Sun. This force can also model the force due to the solar radiation pressure over a spherical or other symmetrical form of a spacecraft by simply reducing the total reflection. As an example, let a spacecraft be equipped with a planar solar sail which normal vector to its sail is pointing in the same direction of the r_1 vector, that is

$$\vec{n} = \frac{\vec{r}_1}{r_1}. \tag{4.79}$$

Hence, the angle between $\vec{n}$ and $\vec{r_1}$ is $\gamma = 0$. Using Eqs. (4.79), (4.13) and (4.7), the ratio area-to-mass required to maintain the equilibrium condition can be written as

$$\frac{A}{m} = \left(\frac{\mu_1}{r_1^3} + \frac{\mu_2}{r_2^3} \right) \frac{r_1^3}{2 p_e R^2}. \tag{4.80}$$

According to Fig. 4.5, the solutions are closer to the Sun than to the Earth, which means that $\mu_1/r_1^3 \gg \mu_2/r_2^3$ and Eq. (4.80) can be approximated as $A/m \approx \mu_1/(2 p_e R^2) = 650.22 \ m^2/kg$. Thus, in the case where the thrust is in the direction of $\vec{r}_1$, the solutions to place this spacecraft in a stationary condition is given by the black curve in Fig. 4.5, with $y = 0$. The results show that there is no other option to place a spacecraft in a stationary condition outside the ecliptic plane. Moreover, a high ratio area-to-mass (A/m) is required to satisfy the points of Fig. 4.5 (about $650 \ m^2/kg$). The ratio area to mass given by Eq. (4.17) must be positive. Hence, the

equilibrium points for a solar sail on the x axis exist when the function $f(x)$ given by Eq. (4.16) is positive. Let x_{L1}, x_{L2}, and x_{L3} be the x coordinates of the collinear lagrangian points L_1, L_2, and L_3, respectively. In the case of the Sun-Earth system, the function $f(x)$ is positive in the region $x_{L3} < x < x_{L1}$ and $d_2 < x < x_{L2}$, but note that this last region is located in the shadow of the Earth. The ratio area to mass required to satisfy the equilibrium condition as a function of x is shown in Fig. 4.6 for the interval $x_{L3} < x < x_{L1}$. Note that, in the case where the planar solar sail is too close to the Sun, i.e. $x \approx 0$, other effects like solar winds should be taken into account.

Figure 4.6 - Thrust in the direction of the $\vec{r}_1$ vector for the Sun-Earth system. The ratio area to mass required to satisfy the equilibrium condition [Eq. (4.17)] as a function of x.
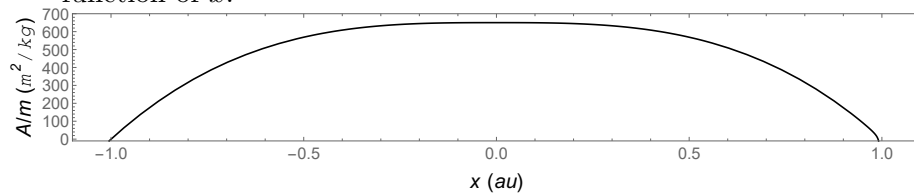
According to subsection 4.3.1.3, the equilibrium points in the ecliptic lie in a circle of radius R around the primary body M_2 and are constrained to $r_1 < R$ for a planar solar sail. In the case of the Sun-Earth system, these equilibrium points are shown in upper side of Fig. 4.7 for a planar solar sail. The ratio area to mass given by Eq. (4.20) required to satisfy the solution of the upper side is shown in the bottom of Fig. 4.7, as a function of x. The solution shown in Fig. 4.7 is in agreement with a more general one presented in (ALIASI et al., 2011).

Figure 4.7 - Thrust in the direction of the $\vec{r}_1$ vector. In the upper panel, points in black
are the ones where the equilibrium condition is possible. These points satisfy
$r_2 = R$ and $r_1 < R$. The red, blue, and green dots represent the position of
the Sun, Earth, and the traditional lagrangian points, respectively. The ratio
area to mass required to satisfy the equilibrium condition [Eq. (4.20)] as a
function of x for the points given in the upper side is shown in the bottom
side.
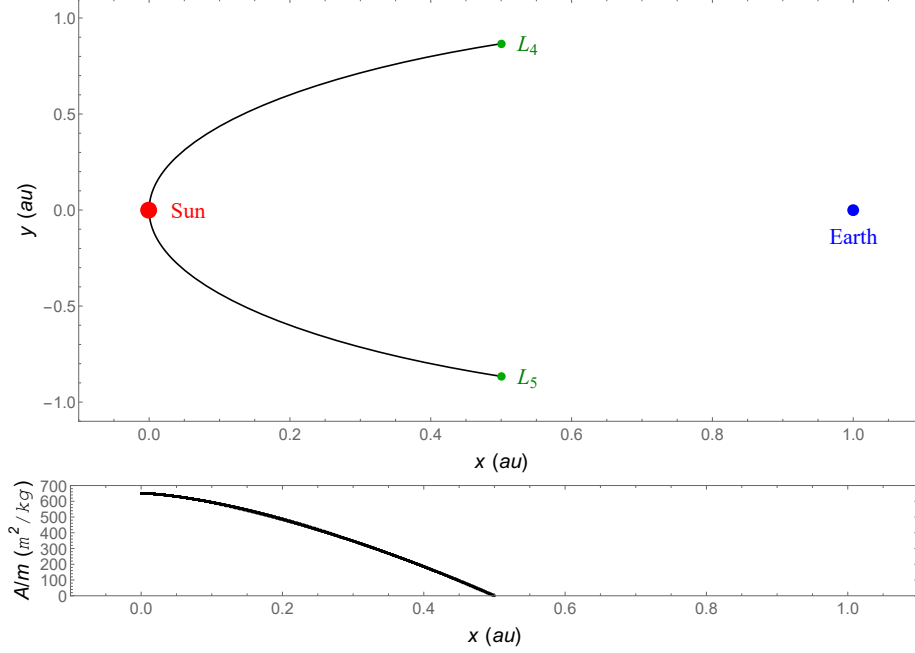
4.4.2   Thrusts in the directions of the $\vec{r}_1$ and $\vec{r}_2$ vectors

Applications to a planar solar sail: according to subsection 4.3.2.1, in the case
where the solutions are out of the ecliptic $(z \neq 0)$, the solution of Eq. (4.30) is drawn
in Fig. 4.8 for several values of the ratio area-to-mass (A/m). Note that, according
to Eq. (4.21), two terms of the respective acceleration are required to satisfy the
equilibrium condition: $f_1(x, y, z)\vec{r}_1$ and $f_2(x, y, z)\vec{r}_2$. The first one comes from the
solar sail described above and the second one may come from other different source,
as electric or magnetic sails, from a laser in the Earth pointed towards the satellite,
or even from a source of thrust that consumes propellant. The norm of this second
acceleration is shown in the color scales in Fig. 4.8. In the upper panel, solutions in
a large region in the x-z plane can be seen for different values of the ratio area-to-
mass. In the lower panel, the solutions are shown for a region closer to the Earth.
A minimum value for the norm of the second acceleration (in the direction of $\vec{r}_2$)
is represented by the region in black, which may be useful for a mission. Note that
the solutions are shown for several values of the ratio A/m available with actual

94

technologies. These points can be used to observe the poles of the Earth, since they are positioned in regions above/below them.

Figure 4.8 - Solutions of Eq. (4.30) for a planar sail in the Sun-Earth system are shown in cyan, red and gray for several ratios A/m. The magnitude of the second thrust in the $\vec{r}_2$ direction is show in the color scale.
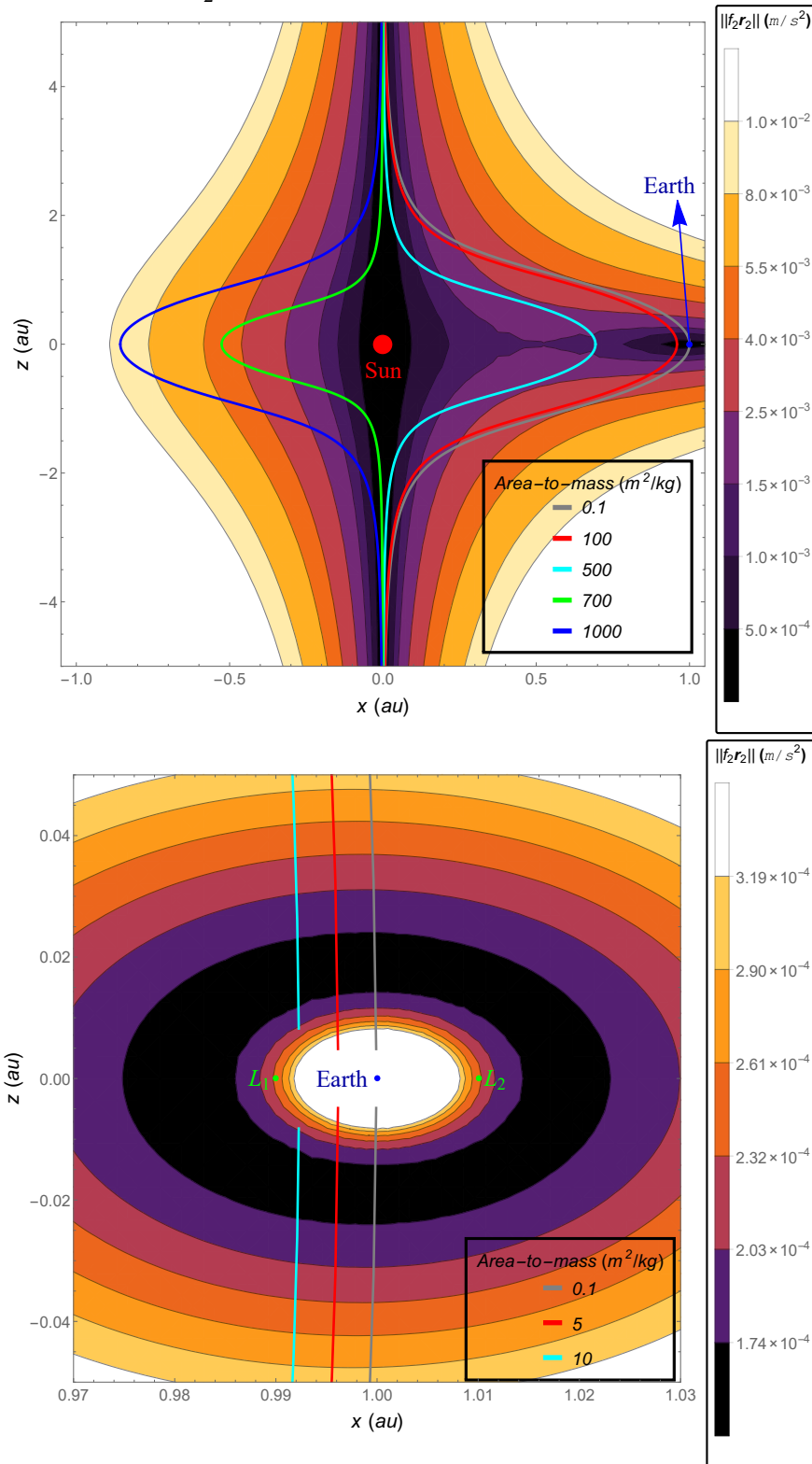
In the case where the solutions lie in the ecliptic ($z = 0$), considering that the acceleration relative to the first term of Eq. (4.21) is given for a solar sail, as described in subsection 4.3.2.2, the solutions are shown in Fig. 4.9 for several different values of the ratio area-to-mass. A larger region is shown in the upper panel, while a zoom closer to the Earth is shown in the bottom panel. The norm of the acceleration relative to the second term is represented in color scale in this same figure. Note that these values are of the order of $10^{-5}m/s^2$ or less around the Earth and of the order of $10^{-8}m/s^2$ or less far from the Earth.

Figure 4.9 - Solutions of Eq. (4.35) for a planar sail in the Ecliptic are shown in cyan, red and gray for several ratios A/m. The norm of the second thrust in the $\vec{r}_2$ direction is show in the color scale.
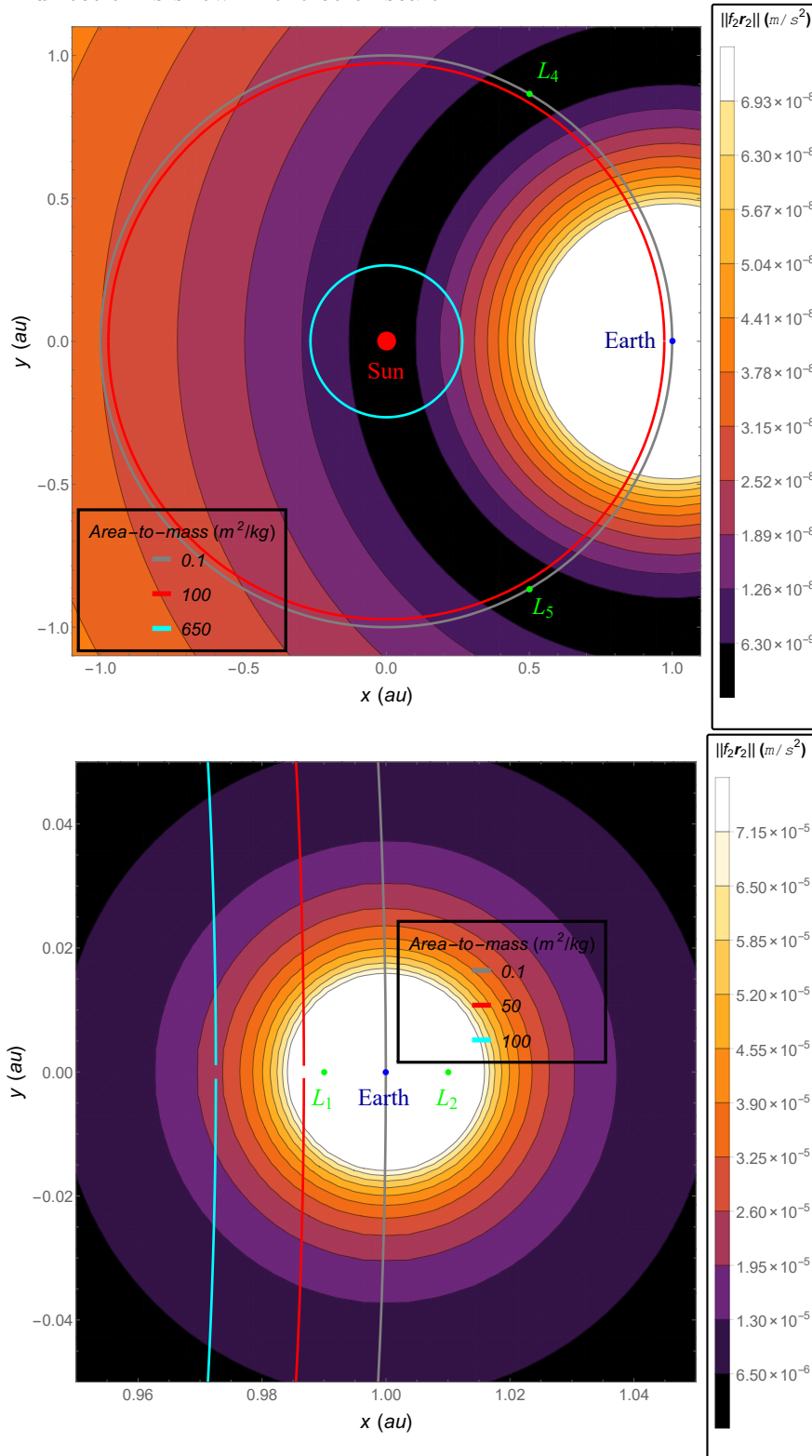
This kind of thrust could also be achieved by the use of a symmetrical sail, like a spherical reflective spacecraft, where the thrust in the direction of $\vec{r}_1$ could be generated by the photons coming from the Sun and the second thrust in the direction of $\vec{r}_2$ could be generated by a laser or a mirror located in the Earth redirecting the photons to the spacecraft.

4.4.3 Thrust in the direction of the x axis

In the case of this kind of thrust, according to subsection 4.3.3, the possible equilibrium points must lie in the ecliptic plane. In the case where $y \neq 0$, these points are given by the solution of Eq. (4.40), and this solution is shown in the upper panel of Fig. 4.10 for the Sun-Earth system. The value of f required to maintain the equilibrium is also shown in the bottom panel of Fig. 4.10, according to Eq. (4.41). The x coordinates of the triangular lagrangian points are given by $x_{L4/L5} = R(\mu_1 - \mu_2)/(2(\mu_1 + \mu_2))$. The value of f represents the direction of the thrust, which must be positive for $x < x_{L4/L5}$. The function f has a root at $x_{L4/L5}$, which means that the traditional libration points L_4 and L_5 belong to the solution set given by Eq. (4.40). The value of f decreases fast as x comes closer to $x = d_2$, due to the gravitational interaction with the Earth, which means that to apply the thrust in the x direction is not effective for AEP near the Earth.

Figure 4.10 - Thrust in the direction of x axis for the Sun-Earth system. In the upper
panel, points in black are the ones where the equilibrium condition is possible.
These points satisfy Eq. (4.40). The red dot represents the position of the
Sun, while the blue dot represents the position of the Earth. The vertical and
horizontal gray straight lines are drawn to guide the eyes. The force required
to maintain the equilibrium [Eq. (4.41)] is shown in the plot of bottom side,
as a function of x, for the points shown in the upper side.
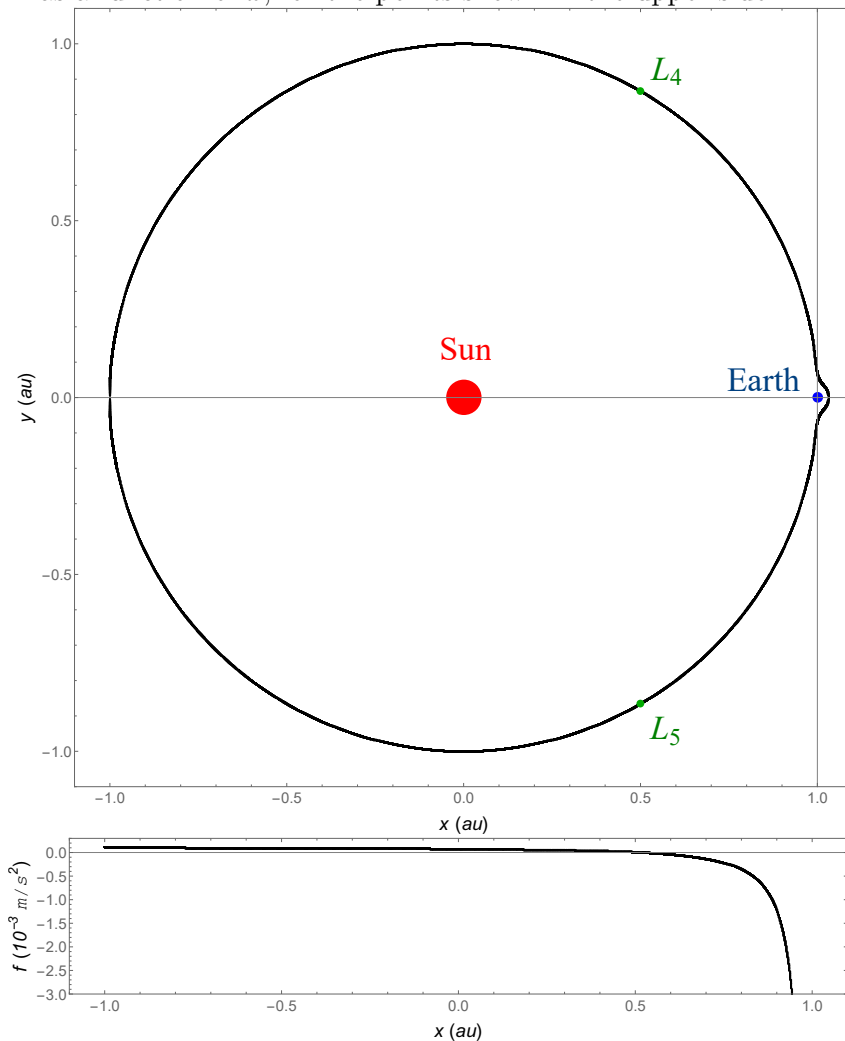
4.4.4 Thrust in the direction of y axis

According to subsection 4.3.4, the possible equilibrium points for this kind of thrust
must lie in the ecliptic and they are represented by the solutions of Eq.(4.46). In
the case of the Sun-Earth system, these solutions are shown in the upper panel
of Fig. 4.11. There are some families of solutions around the Earth. The norm of
the specific thrust required to maintain the equilibrium - i.e. norm of f given by
Eq. (4.48) - is shown in the bottom part of Fig. 4.11. This value is high for solutions

near $x = d_1$. There are minimums ($|f| = 0$) at all the traditional lagrangian points. Locations with high values for the magnitude of the acceleration required to maintain the equilibrium should be avoided in a real mission. A zoom in an interesting region around the Earth is shown in Fig. 4.12, where the possible region to place a spacecraft is drawn in blue, combined with the acceleration required to satisfy Eq. (4.48) as functions of x and y.

Figure 4.11 - Thrust in the direction of the y axis for the Sun-Earth system. Points in black are the ones where the equilibrium condition is possible. These points satisfy Eq. (4.46) combined with $z = 0$. The red dot represents the position of the Sun, while the blue dot represents the position of the Earth. The absolute value of f [Eq. (4.48))] is shown in the bottom side of the plot as a function of x.
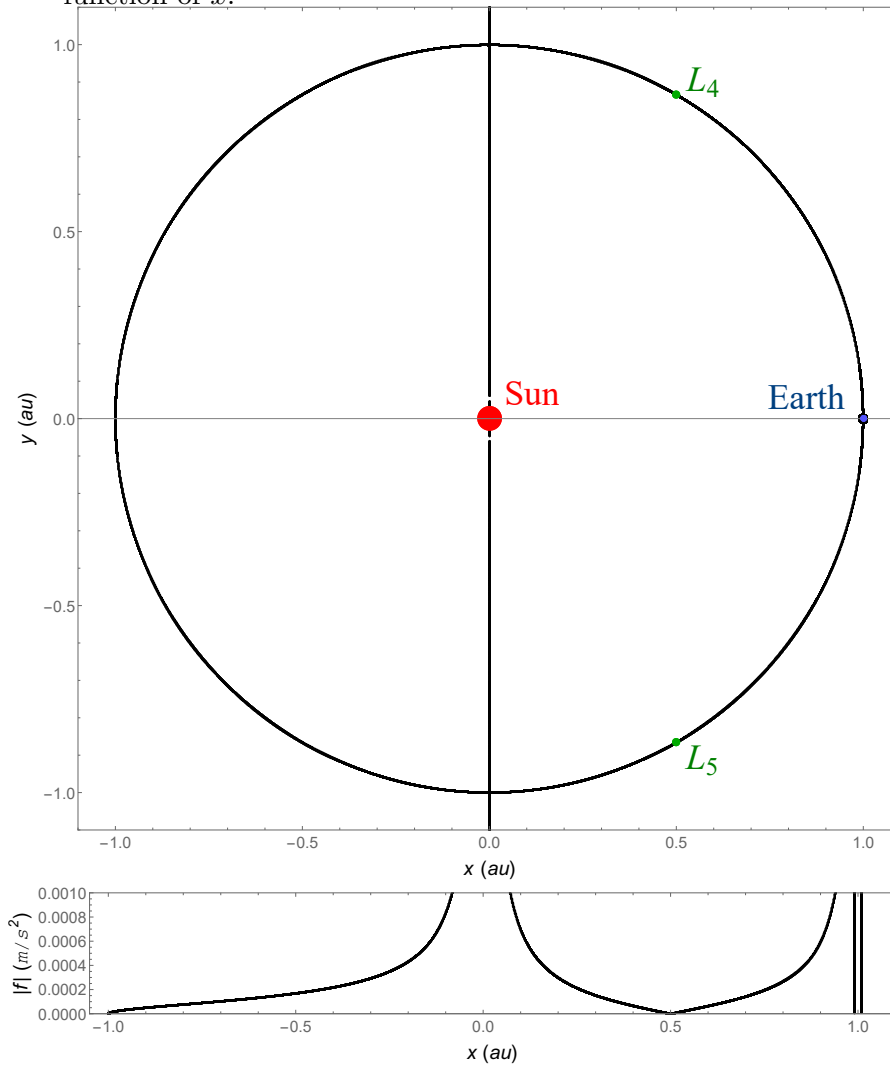
Figure 4.12 - Thrust in the direction of the y axis for the Sun-Earth system. Points in blue are the ones where the equilibrium condition is possible. These points satisfy Eq. (4.46) combined with $z = 0$. The absolute value of f [Eq. (4.48))] is shown in the color scale as a function of x and y.
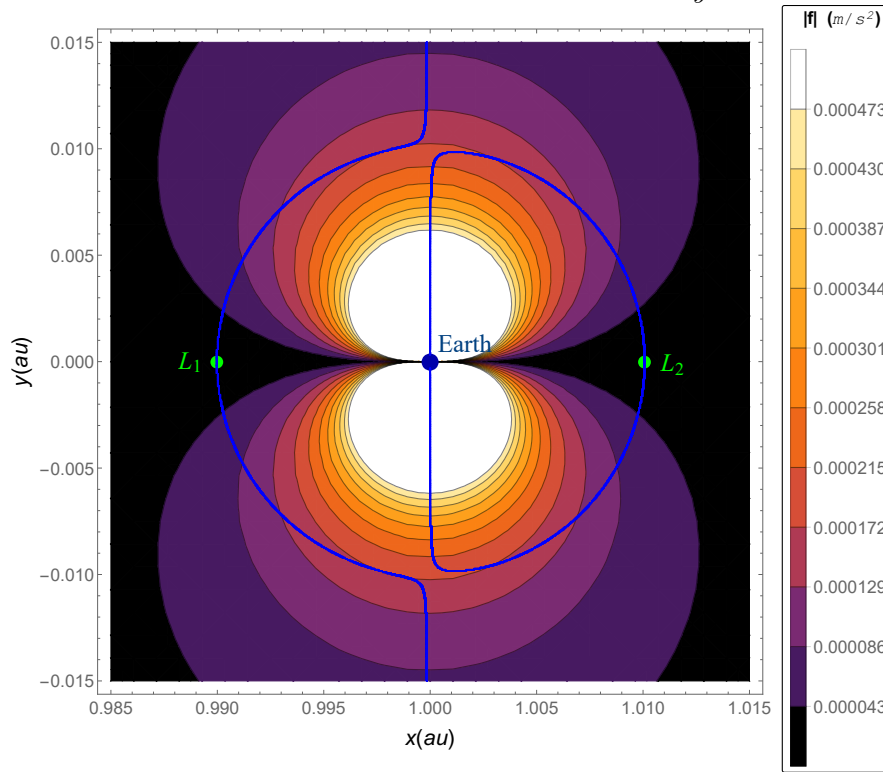
4.4.5 Thrust in the direction of z axis

According to subsection 4.3.5.2, the possible equilibrium points for this kind of thrust out of the x-z plane must be along the circle that crosses the traditional lagrangian points L_4 and L_5, as shown in Fig. 4.2.

According to subsection 4.3.5.1, the equilibrium points in the x-z plane are given by the solution of Eq. (4.51). They are shown in Fig. 4.13 for the case of the Sun-Earth system.

Figure 4.13 - Thrust in the direction of the z axis for the Sun-Earth system. The black curve represents the solutions of Eq. (4.51) with $y = 0$, which corresponds to the equilibrium condition. The red dot represents the position of the Sun, while the blue dot represents the position of the Earth.
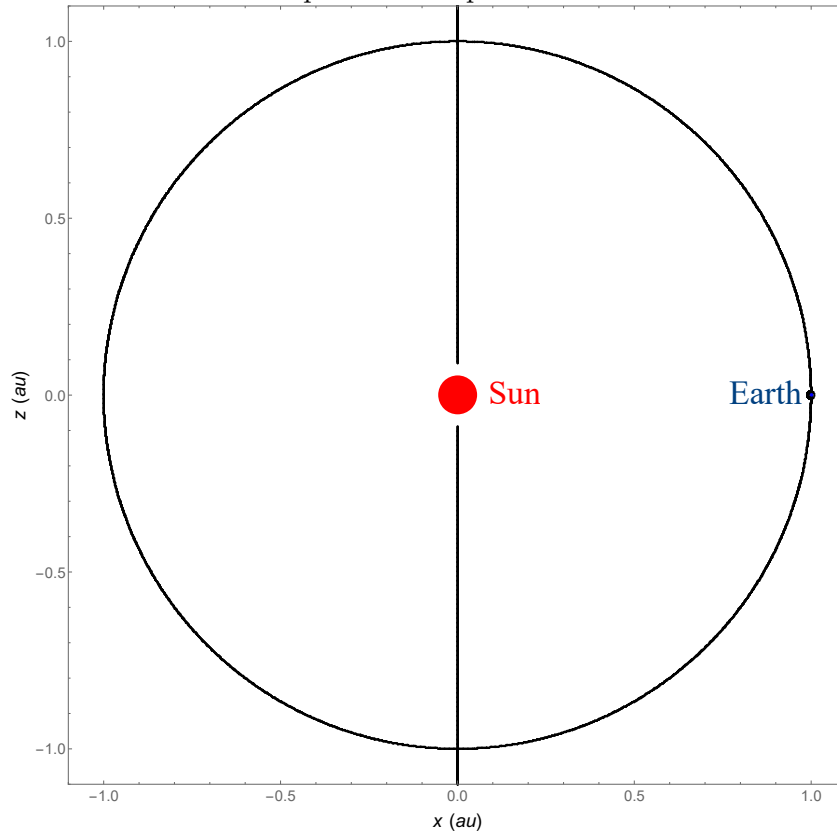
These same equilibrium points in a region closer to the Earth are better shown in Fig. 4.14. In this figure, the points in black are solutions of Eq. (4.51). The specific thrust required to satisfy the absolute value of f given by Eq (4.53) is represented in Fig. 4.14 in the color scale, from blue (low values) to red (high values). Any black point in this figure can be chosen for a mission to park a spacecraft in the Sun-Earth system. Moreover, the respective acceleration required to satisfy the equilibrium condition is shown in the color scale. Note that, in general, the lower the acceleration required to maintain the equilibrium, the better it is for a mission. But there are other constraints. As an example, a spacecraft could park in a position such that it can permanently contact the polar regions of the Earth. Figure 4.14 shows plenty of points that satisfy this demand.

Figure 4.14 - Situation given in subsection 4.3.5.1. The blue dots represent the AEP in the x-z plane for the region around the Earth. These points satisfy Eq. (4.51) with $y = 0$. The color scale represents the magnitude of the acceleration required to maintain the equilibrium condition, according to Eq. (4.53). The Earth and the traditional L_1 and L_2 lagrangian points are also shown as a central blue and green disks, respectively.
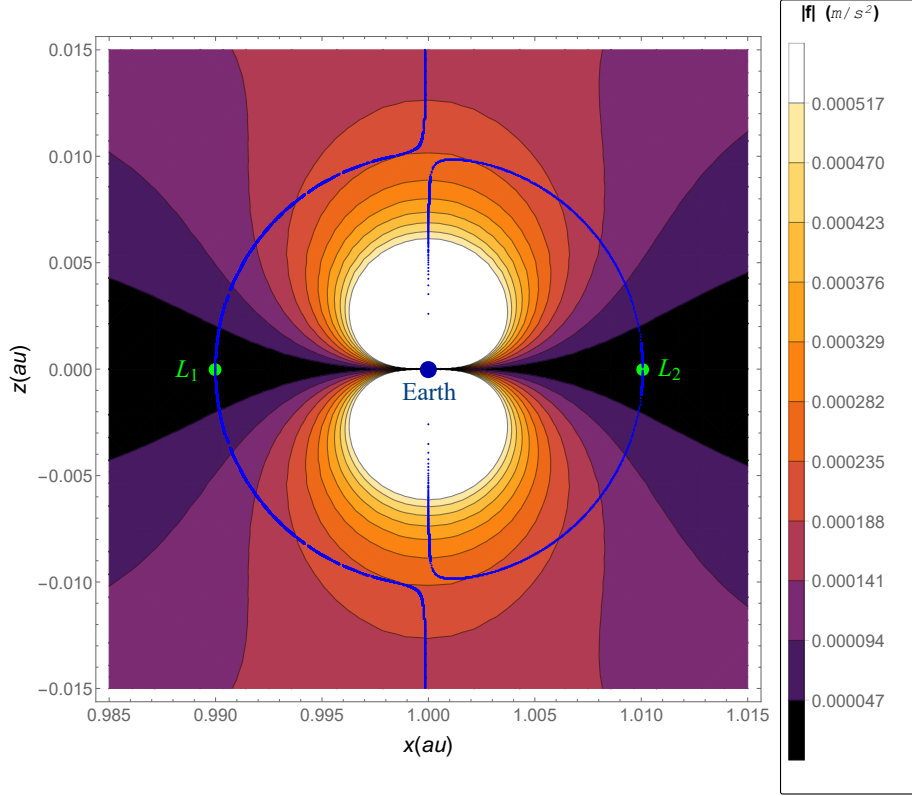
4.4.6 Thrust in the x-z plane

The possible equilibrium points out of the x-z plane is detailed in subsection 4.3.6.1.

The equilibrium in the x-z plane is discussed in subsection 4.3.6.2. In this case, for the Sun-Earth system, the specific thrust $f = \vec{f_p}/m = \sqrt{f_x^2 + f_z^2}$ required to reach the equilibrium condition as a function of the (x, z) coordinates is shown in the color scale of Fig. 4.15. The arrows in this figure represent the direction of the thrust $\vec{f_p}$ required to maintain the equilibrium condition. Note that the acceleration f is relatively weak in the region near the traditional lagrangian point L_3 and also near the Earth. Outside these regions, Fig. 4.15 shows that the cost to maintain the equilibrium condition is increased. Note that the cost near the Earth does not seem as high as it should be in order to compensate its gravitational effect. In order to explore this result, the same acceleration f and also the direction of the thrust

required to maintain the equilibrium condition are shown in Fig. 4.16. Now the gravitational effect of the Earth can be seen. Note that the value of f decreases with $|z|$ above and below the Earth and highly decreases in the regions near the traditional L_1 and L_2, as expected given the dynamical nature of these points. The direction of the thrusts can be seen looking at the arrows of Figs. 4.15 and 4.16 as functions of the x and z coordinates. Note that the opposite directions of the arrows represent the direction of the net acceleration (in the rotating frame) in the case where the thrust is null. In this case, the acceleration in the z direction tends to restore the body to the natural lagrangian points L_1, L_2, and L_3 in the case of small displacements around these points, otherwise, the acceleration in the x direction tends to carry the body far from these points. This type of plot is very important in mapping costs of AEP, so giving choices for the mission designer.

Figure 4.15 - Solutions for the situation given in subsection 4.3.6.2. The magnitude of the specific thrust is shown in the color scale. The direction of the thrust required to satisfy the equilibrium is tangent to the streamlines. The red central disk represents the position of the Sun. The blue disk represents the position of the Earth. The green disk represents the position of the traditional lagrangian point L_3.
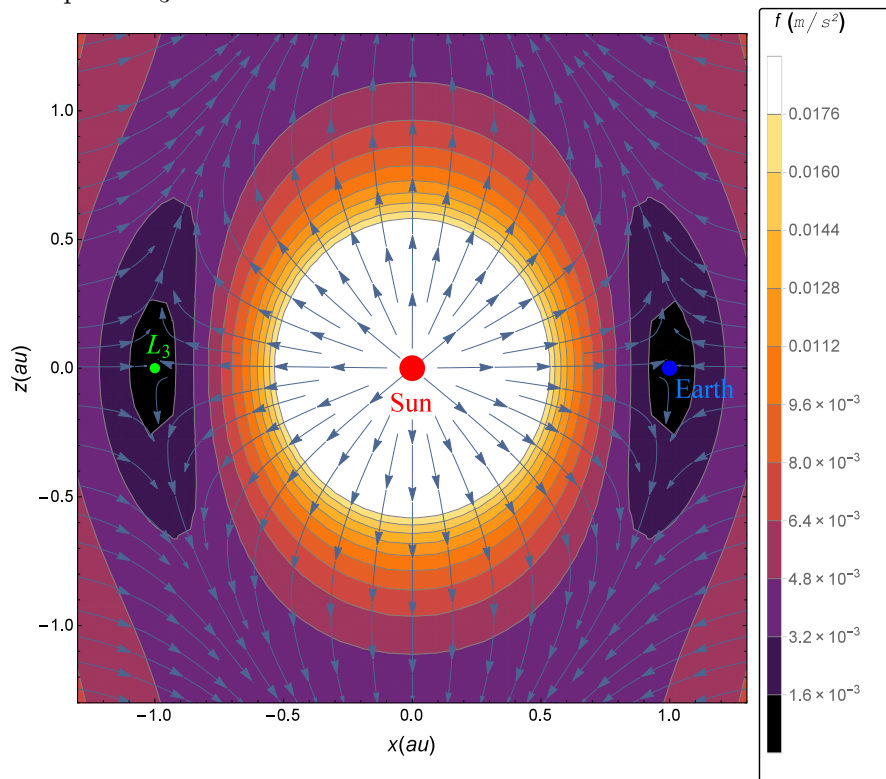
Figure 4.16 - Situation given in subsection 4.3.6.2 for solutions in the x-z plane around the Earth. The color scale represents the magnitude of the specific thrust. The tangent to the streamlines represents the direction of the thrust. The blue central disk represents the position of the Earth. The two green disks represent the position of the traditional L_1 and L_2.
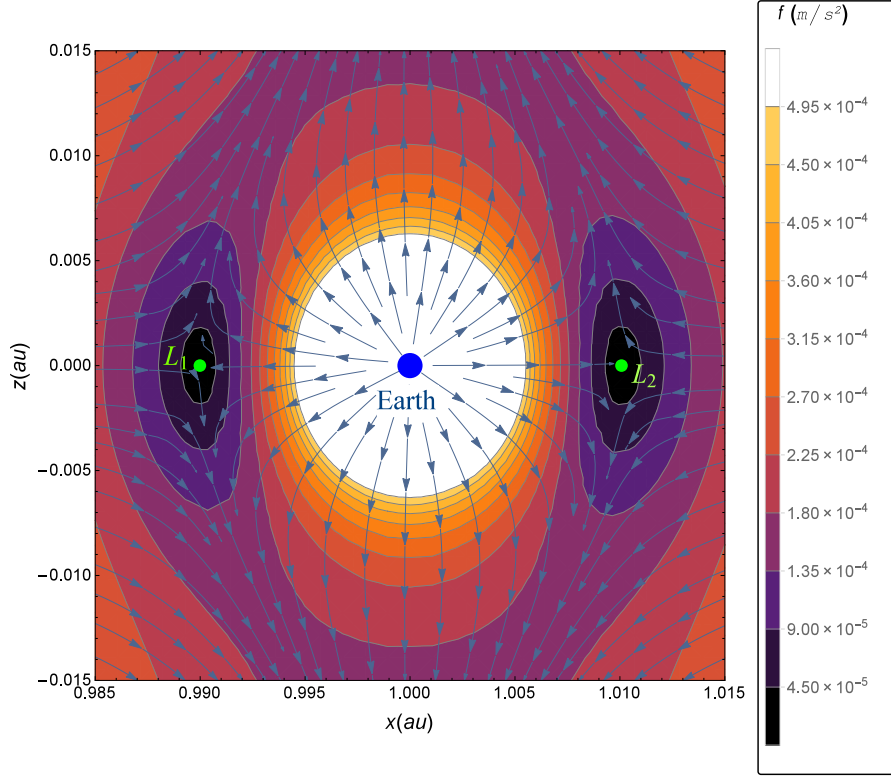
Applications to a planar solar sail: as a practical example using a planar solar sail, suppose that there is a spacecraft located in an AEP in the x-z plane, equipped with a solar sail, which normal vector to the sail is also in the x-z plane. The thrust generated by this solar sail is given by Eq. (4.7). The normal vector to the solar sail can not be partially directed towards the Sun rays, hence the maximum value of $|\gamma|$ is $\pi/2$. This constraint is taken into account in Fig. 4.17, which "forbidden region" describes the regions where $\left|\arccos\left(\frac{\vec{r}_1 \cdot \vec{n}}{r_1}\right)\right| > \frac{\pi}{2}$. The arrows represent the direction that the normal vector of the solar sail must be directed to. The color scale shows the ratio area to mass required to reach the equilibrium condition, according to Eq. (4.8). Note, by comparing Figs. 4.16 and 4.17, that there are many regions where the required thrust is small and the ratio area-to-mass is large. This happens due to the term $\cos^2\gamma$ in Eq. (4.7). The best exploitation of the thrust generated by the planar solar sail is in the case where the normal vector to the sail is in the same direction of r_1, which means $\gamma = 0$, or, as an approximation, when the absolute

value of the z component of the normal vector is minimum.

Figure 4.17 - Situation given in subsection 4.3.6.2 for a planar solar sail in the Sun-Earth system. The color scale represents the absolute ratio area-to-mass required to satisfy the equilibrium condition, given by Eq. (4.8). The tangent to the streamlines represents the direction of the thrust. There is no possible solution for the solar sail inside the light blue forbidden region, which satisfies $\left|\arccos\left(\frac{\vec{r}_1 \cdot \vec{n}}{r_1}\right)\right| > \frac{\pi}{2}$. The blue central disk represents the position of the Earth. The two green disks represent the position of the traditional L_1 and L_2.
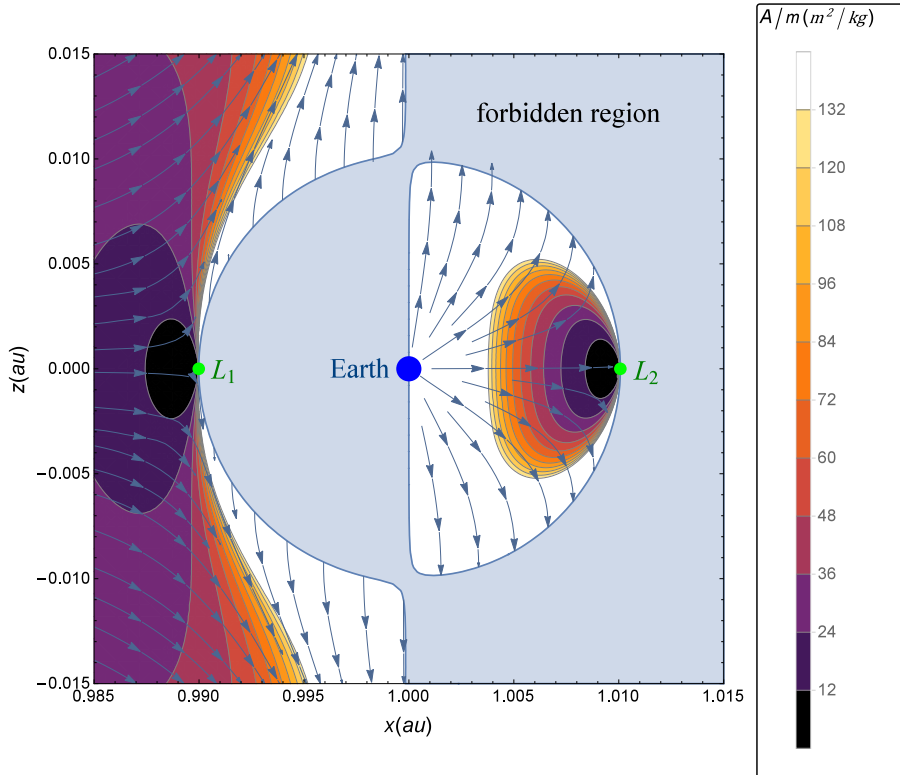
Due to the fact that the Sun is far from the Earth, the tangent of the streamlines in the borders of the forbidden region is approximately pointed along the z axis. Note that this border approximately matches with the solutions in black shown in Fig. 4.14 for the case given in subsection 4.3.5, which can also be seen as a particular case of this one, where $f_x = 0$ and the thrust is in the direction of the z axis.

4.4.7 Thrust in the x-y plane

According to subsection 4.3.7, the equilibrium points must lie in the x-y plane. Let the acceleration f be defined as $f = \sqrt{f_x^2 + f_y^2}$, which is a function of (x, y). This

acceleration is shown in Fig. 4.18 in a color scale for the case of the Sun-Earth system. The directions of the arrows in Fig. 4.18 represent the directions of the thrusts required to maintain the equilibrium. The region where the cost is minimum is around $r \approx R$. The direction of the thrust is changed to the opposite way for values of r greater than R in comparison of r less than R. The same quantities of Fig. 4.18 is better visualized in Fig. 4.19 for values of (x, y) near the Earth. Note that there are four regions of low cost to keep a stationary spacecraft: along the x axis with $y = 0$ near the traditional L_1 and L_2, and for regions where $r \approx R$. Moreover, there are several other low cost possibilities for a mission between these regions.

Figure 4.18 - The Sun-Earth system. The color scale represents the acceleration $f = \sqrt{f_x^2 + f_y^2}$ as a function of (x, y). The streamlines represent the direction of the thrust required to maintain the equilibrium condition. The red, blue and green disks represent the position of the Sun, Earth and traditional lagrangian L_3, respectively.
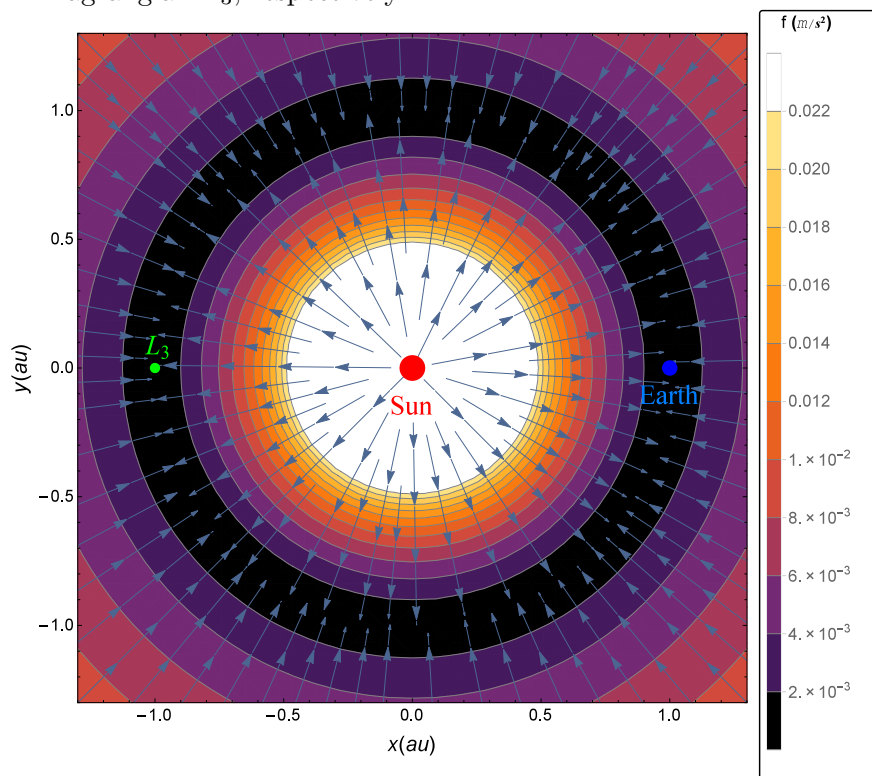
Figure 4.19 - The norm and the direction of the acceleration are shown in a color scale and in streamlines, respectively, for the Sun-Earth system. The blue and green disks represent the position of the Earth and the traditional lagrangians L_1 and L_2, respectively.
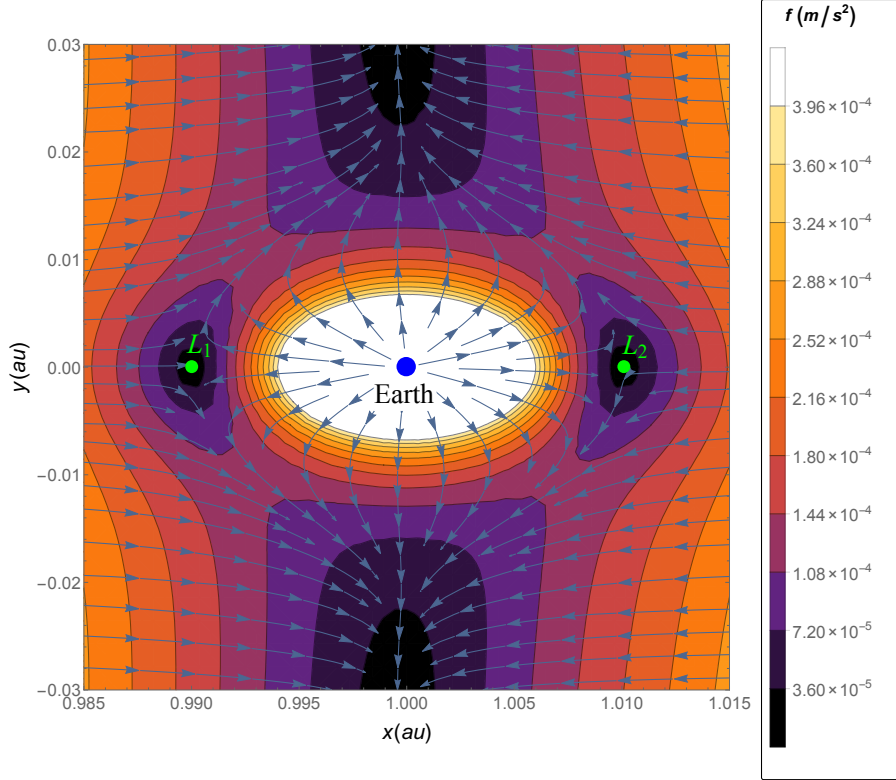
Applications to a planar solar sail: in the case of a spacecraft equipped with a solar sail, the ratio area-to-mass required to maintain the equilibrium condition is given by Eq. (4.7). The direction of the normal vector to the solar sail must be the same of the thrust required to maintain the equilibrium condition. Using the same representation used in the figures previously presented, these two quantities are shown as functions of (x, y) in Fig. 4.20 for the Sun-Earth system. For values of (x, y) close to the Earth, these quantities are shown in Fig. 4.21. The forbidden regions are the ones where the absolute value of the angle between $\vec{r}_1$ and $\vec{n}$ is greater than $\pi/2$. Note, from Fig. 4.20, that the possible regions to park a solar sail is approximately for $r < R$. The maximum value for the ratio area-to-mass is close to the Sun, where the gravitational force balances the force due to the solar sail, which happens when the ratio is $A/m \approx 650 \ m^2/kg$.

The direction and the norm of the thrust are shown in Fig. 4.21 for the regions in the x-y plane close to the Earth. There are four main alternatives to park a spacecraft

with the ratio area-to-mass less than 10 m^2/kg. The regions where the parking is impossible are also shown in this figure.

Figure 4.20 - Solar sail in the Sun-Earth system. The streamlines and the color scale represent the direction of the normal vector to the solar sail and the ratio area-to-mass, respectively, required by the solar sail to reach the equilibrium condition. The forbidden region is the one where the thrust must be pointed outward the Sun. The red central disk represents the position of the Sun.
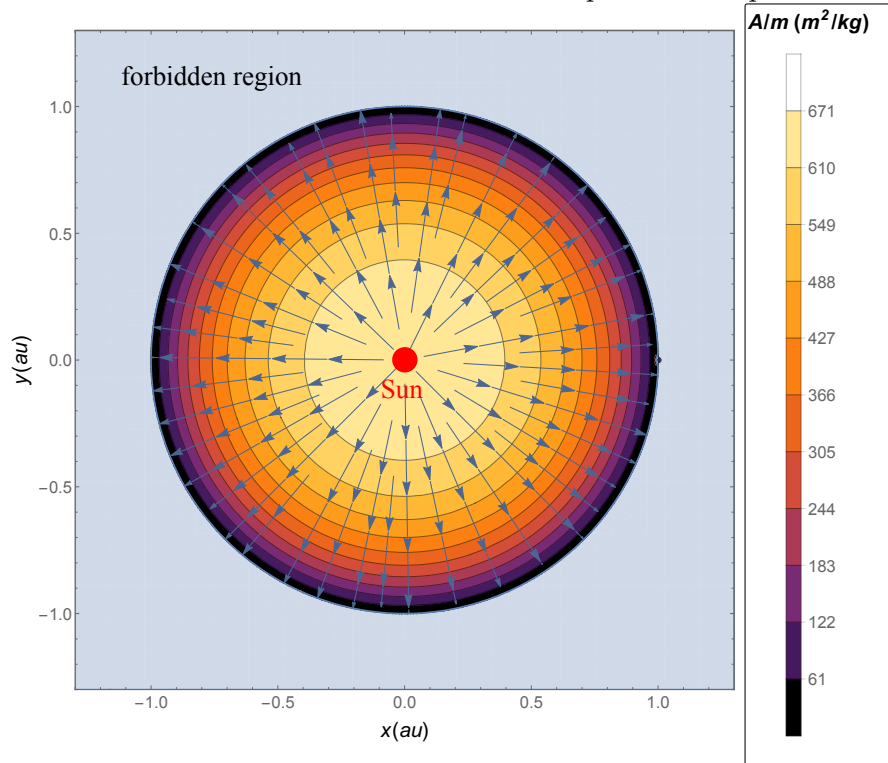
Figure 4.21 - Solar sail nearby the Earth in the Sun-Earth system. The normal vector to the solar sail must be pointed in the direction of the streamlines. The ratio area-to-mass is shown in the color scale of the figure. The forbidden region is the one where $|\gamma| > \pi/2$. The position of the Earth and the L_1 and L_2 traditional points are represented by the blue and green color, respectively.
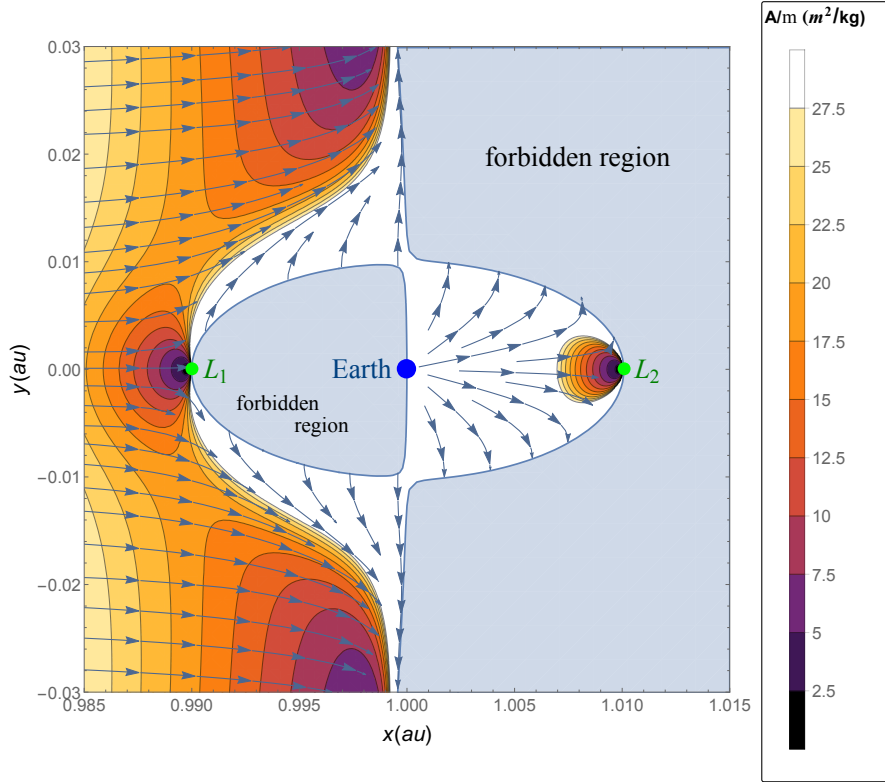
Note that this kind of force depends on the square of the cosine of the angle between the normal vector to the solar sail and $\vec{r}_1$, which means that this force is optimized only in certain regions where both $\vec{r}_s$ and $\vec{n}$ are aligned. On the other hand, an option that does not consume fuel is generally a very attractive option for mission designers.

4.5   Considerations

For all kinds of thrusts studied in this chapter, analytical solutions to the AEP were found in section 4.3 in the ecliptic, in the x-z plane, on the x axis, or in the general three dimensional space. These solutions clearly expose where the AEP can or can not be generated, as a function of the direction of the thrust, for several directions, as explained next:

- In subsection 4.3.1, we showed that the solutions out of the ecliptic must

lie in the x-z plane, in the points where Eq. (4.15) is satisfied. In the ecliptic, the solutions are given in a circle around M_2. These solutions in both planes are shown in Figs. 4.5 and 4.7 for the Sun-Earth system;

- In subsection 4.3.2, a combination of thrusts in the directions of the $\vec{r}_1$ and $\vec{r}_2$ vectors is proposed. Assuming that the thrust in the same direction of $\vec{r}_1$ is generated by a planar solar sail, solutions are found in the x-z and ecliptic planes. Solutions in the x-z plane must satisfy Eq. (4.30). Note from this equation that the coordinate x must be positive for ratios area-to-mass below μ_1/k or x must be negative for area-to-mass above μ_1/k. In the case of the Sun-Earth system, $\mu_1/k \approx 650 \ m^2/kg$ and the solutions are shown in Fig. 4.8 for several values of the ratio. Solutions in the ecliptic only exist for a ratio area-to-mass below μ_1/k and they are placed on a circle around M_1. These solutions are shown in Fig. 4.9 for several values of the ratio;

- In subsection 4.3.3, we studied the case of a thrust in the direction of the x axis. There is only solutions in the ecliptic, which are shown in Fig. 4.10 for the Sun-Earth system;

- A thrust in the y direction is studied in subsection 4.3.4. The solutions are also in the ecliptic, must satisfy Eq. (4.46), and are shown in Figs. 4.11 and 4.12 for the Sun-Earth system;

- In subsection 4.3.5, the solutions were studied for a thrust in the z direction. The solutions in the space out of the x-z plane must be in the circle of radius $3R^2/4$ that passes through the traditional lagrangian points L_4 and L_5. These possible AEP are shown in Fig. 4.2 for a general system. The solutions in the x-z plane must satisfy Eq. (4.51) and they are shown in Figs. 4.13 and 4.14 for the Sun-Earth system. Note that this solution is exactly the same of Eq. (4.46), just interchanging two variables. Hence, the solutions shown in these Figs. are similar to the ones shown in Figs. 4.11 and 4.12, but the magnitude of the thrust as a function of x and z is different. This can be checked by comparing Figs. 4.14 and 4.12.

- In subsection 4.3.6, the AEP were studied for a thrust in the x-z plane. The solutions in the three dimensional space out of the x-z plane must be in the circle parallel to the y-z plane shown in Fig. 4.4. The x coordinate of this circle and the square of its radius are given by Eqs. (4.73) and (4.74), respectively, parametrized with the value of r_2. The solutions obtained in

the space for a thrust in the z direction is a particular case of this one, in which $r_2 = r_1 = R$. The solutions may also lie at any point in the x-z plane. In this case, they are shown in Figs. 4.15 and 4.16 for the Sun-Earth system. These Figs. show the magnitude and direction of the thrust required to satisfy the equilibrium condition. In the case where a planar solar sail is used to generate the thrust, the ratio area-to-mass required to satisfy the AEP is shown in Fig. 4.17 as function of x and z for values encompassing the Earth and the traditional lagrangian L_1 and L_2.

• In the case of a thrust in the x-y plane, studied in subsection 4.4.7, the solutions lie at any point of the ecliptic. For the Sun-Earth system, the magnitude and direction of the thrust as functions of x and y are shown in Figs. 4.18 and 4.19. The ratios area-to-mass required to satisfy the AEP are shown in Figs. 4.20 and 4.21 as functions of x and y as well. The forbidden regions in which the parking is impossible are also shown.

Thus, the present chapter studied the problem of determining the locations of AEP in a binary system of celestial bodies. The main goal is to add several forms of an extra generic continuous thrust to the system to generate new equilibrium points. Those points can be useful to place a spacecraft that benefits from the equilibrium condition to reduce fuel consumption in station-keeping maneuvers. Several types of particular cases are considered, as forces acting in specific directions, like the main axis or planes of the coordinate system. Regions with minimum costs, in terms of fuel consumption, are determined and shown for all the hypothesis considered for the thrust.

In particular, applications using the extra force coming from a planar solar sail was considered, identifying the regions of possible solutions, as well as the area-to-mass ratio involved in each location. This type of force is very important, since it is a natural component of the dynamics, not based in fuel consumption, which reduces the cost of a mission. The results identify AEP located everywhere in space, including positions out of the orbital plane of the binary system, which makes possible the observation of the poles of the components of the binary system. The Sun-Earth system is used in the examples in the simulations made in the present chapter.

The results shown here can help mission designers to evaluate the cost/benefit for the mission in using different locations to place the spacecraft in a stationary position, helping to define the best strategy to observe the bodies. The results also show the magnitude and direction that this continuous thrust should have as a function of

113

the location of the AEP to keep the equilibrium condition.

5 SEARCHING FOR ARTIFICIAL EQUILIBRIUM POINTS TO PLACE SATELLITES "ABOVE AND BELOW" L_3 IN THE SUN-EARTH SYSTEM

Regarding practical applications of L_3 of the Sun-Earth system, there are few studies with the goal of placing a spacecraft at this point, or in orbit around it. One of the main problems in placing a spacecraft near this equilibrium point is the fact that it is located behind the Sun, with respect to the Earth. The Sun would be blocking direct communication between the spacecraft and the Earth. The present research gives several options to solve this problem by using solar sail to place one or two spacecraft above and/or below the Ecliptic plane. This sail could also be used for the mission itself, to collect energy or particles. By using an adequate size, location and attitude of the solar sail, the equilibrium point can be moved from its original location to allow communications between the spacecraft and the Earth. A preliminary study of the solar sail that uses this strategy is shown here.

5.1 Introduction

Once the regions where the parking is possible and not possible were properly studied in chapter 4, including the case where the main primary body (the Sun) is the source of photons, the interpretation of AEP becomes consistent and the tools are now available to solve further related problems, as explained next.

The L_3 lagrangian equilibrium point of the Sun-Earth system is a strategic point of view to observe the Sun. From there, it is possible to observe the momentary opposite face of the Sun with respect to the Earth. Due to the rotation of the Sun, the observation of solar activities of this opposite side of the Sun could provide data to predict coronal mass ejections weeks in advance. Predictions of this kind would be very important in many applications. Other types of physics and astrophysics observations could also be done from this point (TANTARDINI et al., 2010). Despite that, there are few researches done looking for the exploration of the lagrangian point L_3. The reasons may be the natural instability of the point for long time duration missions, the perturbations coming from other planets and also the communication problem mentioned before, due to the location of the Sun, which is exactly between the Earth and the point L_3. The instability exists for the point itself, as well as for orbits around this point. But it is important to remember that this same type of instability also occurs for the other two collinear equilibrium points, L_1 and L_2. Despite of this fact, many missions were planned for those two points (GOMEZ et al., 1993; JORBA; MASDEMONT, 1999; GOMEZ et al., 1998; KOON et al., 2000; LLIBRE et

al., 1985). Stable points are usually better places to locate spacecraft, but unstable points are also an option. In most of the cases, unstable equilibrium points are better places to locate a spacecraft, compared to a point with no equilibrium at all. Of course it is necessary to take care of the instability of the point, and an adequate station-keeping strategy needs to be found to control this natural instability, as well as the other perturbations coming from other forces (TANTARDINI et al., 2010). Due to these reasons, there are some previous researches considering orbits near those points (BARRABES; OLLE, 2006), and even transfer orbits to those points (PRADO, 1995; HOU et al., 2007). The perturbations coming from the other planets, in particular Venus, may be reduced using an adequate choice of the date for the mission (if it is not too long) or by using control techniques.

In that frame, the research related to the thesis at this stage aims to find some simple alternatives to solve the communication problem for a satellite equipped with a solar sail by shifting the location of the equilibrium point from the Ecliptic plane. Solutions are found in the plane that is perpendicular to the Ecliptic plane of the Sun-Earth system and contains the collinear lagrangean points. This is done by considering not only the Sun and Earth gravitational interactions with the satellite, but also the force due to the solar radiation pressure. Under this more complete model, new equilibrium points appear. Their locations are not the same of the ones obtained using only the gravitational forces. It means that a proper choice of the parameters of the solar sail, like its size, attitude, reflectance properties, etc., can generate a location of the point that is not in the orbital plane of the Earth. This out-of-plane component can shift the point such that there is direct visibility from the point to the Earth. This idea could also be used to make measurements related to the relativity theory, by verifying the distortion of the light passing near the border of the solar disk. Basically, there is an appearance of useful AEP obtained with the inclusion of the non-gravitational force given by the solar sail. This concept was already used to study the possibility of placing a mirror around the Earth to increase the temperature of our planet (SALAZAR et al., 2016), and also to decrease the temperature of our planet (MCINNES, 2010). Some other references using this concept in different equilibrium points are proposed in Morimoto et al. (2007) and McInnes et al. (1994). Research in attitude and trajectory stability of solar sails is done in Li et al. (2015). An alternative is to place a second satellite, also equipped with a solar sail, at a new artificial equilibrium point near L_1. Another alternative is to place a spacecraft "below" the traditional equilibrium point L_3 with respect to the ecliptic plane. Out-of-plane displacements of these points can also help the link between the satellite near L_3 and the Earth, as shown in detail later in this chapter.

Thus, three strategies are proposed to remove the problem of visibility between L_3 and the Earth, helping to make this particular point available for astronautical applications. The mathematical models used are described in section 5.2, where the pair of equations representing the AEP of interest is shown. The results are detailed in section 5.3, where three different forms of solutions to the communication problem between L_3 and the Earth are proposed and evaluated as function of the minimum ratio area-to-mass required while using a solar sail. The final considerations of the chapter are written in section 5.4.

5.2 Mathematical models

According the Coriolis theorem (SYMON, 1971), the equation of motion of a spacecraft under the gravitational influence of the Sun and the Earth and subjected to a force due to the solar radiation pressure over its sail written in a non-inertial rotating frame of reference that has the Sun fixed in its center is given by

$$\frac{d^2\vec{r}_s}{dt^2} + 2\vec{\omega} \times \frac{d\vec{r}_s}{dt} + \vec{\omega} \times (\vec{\omega} \times \vec{r}_s) + \frac{d\vec{\omega}}{dt} \times \vec{r}_s = -\frac{\mu_s}{r_s^3}\vec{r}_s - \frac{\mu_e}{r_e^3}\vec{r}_e + \frac{1}{m}\vec{f}_p, \qquad (5.1)$$

where:
$\vec{\omega}$ is the angular velocity of the rotating frame,
$\vec{r}_s$ is the position of the spacecraft,
$\vec{r}_e$ locates the spacecraft with respect to the Earth,
$\vec{f}_p$ is the force over the sail due to the solar radiation pressure,
μ_s is the gravitational parameter of the Sun and
μ_e is the gravitational parameter of the Earth.

Figure 5.1 - rotating frame of reference
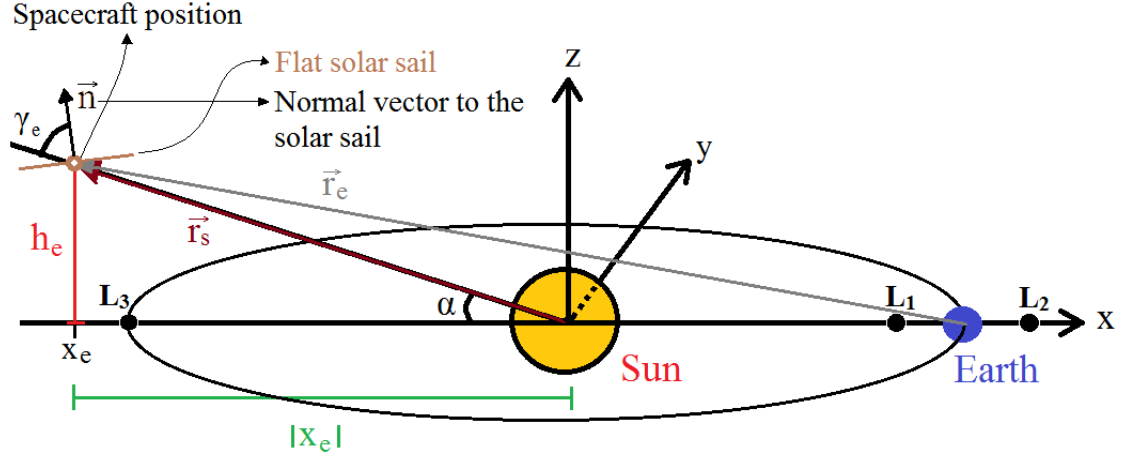
SOURCE: Author's production.

The rotating frame of reference is shown in Fig.5.1, from where the bodies involved (Sun, Earth and spacecraft) and the new artificial equilibrium point near L_3 can be seen. The Sun is placed in the center of the reference system, with the Earth in a circular orbit with radius R. The satellite equipped with a solar sail - a flat one - remains fixed in the artificial equilibrium point near L_3. In particular, the out-of-plane component of its location is noted, marked by h_e. In order to obtain this equilibrium, the vector normal to the solar sail needs to make an angle γ_e with the direction of the solar rays. In this geometry, the line Sun-spacecraft makes an angle α with the orbital plane of the Earth. The force due to the solar radiation pressure over a flat solar sail with perfect reflection is given by MCINNES (2004) as

$$\vec{f_p} = \frac{2p_e A R^2 \cos^2(\gamma_e)}{r_s^2} \vec{n}, \tag{5.2}$$

where R is a positive constant that represents the Sun-Earth distance, p_e is the solar radiation pressure at a distance R from the Sun, A is the total area of the sail, $\vec{n}$ is the vector normal to the flat sail and γ_e is the angle between $\vec{n}$ and $\vec{r_s}$.

For the purpose of this study, the motion of the Earth around the Sun is assumed to be circular and non-perturbed by any force, which indicates a Keplerian orbit. Thus, the angular velocity vector $\vec{\omega}$ can be written as

$$\vec{\omega} = (0, 0, \omega) = \left(0, 0, \sqrt{\frac{\mu_s}{R^3}}\right). \tag{5.3}$$

118

According to Fig.5.1, the $\vec{r}_s$ and $\vec{r}_e$ vectors can be written as

$$\vec{r}_s = (x_e, y_e, h_e) \tag{5.4}$$

and

$$\vec{r}_e = (x_e, y_e, h_e) - (R, 0, 0) = (x_e - R, y_e, h_e), \tag{5.5}$$

where x_e, y_e and h_e are the coordinates of the position of the spacecraft.

The cross products of the third term on the left side of Eq. (5.1) can be calculated through the use of Eqs. (5.3) and (5.4), thus the result is

$$\vec{\omega} \times (\vec{\omega} \times \vec{r}_s) = \left(-\frac{x_e \mu_s}{R^3}, -\frac{y_e \mu_s}{R^3}, 0 \right). \tag{5.6}$$

The equilibrium condition is defined as

$$\frac{d\vec{r}_s}{dt} = 0. \tag{5.7}$$

By using Eq. (5.7) and Eq. (5.3), Eq. (5.1) becomes

$$\vec{\omega} \times (\vec{\omega} \times \vec{r}_s) = -\frac{\mu_s}{r_s^3}\vec{r}_s - \frac{\mu_e}{r_e^3}\vec{r}_e + \frac{1}{m}\frac{2p_e A R^2 \cos^2(\gamma_e)}{r_s^2}\vec{n}. \tag{5.8}$$

Equation (5.8) can be written in a column vector form as

$$\frac{A}{m}\frac{2R^2 p_e \cos^2(\gamma_e)}{r_s^2}\begin{pmatrix} n_{1e} \\ n_{2e} \\ n_{3e} \end{pmatrix} =$$

$$\frac{\mu_s}{r_s^3}\begin{pmatrix} x_e \\ y_e \\ h_e \end{pmatrix} + \frac{\mu_e}{r_e^3}\begin{pmatrix} x_e - R \\ y_e \\ h_e \end{pmatrix} - \frac{\mu_s}{R^3}\begin{pmatrix} x_e \\ y_e \\ 0 \end{pmatrix}, \tag{5.9}$$

where n_{1e}, n_{2e} and n_{3e} are components of the vector $\vec{n}$, respectively, in the x, y and z directions.

Although artificial equilibrium points could be searched in all over the space, this work aims in searching for solutions of the artificial equilibrium points that stay

near L_3 for the main spacecraft and near L_1, L_2 or L_3 for an eventual assistant spacecraft. The locations are above or below the Sun-Earth line, only in the (x, z) plane, which means searching for solutions such that $y_e = 0$. For this condition, the vector $\vec{n}$ can be written as

$$\begin{pmatrix} n_{1e} \\ n_{2e} \\ n_{3e} \end{pmatrix} = \begin{pmatrix} \cos(\alpha + \gamma_e) \frac{x_e}{|x_e|} \\ 0 \\ \sin(\alpha + \gamma_e) \frac{h_e}{|h_e|} \end{pmatrix}, \tag{5.10}$$

where $\alpha = \arctan\left(\left|\frac{h_e}{x_e}\right|\right)$ is the smallest angle between $\vec{r}_s$ and the x axis, as shown in Fig. 5.1.

Using Eq. (5.10), the two non-trivial equations left from the vector components of Eq. (5.9) are written as

$$\left(\frac{A}{m}\right) \frac{2R^2 \cos^2(\gamma_e) p_e}{r_s^2} \cos(\alpha + \gamma_e) \frac{x_e}{|x_e|} = \frac{\mu_s}{r_s^3} x_e + \frac{\mu_e(x_e - R)}{r_e^3} - \frac{x_e \mu_s}{R^3} \tag{5.11}$$

and

$$\left(\frac{A}{m}\right) \frac{2R^2 \cos^2(\gamma_e) p_e}{r_s^2} \sin(\alpha + \gamma_e) \frac{h_e}{|h_e|} = \left(\frac{\mu_s}{r_s^3} + \frac{\mu_e}{r_e^3}\right) h_e, \tag{5.12}$$

where $r_s = \sqrt{(h_e)^2 + (x_e)^2}$ and $r_e = \sqrt{(h_e)^2 + (x_e - R)^2}$.

Table 5.1 shows the values for the respective parameters used in this research.

Table 5.1 - Parameters used in the simulations

R	$1.496 \ 10^{11} m$
p_e	$4.56 \ 10^{-6} \frac{N}{m^2}$
μ_s	$1.3275412528 \ 10^{20} \frac{m^3}{s^2}$
μ_e	$3.98588738352 \ 10^{14} \frac{m^3}{s^2}$

Using the values for the respective parameters given by Table 5.1, there are four unknown variables left in Eqs. (5.11) and (5.12). They are: x_e, h_e, γ_e and the ratio $\frac{A}{m}$. By fixing two of them it is possible to find the other two, such that all of them satisfy both Eqs. (5.11) and (5.12), if solutions exist.

This work presents three kind of solutions for the communication problem. For the particular case of communication solution 3, the one shown in subsection 5.3.3,

the angle between the vector normal to the solar planar sail and the solar rays is constrained such that the reflected rays are in the direction of the z axis. This constraint means:

$$\gamma_e = \frac{\pi}{4} - \frac{\alpha}{2}. \tag{5.13}$$

The total force due to the solar radiation pressure over each of the solar sail is given by the sum of each of the photons' flux pushing the solar sail, as shown in Eq. (5.14), for the case of communication solution 3. Due to the geometrical symmetry of this solution, both the incident rays that come directly from the Sun and the ones coming from the Sun reflected by the other spacecraft make the same angle γ_e with the vector normal to the solar sail. The details of the solution are given in subsection 5.3.3.

$$\vec{f_p} = \frac{2p_e A R^2 \cos^2(\gamma_e)}{r_s^2}\vec{n} + \frac{2p_e A R^2 \cos^2(\gamma_e)}{(r_s + 2h_e)^2}\vec{n} \tag{5.14}$$

Therefore, if Eq. (5.14) replaces Eq. (5.2), then Eqs. (5.11) and (5.12) are replaced by

$$\left(\frac{A}{m}\right)2R^2\cos^2(\gamma_e)p_e\cos(\alpha + \gamma_e)\left(\frac{1}{r_s^2} + \frac{1}{(r_s + 2h_e)^2}\right)\frac{x_e}{|x_e|} =$$
$$\frac{\mu_s}{r_s^3}x_e + \frac{\mu_e(x_e - R)}{r_e^3} - \frac{x_e\mu_s}{R^3}, \tag{5.15}$$

and

$$\left(\frac{A}{m}\right)2R^2\cos^2(\gamma_e)p_e\sin(\alpha + \gamma_e)\left(\frac{1}{r_s^2} + \frac{1}{(r_s + 2h_e)^2}\right)\frac{h_e}{|h_e|} =$$
$$\left(\frac{\mu_s}{r_s^3} + \frac{\mu_e}{r_e^3}\right)h_e, \tag{5.16}$$

where $\alpha = \arctan\left(\left|\frac{h_e}{x_e}\right|\right)$ and γ_e is given by Eq. (5.13).

A particular algorithm is used to find less accurate solutions of Eqs. (5.11) and (5.12), or Eqs. (5.15) and (5.16), and the Newton method for two variables is used to improve the accuracy, starting from these less accurate solutions. Each solution set presented in this research satisfies Eqs. (5.11) and (5.12) or Eqs. (5.15) and (5.16), with a minimum accuracy in the order of 10^{-10} for each of them.

5.3 Results and solutions

A wide range of solutions sets (x_e, h_e, γ_e and the ratio $\frac{A}{m}$) that satisfy the equilibrium condition (Eq. (5.7)) is found. For clarity purposes, Figs. 5.2-5.4 show the solutions sets for $\frac{A}{m} = 12 \frac{m^2}{kg}$ near L_1, L_2 and L_3, respectively. The three points are considered, although the main goal of the chapter is to search for artificial equilibrium points near L_3, because the two other colinear equilibrium points are also candidates to receive a second spacecraft to complete the communication system. In that way, artificial equilibrium points near those points are useful to attend the goal of the present research. In these figures, each of the brown straight lines represent the solar sail and its respective inclination (γ_e), which is the angle between the vector normal to the solar sail and the vector in the direction of the rays coming from the Sun. The solar radiation pressure comes from the left side for the solutions sets near L_1 and L_2 and from the right side for the solutions sets near L_3. Figures 5.2-5.4 also show that, for $\gamma_e = \frac{\pi}{2}$, the only possible solutions are the L_1, L_2 or L_3 lagrangian traditional points, which are located very close to $\frac{x_e}{R} = 0.99$, $\frac{x_e}{R} = 1.01$ and $\frac{x_e}{R} = -1$, respectively. This happens because the solar sail is assumed to be flat, so there is no solar radiation pressure effects over the sail when it is parallel to the rays of the Sun. A physical analysis of the figures can be done to explain their behavior. The first fact noticed is that the new equilibrium points are shifted towards the Sun. This means a shift to the left for the points L_1 and L_2 and to the right for the point L_3. Therefore, the net result of adding the solar radiation pressure is that it combines with the centrifugal force and the gravity forces of the Sun and the Earth to install again the equilibrium condition in another position. Another fact noted in Figs. 5.2-5.4 is the behavior of the angle γ_e, which defines the attitude of the solar sail. It starts perpendicular to the rays of the Sun at the original lagrangian point, to have a zero effect from the solar radiation pressure. Then, it starts to decrease, making the vertical component of the force to get stronger, thus h_e increases and a maximum value is reached. After that, the solar sail rotates until it faces the Sun. At this point there is no vertical component of the force and the equilibrium point goes back to the horizontal axis, in its minimum distance from the Sun.

Similar patterns can be obtained for other values of the ratio $\frac{A}{m}$, but with other values for the maximum h_e reached, as shown in Fig. 5.5. It is interesting to note that different values of the maximum distance from the orbital plane of the Earth are reached in each situation. The equilibrium points take into account the effects of the gravity forces and the solar radiation pressure. Near L_3 the gravity forces are weaker, because it is the point located far away from the Earth. Therefore, it is the

point where h_e is larger, compared to the other points, for a given value of the ratio $\frac{A}{m}$. In the points L_1 and L_2, the gravity forces of the Earth are quite relevant, but the solar radiation pressure effects are weaker in L_2. Thus, the point L_2 has the smallest values for the maximum h_e and the middle of the two primaries is the intermediate case in the aspect of larger h_e reached. Of course, the values of h_e increase with $\frac{A}{m}$ for all the points, as expected, and these values are quantified in Fig. 5.5. In all the results presented here, the Earth shadow is neglected, because the equilibrium points of interest are not in the orbital plane of the Earth, so they are outside the region of possible shades.

Figure 5.2 - Black dots represent the solutions sets for $\frac{A}{m} = 12\frac{m^2}{kg}$ near L_1. Red dots are also solutions. Their respective angles γ_e (in radians) of the normal to the sail relative to the rays of the Sun are shown. Solar rays come from the left side of the figure. The brown straight lines represent the inclination of the planar solar sail (not in scale).

SOURCE: Author's production.

123
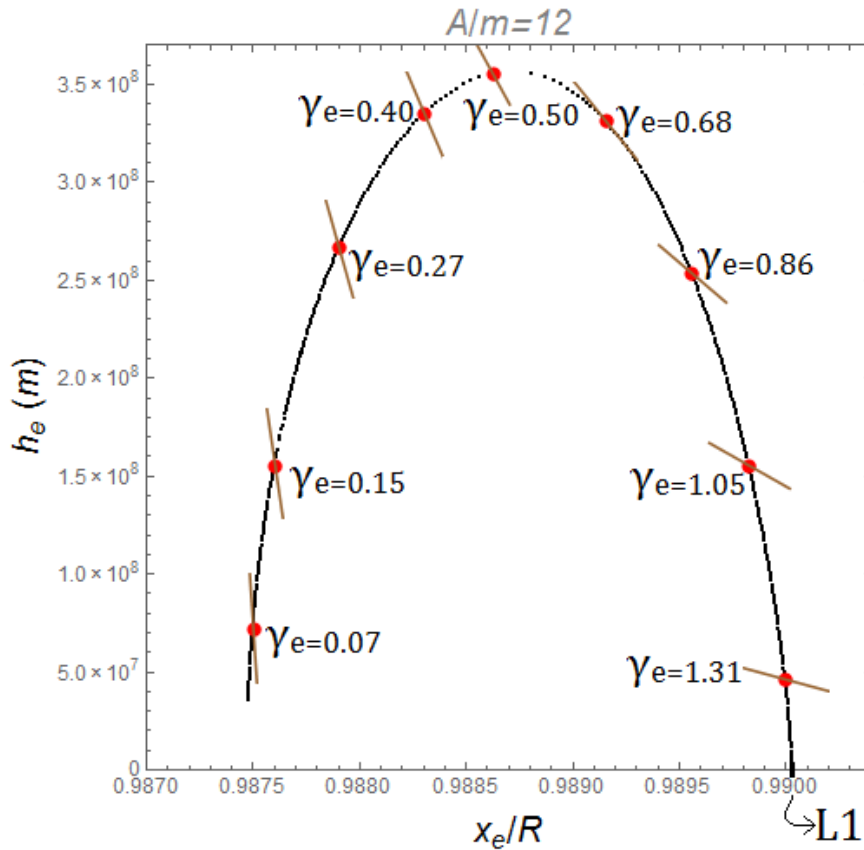
Figure 5.3 - Black dots represent the solutions sets for $\frac{A}{m} = 12\frac{m^2}{kg}$ near L_2. Red dots are also solutions. Their respective angles γ_e (in radians) of the normal to the sail relative to the rays of the Sun are shown. Solar rays come from the left side of the figure. The brown straight lines represent the inclination of the planar solar sail (not in scale).
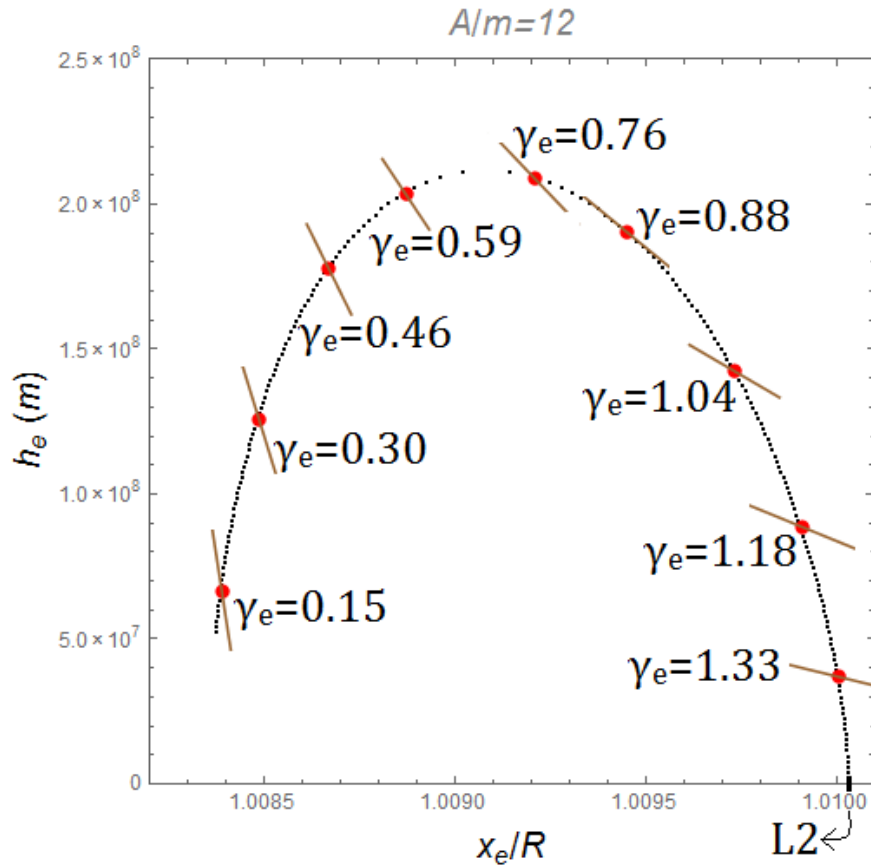
SOURCE: Author's production.

Figure 5.4 - Black dots represent the solutions sets for $\frac{A}{m} = 12\frac{m^2}{kg}$ near L_3. Red dots are also solutions. Their respective angles γ_e (in radians) of the normal to the sail relative to the rays of the Sun are shown. Solar rays come from the right side of the figure. The brown straight lines represent the inclination of the planar solar sail (not in scale).
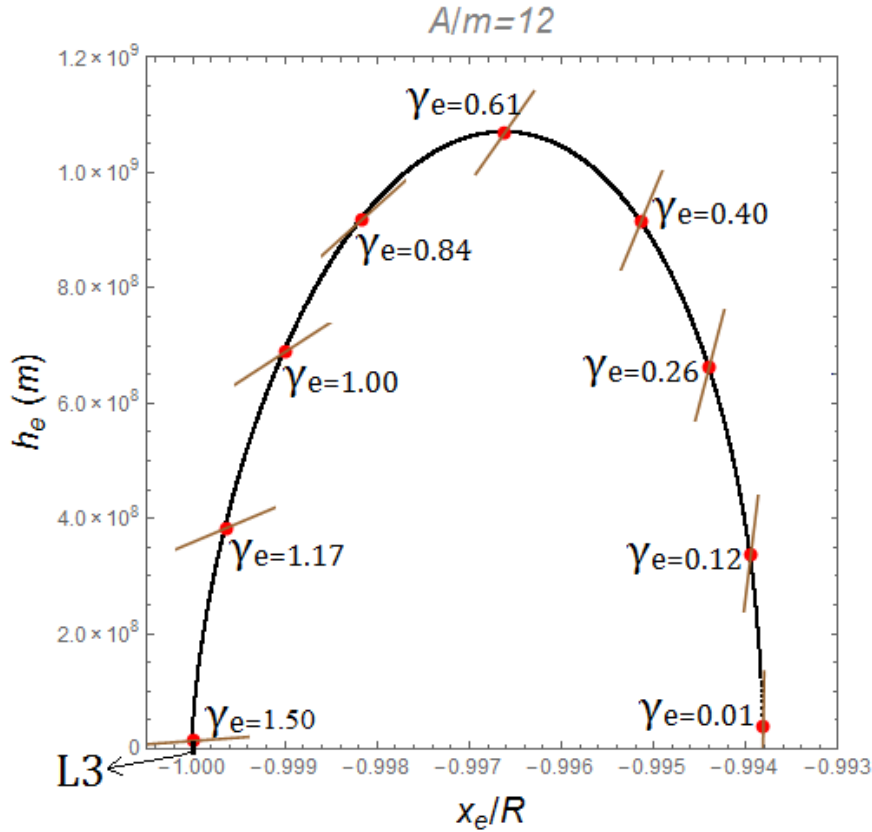
SOURCE: Author's production.

The next step is to combine those results to obtain geometries that allow the communication between L_3 and the Earth. Figure 5.6 represents the solutions sets for x_e and h_e coordinates for its respective value of the ratio $\frac{A}{m}$. The red line at $x_e = 0$ represents the size of the radius of the Sun. The blue straight line connects the highest point near L_3, the point with maximum value for h_e, to the highest point reached near the lagrangian point L_1. The green straight line connects the highest point near L_3 to the center of the Earth. The values for γ_e are omitted from this figure for clarity purposes, but each set of solution contains its respective value for γ_e.

Figure 5.5 shows an approximated linear relation between the maximum value for

h_e reached near L_1, L_2 and L_3 as a function of $\frac{A}{m}$. The results come from the data obtained by the algorithm to solve the set of equations that represent the equilibrium conditions. The absolute value of the acceleration of the solar radiation pressure is also proportional to $\frac{A}{m}$, which means that the maximum h_e reached is proportional to the absolute value of the force due to the solar radiation pressure. If the reflection of the solar sail is not perfect (a real solar sail), then the resultant force of the solar sail would be smaller for a given ratio A/m and this linear relation should be considered.

Note that exactly the same results presented in this study could be obtained for $z = -h_e$, instead for $z = h_e$, due to the symmetry of the problem between "above" and "below" the Ecliptic plane. In fact, there is an infinite number of solutions with the equilibrium point being visible just in the limit of the solar disk, but in any direction (not in the x, z plane). It gives different points of observation for the spacecraft, which can be used to attend different goals of the mission. Besides that, orbits around those artificial equilibrium points are also an option, but neither of the cases are in the scope of the present chapter.

The effects of the interference in the communication signs due to the electromagnetic waves as they pass near the Sun are ignored in this work. The calculations are made taking into account that the radius of the Sun is approximately $6.96 \times 10^8 m$. Thus, if the value for h_e near L_3 is more than twice this value, the spacecraft can communicate directly with the Earth and the Sun is no longer an obstacle.

Figure 5.5 - Color dots represent the solutions sets for the maximum value of h_e reached for the respective value of the parameter $\frac{A}{m}$ $\left(\frac{m^2}{kg}\right)$ near L_3 (black dots), L_1 (red dots) and L_2 (blue dots).
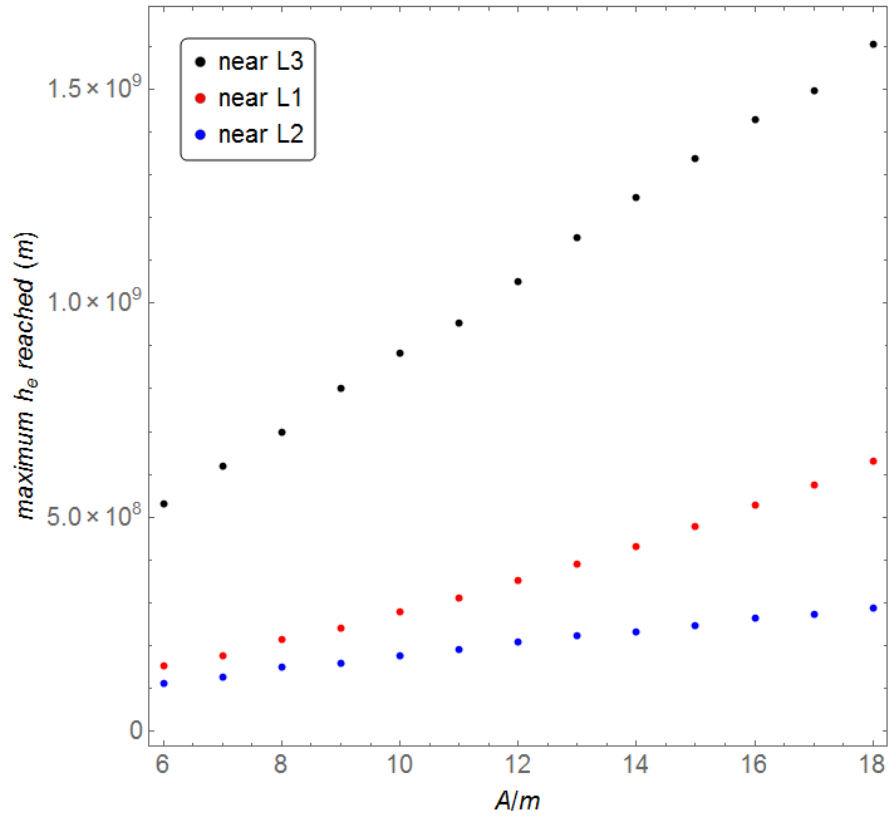
SOURCE: Author's production.

Figure 5.6 - Black dots represent the solutions sets for $\frac{A}{m} = 8, 10, 12, 14, 16$ and $18 \ \frac{m^2}{kg}$, respectively, in each plot. The red straight line represents the radius of the Sun. The green straight line connects the maximum value of h_e reached near L_3 to the center of the Earth. The blue straight line connects the maximum value for h_e reached near L_3 to the maximum value for h_e reached near L_1. Note that the solutions sets near $x_e/R \approx -1$ form a black column near L_3, the solutions sets near $x_e/R \approx 0.99$ form a black column near L_1, and the solutions sets near $x_e/R \approx 1.01$ form a black column near L_2. These columns are better detailed in Figs. 5.2-5.4.
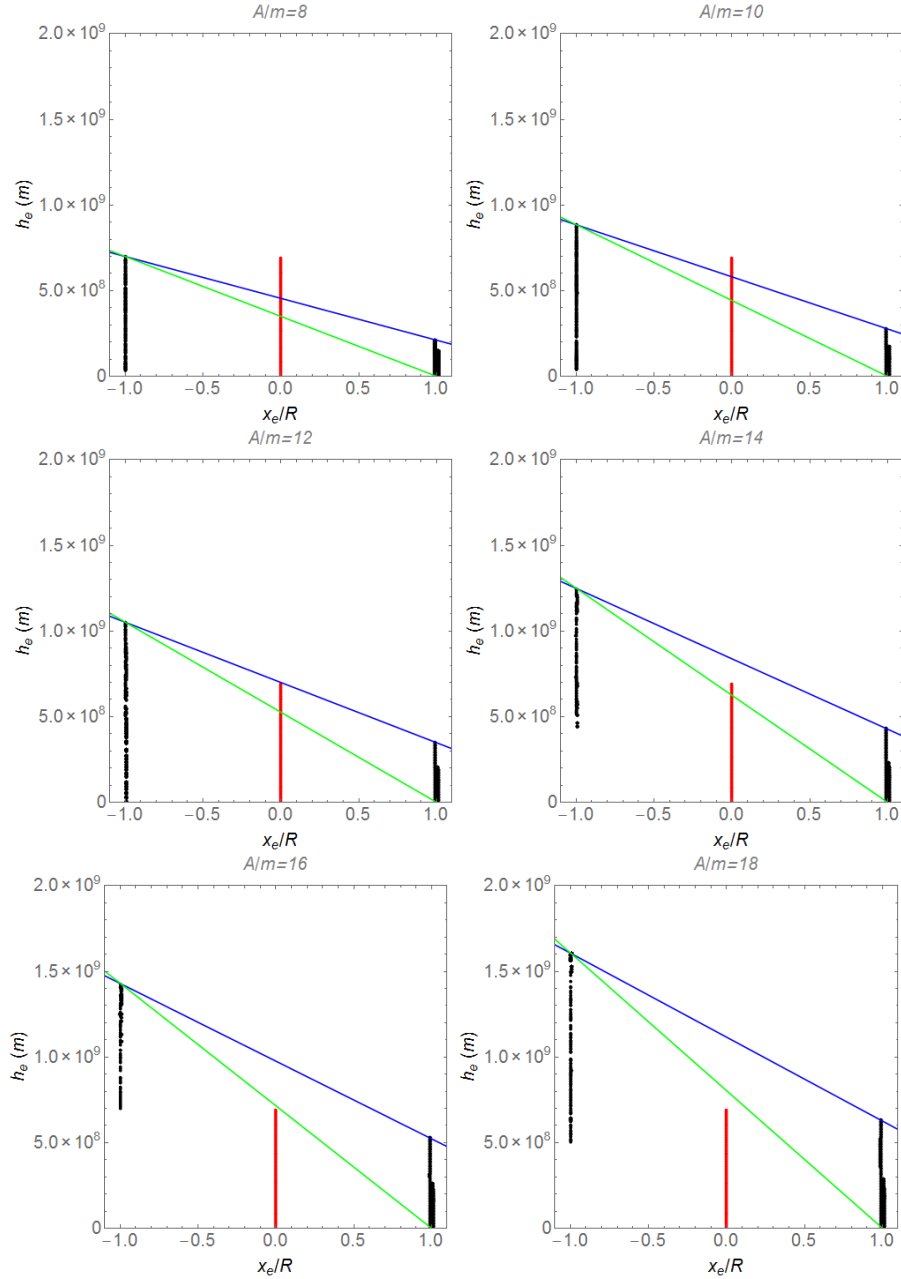
SOURCE: Author's production.

5.3.1 Communication solution 1

As mentioned before, three classes of solutions are shown to solve the communication problem. The first of them requires a spacecraft with a ratio area-to-mass $\frac{A}{m} = 16\frac{m^2}{kg}$ or more, because the spacecraft near L_3 placed in the (x, z) plane must have a coordinate in the z axis to be at least $1.4 \times 10^9 m$ to communicate directly with the Earth, as can be seen from Fig. 5.5. Figure 5.6 ($\frac{A}{m} = 16$) shows that the green straight line connects the solution point with the highest value for h_e near L_3 to the Earth. This green straight line does not cross the radius of the Sun, thus the spacecraft located in this solution can communicate freely with the Earth. Figure 5.7 shows a drawing for this kind of solution.

Figure 5.7 - Geometry of the communication solution 1. The communication electromagnetic waves path does not cross the radius of the Sun.
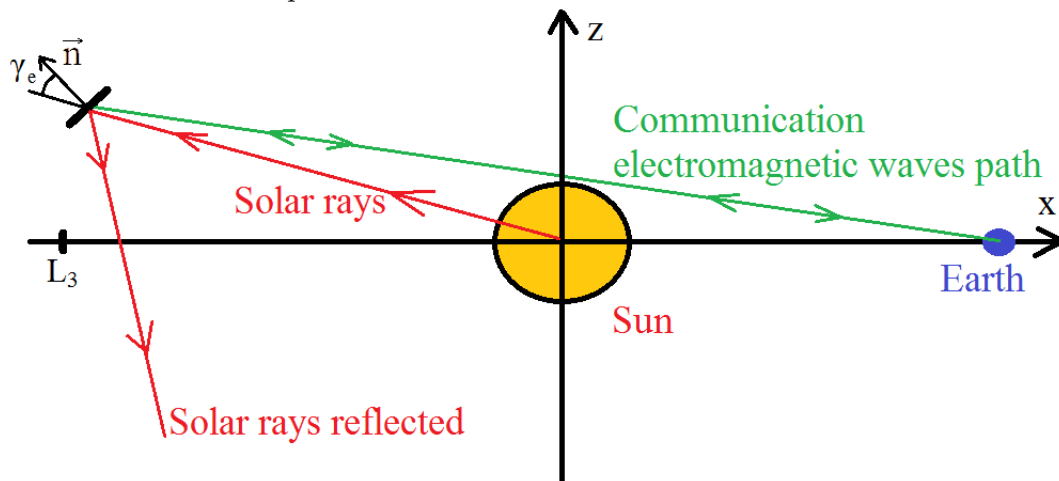
SOURCE: Author's production.

The advantage of this solution is that it is satisfied with just one spacecraft, to the expense of a large area-to-mass vehicle. To have an idea of this ratio, a spacecraft with 100 kg would require an area of 1600 m^2, which means a square sail with each side measuring 40 meters. The solar sail of the spacecraft for the Ikaros mission had approximately a square sail with 14 m each side (TSUDA et al., 2013).

It is important to mention that a large area for the sail may have some advantages, depending on the goal of the mission. It can be used to get solar energy, so reducing or eliminating the need of a power supply. There are also some important observations

related to the flux of particles in the space that requires a large surface to collect the particles (WILLIAMS, 2003). Thus, the effort to build a large solar sail is not only used to shift the equilibrium point. The values of the parameters and the position of the spacecraft near L_3 used for this kind of solution are given in Table 5.2.

Table 5.2 - Parameters and positions used in communication solution 1.

	Spacecraft near L_3
$\frac{A}{m}$	$16\frac{m^2}{kg}$
x_e	$-1.48897776339213\ 10^{11}m \approx -0.995R$
h_e	$1.428\ 10^9 m$
γ_e	0.595011210480688

5.3.2 Communication solution 2

The second alternative to solve the problem uses two spacecraft equipped with solar sails to keep the equilibrium condition (Eq. (5.7)) at very different positions. This kind of solution requires two spacecraft with ratio $\frac{A}{m} = 12\ \frac{m^2}{kg}$. One of them is positioned in the solution point with the maximum value for h_e near L_3 and the other one in the solution point with the maximum value for h_e near L_1. The geometry of this solution is shown in Fig. 5.8.

Figure 5.8 - Drawing of the communication solution 2. The spacecraft 2 acts as a communication bridge between Earth and spacecraft 1 near L_3.
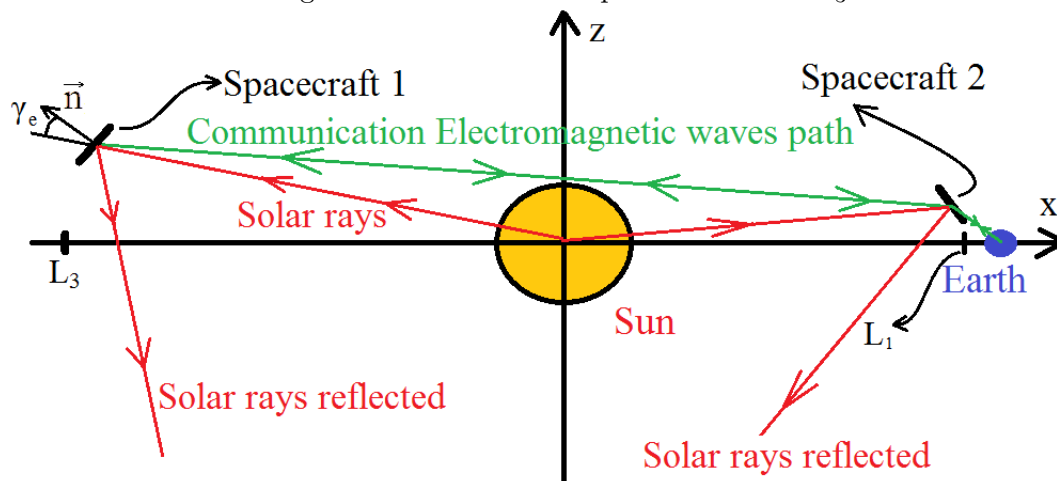
SOURCE: Author's production.

The blue straight lines of Fig. 5.6 ($\frac{A}{m} = 12$) represents the path of the electromagnetic wave used for communication between both spacecraft. This path does not cross the radius of the Sun, then both spacecraft can communicate with each other freely. The spacecraft near L_1 can communicate with the Earth directly, consequently it works as a communication bridge between the spacecraft located near L_3 and the Earth.

This type of solution requires two spacecraft, but each of them with a smaller A/m compared with the first type of solution. Having two spacecraft helps to make observations from two different points in space, which can be interesting for the mission itself, not only to reduce the A/m ratio. On the other hand, it requires two equipments, increasing the costs and the risks of failures. Of course there is also an infinite number of combinations of solutions of this type, because both spacecraft may not have the same area-to-mass ratio. The best combination depends on other constraints coming from the mission. This is an interesting flexibility for mission designers. The parameters and the position of the spacecraft near L_3 and L_1 used for this solution are given by Table 5.3.

Table 5.3 - Parameters and positions used in communication solution 2.

	Spacecraft near L_3	Spacecraft near L_1
$\frac{A}{m}$	$12\frac{m^2}{kg}$	$12\frac{m^2}{kg}$
x_e	$-1.49175472073972\ 10^{11}m \approx -0.997R$	$1.47905589503409\ 10^{11}m \approx 0.989R$
h_e	$1.051\ 10^9 m$	$3.56\ 10^8 m$
γ_e	0.689928275818861	0.5150135706943621

5.3.3 Communication solution 3

The third kind of solution involves two spacecraft with the same area and mass, both near L_3, positioned as shown in Fig. 5.9. The spacecraft 1 is located above the x axis with the z coordinate equals to h_e and the spacecraft 2 is located symmetrically opposite, below the x axis, with z coordinate equals to $-h_e$. The angle γ_e of both spacecraft are such that the reflected solar rays go vertically directly to the other spacecraft, which stays symmetrically opposite positioned in the z axis, as shown in Fig. 5.9. This is the reason why the parameter γ_e is not an independent variable anymore. In this configuration, the spacecraft can interact with each other through the reflected solar rays. In this figure, the second spacecraft is subjected to part of the projected area of the first spacecraft over the second (and vice versa) and the total distance of the rays that come from the Sun and are reflected from the other

spacecraft is $\sqrt{x_e^2 + h_e^2} + 2h_e$. Then, the total force due to the solar radiation pressure over each spacecraft is the one that comes from these rays reflected by the other spacecraft plus the force due to the rays that comes normally directly from the Sun. The resultant force due to the solar radiation pressure is almost doubled in each spacecraft, in comparison with the configuration with a single spacecraft alone.

Figure 5.9 - Drawing of the solution 3. Solar rays that hit each spacecraft are reflected in the direction of the other spacecraft. The resultant force due to the solar radiation pressure is doubled in the spacecraft.
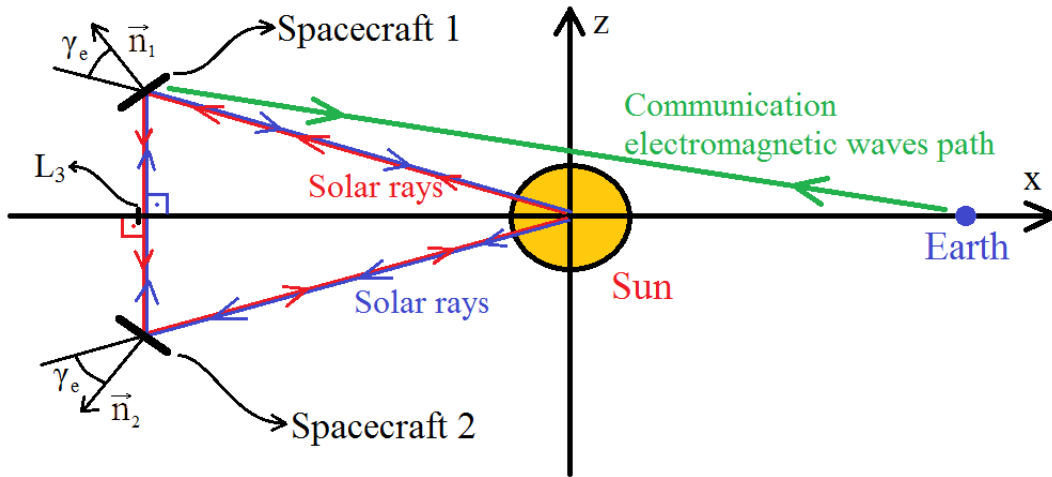
SOURCE: Author's production.

In comparison with the other types of solution, communication solution 3 demands a considerable smaller ratio A/m, just $9 \frac{m^2}{kg}$, but it also requires an almost perfect planar solar sail in order to make reflection towards a distance equals to $2h_e$ in the direction of the other spacecraft. In comparison with the first type of solution, for a fixed mass, the area of the solar sail is almost halved. The angle γ_e must be controlled almost perfectly to make the reflected rays to hit the other spacecraft. This kind of solution requires high precise technologies to be implemented. Table 5.4 shows the values for the positions and parameters for the spacecraft 1 and 2, in the configuration given by this third kind of communication solution. The technology for such high accuracy may not be available now, but the idea of the present chapter is to show this potential possibility for the future, as well as to compare this solution with the other two solutions previously showed.

132

Table 5.4 - Parameters and positions for spacecraft 1 and 2 used in communication solution 3.

	Spacecraft 1 (above the x axis):	Spacecraft 2 (below the x axis):
$\frac{A}{m}$	$9\ \frac{m^2}{kg}$	equals spacecraft 1
x_e	$-1.49110398621742\ 10^{11}m \approx -0.997R$	equals spacecraft 1
h_e	$1.45241181117863\ 10^9 m$	$-1.45241181117863\ 10^9 m$
γ_e	0.780528060797507	equals spacecraft 1

The maximum value reached for a spacecraft for h_e for a given ratio A/m is significantly increased (almost doubled) for the configuration of the spacecraft given in communication solution 3 in comparison with the other previously given solutions, as shown in Fig. 5.10.

Figure 5.10 - Color dots are the solutions sets in the (x, z) plane represented by the values h_e and x_e/R, for the respective values of the parameter A/m $(\frac{m^2}{kg})$ near L_3 for the communication solution 3.
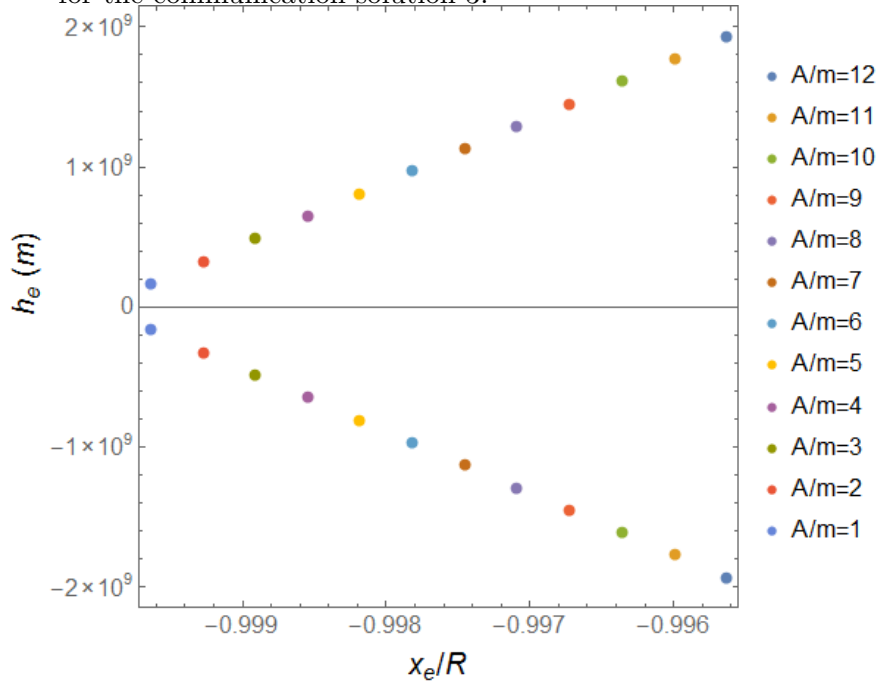
SOURCE: Author's production.

This kind of solution uses two spacecraft with the same ratio A/m with symmetry

in the z axis with respect to the x axis in the (x, z) plane, so, both spacecraft can communicate directly with Earth. Solutions in the (x, z) plane with different ratio A/m could also be searched. For example, the main and heaviest spacecraft (with smaller ratio A/m) could be positioned in an artificial equilibrium point below the x axis, right close to it, and the other spacecraft positioned with larger value for $|h_e|$, such that this last spacecraft could serve as a bridge for communications between the first spacecraft and the Earth. Of course the exactly positions would depend on all the parameters of each spacecraft, including γ_e, but this can also be an interesting flexibility for mission designers.

Additionally, this kind of solution is not restricted to place a spacecraft near L_3. As an example of an expansion of this idea, two spacecraft can be placed around the Earth, one below the Ecliptic plane and the other one symmetrically opposite placed above the Ecliptic plane. The first one would have a permanent contact with the region of low latitude, near the south pole, while the other one would be in permanent contact with the region with high latitude, near the north pole. The idea of maintaining a spacecraft equipped with a solar sail in permanent contact with high latitude regions of the Earth was first presented and patented by Forward (1991), but the kind of solution presented here takes the advantage of two spacecraft with less area-to-mass ratio than just one, as presented by Forward. The maximum value for h_e reached is approximately linearly dependent on the ratio A/m, as shown in Figs. 5.5 and 5.10. The configuration presented in this kind of solution almost doubles the resultant force due to the solar radiation pressure, because Eq. (5.14) replaces Eq. (5.2) for this configuration, therefore the net effect is that the ratio A/m can be almost halved if the objective is to maintain the same value for h_e, in comparison with the solutions with a single spacecraft, like the solution of Forward or the communication solution 1 presented here. Besides that, both of them can simultaneously be useful, one to interact with regions near the south pole and the other one to interact with regions near the north pole. Figure 5.11 illustrates the extension of this kind of solution.

Figure 5.11 - The idea of communication solution 3 applied to permanent observations of both poles of the Earth.
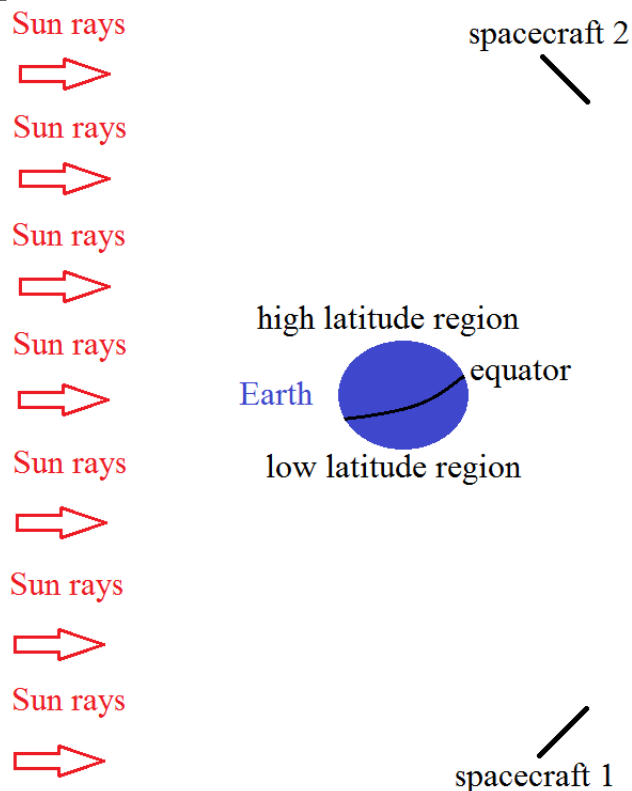
SOURCE: Author's production.

5.4 Considerations

The main purpose of this research is to offer new options of solutions for the communication problem between a spacecraft orbiting the Sun in a point near L_3 and the Earth, in the Sun-Earth system.

The idea is to take advantage of a large solar sail, which can also be used for other purposes of the mission, to find new artificial equilibrium points, which are not behind the Sun when looking from the Earth. A large number of solutions for each given value of the area-to-mass ratio is found. The results showed the exact locations and the attitude of the solar sail for the three collinear equilibrium points.

Three types of solutions are proposed. The first of them uses only one spacecraft, but it requires a large area-to-mass ratio, in the order of $16 \frac{m^2}{kg}$. The second solution uses two spacecraft, each one having a solar sail and located at the artificial equilibrium

points near L_3 and L_1. For this type of solution a ratio $\frac{A}{m} = 12 \ \frac{m^2}{kg}$ is enough to obtain communication. The third kind of solution requires considerable smaller area-to-mass ratio ($\frac{A}{m} = 9 \ \frac{m^2}{kg}$). This solution has high precision technological challenges, but the present chapter has the goal of showing this potential for the future, not considering the details of implementations.

In this way, three options of solutions are shown. Removing the negative aspect of the communication problem, the point L_3 can be better considered for practical applications, in the same way that the other two unstable collinear points (L_1 and L_2) are under consideration for a long time now.

Of course this is a preliminary study, and more sophisticated models for the solar sail can be used to improve the results obtained here. Specific models, including other perturbations, can also be used to calculate new sets of solutions for the three types of communication solutions presented in this research.

6 SOLUTIONS FOR A SPACECRAFT MOTION AROUND ARTIFICIAL EQUILIBRIUM POINTS

The main goal of this chapter is to describe the motion of a spacecraft around an artificial equilibrium point in the circular restricted three-body problem. The spacecraft is under the gravitational influence of the Sun and the Earth, as primary and secondary bodies, subjected to the force due to the solar radiation pressure and some extra perturbations. Analytical solutions for the equations of motion of the spacecraft are found using several methods and for different extra perturbations. These solutions are strictly valid at the artificial equilibrium point, but they are used as approximations to describe the motion around this artificial equilibrium point. As an application of the method, the perturbation due to the gravitational influence of Jupiter and Venus is added to a spacecraft located at a chosen artificial equilibrium point, near the L_3 lagrangian point of the Sun-Earth system. The system is propagated starting from this point using analytical and numerical solutions. Comparisons between analytical-analytical and analytical-numerical solutions for several kinds of perturbations are made to guide the choice of the best analytical solution, with the best accuracy.

6.1 Introduction

The Lagrangian equilibrium points that appear in the restricted three-body problem are convenient for astronautical applications. They are good candidates to place spacecraft, since their equilibrium conditions help to reduce the fuel consumption for station-keeping maneuvers. An interesting application is described in chapter 5, which is the use of one of these points (L_3) in the Sun-Earth system to place a spacecraft. Such spacecraft could help to observe and detect solar activities in the momentary opposite side of the Sun from the perspective of the Earth. Combined with the rotation of the Sun, these detections could improve the prediction of coronal mass ejection in the direction of the Earth weeks in advance. This advantageous point can be useful for many others spacecraft missions, such as collections of particles traveling in space (WILLIAMS, 2003) or for parallax measurements. Even considering these benefits, there are only a few investigations performed to explore this point. One of the reasons is its instability. Another important problem is the strong perturbations coming from other planets, in particular Jupiter and Venus (TANTARDINI et al., 2010). This is specially true during the times that they are closer to this point. The instability problem exists not only for the point itself, but also for the motion around this point (JIANG et al., 2016). This instability is also

present in the other two collinear equilibrium points, called L_1 and L_2, but many real applications are considered for these two points (GOMEZ et al., 1993; JORBA; MASDEMONT, 1999; GOMEZ et al., 1998; KOON et al., 2000; LLIBRE et al., 1985). It is necessary to study options to control this instability, but it can be done using an adequate station-keeping strategy. Among the few studies related to this particular point, it can be mentioned reference (BARRABES; OLLE, 2006), which consider motions around these points, and researches studying transfer orbits (PRADO, 1995; HOU et al., 2007).

In this context and considering the AEP studied in chapters 4 and 5, the actual stage of the research is represented by the goal of searching for solutions for the motion of a spacecraft near an artificial equilibrium point. It is assumed that the spacecraft is subjected to the force coming from the solar radiation pressure, besides the forces given by the circular restricted three-body problem Sun-Earth-spacecraft. It is also considered that the spacecraft is equipped with a solar sail. An adequate choice of the parameters involved in the solar sail, like its attitude, reflectance properties, area, etc, can generate families of locations for these new artificial equilibrium points described before, with some of them lying outside the orbital plane of the Earth. Of course, there is an extra engineering work in building solar sails with large ratio area-to-mass, but they can also be used in scientific experiments, like producing energy or collecting particles traveling in space (WILLIAMS, 2003). Thus, a perturbation is added to the problem through its equations of motion, and then, analytical solutions of these equations are found. Analytical solutions for the equations of motion are found for some different forms of perturbations and through the use of different methods, either direct analytical solution or the analytical solution of the linearized equations of motion. From these analytical solutions, it is possible to study the motion of the spacecraft in details. The method is applied considering the important perturbations coming from Jupiter and Venus or Jupiter only gravitational interactions with the spacecraft located near the L_3 lagrangian point of the Sun-Earth system. These two planets represent the largest forces acting as perturbations over a spacecraft in this location. Hence, specific values of the parameters and perturbations are given. Results coming from the different analytical methods are shown, as well as coming from a numerical method. Thus, the results are compared with each other. These comparisons guide the choice of the best model to be used, as a function of the accuracy desired for the problem and the time span involved.

This stage of the research is written in this chapter and divided as follows. Mathematical models are presented in section 6.2. In subsections 6.2.1-6.2.3, solutions

are found through different methods and forms for the perturbation. In section 6.3, results are obtained for some specific cases shown in subsections 6.3.1-6.3.4. Final considerations of the chapter are shown in section 6.4.

6.2 Formulation of the problem and description of the mathematical models used

Suppose a spacecraft under the gravitational influence of the Sun and the Earth, subjected to a force due to the solar radiation pressure over its sail, and to perturbations from other sources. In a non-inertial rotating frame of reference, that has the Sun fixed in its center and the Earth fixed along the x axis, according Coriolis theorem (SYMON, 1971), the equation of motion of such spacecraft is given by

$$\frac{\mathrm{d}^2 \vec{r}_s}{\mathrm{d}t^2} + 2\vec{\omega} \times \frac{\mathrm{d}\vec{r}_s}{\mathrm{d}t} + \vec{\omega} \times (\vec{\omega} \times \vec{r}_s) + \frac{\mathrm{d}\vec{\omega}}{\mathrm{d}t} \times \vec{r}_s = -\frac{\mu_s}{r_s^3}\vec{r}_s - \frac{\mu_e}{r_e^3}\vec{r}_e + \frac{1}{m}\vec{f}_p + \vec{a}, \quad (6.1)$$

where:
$\vec{\omega}$ is the angular velocity of the rotating frame;
$\vec{r}_s$ is the position of the spacecraft;
$\vec{r}_e$ locates the spacecraft with respect to the Earth;
$\vec{f}_p$ is the force over the solar sail due to the solar radiation pressure;
$\vec{a}$ is the perturbative acceleration vector acting in the spacecraft;
μ_s is the gravitational parameter of the Sun;
μ_e is the gravitational parameter of the Earth.

Figure 6.1 - Geometry of the problem in the rotating frame of reference
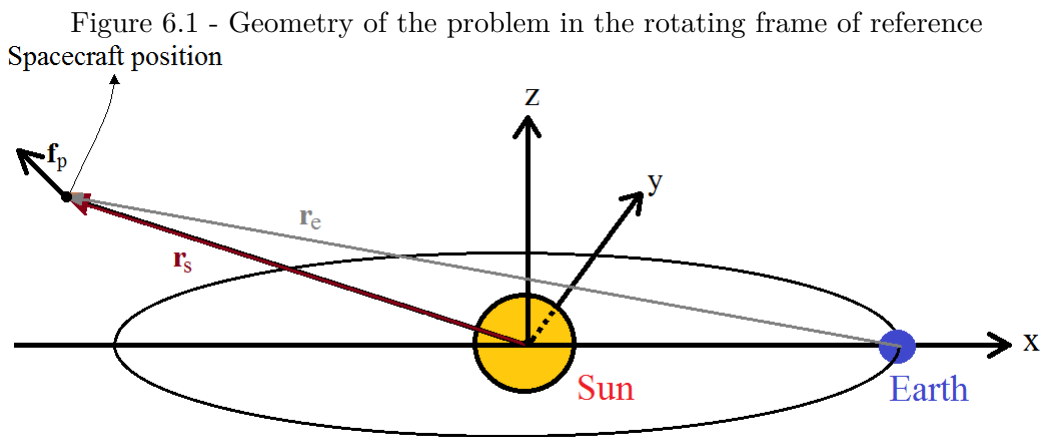
SOURCE: Author's production.

The rotating frame of reference and the geometry of the problem are shown in Fig.6.1, from where it is possible to see the bodies involved (Sun, Earth and spacecraft). The Sun is placed in the center of the reference system, not in the baricenter. For the purpose of this work, the motion of the Earth around the Sun is circular and non-perturbed by any force, which indicates

$$\vec{\omega} = (0, 0, \omega), \tag{6.2}$$

where ω is a constant.

The equation of motion (Eq. (6.1)) now becomes

$$\frac{\mathrm{d}^2 \vec{r}_s}{\mathrm{d}t^2} + 2\vec{\omega} \times \frac{\mathrm{d}\vec{r}_s}{\mathrm{d}t} + \vec{\omega} \times (\vec{\omega} \times \vec{r}_s) = -\frac{\mu_s}{r_s^3}\vec{r}_s - \frac{\mu_e}{r_e^3}\vec{r}_e + \frac{1}{m}\vec{f}_p + \vec{a}. \tag{6.3}$$

The artificial equilibrium point (AEP) is defined by the condition given by

$$\frac{1}{m}\vec{f}_p = \vec{\omega} \times (\vec{\omega} \times \vec{r}_s) + \frac{\mu_s}{r_s^3}\vec{r}_s + \frac{\mu_e}{r_e^3}\vec{r}_e. \tag{6.4}$$

The reason why this condition can be called an AEP will be explained later in this section. If Eq. (6.4) is true, then Eq. (6.3) becomes:

$$\frac{\mathrm{d}^2 \vec{r}_s}{\mathrm{d}t^2} + 2\vec{\omega} \times \frac{\mathrm{d}\vec{r}_s}{\mathrm{d}t} = \vec{a} \tag{6.5}$$

Using Eq. (6.2), the components of Eq. (6.5) can be written as

$$\frac{\mathrm{d}^2 x}{\mathrm{d}t^2} - 2\frac{\mathrm{d}y}{\mathrm{d}t}\omega - a_x(x, y, z, t) = 0, \tag{6.6}$$

$$\frac{\mathrm{d}^2 y}{\mathrm{d}t^2} + 2\frac{\mathrm{d}x}{\mathrm{d}t}\omega - a_y(x, y, z, t) = 0, \tag{6.7}$$

and

$$\frac{\mathrm{d}^2 z}{\mathrm{d}t^2} - a_z(x, y, z, t) = 0, \tag{6.8}$$

where x, y and z are the components of the position vector $\vec{r}_s$ and $a_x(x, y, z, t)$, $a_y(x, y, z, t)$ and $a_z(x, y, z, t)$ are the components of the perturbation vector $\vec{a}$ and may depend on the position and time variables.

Equations (6.6)-(6.8) form a set of coupled ordinary differential equations. Depend-

ing on the form of the perturbation vector $\vec{a}$, analytical solutions for these equations may be easily obtained. In the case where the components of the perturbation vector $\vec{a} = (a_x, a_y, a_z)$ is given by

$$a_x = \frac{1}{2\omega}\frac{\mathrm{d}X(x)}{\mathrm{d}t} + Y(y) + T_x(t) \tag{6.9}$$

$$a_y = X(x) - \frac{1}{2\omega}\frac{\mathrm{d}Y(y)}{\mathrm{d}t} + T_y(t) \tag{6.10}$$

and

$$a_z = Z(z) + T_z(t), \tag{6.11}$$

where $X(x)$, $Y(y)$, and $Z(z)$ are any functions of x, y, and z only, respectively, and $T_x(t)$, $T_y(t)$, and $T_z(t)$ are any explicit functions of time only, then Eqs. (6.6)-(6.8) can be rewritten as

$$\frac{\mathrm{d}^3 x}{\mathrm{d}t^3} + 4\omega^2\frac{\mathrm{d}x}{\mathrm{d}t} - 2\omega X - 2\omega T_y - \frac{1}{2\omega}\frac{\mathrm{d}^2 X}{\mathrm{d}t^2} - \frac{\mathrm{d}T_x}{\mathrm{d}t} = 0, \tag{6.12}$$

$$\frac{\mathrm{d}^3 y}{\mathrm{d}t^3} + 4\omega^2\frac{\mathrm{d}y}{\mathrm{d}t} + 2\omega Y + 2\omega T_x + \frac{1}{2\omega}\frac{\mathrm{d}^2 Y}{\mathrm{d}t^2} - \frac{\mathrm{d}T_y}{\mathrm{d}t} = 0, \tag{6.13}$$

and

$$\frac{\mathrm{d}^2 z}{\mathrm{d}t^2} - Z - T_z = 0. \tag{6.14}$$

Equations (6.12)-(6.14) form a set of three uncoupled ordinary differential equations. Depending on the form of X, Y, Z, T_x, T_y, and T_z, analytical solutions for these equations may be obtained.

Supposing a perturbation caused by the gravitational interaction of the spacecraft with another planet, it depends on the relative position of the spacecraft with respect to the planet, which means that it depends only on the position of the spacecraft and the time t, since the position of the perturbing planet is usually supposed to be known as a function of time. The major variation of the relative position between the spacecraft and the perturbing planet is due to the variation of the position of the planet itself in the frame of reference, because, in comparison, the displacement of the spacecraft in this same frame of reference is supposed to be small around the AEP. Therefore, it is assumed here the approximation that the perturbing force may be calculated using the relative position between the planet and the AEP. Note that, in this approximation, the advantage that the perturbing force becomes only a function of time t is used in the next solution.

6.2.1 Analytical Solution 1 - perturbation linearly dependent on time

If the gravitational forces (or accelerations) due to Venus and Jupiter are used as an example of perturbation, then this perturbation is a function of the position of the spacecraft and time, because the motion of Venus and Jupiter around the Sun can be predicted as a function of time. The motion is close around the AEP, then the perturbation can be approximated by a function of time only, calculated at the initial position of the spacecraft. More than that, the components of the perturbation are assumed to be linear functions of time in the following forms:

$$a_x(x, y, z, t) = a_x(x_0, y_0, z_0, t) = a_x(x_0, y_0, z_0, 0) + \alpha_x t, \tag{6.15}$$

$$a_y(x, y, z, t) = a_y(x_0, y_0, z_0, t) = a_y(x_0, y_0, z_0, 0) + \alpha_y t, \tag{6.16}$$

and

$$a_z(x, y, z, t) = a_z(x_0, y_0, z_0, t) = a_z(x_0, y_0, z_0, 0) + \alpha_z t, \tag{6.17}$$

where x_0, y_0 and z_0 are the initial position components and α_x, α_y and α_z are assumed to be constants calculated as explained now. For a given time $t = t_f > 0$, the value of the constant α_x is calculated using Eq. (6.15) itself, because the perturbation $a_x(x_0, y_0, z_0, t_f)$ at the time $t = t_f$ and the perturbation $a_x(x_0, y_0, z_0, 0)$ at the time $t = 0$ are assumed to be known. In the same way, Eqs. (6.16) and (6.17) can be used to calculate the values of α_y and α_z, respectively. For brevity and simplicity, instead of using the notation given by Eqs. (6.15-6.17), the perturbation components are written by following the notation

$$a_x = a_{x0} + \alpha_x t, \tag{6.18}$$

$$a_y = a_{y0} + \alpha_y t, \tag{6.19}$$

and

$$a_z = a_{z0} + \alpha_z t, \tag{6.20}$$

where $a_{x0} = a_x(x_0, y_0, z_0, 0)$ and $\alpha_x = \frac{1}{t_f}[a_x(x_0, y_0, z_0, t_f) - a_x(x_0, y_0, z_0, 0)]$ in Eq. (6.18) and analogously for Eqs. (6.19) and (6.20).

If the relations $X(x) = 0$; $Y(y) = 0$; $Z(z) = 0$; $T_x(t) = a_{x0} + \alpha_x t$; $T_y(t) = a_{y0} + \alpha_y t$; and $T_z(t) = a_{z0} + \alpha_z t$ are put into Eqs. (6.9)-(6.11), the components of the perturbation given by Eqs. (6.18)-(6.20) are satisfied. Therefore, using these relations, the uncoupled Eqs. (6.12)-(6.14) becomes

$$\frac{\mathrm{d}^3 x}{\mathrm{d}t^3} + 4\omega^2 \frac{\mathrm{d}x}{\mathrm{d}t} - 2\omega T_y - \frac{\mathrm{d}T_x}{\mathrm{d}t} = 0, \tag{6.21}$$

$$\frac{\mathrm{d}^3 y}{\mathrm{d}t^3} + 4\omega^2 \frac{\mathrm{d}y}{\mathrm{d}t} + 2\omega T_x - \frac{\mathrm{d}T_y}{\mathrm{d}t} = 0, \tag{6.22}$$

and

$$\frac{\mathrm{d}^2 z}{\mathrm{d}t^2} - T_z = 0. \tag{6.23}$$

Equations (6.21)-(6.23) form a set of uncoupled ordinary differential equations. The analytical solution for these equations can be easily obtained and they are written as functions of the initial positions and velocities as

$$
\begin{aligned}
x(t) &= \frac{\sin(2t\omega)\left(-\frac{a_{y0}}{2\omega} + v_{x0} - \frac{\alpha_x}{4\omega^2}\right)}{2\omega} + \frac{\cos(2t\omega)\left(-\frac{a_{x0}}{2\omega} - v_{y0} + \frac{\alpha_y}{4\omega^2}\right)}{2\omega} + \\
&\quad t\left(\frac{a_{y0}}{2\omega} + \frac{\alpha_x}{4\omega^2}\right) + \frac{a_{x0}}{4\omega^2} + \frac{t^2 \alpha_y}{4\omega} + \frac{v_{y0}}{2\omega} + x_0 - \frac{\alpha_y}{8\omega^3},
\end{aligned} \tag{6.24}
$$

$$
\begin{aligned}
y(t) &= \frac{\cos(2t\omega)\left(-\frac{a_{y0}}{2\omega} + v_{x0} - \frac{\alpha_x}{4\omega^2}\right)}{2\omega} + \frac{\sin(2t\omega)\left(\frac{a_{x0}}{2\omega} + v_{y0} - \frac{\alpha_y}{4\omega^2}\right)}{2\omega} + \\
&\quad t\left(\frac{\alpha_y}{4\omega^2} - \frac{a_{x0}}{2\omega}\right) + \frac{a_{y0}}{4\omega^2} - \frac{t^2 \alpha_x}{4\omega} - \frac{v_{x0}}{2\omega} + \frac{\alpha_x}{8\omega^3} + y_0,
\end{aligned} \tag{6.25}
$$

and

$$z(t) = \frac{t^2 a_{z0}}{2} + \frac{t^3 \alpha_z}{6} + t v_{z0} + z_0. \tag{6.26}$$

where $(x_0, y_0, z_0) = (x(0), y(0), z(0))$ and $(v_{x0}, v_{y0}, v_{z0}) = (v_x(0), v_y(0), v_z(0))$ are the position and velocity initial conditions of the motion.

The derivatives with respect to time are the respective velocity components and they are written as

$$
\begin{aligned}
v_x(t) &= \cos(2t\omega)\left(-\frac{a_{y0}}{2\omega} + v_{x0} - \frac{\alpha_x}{4\omega^2}\right) - \\
&\quad \sin(2t\omega)\left(-\frac{a_{x0}}{2\omega} - v_{y0} + \frac{\alpha_y}{4\omega^2}\right) + \frac{a_{y0}}{2\omega} + \frac{t\alpha_y}{2\omega} + \frac{\alpha_x}{4\omega^2},
\end{aligned} \tag{6.27}
$$

$$
\begin{aligned}
v_y(t) &= -\sin(2t\omega)\left(-\frac{a_{y0}}{2\omega} + v_{x0} - \frac{\alpha_x}{4\omega^2}\right) + \\
&\quad \cos(2t\omega)\left(\frac{a_{x0}}{2\omega} + v_{y0} - \frac{\alpha_y}{4\omega^2}\right) - \frac{a_{x0}}{2\omega} - \frac{t\alpha_x}{2\omega} + \frac{\alpha_y}{4\omega^2},
\end{aligned} \tag{6.28}
$$

and

$$v_z(t) = t a_{z0} + \frac{t^2 \alpha_z}{2} + v_{z0}. \tag{6.29}$$

6.2.2 Analytical Solution 2 - constant perturbation

In a simpler and more direct case, the perturbation $\vec{a}$ is a constant vector, calculated at the AEP in the time $t = 0$, being $a_x(x, y, z, t) = a_{x0}$, $a_y(x, y, z, t) = a_{y0}$ and $a_z(x, y, z, t) = a_{z0}$. This is a particular case of the situation shown in subsection 6.2.1, where $\alpha_x = \alpha_y = \alpha_z = 0$. Therefore, using these relations, the solutions given by Eqs. (6.24)-(6.29) becomes

$$
\begin{aligned}
x(t) = \frac{1}{2\omega} \Bigg(& -(v_{y0} + \frac{a_{x0}}{2\omega})\cos(2\omega t) + (v_{x0} - \frac{a_{y0}}{2\omega})\sin(2\omega t) + \\
& a_{y0}t + (v_{y0} + \frac{a_{x0}}{2\omega}) + 2\omega x_0 \Bigg),
\end{aligned}
\tag{6.30}
$$

$$
\begin{aligned}
y(t) = \frac{1}{2\omega} \Bigg(& (v_{x0} - \frac{a_{y0}}{2\omega})\cos(2\omega t) + (v_{y0} + \frac{a_{x0}}{2\omega})\sin(2\omega t) - \\
& a_{x0}t - (v_{x0} - \frac{a_{y0}}{2\omega}) + 2\omega y_0 \Bigg),
\end{aligned}
\tag{6.31}
$$

$$
z(t) = \frac{a_{z0}t^2}{2} + v_{z0}t + z_0,
\tag{6.32}
$$

$$
v_x(t) = (v_{y0} + \frac{a_{x0}}{2\omega})\sin(2\omega t) + (v_{x0} - \frac{a_{y0}}{2\omega})\cos(2\omega t) + \frac{a_{y0}}{2\omega},
\tag{6.33}
$$

$$
v_y(t) = -(v_{x0} - \frac{a_{y0}}{2\omega})\sin(2\omega t) + (v_{y0} + \frac{a_{x0}}{2\omega})\cos(2\omega t) - \frac{a_{x0}}{2\omega},
\tag{6.34}
$$

and

$$
v_z(t) = a_{z0}t + v_{z0}.
\tag{6.35}
$$

Now, an explanation is given for the reason why the condition given by Eq. (6.4) defines an AEP. In a scenario with no perturbation ($a_{x0} = a_{y0} = a_{z0} = 0$), supposing that the initial velocity is given by $(v_{x0}, v_{y0}, v_{z0}) = (0, 0, 0)$, then, if Eq. (6.4) is true, the solutions given by Eqs. (6.30-6.35) are rewritten as

$$
x(t) = x_0
\tag{6.36}
$$

$$
y(t) = y_0
\tag{6.37}
$$

$$
z(t) = z_0
\tag{6.38}
$$

$$v_x(t) = 0 \tag{6.39}$$

$$v_y(t) = 0 \tag{6.40}$$

$$v_z(t) = 0 \tag{6.41}$$

Equations (6.36)-(6.41) show that, if there is no perturbation, the initial velocity is zero and $\vec{f}_p$ is adjusted such that Eq. (6.4) is satisfied at least in a single point (X_0, Y_0, Z_0), then all the components of the accelerations are balanced and the spacecraft would be in a stationary condition at the AEP. Despite the name, it is important to note that an AEP is not only a point in the 3D space, because it also requires other variables (or parameters) implicit in the force function $\vec{f}_p$ to assume values such that Eq. (6.4) is satisfied. In this sense, an AEP is a set of conditions.

A more direct engineering application is found if the force $\vec{f}_p$ due to the solar radiation pressure over the solar sail can be controlled such that Eq. (6.4) is true along all the path. Therefore, the solutions given by Eqs. (6.24)-(6.29) or Eqs. (6.30-6.35) can describe the motion for a linearly time dependent or a constant perturbation, respectively. But, considering an engineering problem, it is common that the force $\vec{f}_p$ can not be controlled during all the time. It means that Eq. (6.4) can not be true along all the path and the solution given by Eqs. (6.24)-(6.29) or Eqs. (6.30)-(6.35) depends on this condition to be valid. However, suppose that Eq. (6.4) is satisfied for a single point, called AEP. If this AEP is the starting point of the motion of a spacecraft, then it is expected that, even if this condition is not satisfied outside the AEP, Eq. (6.5) can describe the motion of the spacecraft around the AEP with some degree of accuracy. The closer the spacecraft is from the AEP, the higher the accuracy.

A similar approximation analysis can be made for the perturbation. Equations (6.24)-(6.29) or (6.30)-(6.35) are valid as solutions of Eqs. (6.6-6.8) only if the perturbation is linearly dependent on the time or is a constant vector. Even if this is not true, with the motion starting at the AEP, it is expected that the analytical solution given by Eqs. (6.24)-(6.29) or (6.30)-(6.35) can describe the motion originated by Eqs. (6.6-6.8) if the perturbation is approximated accordingly, being constant or linearly dependent on time.

6.2.3 Linear Analytical Solution

Analytical solutions for Eqs. (6.6)-(6.8) strictly valid around the AEP can also be obtained using a well known method presented in this subsection (BOYCE; DIPRIMA,

2001). The simpler case of a constant perturbation is used, but this method could also be used to search for solutions in the case of other forms of perturbations. On the other side, as will be shown later, the method presented in this subsection is highly expensive. It requires the evaluation of the eigenvectors of a 6×6 matrix and other expensive steps in order to find the final solution. Despite the costs, the solution obtained through the use of this method will be useful for comparisons and validations of the more direct analytical solutions previously presented. According Eq. (6.3), the equation of motion with no perturbation is

$$\frac{\mathrm{d}^2 \vec{r}_s}{\mathrm{d}t^2} = -2\vec{\omega} \times \frac{\mathrm{d}\vec{r}_s}{\mathrm{d}t} - \vec{\omega} \times (\vec{\omega} \times \vec{r}_s) - \frac{\mu_s}{r_s^3}\vec{r}_s - \frac{\mu_e}{r_e^3}\vec{r}_e + \frac{1}{m}\vec{f}_p. \qquad (6.42)$$

If the velocity components are defined as new variables, this system of three second order ordinary differential equations can be converted in a system of 6 first order ordinary differential equations as

$$\frac{\mathrm{d}\vec{X}}{\mathrm{d}t} = \vec{F}(\vec{X}), \qquad (6.43)$$

where $\vec{X}$ is the vector of the variables and $\vec{F}(\vec{X})$ is the vector that represents the functions of each respective component equation, which are functions of the variables $\vec{X}$.

A vector $\vec{Y}$ is defined as a displacement $\delta\vec{X}$ in the following way: $\vec{Y} = \vec{X} - \vec{X}_{AEP}$, where $\vec{X}_{AEP}$ is the vector $\vec{X}$ calculated at the AEP. Each component of the function vector $\vec{F}(\vec{X})$ can be expanded in Taylor series around the AEP. In this series expansion, if the terms of the components of $\vec{Y}$ of order two or more are neglected, as well as crossed terms among the components of $\vec{Y}$, Eq. (6.43) is said to be linearized around the AEP and the result is written as

$$\frac{\mathrm{d}\vec{Y}}{\mathrm{d}t} = \vec{A}_{6\times6}\vec{Y}, \qquad (6.44)$$

where $\vec{A}_{6\times6}$ is a 6x6 matrix, representing the Jacobian of the function vector $\vec{F}(\vec{X})$, calculated at the AEP. A perturbation may be added to Eq.(6.44) and the result is written as

$$\frac{\mathrm{d}\vec{Y}}{\mathrm{d}t} = \vec{A}_{6\times6}\vec{Y} + \vec{p}_a, \qquad (6.45)$$

146

where $\vec{p_a}$ is the vector due to the perturbation of the system, that comes directly from $\vec{a}$ in Eq. (6.1). The perturbation $\vec{p_a}$ is assumed to be constant for this kind of solution.

Equation (6.45) is known as a system of non-homogeneous coupled linear ordinary differential equations of first order with constant coefficients. As said before, this method is expensive, thus a general solution for general parameters could not be obtained due to the large number of therms contained in the eigenvalues of $\vec{A}_{6\times6}$. On the other hand, if all the values of the parameters are explicitly defined, the analytical solution $\vec{Y}(t)$ of Eq. (6.45) is obtained through the use of the method of combinations of the eigenvectors of $\vec{A}_{6\times6}$ plus a particular solution of this equation, taking into account that the initial conditions are given at the AEP ($\vec{Y_0} = \vec{0}$).

Linear stability analysis for different explicit possible forms of $\vec{f_p}$ could be done using $\vec{A}_{6\times6}$. On the other side, linear stability analysis of AEP in space has already been done in the case of a radial propulsive acceleration (ALIASI et al., 2011) or a general propulsive acceleration (BOMBARDELLI; PELAEZ, 2011).

6.3 Results and Analysis

In this section, the results of the solutions are shown for several more realistic cases, that consider the gravitational perturbations of Jupiter and Venus or just Jupiter. In order to give an estimation of the accuracy of the analytical solutions with the assumptions made by the approximations, numerical simulations of the complete equation of motion (Eq. (6.3)) are used for comparison purposes.

A spacecraft which parameters and positions variables are such that the conditions of an AEP are satisfied near the lagrangian point L_3 of the Sun-Earth system is subjected to the perturbation of the gravitational interaction of Jupiter and Venus in the Epoch December 16, 2016. The equation of motion of such spacecraft is described by Eq. (6.3). An AEP implies that Eq. (6.4) is satisfied. In order to show a more explicit example, suppose that $\vec{f_p}$ given in Eq. (6.4) is the force due to the solar radiation pressure acting over the surface of the solar sail of a spacecraft and it is given by (MCINNES, 2004)

$$\vec{f_p} = \frac{2p_e A R^2 \cos^2(\gamma_e)}{r_s^2}\vec{n}, \tag{6.46}$$

where R is the Sun-Earth distance, p_e is the solar radiation pressure at a distance R from the Sun, A is the total area of the flat solar sail, $\vec{n}$ is the vector normal to

the solar sail and γ_e is the angle between $\vec{n}$ and $\vec{r_s}$.

The values of the parameters used for all the calculations are given in Table 6.1. If the force due to the solar radiation pressure is given by Eq. (6.46), which parameters and variables values are given by Table 6.2, then Eq. (6.4) is satisfied and the spacecraft is located at an AEP.

Table 6.1 - Values of parameters used in this chapter.

$R =$	$1.495978707\ 10^{11}\ m = 1\ au$
$p_e =$	$4.56\ 10^{-6}\ N/m^2$ (MCINNES, 2004)
$\mu_s =$	$1.32712440041\ 10^{20}\ m^3/s^2$ (LUZUM et al., 2011)
$\mu_e =$	$\mu_s/328900.56$ (LUZUM et al., 2011)
$\mu_j =$	$\mu_s/1047.3486$ (LUZUM et al., 2011)
$\mu_v =$	$\mu_s/408523.71$ (LUZUM et al., 2011)

Table 6.2 - Parameter values of the artificial equilibrium point.

$\frac{A}{m} =$	$12\ m^2/kg$
$\gamma_e =$	$0.670259715053405\ rad$
$x_0 =$	$-1.49152431572918\ 10^{11} m$
$y_0 =$	$0\ m$
$z_0 =$	$1.0595\ 10^9 m$

At this equilibrium point, Eq. (6.3) becomes Eq. (6.5). For the analytical solution 2, the perturbations of Jupiter and Venus are considered constant for the integration time, which is a whole day. This time is very short compared to the orbital periods of Venus and Jupiter, so their positions are considered constants for the analytical solution 2 and also for the linear analytical solution. In the case of the analytical solution 1, the perturbation of Venus and Jupiter are calculated at the AEP, but it varies linearly with time. Then, the motion of the spacecraft around the AEP can be determined by the analytical solutions of the equations of motion, which are Eqs. (6.30-6.35), Eqs. (6.24-6.29) and Eq. (6.45). These solutions are exact solutions at the AEP, but they are approximations outside this point. The accuracy of each kind of solution is shown and it is expected to be better when the spacecraft is positioned near the AEP.

For the examples shown here, the spacecraft under the gravitational influence of the

Sun, Earth, Venus and Jupiter is positioned at the AEP according Table 6.2, with initial velocities given by $v_{x0} = v_{y0} = v_{z0} = 0\,m/s$ at the time zero. The evolutions of their respective motion are determined and compared by the analytical solution 1 (Eqs. (6.24-6.29)), the analytical solution 2 (Eqs. (6.30-6.35)), the analytical solution of the linear expansion (solution of Eq. (6.45)) and the numerical solution integrated via Runge Kutta of fourth order, as shown in the next figures.

6.3.1 Case 1 - Jupiter and Venus in 12/16/16

In this first case, the positions of Venus and Jupiter relative to the frame of reference are calculated for the approximated real data (JET PROPULSION LABORATORY, 2018) in the date of 12/16/16. These positions at the initial integration time ($t = 0$) are given by Table 6.3. For the analytical solution 2 and the linear analytical solution, the perturbation is assumed to be constant and its value is calculated at the initial conditions (the AEP and $t = 0$). For the analytical solution 1, the perturbation is calculated at the AEP at the time $t = 0$ and at the AEP at the time $t = t_f$, where t_f is the final integration time. Thus, two steps are needed: one to calculate the values of α for each component of perturbation and another to calculate the values of the solutions. For the numerical solution, the positions of Jupiter and Venus are updated for each step of the numerical integration, so this solution takes into account the influence of the motions of Jupiter and Venus around the Sun into the perturbation of the system.

Table 6.3 - Values of the positions of Jupiter and Venus (JET PROPULSION LABORATORY, 2018) in 12/16/2016 in the rotating frame of reference. The last line shows the total distance from the Sun. All values are given in meters.

coordinate	Jupiter	Venus
x	-166397914578	54185387000
y	-721781287016	93293222036
z	16846403798	-4976020886
$\sqrt{x^2 + y^2 + z^2}$	740905050316	108002047323

There are two sources of errors in the analytical solutions. The displacement of the spacecraft position from the AEP, since the analytical solution assumes that Eq. (6.4) is always true, and the accelerations due to the perturbation, since the analytical solution 2 and the linear analytical solutions are obtained assuming a constant perturbation, while the analytical solution 1 assumes that this perturbation varies linearly with time. In order to know which of them is better to describe

the motion of the spacecraft, the numerical calculations are made considering the perturbation due to the gravitational forces of Jupiter and Venus and updating their values for each integration step for the respective position of the spacecraft, as the solution evolves in time. The updating of the position of Jupiter and Venus in time are obtained through an algorithm given in (JET PROPULSION LABORATORY, 2018). Due to this step update, the numerical solution is closer to reality, among these models.

In order to give an idea of the differences of the solutions at the end of the integration time, a delta function is defined as the analytical minus the numerical solution, for each analytical solution and for each of the components of the position and velocity as functions of time, as shown in Eq. (6.47). Their respective values are shown in Tables (6.4-6.7), always calculated at the final time of the integration interval ($t_f = 86400s$).

$$\Delta x = (x - x_0)\big|_{analytical} - (x - x_0)\big|_{numerical}$$
$$\Delta v_x = v_x\big|_{analytical} - v_x\big|_{numerical}$$
$$\Delta y = (y - y_0)\big|_{analytical} - (y - y_0)\big|_{numerical}$$
$$\Delta v_y = v_y\big|_{analytical} - v_y\big|_{numerical}$$
$$\Delta z = (z - z_0)\big|_{analytical} - (z - z_0)\big|_{numerical}$$
$$\Delta v_z = v_z\big|_{analytical} - v_z\big|_{numerical}. \tag{6.47}$$

The differences between the values of the positions as functions of t and their values in the initial conditions are shown in Fig. 6.2 with the respective values of Δ. The values of the components of the velocity is shown in Fig. 6.3 also with the respective values of Δ. The total components of the perturbation $\vec{a}$ at the AEP are $a_x = 9.1\,10^{-11}\ m/s^2$, $a_y = -2.4\,10^{-7}\ m/s^2$ and $a_z = 5.1\,10^{-9}\ m/s^2$. The large differences among these components explains why the motion is larger in the y axis, as seen in Fig. 6.2. It can be noted, from this figure, that the the analytical and numerical solutions apparently diverge faster for x. They are almost identical for y and they are slightly divergent for z. It can also be noted that, as expected, the solutions are almost coincident for low values of t, starting from a perfect match at $t = 0$. The range of the validity of the analytical solutions depends on the accuracy required. For the example shown in Fig. 6.2, the major difference is in the x component. In the worst case of the x-axis, the errors (differences between analytical and numerical solutions) are bellow $0.2\,m$ in position and $10^{-4}\,m/s$ in velocity in the first $20000\,s$,

which is more than 5 *hours*. This means a result good enough to consider that the analytical equations are useful, even if Eq. (6.4) is true only in a single point, which is the starting point of the motion. Figure 6.2 also shows that the analytical solution 2 and the linear solution are almost coincident with each other and the analytical solution 1 approximates the numerical solution more than the other two options. The solution is better when the curve that represents Δ shown in the right side of Figs. 6.2 and 6.3 is closer to zero. The comparisons among the curves in these figures also indicates that, for the x coordinate, approximately half of the error of the analytical solution 2 and the linear solution are due to the assumption that the perturbations from Venus and Jupiter over the spacecraft are constants.

Figure 6.2 - Case 1 - components of the differences between the position and the initial
position are shown in the three figures of the left side as functions of time
evaluated numerically (red), analytically via solution 1 (blue), analytically via
solution 2 (green) and analytically via linearized equations of motion (black).
The functions Δ defined in Eq. (6.47) are shown in the figures of the right
side for the components of the position. At the time $t = 0$, the spacecraft is
located at the AEP given in Table 6.2 with velocities $v_{x0} = v_{y0} = v_{z0} = 0 \, m/s$.
The motions of the perturbing planets Jupiter and Venus around the Sun are
calculated using JET PROPULSION LABORATORY (2018). Overlays of the
curves may arise hiding firstly the red one in the figures of the left side.
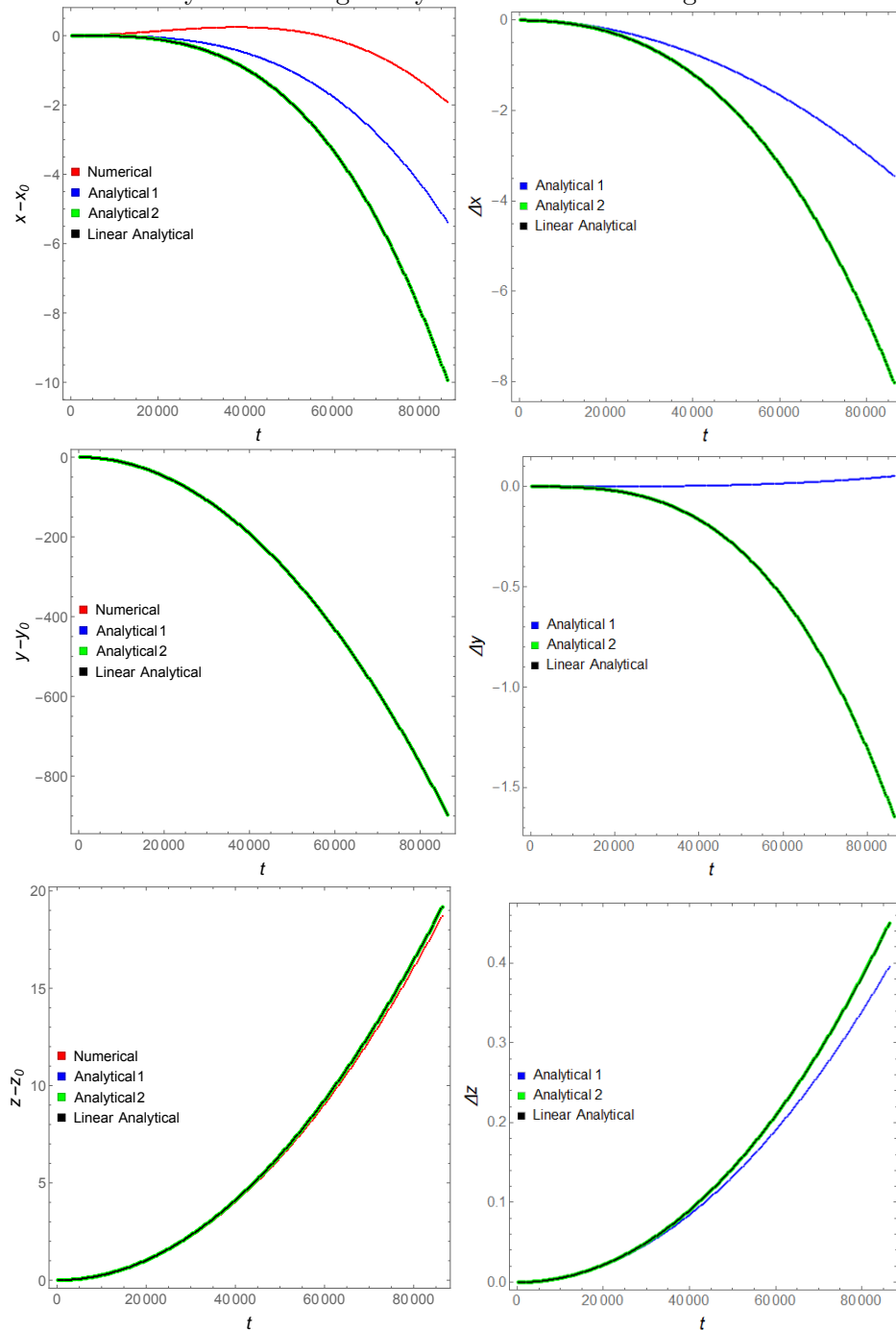
SOURCE: Author's production.

Figure 6.3 - Case 1 - components of the velocity are shown in the three figures of the left side as functions of time evaluated numerically (red), analytically via solution 1 (blue), analytically via solution 2 (green) and analytically via linearized equations of motion (black). The functions Δ defined in Eq. (6.47) are shown in the figures of the right side for the components of the velocity. At the time $t = 0$, the spacecraft is located at the AEP given in Table 6.2 with velocities $v_{x0} = v_{y0} = v_{z0} = 0\ m/s$. The motions of the perturbing planets Jupiter and Venus around the Sun are calculated using JET PROPULSION LABORATORY (2018). Note that overlays of the curves may arise hiding firstly the red one in the figures of the left side.
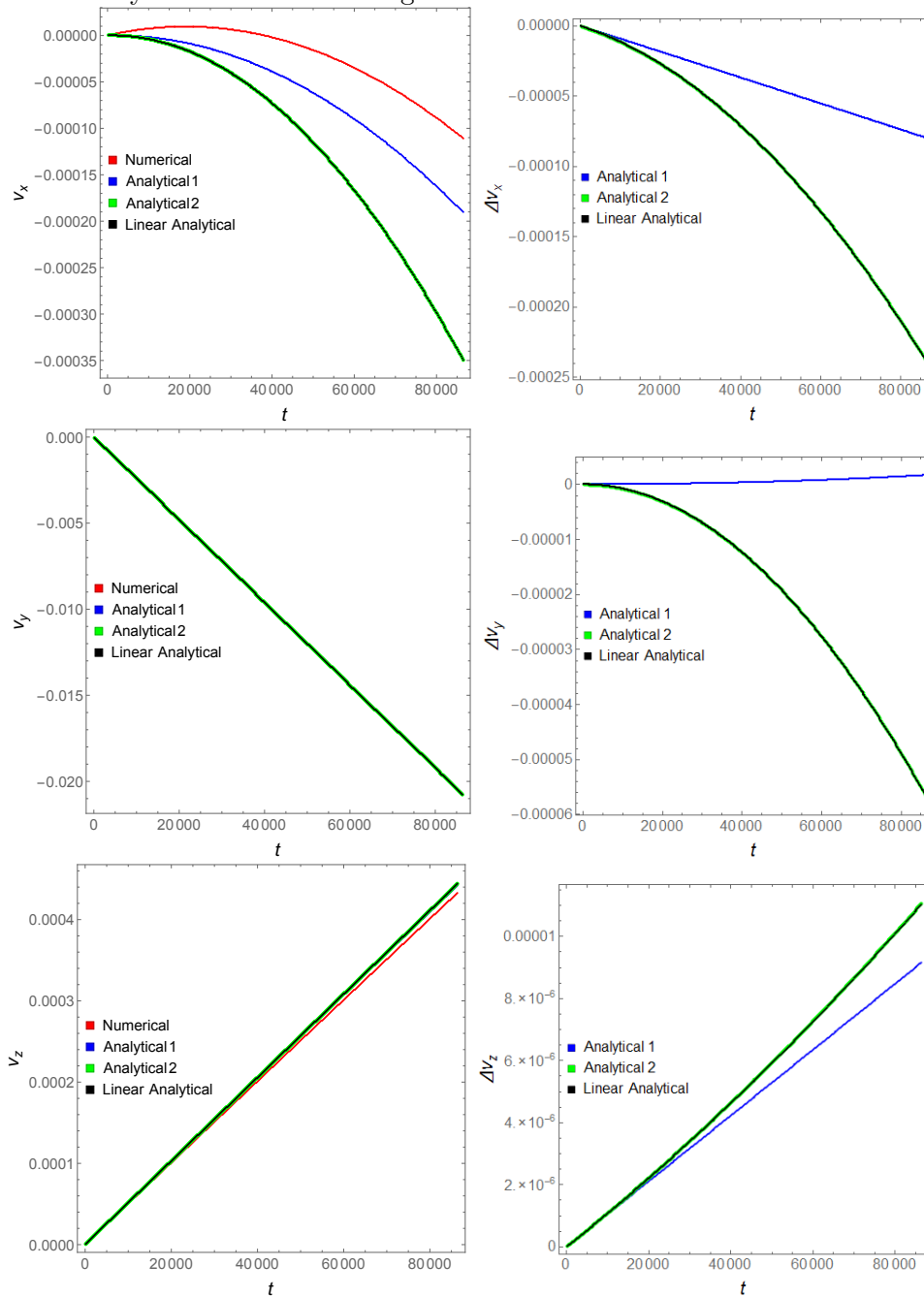
SOURCE: Author's production.

Table 6.4 - Case 1 - delta function of the components of the position and velocity calculated at the time $t_f = 86400s$ for the linear analytical solution, the analytical solution 1 and the analytical solution 2. The perturbations are given by Jupiter and Venus with their respective positions in the date 12/16/2016. The delta function is the difference between the analytical and the numerical solutions. The units are *meters* for the differences of positions and m/s for the differences of velocities.

	Linear Analytical	**Analytical Sol. 2**	**Analytical Sol. 1**
Δx	-8.0141$\times 10^{-0}$	-8.0136$\times 10^{-0}$	-3.4466$\times 10^{-0}$
Δy	-1.6452$\times 10^{-0}$	-1.6454$\times 10^{-0}$	5.2743$\times 10^{-2}$
Δz	0.4496$\times 10^{-0}$	0.4501$\times 10^{-0}$	0.3955$\times 10^{-0}$
Δv_x	-2.3854$\times 10^{-4}$	-2.3851$\times 10^{-4}$	-7.9772$\times 10^{-5}$
Δv_y	-5.6823$\times 10^{-5}$	-5.6832$\times 10^{-5}$	1.6736$\times 10^{-6}$
Δv_z	1.1041$\times 10^{-5}$	1.1062$\times 10^{-5}$	9.1654$\times 10^{-6}$

Table 6.4 indicates that the delta of the analytical solution 1 is the function that tends to get closer to zero, which means that this is the solution closer to the numerical solution, for the given perturbation.

6.3.2 Case 2 - Jupiter and Venus at $(-R_J, 0, 0)$ and $(-R_V, 0, 0)$, respectively

In order to continue the analysis of the influence of the perturbations over the differences between the four kinds of analytical and numerical solutions for more situations, Jupiter is set to be in the nearest position of the spacecraft (located near L_3) in the initial position in the frame of reference $(x, y, z) = (-R_J, 0, 0)$. Venus is also set to be in the nearest position of the spacecraft, so its positions is $(x, y, z) = (-R_V, 0, 0)$, where R_J and R_V are the distance of these planets from the Sun at 12/16/16. The values of R_J and R_V are given by $\sqrt{x^2 + y^2 + z^2}$ in Table 6.3, for each planet. Their motion are assumed to be circular around the Sun with the constant angular velocity given by $\sqrt{\mu_s/R_J^3} - w$ for Jupiter and $\sqrt{\mu_s/R_V^3} - w$ for Venus during the interval of integration time, which is a day ($t_f = 86400\ s$). The results are shown in Fig. 6.4 and Table 6.5, as the difference of the positions as functions of time and the Δ functions.

Figure 6.4 - Case 2 - components of the differences between the position and the initial position are shown in the three figures of the left side as functions of time evaluated numerically (red), analytically via solution 1 (blue), analytically via solution 2 (green) and analytically via linearized equations of motion (black). The functions Δ defined in Eq. (6.47) are shown in the figures of the right side for the components of the position. At the time $t = 0$, the spacecraft is located at the AEP given in Table 6.2 with velocities $v_{x0} = v_{y0} = v_{z0} = 0\ m/s$. Jupiter and Venus are initially positioned at the nearest position to the spacecraft at $(-740905050316, 0, 0)$ and $(-108002047323, 0, 0)$, respectively. Overlays of the curves may arise hiding firstly the red one in the figures of the left side.

Table 6.5 - Case 2 - delta function of the components of the position and velocity cal-
culated at the time $t_f = 86400s$ for the linear analytical solution, the ana-
lytical solution 1 and the analytical solution 2. The perturbations are given
by Jupiter and Venus initially positioned at $t = 0$ in $(-740905050316, 0, 0)$
and $(-108002047323, 0, 0)$, respectively. The delta function is the difference
between the analytical and the numerical solutions. The units are *meters* for
the differences of positions and m/s for the differences of velocities.

	Linear Analytical	Analytical Sol. 2	Analytical Sol. 1
Δx	-3.3263×10^{-0}	-3.2793×10^{-0}	-3.5030×10^{-0}
Δy	-1.9969×10^{-0}	-1.9972×10^{-0}	4.7333×10^{-2}
Δz	0.3896×10^{-0}	0.3890×10^{-0}	0.3994×10^{-0}
Δv_x	-7.4608×10^{-5}	-7.2433×10^{-5}	-7.9996×10^{-5}
Δv_y	-6.9422×10^{-5}	-6.9441×10^{-5}	1.5703×10^{-6}
Δv_z	8.8993×10^{-6}	8.8704×10^{-6}	9.2303×10^{-6}

6.3.3 Case 3 - Jupiter and Venus at $(R_J, 0, 0)$ and $(R_V, 0, 0)$, respectively

The same analysis can be made by changing the position of Jupiter in the frame
of reference to $(x, y, z) = (R_J, 0, 0) = (740905050316, 0, 0)$ and Venus to $(x, y, z) =
(R_V, 0, 0) = (108002047323, 0, 0)$. Their motions around the Sun are also assumed to
be circular with constant angular velocity during the integration time. The results
are shown in Fig. 6.5 and Table 6.6 as the difference of the positions as functions of
time and the Δ functions.

Figure 6.5 - Case 3 - components of the differences between the position and the initial
position are shown in the three figures of the left side as functions of time
evaluated numerically (red), analytically via solution 1 (blue), analytically via
solution 2 (green) and analytically via linearized equations of motion (black).
The functions Δ defined in Eq. (6.47) are shown in the figures of the right side
for the components of the position. At the time $t = 0$, the spacecraft is located
at the AEP given in Table 6.2 with velocities $v_{x0} = v_{y0} = v_{z0} = 0\ m/s$. The
position of Jupiter and Venus at $t = 0$ is $(x, y, z) = (740905050316, 0, 0)$ and
$(x, y, z) = (108002047323, 0, 0)$, respectively. Note that overlays of the curves
may arise hiding firstly the red one in the figures of the left side.

SOURCE: Author's production.

157

Table 6.6 - Case 3 - delta function of the components of the position and velocity calculated at the time $t_f = 86400s$ for the linear analytical solution, the analytical solution 1 and the analytical solution 2. The perturbations are given by Jupiter and Venus initially positioned at $t = 0$ in $(740905050316, 0, 0)$ and $(108002047323, 0, 0)$, respectively. The delta function is the difference between the analytical and the numerical solutions. The units are *meters* for the differences of positions and m/s for the differences of velocities.

	Linear Analytical	Analytical Sol. 2	Analytical Sol. 1
Δx	-3.4025×10^{-0}	-3.4481×10^{-0}	-3.4800×10^{-0}
Δy	2.5986×10^{-0}	2.5989×10^{-0}	3.8396×10^{-2}
Δz	0.3948×10^{-0}	0.3949×10^{-0}	0.3949×10^{-0}
Δv_x	-7.8135×10^{-5}	-8.0242×10^{-5}	-8.1607×10^{-5}
Δv_y	9.0268×10^{-5}	9.0286×10^{-5}	1.3852×10^{-6}
Δv_z	9.1397×10^{-6}	9.1438×10^{-6}	9.1433×10^{-6}

6.3.4   Case 4 - Jupiter only

In order to analyze the behavior of the analytical solutions for a gravitational perturbation caused only by a single planet, the same results obtained before with the perturbations coming from Jupiter and Venus (Figs. 6.2 and 6.3 and Table 6.4) are shown neglecting the Venus gravitational influence over the spacecraft. This means that the perturbation is caused only by the gravitational influence of Jupiter. The results are shown in Fig. 6.6 and in Table 6.7.

Figure 6.6 - Case 4 - components of the differences between the position and the initial
position are shown in the three figures of the left side as functions of time
evaluated numerically (red), analytically via solution 1 (blue), analytically via
solution 2 (green) and analytically via linearized equations of motion (black).
The functions Δ defined in Eq. (6.47) are shown in the figures of the right side
for the components of the position. At the time $t = 0$, the spacecraft is located
at the AEP given in Table 6.2 with velocities $v_{x0} = v_{y0} = v_{z0} = 0 \ m/s$. The
perturbation is given only by the gravitational force of Jupiter calculated using
(JET PROPULSION LABORATORY, 2018). Note that overlays of the curves may
arise hiding firstly the red one in the figures of the left side.
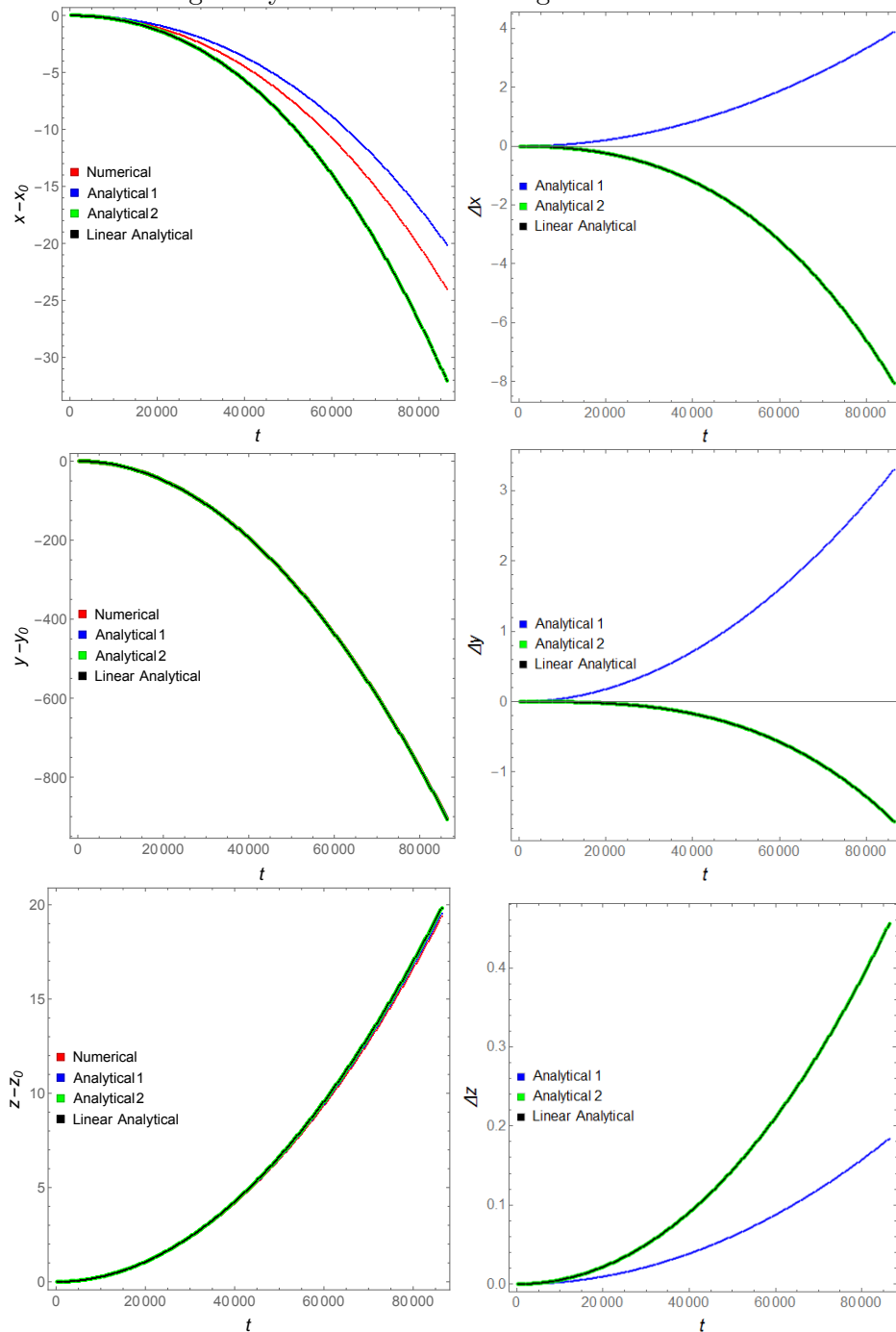
SOURCE: Author's production.

Table 6.7 - Case 4 - delta function of the components of the position and velocity calculated at the time $t_f = 86400s$ for the linear analytical solution, the analytical solution 1 and the analytical solution 2. The perturbation is given only by Jupiter with its respective position in the date 12/16/2016. The delta function is the difference between the analytical and the numerical solutions. The units are *meters* for the differences of positions and m/s for the differences of velocities.
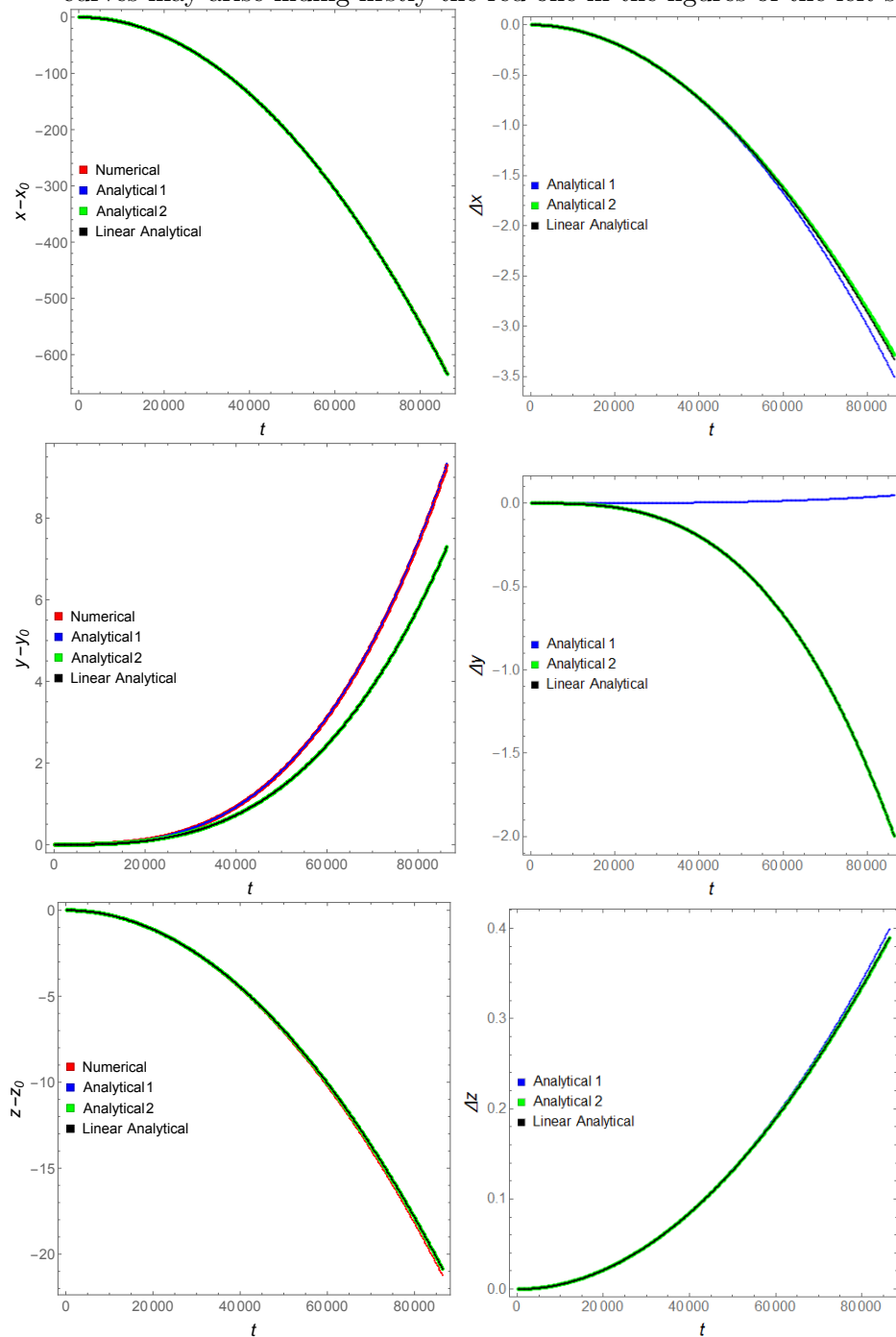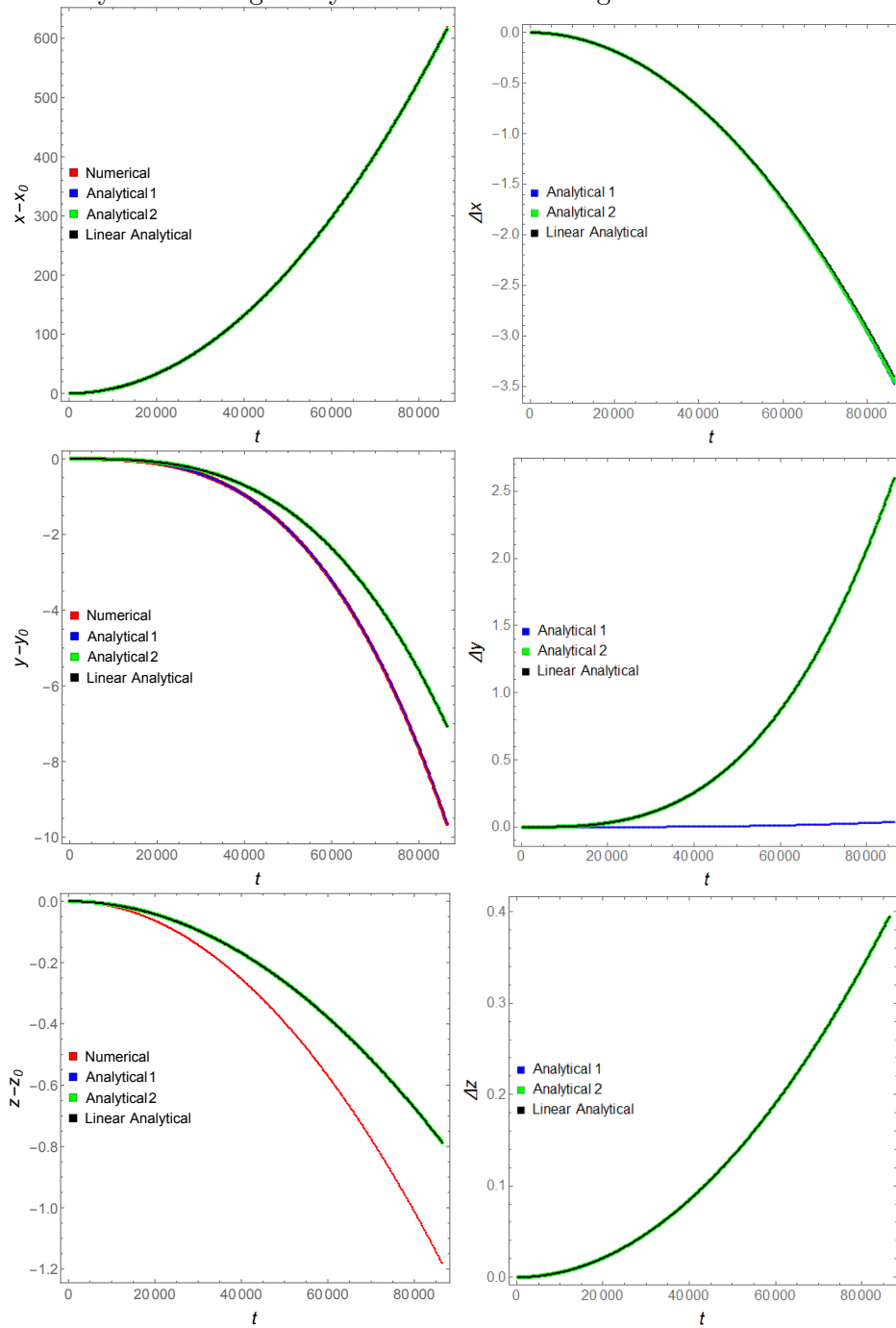
	Linear Analytical	Analytical Sol. 2	Analytical Sol. 1
Δx	-8.0470×10^{-0}	-8.0449×10^{-0}	3.8823×10^{-0}
Δy	-1.6990×10^{-0}	-1.6992×10^{-0}	3.2995×10^{-0}
Δz	0.4558×10^{-0}	0.4563×10^{-0}	0.1840×10^{-0}
Δv_x	-2.3969×10^{-4}	-2.3858×10^{-4}	1.7505×10^{-4}
Δv_y	-5.8687×10^{-5}	-5.8697×10^{-5}	1.1368×10^{-4}
Δv_z	1.1255×10^{-5}	1.1277×10^{-5}	1.8235×10^{-6}

6.4 Considerations

Three kinds of solutions were developed analytically with the objective to describe the motion of a spacecraft around an AEP. The three solutions are analytical 1 (Eqs. (6.24-6.29)), analytical 2 (Eqs. (6.30-6.35)), and the linear analytical (given by the solution of Eq. (6.45)). All of them can describe the motion around the AEP.

The numerical solution is the closest to the reality among the solutions, because it does not use approximations for the condition given by Eq. 6.4 outside the AEP and the values of the perturbations are updated in each small step of the integration time. This means that the definitions given by Eqs. (6.47) for the delta functions allow them to describe the error associated with each one of the analytical solutions found in this research. Of course this error decreases with the decreasing of the time and it tends to zero for shorter integration times. Thus, all the solutions are able to describe the motion of the spacecraft around the AEP with some degree of accuracy, which also means that an error is associated to each one of the analytical solutions outside the AEP. In this research, these errors are estimated for some cases, allowing the reader to analyze the behavior of the error when the system is evolved for a day.

Tables 6.4 - 6.7 show that the maximum absolute values of the delta function are of the order of 1 m for the components of the position and of the order of $10^{-4}m/s$ for the components of the velocity, if the systems are propagated for a whole day. This means that a day of integration time can associate any of the solutions obtained in this research with errors that could fit in the design of some spacecraft missions.

The analytical solution 2 and the linear analytical solution are always practically

coincident for all the positions of Jupiter and Venus used in section 6.3, as can be seen in Figs. 6.2 - 6.6 and Tables 6.4 - 6.7. This is an expected result, since both of them consider the perturbation as a constant of motion. On the other hand, both solutions are obtained through two completely different methods. Linear analytical solution require very complex steps and its final solution $\vec{Y}(t)$ is only found if the parameters are explicit. On the other side, analytical solution 2 takes the advantage of a general solution obtained in a closed form for all values of the parameters.

Tables 6.4 - 6.7 show that the absolute values of the delta function for analytical solution 1 is the one among all analytical solutions that tends to be closer to zero, but there are some exceptions. For the first case, showed in subsection 6.3.1, the absolute values of the delta functions for analytical solution 1 are smaller than both linear analytical and analytical solution 2 for every position and velocity components. For the second case, showed in subsection 6.3.2, Table 6.5 shows that the absolute values of the delta function is slight larger for the analytical solution 1 than others, both for x and z axis components, but all these errors are small if compared to the respective axis displacement. The errors are about 0.5% of the displacement for x and about 2% for z position components. Otherwise, an analysis in the y position components shows that the error is larger for the analytical solution 2 and the linear analytical solution. These errors are larger if compared to the displacement, about 25% of the displacement for the analytical solution 2 and for the linear analytical solution. On the other hand, the comparative error for the analytical solution 1 shows that the error is only about 0.05% of the displacement in the y position components. This fact indicates that, for this case, analytical solution 1 is the best choice. For the third case, showed in subsection 6.3.3, an analysis of Table 6.6 shows quite similar results compared to the second case, except that all the solutions show significant errors for the z position component. The error is about 33% in the displacement, but the z displacement is much smaller for this case than for the other two situations shown before. For the fourth case, showed in subsection 6.3.4, Table 6.7 shows that the absolute values of the delta function for analytical solution 88 is smaller for x and z components position and it is larger for y component position. For the linear analytical solution and analytical solution 2, the errors are: about 26% of the displacement for x coordinate, about 0.17% of the displacement for y coordinate and about 2.3% of the displacement for z coordinate. This same Table shows that the errors for the analytical solution 88 are about 12.6% of the displacement for x coordinate, about 0.33% of the displacement for y coordinate and about 0.9% of the displacement for z coordinate. Again, when the relative error is large, the analytical solution 1 is much better than the other two analytical solutions. All these results

can be also analyzed through Figs. 6.2 - 6.6, because they show the differences between the analytical solutions for all the interval of the integration, not only in the final time. Thus, the conclusion is that the errors of the analytical solution 1 tend to be smaller than the errors of the analytical solution 2, which in turn are quite similar to the errors of the linear analytical solution.

If Eq. (6.4) is satisfied along all the path, then analytical solutions 1 and 2 are exact ones for their respective given perturbations. Moreover, all kinds of analytical solutions presented in this chapter can be considered as approximated ones in more realistic cases, where Eq. (6.4) is satisfied only in the initial conditions of the motion and the perturbations are approximated as constants or linearly dependent on time. In these more realistic cases, the numerical solution is closer to reality. On the other hand, for the numerical calculations, more than a million operations are needed in order to reach the results, while the analytical calculations could be made for any time with less than a thousand operations. An analytical solution can be useful for many purposes, including to lower time computation costs or analytical calculations of station-keeping costs, trajectories, etc.

7 SEARCHING FOR ORBITS TO OBSERVE THE POLES OF CE-LESTIAL BODIES

The objective of the present chapter is to show a method to find orbits near artificial equilibrium points for a satellite equipped with a continuous thrust that allows it to stay near the poles of a celestial body. The physical system includes the presence of a moon of the celestial body under observation, and the perturbation caused by this moon is used to help the satellite to stay close to its original position. Some considerations are made and an analytical solution for the equations of motion is obtained and analyzed. Analogous considerations are applied to the spacecraft. A numerical simulation is obtained, which results are obligated to be find in agreement with the analytical solution using periodic adjustments of the thrust. This agreement means that the motion of the spacecraft remains bounded close to its initial position for long times. Several systems with different sizes and mass parameters are used as examples, like Sun-Earth-Moon, Sun-Ida-Dactyl and Sun-Saturn-Titan systems. The results also indicate the location of the points with minimum thrust required, as well as the total annual increment of velocity required to keep the satellite near its initial position. Several analyzes are made about practical applications of the method.

7.1 Introduction

A new solution describing the spacecraft motion around AEP were shown in the research written in chapter 6. Therefore, once again, new tools are now available to solve further related problems. One of them is explained next.

The restricted three-body problem accepts four different solutions: periodic orbits, quasi-periodic orbits, chaotic orbits, and equilibrium points. In the case of natural solutions, i. e., a system without interference of external forces, the equilibrium points of the restricted three-body problem are the well known Lagrangian points. The collinear points have been used for space missions along the last years, and a more recent example is the James Webb Space Telescope, which is in phase of construction, with a planned date of launch in 2020. This space telescope will be placed in the L_2 Sun-Earth Lagrangian point [1]. Although useful points for space exploration, these points have limitation, since they are always in the plane of the secondary orbit. The use of continuous thrust by the spacecraft can change this restriction, since the use of thrust allows the rise of families of artificial equilibrium points all over the

_____

[1]https://jwst.nasa.gov/orbit.html

space (MCINNES et al., 1994). The type of continuous thrust required to create these points can be generated by engines that require low propellant consumption, like ion engines (GOEBEL; KATZ, 2008), or no propellant consumption at all, by using solar sails (MCINNES, 2004), electric sails (JANHUNEN, 2004; JANHUNEN; SANDROOS, 2007; MENGALI; QUARTA, 2009), magnetic sails (ZUBRIN; ANDREWS, 1991; UENO et al., 2009), or magneto-plasma sails (YAMAKAWA et al., 2006). In previous work (DE ALMEIDA JUNIOR et al., 2017a), AEP located near the Lagrangian point L_3 Sun-Earth, but above and below the Ecliptic plane, were found. These orbits could be a possible solution for the communication problem between Earth and the classical L_3. AEPs out of the Ecliptic plane can also be useful for placing a spacecraft in a region where it can be maintained in constant contact with the poles of a celestial body (FORWARD, 1991). Stable AEP exists only in a region around the triangular Lagrangian points (ALIASI et al., 2011; BOMBARDELLI; PELAEZ, 2011). In order to solve the stability problem, Halo orbits have been found and extensively investigated (FARQUHAR; KAMEL, 1973; HOWELL, 1984). In recent researches, some of these orbits are under study for a satellite equipped with solar sail (FARRÉS; JORBA, 2014; HEILIGERS et al., 2015).

The main objective in this stage of the work is to develop a method to find orbits for a spacecraft equipped with a continuous thrust that allow it to stay near an AEP located above or below the poles of a celestial body for a long period of time, despite its linear stability. This type of artificial equilibrium points is of great importance to place a spacecraft, because it can be used as an observation, communication or research spot. A satellite like that would be perfect to be used in regions near the poles as a "geosynchronous satellite" (FORWARD, 1991), as an option for the satellites placed in Molniya orbits. The gravitational interaction with a third body (which will be called here a moon) will be considered as an additional perturbation. The presence of the third body shall help the spacecraft to keep its location close to the original position. To complete this task, an analytical solution is created by using a new tool (DE ALMEIDA JUNIOR et al., 2018) developed in chapter 6 that requires direct integration of differential equations. Thus, the oscillatory terms of this solution are identified, and the same conditions that were used to the analytical oscillatory solution are applied to the spacecraft. The result of this process is such that the motion of the spacecraft is bounded close to its initial position for a large period of time, considering the perturbation of the moon. Additionally, an estimate about the ratio area-to-mass required to satisfy the generic thrust is shown through a solution using the solar radiation pressure coming from the Sun (primary body) and reflected to the spacecraft through a mirror installed on the surface of the secondary

body.

The last stage of the research is written in this chapter and divided as follows. In section 7.2, an introductory definition is made using the respective mathematical models. The equations of motion are simplified using some considerations and approximations. The analytical solutions for the simplified equations are exactly obtained and analyzed. The same considerations used to simplify the equations are applied to the spacecraft through periodic approximations by slightly changing the thrust. A numerical solution to the complete equations of motion is also obtained. The results are presented in section 7.3 and they show how the numerical solution comes closer to the analytical one, as function of the period in which the thrust is adjusted for three different systems. The final considerations of the chapter are written in section 7.4.

7.2 Mathematical models

Let two main bodies M_1 and M_2 move around their center of mass. The equations of motion of a spacecraft subject to a perturbation, its own thrust and the gravitational interaction with M_1 and M_2 in the rotating reference frame is given by

$$\frac{d^2\vec{r}}{dt^2} + 2\vec{\omega} \times \frac{d\vec{r}}{dt} + \vec{\omega} \times (\vec{\omega} \times \vec{r}) + \frac{d\vec{\omega}}{dt} \times \vec{r} = -\frac{\mu_1}{r_1^3}\vec{r_1} - \frac{\mu_2}{r_2^3}\vec{r_2} + \vec{f_t} + \vec{a}, \qquad (7.1)$$

where: $\vec{r}$ denotes the position of the spacecraft, which coordinates are x, y, z; $\vec{\omega}$ is the angular velocity of the rotating frame of reference; $\vec{r_1}$ is the position of the spacecraft with respect to the body M_1; r_1 is the absolute value of $\vec{r_1}$; $\vec{r_2}$ locates the spacecraft with respect to the body M_2; r_2 is the absolute value of $\vec{r_2}$; $\vec{f_t}$ is an acceleration acting over the spacecraft due to its thrust; μ_1 is the gravitational parameter of M_1; μ_2 is the gravitational parameter of M_2; and $\vec{a}$ is an acceleration due to an additional force. Using $\vec{i}$, $\vec{j}$, and $\vec{k}$ as the unitary vectors along the x, y, and z axes, respectively, and the classic definition of center of mass, the relative positions $\vec{r_1}$ and $\vec{r_2}$ are given by $\vec{r_1} = \vec{r} + x_{M_1}\vec{i}$ and $\vec{r_2} = \vec{r} - x_{M_2}\vec{i}$, where $x_{M_1} = R/(1 + \mu_1/\mu_2)$ and $x_{M_2} = R/(1 + \mu_2/\mu_1)$, with R the distance between the two main bodies. In the case where the motion of the main bodies are circular around their center of mass, Eq. (7.1) becomes

$$\frac{d^2\vec{r}}{dt^2} + 2\vec{\omega} \times \frac{d\vec{r}}{dt} - \omega^2\left(\vec{r} - z\vec{k}\right) = -\frac{\mu_1}{r_1^3}\vec{r_1} - \frac{\mu_2}{r_2^3}\vec{r_2} + \vec{f_t} + \vec{a}. \qquad (7.2)$$

Let a moon of the primary M_2 be in a circular orbit around it, which semi-major axis is R_m and the angular velocity is ω_m. The vector that locates this moon is given by

$$\vec{r}_m = (x_{M_2} + R_m \cos(\omega_m t + \theta))\, \vec{i} + (R_m \sin(\omega_m t + \theta))\, \vec{j}. \qquad (7.3)$$

The main bodies, the moon, and the spacecraft are shown in Fig. 7.1.

Figure 7.1 - The spacecraft and the bodies involved.
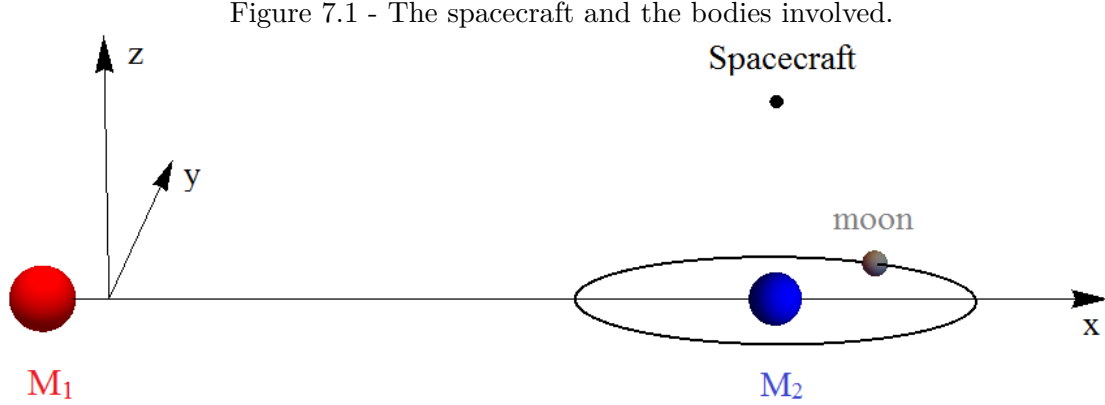
SOURCE: Author's production.

The acceleration over the spacecraft due to its gravitational attraction with the moon is

$$\vec{a} = \frac{\mu_m}{\|\vec{r}_m - \vec{r}\|^3}\, (\vec{r}_m - \vec{r})\,, \qquad (7.4)$$

where μ_m is the gravitational parameter of the moon. Hence, Eq. (7.2) becomes

$$\frac{d^2\vec{r}}{dt^2} + 2\vec{\omega} \times \frac{d\vec{r}}{dt} - \omega^2\left(\vec{r} - z\vec{k}\right) = -\frac{\mu_1}{r_1^3}\vec{r}_1 - \frac{\mu_2}{r_2^3}\vec{r}_2 + \vec{f}_t + \frac{\mu_m}{\|\vec{r}_m - \vec{r}\|^3}\, (\vec{r}_m - \vec{r})\,. \quad (7.5)$$

7.2.1 Analytical solution valid for a short integration time

Let the acceleration $\vec{f}_t$ due to its own thrust applied over the spacecraft be given by

$$\vec{f}_t = \left(-\omega^2\vec{r} + \left(\omega^2 z + \frac{\mu_m}{\|\vec{r}_m - \vec{r}\|^3}z\right)\vec{k} + \frac{\mu_1}{r_1^3}\vec{r}_1 + \frac{\mu_2}{r_2^3}\vec{r}_2\right) \qquad (7.6)$$

at an arbitrary point (x_0, y_0, z_0), which will be called a pseudo artificial equilibrium point (PAEP). The PAEP would be an equilibrium point if only the z component of the perturbation $\vec{a}$ would be taken into account, neglecting the x and y components

166

of this perturbation, which is not possible in the real case. This is the reason why this point is called a PAEP and not an artificial equilibrium point. The components of Eq. (7.2) can be rewritten at the PAEP as

$$\frac{\mathrm{d}^2 x}{\mathrm{d}t^2} - 2\frac{\mathrm{d}y}{\mathrm{d}t}\omega - \left(\frac{\mu_m}{\|\vec{r}_m - \vec{r}\|^3}\left(R_m\cos(\omega_m t + \theta) + (x_{M_2} - x)\right)\right) = 0, \qquad (7.7)$$

$$\frac{\mathrm{d}^2 y}{\mathrm{d}t^2} + 2\frac{\mathrm{d}x}{\mathrm{d}t}\omega - \left(\frac{\mu_m}{\|\vec{r}_m - \vec{r}\|^3}\left(R_m\sin(\omega_m t + \theta) - y\right)\right) = 0, \qquad (7.8)$$

$$\frac{\mathrm{d}^2 z}{\mathrm{d}t^2} = 0. \qquad (7.9)$$

Note that this set of equations is valid only at the PAEP. On the other hand, it can describe the motion around the PAEP with some accuracy (DE ALMEIDA JUNIOR et al., 2018). Let the term $x_{M_2} - x$ of Eq. (7.7) and the term y in right side of Eq. (7.8) be approximated by $x_{M_2} - x_0$ and y_0, respectively. Let the quantity α be defined as $\alpha = R_m\mu_m/\|\vec{r}_m - \vec{r}\|^3$. It is also assumed that α is a constant during the motion, where $\vec{r}$ is evaluated at x_0, y_0, z_0 and $\vec{r}_m$ is evaluated at the initial time of the motion. Due to the fact that the motion of the moon is circular around M_2, this approximation is exact if the satellite is located at any point above M_2, it is also a good approximation for points around it, which is the case that will be explored in the present chapter. Considering the above assumptions, Eqs. (7.7) and (7.8) become

$$\frac{\mathrm{d}^2 x}{\mathrm{d}t^2} - 2\frac{\mathrm{d}y}{\mathrm{d}t}\omega - \alpha\left(\cos(\omega_m t + \theta) + (x_{M_2} - x_0)\right) = 0, \qquad (7.10)$$

$$\frac{\mathrm{d}^2 y}{\mathrm{d}t^2} + 2\frac{\mathrm{d}x}{\mathrm{d}t}\omega - \alpha\left(\sin(\omega_m t + \theta) - y_0\right) = 0, \qquad (7.11)$$

which solutions are exactly given by

$$\begin{aligned} x(t) \;=\; & \frac{1}{4\omega^2\omega_m(\omega_m + 2\omega)}\Bigg[2\alpha\omega\cos(\theta)(\omega_m + 2\omega) + \omega_m\bigg((\omega_m + 2\omega)\Big(\alpha(x_{M_2} - x_0) + \\ & 2\omega(-\alpha t y_0 + v_{y0} + 2x_0\omega) + \sin(2t\omega)(2\omega v_{x0} + \alpha y_0)\Big)\bigg) - (\omega_m + 2\omega)\cos(2t\omega) \\ & \Big(\alpha(x_{M_2} - x_0) + 2\omega v_{y0}\Big) - 2\alpha\omega\cos(\theta - 2t\omega)\bigg) - 4\alpha\omega^2\cos(\theta + t\omega_m)\Bigg], \quad (7.12) \end{aligned}$$

$$y(t) = \frac{1}{4\omega^2 \omega_m (\omega_m + 2\omega)} \Bigg[(\omega_m + 2\omega)\,\omega_m \bigg(-2\omega\,(\alpha t\,(x_{M_2} - x_0) + v_{x0}) +$$

$$\sin(2t\omega)\,(\alpha x_{M_2} + 2\omega v_{y0} - \alpha x_0) + \cos(2t\omega)\,(2\omega v_{x0} + \alpha y_0) - y_0\left(\alpha - 4\omega^2\right) \bigg) +$$

$$2\alpha\omega \sin(\theta) \bigg(-\omega_m \cos(2t\omega) - 2\omega\cos(t\omega_m) + \omega_m + 2\omega \bigg) +$$

$$2\alpha\omega\cos(\theta)\,(\omega_m \sin(2t\omega) - 2\omega\sin(t\omega_m)) \Bigg], \tag{7.13}$$

where $x_0 = x(0)$, $y_0 = y(0)$, $v_{x0} = v_x(0)$, and $v_{y0} = v_y(0)$ are the initial conditions of the motion.

7.2.2 Numerical calculation

The numerical solution is obtained through a direct numerical integration of Eq. (7.5) using a Runge-Kutta method. In this case, the acceleration $\vec{f_t}$ is evaluated at the PAEP using Eq. (7.6) and it is assumed to be constant during every part of the motion.

7.2.3 Chasing the analytical solution

The secular terms present in Eqs. (7.12) and (7.13) are linearly dependent on t and they also depend on the initial position of the motion. These secular terms vanish in the case where the satellite is initially positioned above M_2 at $(x_0, y_0, z_0) = (x_{M_2}, 0, z_0)$. Hence, there will be only oscillatory terms left in the solution. The problem is that this solution requires that Eq. (7.6) is satisfied over all the path. Since Eq. (7.6) is satisfied only at the initial condition of the motion, the analytical solution is valid only for short times of integration. In general, after some time, which may vary depending on the parameters, the numerical solution diverges from the analytical one and the satellite will tend to escape from its initial position. In order to solve this problem, the thrust will be adjusted every period of time such that Eq. (7.6) will be valid again, right after the adjustment. Even in the case where the initial position is not right above M_2, the secular terms are not a problem anymore, because the analytical solution is used again at every period of time.

The process is described next. The analytical solution is used to predict the motion after a given period of time. The new position will be used to slight adjust $\vec{f_t}$, such that Eq. (7.6) is valid again. The new position and velocity will be used as initial conditions to repeat the process for a new period of time. This sequence is repeated as many times as necessary, until the duration of the mission is reveryed. In the

case where the numerical solution is used, the process is the same, except that the integration over every period of time is made using a Runge-Kutta method.

The objective of this method is to force the motion to try to chase the analytical solution, hence the satellite will be kept around the PAEP for a longer time.

7.2.4 Thrust using a solar sail

The acceleration $\vec{f_t}$ can be provided by a solar sail attached to the satellite, due to the solar radiation pressure or other source of photons as (MCINNES, 2004)

$$\vec{f_s} = \beta \frac{A}{m} \frac{k \cos^2(\gamma)}{r_n^2} \vec{n}, \tag{7.14}$$

where β is a positive non-dimensional parameter less than 1 ($\beta = 1$ means a perfect reflection), k is a parameter that depends on the luminosity of the body, A is the area of the flat solar sail, m is the mass of the satellite, $\vec{r_n}$ is the vector that locates the sail with respect to the source of photons, $\vec{n}$ is the vector normal to the solar sail and γ is the angle between $\vec{r_n}$ and $\vec{n}$, which is given according to $\cos \gamma = (\vec{r_n} \cdot \vec{n} / r_n)$. Note that the parameter β is used to represent many forms of practical applications, such as a satellite which reflexivity of its panel can be changed (FUNASE et al., 2011; HUA et al., 2016), as well as a satellite which effective area is adjustable (ROMAGNOLI; OEHLSCHLAGEL, 2011; RODRIGUEZ-SOLANO et al., 2012). This acceleration can be used to keep the satellite at the PAEP. On the other hand, it can be useful even if its magnitude is not large enough to satisfy the magnitude of $\vec{f_t}$, because it is possible to combine this acceleration with a propulsion system.

In the case where the acceleration $\vec{f_t}$ is given totally by the planar solar sail, in order to make the analytical solutions given by Eqs. (7.12) and (7.13) valid, the condition $\vec{f_s} = \vec{f_t}$ must be satisfied at he PAEP. Hence, $\vec{f_t}$ can be calculated at the PAEP using Eq. (7.6), where $\vec{r}$ and $\vec{r_m}$ must be evaluated at an arbitrary point (x_0, y_0, z_0) and in the initial time of the motion, respectively. Let the components of $\vec{f_t}$ be written as $\vec{f_t} = \left(f_x \vec{i} + f_y \vec{j} + f_z \vec{k} \right)$. Hence, the unitary vector normal to the solar sail is given by

$$\vec{n} = \frac{f_x \vec{i} + f_y \vec{j} + f_z \vec{k}}{\sqrt{f_x^2 + f_y^2 + f_z^2}}. \tag{7.15}$$

The value of the parameter k depends on the luminosity of the body. Let k_1 be the value of k in the case where M_1 is the source of photons, then $k_1 = 2 p_e R_e^2$ in the case where the Sun is the source, where R_e is the distance Sun-Earth and

$p_e = 4.56 \times 10^{-6} kg/(ms^2)$ holds for the solar radiation pressure at a distance R_e from the Sun. Therefore, the above conditions require that, at the PAEP, the ratio $\beta A/m$ is given by

$$\beta \frac{A}{m} = \frac{1}{k_1} \frac{\left(f_x^2 + f_y^2 + f_z^2\right)^{\frac{3}{2}} r_1^4}{\left((x + x_1)f_x + yf_y + zf_z\right)^2}. \qquad (7.16)$$

The locations of interest used in this chapter are above M_2, which means that the direction of $\vec{f_t}$ is almost totally given in the z direction, while the vector $\vec{r_1}$ is almost totally given in the x direction. This means that, if M_1 is the source of photons, the force given by Eq. (7.14) is highly attenuated by the term $\cos^2(\gamma)$. A very high value for the ratio A/m is required in order to compensate the attenuation of this term. On the other hand, if this term would not be taken into account, that is, if $\vec{n}$ was positioned in the same direction of the rays, a solar sail with a reasonable ratio area-to-mass could generate an acceleration capable to satisfy the absolute value of $\vec{f_t}$, but with distinct direction. In order to solve this problem, a solution is proposed here where the direction of the rays will be changed at the surface of M_2. It will be assumed that there is a small planar mirror located at M_2, permanently reflecting the rays coming from M_1 to the satellite. The size of this mirror can be of the same order of the area of the satellite. Depending on M_2, which can be a planet or an asteroid, there are engineering challenges to implement this solution (a rolling mirror on it) that will not be discussed here. In the same way, the problems related to point the mirror to the satellite is out of the scope of the present chapter. In the configuration for this solution, the mirror is located at $(x_{M_2}, 0, l)$, where l is the radius of M_2. The vector $\vec{r_A}$ locates the mirror with respect to M_1 and the vector $\vec{r_B}$ locates the solar sail with respect to the mirror. They are written as $\vec{r_A} = (x_{M_2}, 0, l)$ and $\vec{r_B} = (x - x_{M_2}, y, z - l)$. A sketch of this solution is shown in Fig. 7.2.

Figure 7.2 - A solution to redirect the photons coming from M_1 to the solar sail.
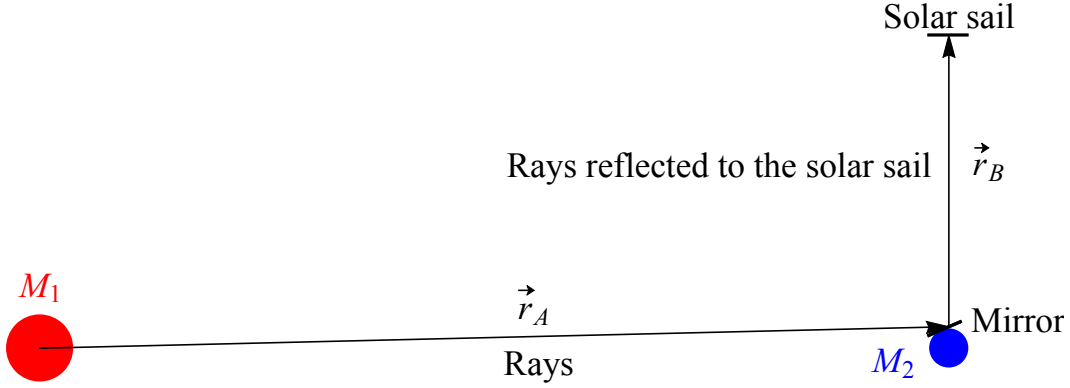
SOURCE: Author's production.

In this solution, the force per unit of mass can be written as

$$\vec{f}_s = \beta \frac{A}{m} \frac{k_1 \cos^2(\gamma)}{(\|\vec{r}_A\| + \|\vec{r}_B\|)^2} \vec{n},$$ (7.17)

where $\cos\gamma = (\vec{r}_B \cdot \vec{n}/\|\vec{r}_B\|)$. The ratio $\beta A/m$ required to satisfy the equilibrium condition is

$$\beta \frac{A}{m} = \frac{1}{k_1 \left(f_z(z-l) + f_x(x - x_{M_2}) + yf_y\right)^2} \left[\left(f_x^2 + f_y^2 + f_z^2\right)^{3/2} \left((x - x_{M_2})^2 + \right.\right.$$

$$\left.\left. y^2 + (l-z)^2\right) \left(\sqrt{l^2 + x_{M_2}^2} + \sqrt{(l-z)^2 + (x - x_{M_2})^2 + y^2}\right)^2 \right].$$ (7.18)

7.3 Results

Let the acceleration $\vec{f}_t$ be slightly adjusted every period of time such that Eq. (7.6) is satisfied at the positions in these discrete periods of time and it remains constant during the motion. The trajectory of the satellite can be evaluated using both the analytical solution given by Eqs. (7.12) and (7.13) or the direct numerical integration of the equations of motion [Eq. (7.5)]. In the numerical case, the vector $\vec{f}_t$ is adjusted at every period of time, such that Eq. (7.6) is satisfied, while the analytical solution is already obtained with the assumption that Eq. (7.6) is satisfied over all the path. After this period of time, the values of the position and velocity are used as initial conditions for the integration during the next same period of time using both solutions.

Let the components of the initial velocity of the motion be $v_{x0} = v_{y0} = v_{z0} = 0$ and the coordinates of the PAEP at $t = 0$ be $(x_0, y_0, z_0) = (x_{M_2}, 0, z_0)$, where x_{M_2} is the x coordinate of the body M_2. Assuming $\theta = 0$, the only parameter left is the altitude z_0, which is the initial distance from M_2. All the other parameters depend on the configurations of the system given by M_1, M_2 and the moon that rotates around M_2. Thus, the satellite is initially located above M_2 with a z_0 coordinate for three different systems: the Sun-Earth-Moon, Sun-Saturn-Titan, and Sun-Ida-Dactyl taking place of M_1-M_2-moon. The absolute value of the force per unit of mass required to maintain the PAEP at $t = 0$ as function of the initial coordinate z_0 is shown for the respective systems, as well as the ratio $\beta A/m$ required to satisfy the PAEP using a solar thrust and a mirror at "the top" of M_2 reflecting the rays towards the satellite for the case of the Sun-Ida-Dactyl, according to the scheme shown in Fig. 7.2. The initial coordinate z_0 is chosen as the one that minimizes the absolute value of the force required to satisfy the PAEP in the case of the Sun-Earth-Moon and Sun-Saturn-Titan systems. In the case of the Sun-Ida-Dactyl system, this coordinate is chosen closer to Dactyl such that its gravitational effect over the trajectories is stronger. Thus, the system is evolved and the projection of trajectories in the x-y plane are shown for the respective system for different period of times that the thrust is adjusted in order to satisfy Eq. (7.6).

7.3.1 Sun-Earth-Moon system

Table 7.1 - Values of the parameters for the Sun-Earth-Moon system.

R	$1.495978707 \times 10^{11}\ m = 1\ AU$
μ_1	$1.32712440041 \times 10^{20}\ m^3/s^2$ (LUZUM et al., 2011)
μ_2	$\mu_1/328900.56$ (LUZUM et al., 2011)
μ_m	$0.0123000371\mu_2$ (PITJEVA; STANDISH, 2009)
R_m	$3.84402 \times 10^8 m$
ω_m	$2\pi/(27.321582\ days)$

In the case where M_1 is the Sun, M_2 is the Earth and the generic moon is the Moon, which parameters are shown in Table 7.1, the absolute value of the force required to satisfy the PAEP [Eq. (7.6)] is shown in Fig. 7.3. The absolute value of the acceleration has a minimum of $\|\vec{f}_t\| = 0.162974 \times 10^{-3} m/s^2$ at $z_0 = 0.01832589841874661\ AU$, where $AU = 149597870700\ m$ is the astronomical unit. This acceleration implies in a total increment in velocity of 5.1 km/s every year. This point is attractive due to the costs of the thrust. It is an indication of

a very good region to place the spacecraft, independent of the control technique to keep it there. This figure also shows the increase in the costs with the value of z_0 in the case of the specifications of the mission do not allow the use of the minimum point. This information is also used in the case of a constellation of spacecraft along the z axis is planned. The implementation of the mirror over M_2 explained in the subsection 7.2.4 may be very difficult for the Sun-Earth-Moon system, a case where M_2 is the Earth, but once this problem is solved, an evaluation using Eq. (7.18) shows that the minimum ratio $\beta A/m$ reveryed is $\beta A/m = 18.53 \ m^2/kg$ at $z_0 = 0.01799601960829353 \ AU$. This type of solution is used here to express that the required amount of force per unit of mass could be reveryed using current technology for the ratio $\beta A/m$ (TSUDA et al., 2013). Alternatively, this force per unit of mass can be reveryed by the use of ionic thrust[2].

Figure 7.3 - The absolute value of $\vec{f_t}$ given by Eq. (7.6) evaluated at the PAEP located at $(x_{M_2}, 0, z_0)$ as a function of z_0 for the Sun-Earth-Moon system.
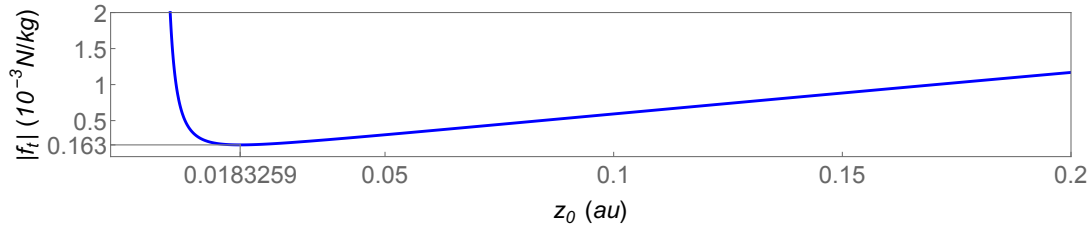
SOURCE: Author's production.

In the case of the Sun-Earth-Moon system, the solution for $x(t)$, $y(t)$, and $z(t)$ are shown in Fig. 7.4 for a fixed period of adjustment of 24 h. The black curve of these figures represent the analytical solution given by Eqs. (7.12) and (7.13), while the red curve represents a numerical integration via Runge-Kutta method of the complete equations of motion [Eq. (7.5)]. The (x, y) coordinates of the trajectories are shown in Fig. 7.5 for one year of integration time using $z_0 = 0.01832589841874661 \ AU$. The blue dots represent the initial position of the motion, while the lighter red and the gray dots represent the final position of the satellite after one year for the numerical an analytical solutions, respectively. The trajectories are changed for different periods of the adjustments where the continuous thrust satisfy Eq. (7.6) at the respective position. These periods vary from no adjustment at all in the top left

---

[2]http://www.adastrarocket.com/aarc/technology

plot of the figure to every hour of adjustment in the bottom right plot of the figure.

Figure 7.4 - Displacements in the x, y, and z directions as function of time in the case of the Sun-Earth-Moon system for a spacecraft initially located at $(x_{M_2}, 0, z_0)$, where $z_0 = 0.01832589841874661\ AU$. The thrust is adjusted every 24 $hours$.

SOURCE: Author's production.

Figure 7.5 - Projection of the trajectories in the x-y plane for 365 days of integration time in the case of the Sun-Earth-Moon system for a spacecraft initially located at $(x_{M_2}, 0, z_0)$, where $z_0 = 0.01832589841874661\ AU$. The thrust is not adjusted in the top left figure and it is adjusted every $90, 30, 7,$ and $1\ days$ and every $1\ h$ in the respective subsequent figures.
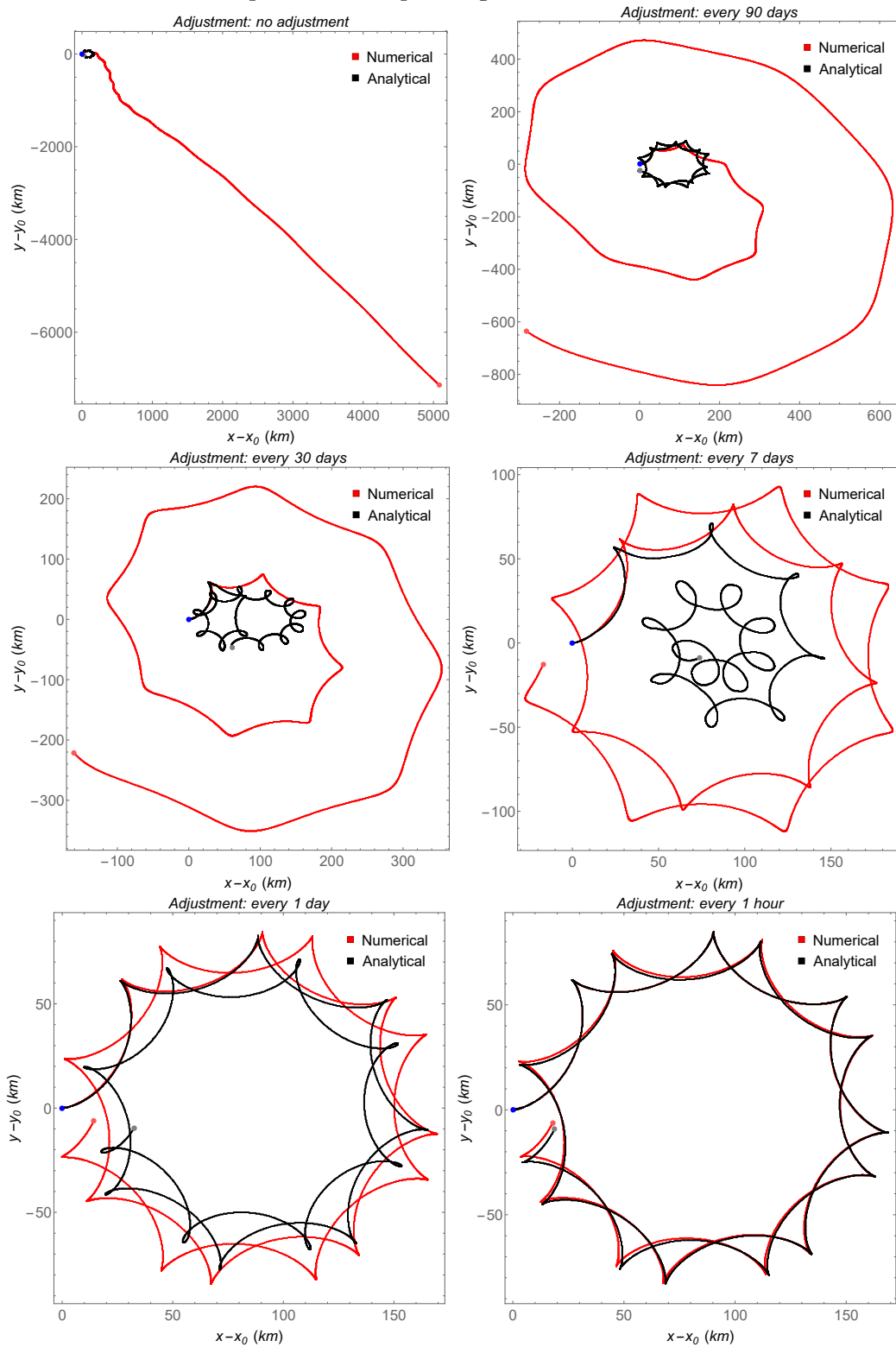
SOURCE: Author's production.

7.3.2 Sun-Ida-Dactyl system

Table 7.2 - Values of the parameters for the Sun-Ida-Dactyl system.

R	2.863914916076813 AU (JET PROPULSION LABORATORY, 2018)
μ_1	$1.32712440041 \times 10^{20} \ m^3/s^2$ (LUZUM et al., 2011)
μ_2	$3 \times 10^6 \ m^3/s^2$ (BELTON et al., 1996)
μ_m	$9 \times 10^{-5} \ \mu_2$ (BELTON et al., 1995)
R_m	90.5 km (BELTON et al., 1996)
ω_m	$-\sqrt{\mu_2/R_m^3}$ (retrograde) (BELTON et al., 1996)

The same procedure used for the Sun-Earth-Moon system in section 7.3.1 is presented in this subsection for the Sun-Ida-Dactyl system, which parameters are given in Table 7.2. The force per unit of mass required to satisfy the PAEP at the initial condition of the motion is shown in the upper side of Fig. 7.6. A solar sail receiving the reflected rays through a mirror at Ida can generate a thrust to satisfy Eq. (7.6) for the ratio $\beta A/m$ shown as function of z_0 in the bottom side of Fig. 7.6. Note, from this figure, that the minimum absolute value of the acceleration or the ratio $\beta A/m$ is reveryed at $z_0 \approx 15.26 \times 10^3 km$. The trajectories are shown in Fig. 7.7 in the case where the z component of the initial position of the satellite is $z_0 = 1000 \ m$ for different periods of adjustments. The numerical trajectories vary from a range of 50 km in the case where there is no adjustment at all to a range closer to the analytical solution near the start position of the motion in the case where the adjustments are made at a period of every hour. It is noted that, in this system, the force per unit of mass is much smaller, due to the smaller dimensions of the bodies involved. The minimum is now $\|\vec{f_t}\| \approx 3.9 \times 10^{-8} N/kg$ at $z_0 \approx 15.26 \times 10^3 \ km$. This value is four orders of magnitude compared to the Sun-Earth-Moon system. The annual Δv defined as $\Delta v_{annual} = \|\vec{f_t}\| \times 1 \ year$ would be approximately equal to $1.2 \times 10^{-3} \ km/s$. These values are very small, and easy to be made using current technology. It means that the idea proposed here is very practical when considering binaries asteroids or other small bodies which mass ratio are much less than one.

Figure 7.6 - The absolute value of $\vec{f_t}$ given by Eq. (7.6) and the ratio $\beta A/m$ given by Eq. (7.18) evaluated at the PAEP located at $(x_{M_2}, 0, z_0)$ as a function of z_0 for the Sun-Ida-Dactyl system.
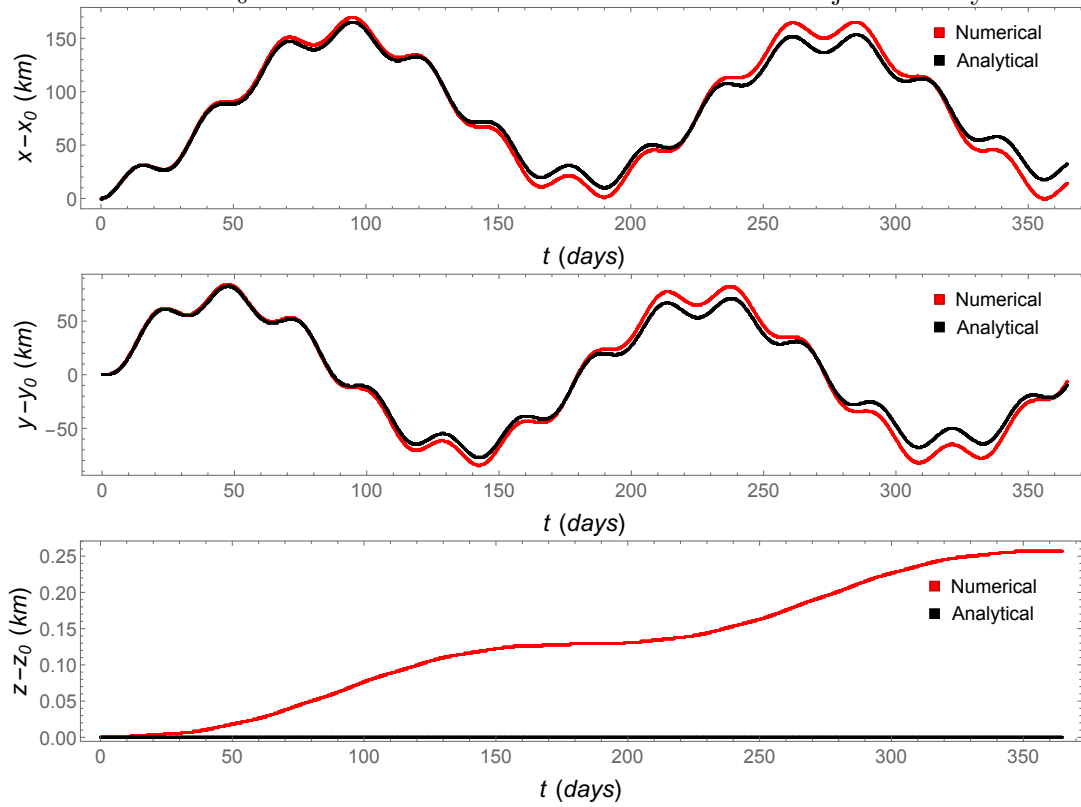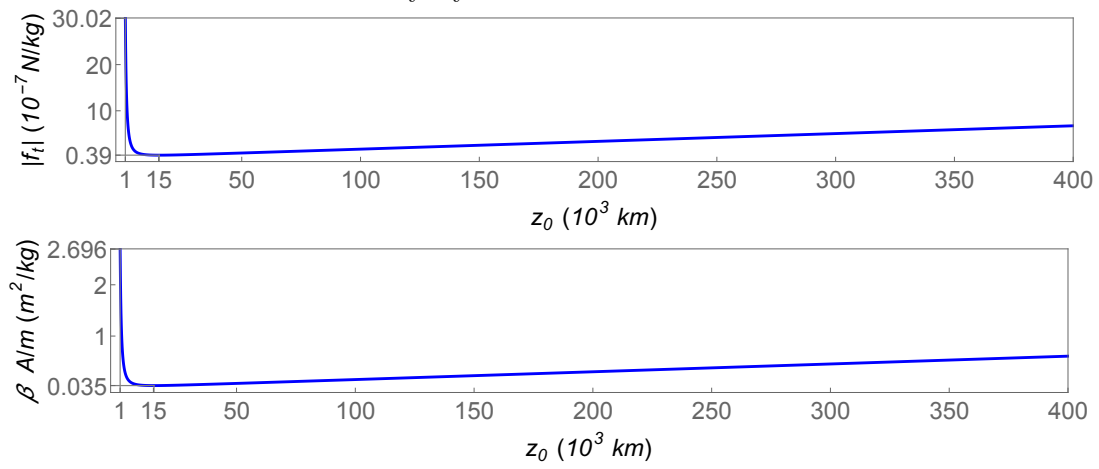

SOURCE: Author's production.

Figure 7.7 - Projection of the trajectories in the x-y plane for 365 days of integration time in the case of the Sun-Ida-Dactyl system for a spacecraft initially located at $(x_{M_2}, 0, z_0)$, where $z_0 = 1000\ km$. The thrust is not adjusted in the top left figure and it is adjusted every $90, 30, 7$, and $1\ days$ and every $1\ h$ in the respective subsequent figures.
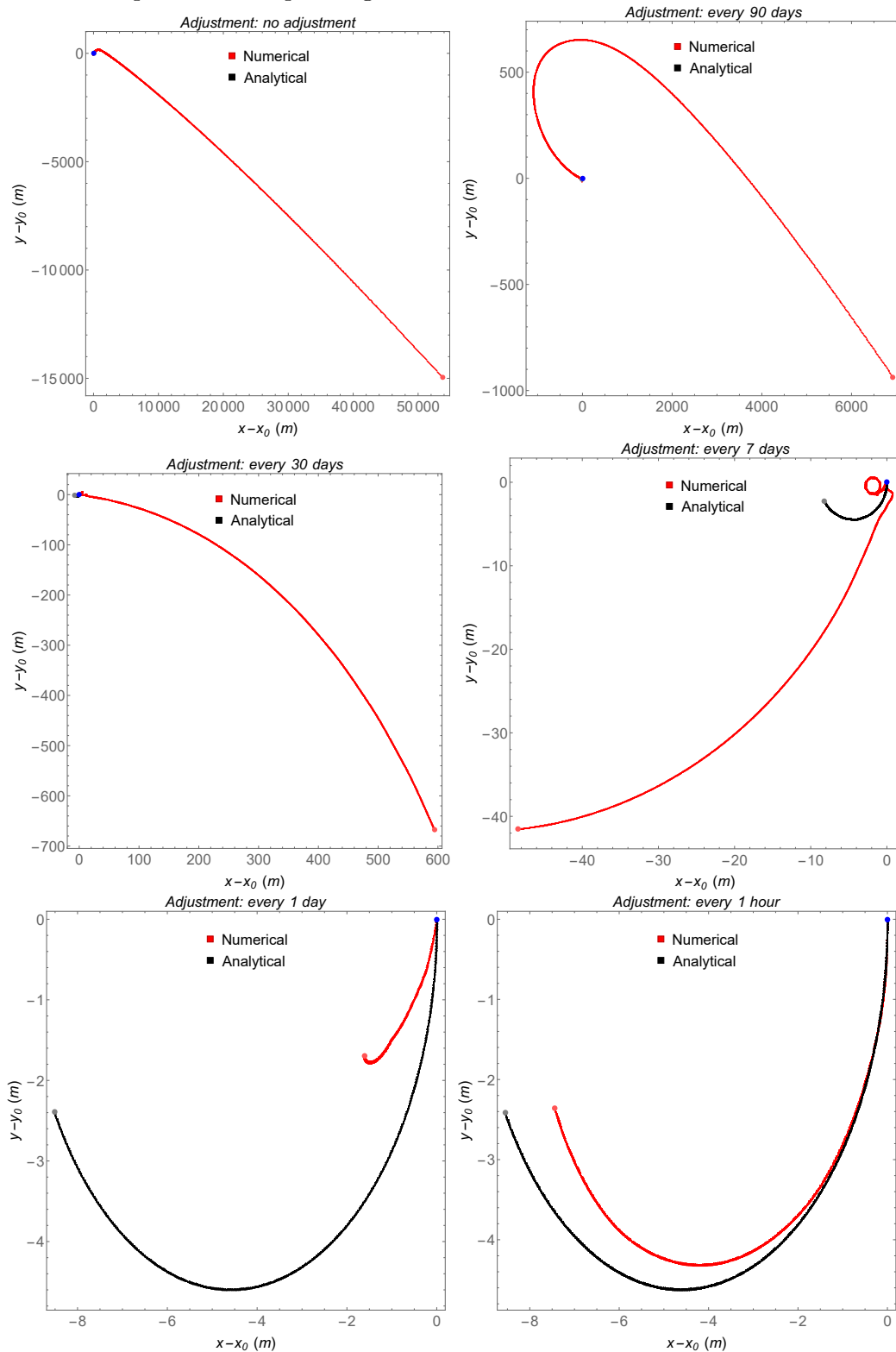
7.3.3 Sun-Saturn-Titan system

Table 7.3 - Values of the parameters for the Sun-Saturn-Titan system.

R	$9.5820172\ AU$
μ_1	$1.32712440041 \times 10^{20}\ m^3/s^2$ (LUZUM et al., 2011)
μ_2	$3.793947517 \times 10^{16}\ m^3/s^2$
μ_m	$8.977972416 \times 10^{12}\ m^3/s^2$
R_m	$1.221870000 \times 10^9 m$
ω_m	$\sqrt{\mu_2/R_m^3}$

The same procedure is used for the Sun-Saturn-Titan system. It is shown in Fig. 7.8 that the minimum value of the absolute value of the acceleration given by Eq. (7.6) is reveryed at $z_0 \approx 0.8\ AU$, which is relatively far from the heavy bodies of Saturn and Titan. On the other side, the absolute value of the acceleration required to satisfy the PAEP is two orders of magnitude less than the minimum for the Sun-Earth-Moon system. It means that the total Δv_{annual} is approximately equal to $0.25285\ km/s$. Note that this value was evaluated at the initial position, hence it is an approximation for the complete trajectory, since the acceleration $\|\vec{f_t}\|$ slightly changes as the spacecraft is displaced from its initial position. It is evaluated at every period of time of the respective adjustments and is constant during these intervals. Evaluating the index Δv at every period of time of the adjustments and adding them, in the case in which the adjustment is made every 1 day, the value of Δv_{annual} is equal to $0.25268\ km/s$. Those values of accelerations and Δv are small, and not difficult to be implemented with current technology. It means that in a system of primaries like that, this concept can be used. In the case where the initial condition is given at the PAEP at $z_0 = 0.7982524313795235\ AU$, the projection of the trajectories in the x-y plane is shown in Fig. 7.9. Due to the large distance of the satellite from the massive bodies, it does not move far away from the initial position in this case, but other value z_0 can also be chosen to bring the numerical solution closer to the analytical one.

Figure 7.8 - The absolute value of $\vec{f_t}$ given by Eq. (7.6) evaluated at the PAEP located at $(x_{M_2}, 0, z_0)$ as a function of z_0 for the Sun-Saturn-Titan system.

SOURCE: Author's production.

Figure 7.9 - Projection of the trajectories in the x-y plane for 365 days of integration time in the case of the Sun-Saturn-Titan system for a spacecraft initially located at $(x_{M_2}, 0, z_0)$, where $z_0 = 0.7982524313795235$ AU. The thrust is not adjusted in the top left figure and it is adjusted every $90, 30, 7$, and 1 $days$ and every 1 h in the respective subsequent figures.
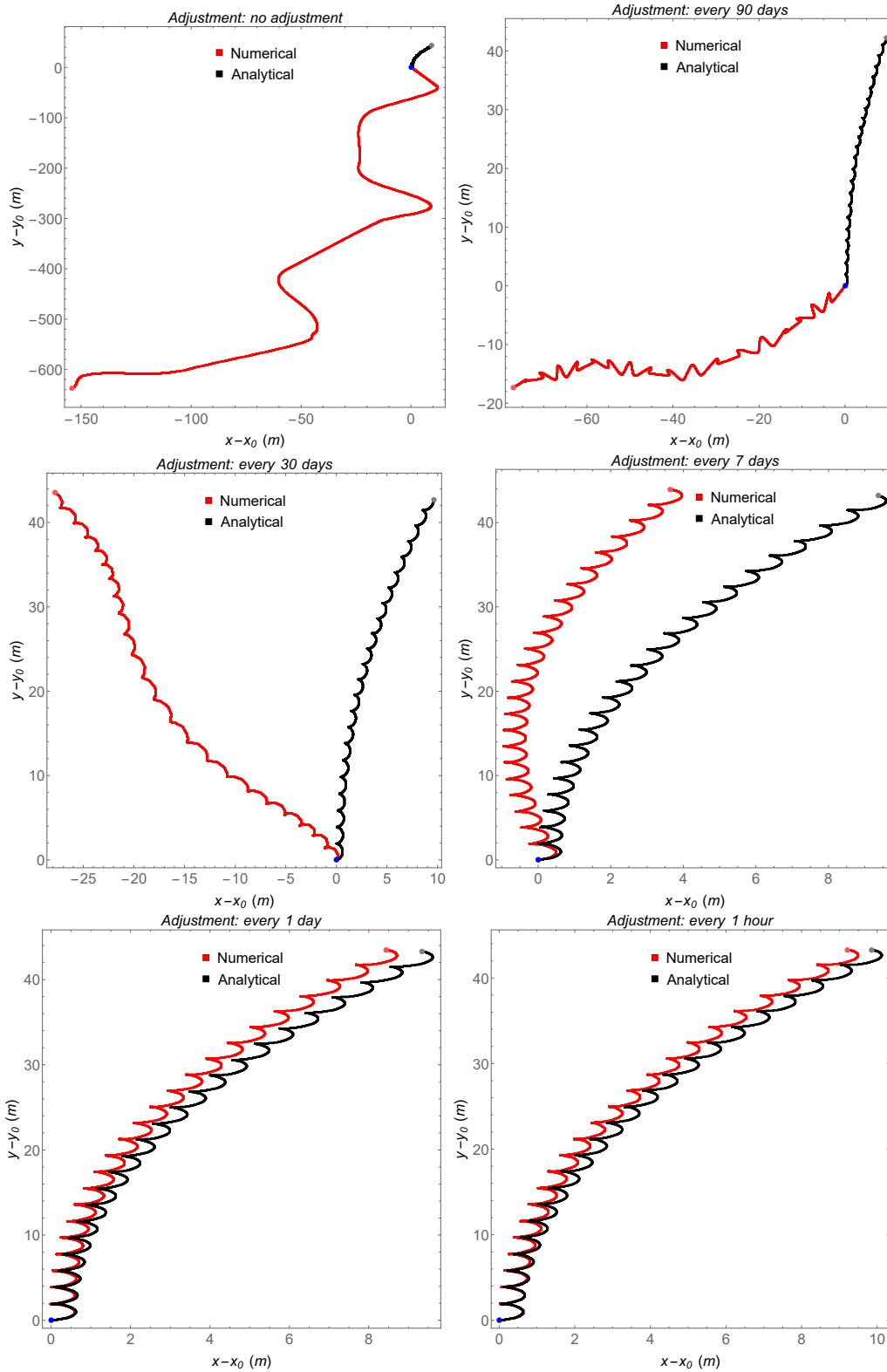
7.4 Considerations
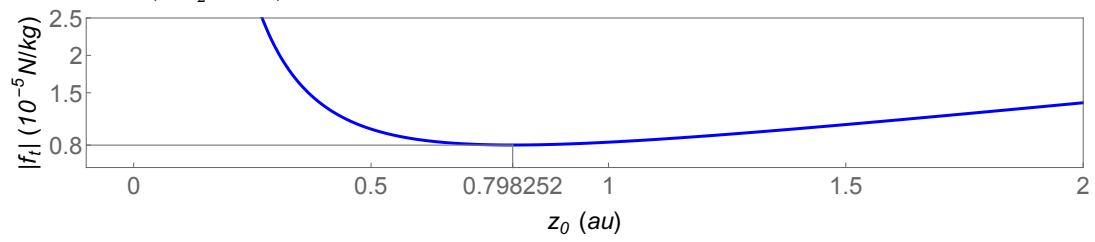
The present chapter focused in finding pseudo artificial equilibrium points to place a satellite equipped with a continuous thrust to observe the poles of a celestial body that has a moon around it. It is made an analytical and a numerical study, which have a good agreement with each other. Solutions were found for the Sun-Earth-Moon, Sun-Ida-Dactyl and Sun-Saturn-Titan systems. The results showed that the acceleration required has a strong dependency with the altitude of the equilibrium point, with a very clear minimum. They also show the annual increment of velocity required to keep the satellite fixed in the equilibrium points found. Comparing the systems, it is very clear that smaller bodies, like asteroids, have very low thrust required to keep the equilibrium points. The magnitude of the accelerations required for the thrusts are of the order 10^{-4} m/s^2 for the Sun-Earth-Moon system, with an annual velocity increment of 5.1 km/s. These number go to the order of 10^{-8} m/s^2 for the Sun-Ida-Dactyl system, with an annual velocity increment of 1.2×10^{-3} km/s. It means that this type of solution is relatively expensive for some systems, but very affordable in others.

The results also showed that, depending on the z_0 coordinate, without using the method presented here, the trajectory of the satellite can oscillate around its initial position $(x_0, y_0, z_0) = (x_{M_2}, 0, z_0)$ for a short term, but it will eventually escape due to the perturbation, which is the gravitational interaction with the moon. For the majority of the values of z_0, the satellite tends to escape very fast from its initial position. On the other side, using the method presented in this chapter, the spacecraft is obligated to follow a previously developed analytical solution and so it will keep an orbit around the PAEP for longer times, at the cost that, in every period of time, which is defined by the mission designer, the direction and the absolute value of the thrust must be slightly adjusted.

In comparison with a spacecraft which thrust is able to cancel all the accelerations to keep itself in the equilibrium condition permanently, continuously changing the absolute value and the direction of the thrust, the presented method has the advantage that the spacecraft does not need to cancel the x-y plane component of the perturbation due to the gravitational interaction with the moon, which means that a thrust with lower intensity is required, besides the fact that it does not need to be adjusted continuously, only in periods of every hour or some days. Hence, an important restriction is withdrawn over its construction, besides the wear of material to keep the thrust being changed continuously.

8 CONCLUSIONS

The use of *integral indices* to measure the perturbation level of a particular trajectory has several advantages. The integration of the perturbing forces can be made analytically or numerically, depending on the disturbing force. Therefore, any perturbation can be added to the system, even the ones that needs complex mathematical models to be represented. It is not necessary to add or subtract forces in the dynamical model to measure their effects, which is interesting because those techniques modify the trajectories of the spacecraft, so interfering in the results obtained. The mappings can be made for each individual force, so it is possible to measure the contribution of each force individually. Therefore, it is possible to use the results to decide which forces should be included in the force model of a specific problem, according to the accuracy level required by the mission. As mentioned above, these indices identify the less perturbed orbits, which have a good potential to show less oscillations in the orbital parameters. It means that they are good candidates to locate a spacecraft in missions that benefits from near Keplerian orbits. Those orbits may also require less fuel for the station-keeping maneuvers. The results of the research on the subject "Integral indices" shown in chapter 2 show that the exclusion of non-Keplerian terms in the evaluation of an index lead to the assumption of neglecting terms that may be of the same order of magnitude of the index itself when used to compare it with the specif impulse. Thus, in chapter 3, several indices were defined using non-Keplerian terms in their evaluations. The results of the chapter show that some of them are still not useful, but the index defined in Eq. (3.83) gives expected results, as can be checked using Figs. 3.15-3.17. The results of this index are in agreement with the ones obtained using an index based in the displacement of the perturbed orbit relative to the Keplerian one, given in Eq. (3.84). The final contribution of this research is that this index can be useful when used to predict the effects of the perturbation over an orbit without the need of the evaluation of the complete system for long times.

The first research on the subject *artificial equilibrium points* is shown in chapter 4, which clarifies the points in the Sun-Earth system where the parking is possible for several different kinds of thrusts and quantified the required thrust. As an example, in the case where the thrust is given in the x-z plane direction, the spacecraft can be located in a stationary condition over a circle around the x axis, as can be noted in Fig. 4.4, which radius is given by Eq. (4.74). In other situations, the directions of the thrusts are represented as arrows and their norm as color scale in Figs. 4.14, 4.15, 4.16, 4.18, and 4.19. In the case where a solar sail is used, the ratio area to mass is

represented in color scale as function of the position in Fig. 4.17 for the case of a thrust given in the direction of the x-z plane, in Figs. 4.20 and 4.21 for the case of a thrust given in the x-y plane direction, and in the bottom side of Fig. 4.7 for the case of a thrust given in the direction of the $\vec{r}_1$ vector. The forbidden regions represent locations where the parking is not possible for a solar sail due to the constraint of the angle γ, which value must be in the interval $(-\pi/2, \pi/2)$. The results of the research of this chapter offer valuable informations for a mission designer in order to take advantage of lower ratio are-to-mass or consumption of propellant. Note that the forbidden zones expressed shown in the results are also important informations.

The second research on the subject *artificial equilibrium points* is written along chapter 5, where a problem is proposed and solved in three different forms. Among them, the communication solution 1 shown in subsection 5.3.1 offers the simpler form to solve the problem, where a solar sail placed near L_3 is sustained above the Ecliptic about twice the radius of the Sun, by redirecting the solar rays. The ratio area-to-mass required in this solution is about 16 m^2/kg. The second kind of solution requires a system of two spacecraft equipped with solar sails, one near L_3 and the other near L_1, both above the Ecliptic. The spacecraft near L_1 works as a bridge of information between the spacecraft located near L_3 and the Earth. This solution requires two spacecraft with lower ratio area-to-mass, about 12 m^2/kg each. The last kind of solution combines two spacecraft equipped with solar sails near L_3, one redirecting the solar rays to the other, helping each other to be sustained by this redirection of the solar rays. Yet it requires technological challenges in order to precisely point the rays towards its pair, this solution requires two solar sails with a ratio area-to-mass only about 9 m^2/kg. Finally, the last contribution in this stage of the research is proposing this kind of solution to be applied to sustain a spacecraft above the Ecliptic near the Earth, making permanently contact with its poles.

Analytical solutions to describe the *spacecraft motion around artificial equilibrium points* are found in the research written in chapter 6. The linear analytical solution is expensively obtained by linearizing the system of equations and solving it, while the other two are obtained using a new proposed method, which is also created in this research and valid for a general previously given form of the perturbation shown in Eqs. (6.9)-(6.11). In the case where Eq. (6.4) is always true, the analytical solutions obtained using the new proposed method are exact ones. On the other side, the range of validity in time of the analytical solutions is investigated by making a comparison with numerical evaluations of the same system in the case where Eq. (6.4) is valid only in the initial position of the motion. In their range of validity, such

kind of analytical solutions can be used to lower time computation costs, analytical evaluations of stations-keeping costs and trajectories, or they can be used to develop a new method to maintain a spacecraft above one of the primaries with respect to the ecliptic for long times.

The second research on the subject *spacecraft motion around artificial equilibrium points* is written in chapter 7, where the method described in chapter 6 is used to obtain analytical solutions for a spacecraft perturbed by a general moon after some considerations. These analytical solutions are analyzed and their periodic and secular terms are identified. The initial position is chosen such that the secular terms are negligible, which is right above one of the primaries, including the presence of a moon. Adjustments are applied to the spacecraft each determined period of time with the goal of making the pseudo artificial equilibrium point valid again. A numerical solution is obtained by integrating the complete equations of motion using a numerical method. The results shown in section 7.3 present the solutions applied to the Sun-Earth-Moon, Sun-Ida-Dactyl and Sun-Saturn-Titan systems, which are shown in Figs. 7.5, 7.7, and 7.9, respectively. The results clearly show that the higher is the frequency of the adjustments, the closer the numerical solution is with respect to the analytical one, which in time is restricted to periodic terms. Therefore, the spacecraft is kept near its initial position for long times, despite its linear stability. This initial position can be used to place a satellite in permanent contact with regions near the poles of one of the primaries and even the poles of its moon, in a strategical point of view, as an option to the solution presented by Forward (1991) or the Molniya orbits.

Some ideas for further researches crossing the subjects of this thesis are presented next, as a final contribution. The effects of an additional perturbation over the trajectory of a spacecraft motion around an artificial equilibrium point could be identified using the integral index defined in Eq. (3.83). The range of validity for analytical solutions of the kinds shown here could also be investigated using this type of index. On the other hand, analytical solutions can be obtained for other extra forms of the perturbation, which can be used to validate or to invalidate integral indices, or even to other purposes.

REFERENCES

ABBASI, N. M. 2017. Available from: <http://12000.org/my_notes/vanderpol/vanderpol_perturbation/index.htm>. Access in: 15 June 2017. 21

AKELLA, M.; BROUCKE, R. Anatomy of the constant radial thrust problem. **Journal of Guidance, Control, and Dynamics**, v. 25, n. 3, 2002. 27

ALIASI, G.; MENGALI, G.; QUARTA, A. Artificial equilibrium points for a generalized sail in the circular restricted three-body problem. **Celestial Mechanics and Dynamical Astronomy**, v. 110, n. 4, p. 343–368, 2011. 71, 77, 91, 93, 147, 164

_____. Artificial equilibrium points for a generalized sail in the elliptic restricted three-body problem. **Celestial Mechanics and Dynamical Astronomy**, v. 114, p. 181–200, 2012. 72

BAIG, S.; MCINNES, C. Artificial halo orbits for low-thrust propulsion spacecraft. **Celestial Mechanics and Dynamical Astronomy**, v. 104, p. 321, 2009. 72

BAOYING, H.; MCINNES, C. Solar sail halo orbits at the sun–earth artificial l1 point. **Celestial Mechanics and Dynamical Astronomy**, v. 94, p. 155, 2006. 72

BARRABES, E.; OLLE, M. Invariant manifolds of l3 and horseshoe motion in the restricted three-body problem. **Nonlinearity**, v. 9, p. 2065–2090, 2006. 116, 138

BATTIN, R. H. **An introduction to the mathematics and methods of astrodynamics**. Reston, VA: American Institute of Aeronautics and Astronautics, 1999. 28, 34

BELTON, M. J.; CHAPMAN, C. R.; THOMAS, P. C.; DAVIES, M. E.; GREENBERG, R.; KLAASEN, K.; BYRNRES, D.; D'AMARIO, L.; SYNNOTT, S.; JOHNSON, J. V.; Mc EWEN, A.; MERLINE, W. J.; DAVIS, D. R.; PETIT, J. M.; STORRS, A.; VEVERKA, V.; ZELLNER, B. Bulk density of asteroid 243 Ida from the orbit of its satellite Dactyl. **Nature**, v. 374, n. 6525, p. 785–788, 1995. ISSN 00280836. Available from: <https://doi.org/10.1038/374785a0>. 176

BELTON, M. J.; MUELLER, B. E.; D'AMARIO, L. A.; BYRNES, D. V.; KLAASEN, K. P.; SYNNOTT, S.; BRENEMAN, H.; JOHNSON, T. V.;

THOMAS, P. C.; VEVERKA, J.; HARCH, A. P.; DAVIES, M. E.; MERLINE, W. J.; CHAPMAN, C. R.; DAVIS, D.; DENK, T.; NEUKUM, G.; PETIT, J. M.; GREENBERG, R.; STORRS, A.; ZELLNER, B. The discovery and orbit of 1993 (243)1 Dactyl. **Icarus**, v. 120, n. 1, p. 185–199, 1996. ISSN 00191035. Available from: <https://doi.org/10.1006/icar.1996.0044>. 176

BOMBARDELLI, C.; PELAEZ, J. On the stability of artificial equilibrium points in the circular restricted three-body problem. **Celestial Mechanics and Dynamical Astronomy**, v. 109, n. 1, p. 13–26, 2011. 71, 147, 164

BOYCE, W.; DIPRIMA, R. C. **Elementary differential equations and boundary value problems**. 7.ed. New York: John Wiley and Sons, 2001. 146

BROSCHART, S.; SCHEERES, D. Control of hovering spacecraft near small bodies: application to asteroid 25143 itokawa. **Journal of Guidance, Control, and Dynamics**, v. 28, n. 2, p. 343, 2005. 71

BROUCKE, R. Notes on the central force r^n. **Astrophysics and Space Science**, v. 72, n. 1, p. 33, 1980. 35

BROUWER, D.; CLEMENCE, G. M. **Celestial mechanics**. London: Academic Press, 1961. 41

BU, S.; LI, S.; YANG, H. Artificial equilibrium points in binary asteroid systems with continuous low-thrust. **Astrophysics and Space Science**, v. 362, p. 137, 2017. 71

CARVALHO, J.; MORAES, R.; PRADO, A. Searching less perturbed circular or-bits for a spacecraft travelling around europa. **Mathematical Problems in Engineering**, v. 2014, 2014. 11

DE ALMEIDA JUNIOR, A. K.; PRADO, A. F. B. A.; SANCHEZ, D. M.; YOKOYAMA, T. Searching for artificial equilibrium points to place satellites "above and below" l_3 in the sun-earth system. **Revista Mexicana de Astronomia y Astrofisica**, v. 53, p. 349, 2017. Available from: <http://www.astroscu.unam.mx/rmaa/RMxAA..53-2/PDF/RMxAA..53-2_aalmeida.pdf>. 5, 72, 164

DE ALMEIDA JUNIOR, A. K.; PRADO, A. F. B. A.; VILHENA, R. M.; LARA, M. Analyzing "integral indices" to quantify the effects of a perturbing force in the harmonic and duffing oscillators. **Computational and Applied Mathematics**, 2017. Available from: <https://doi.org/10.1007/s40314-017-0471-8>. 3, 27

DE ALMEIDA JUNIOR, A. K.; PRADO, A. F. B. A.; YOKOYAMA, T.;
SANCHEZ, D. M. Spacecraft motion around artificial equilibrium points.
Nonlinear Dynamics, v. 91, p. 1473, 2018. Available from:
<https://doi.org/10.1007/s11071-017-3959-2>. 6, 72, 164, 167

DEPRIT, A.; ROM, A. The main problem of artificial satellite theory for small
and moderate eccentricities. **Celestial Mechanics**, v. 2, n. 2, p. 166, 1970. 42

DUSEK, H. M. Motion in the vicinity of libration points of a generalized restricted
three-body model. **Progress in Astronautics and Rocketry**, v. 17, p. 37, 1966.
71

ESMAILZADEH, E.; MEHRI, B.; NAKHAIE-JAZAR, G. Periodic solution of a
second order, autonomous, nonlinear system. **Nonlinear Dynamics**, v. 10, p.
307–316, 1996. 14

FARQUHAR, R. W.; KAMEL, A. A. Quasi-periodic orbits about the translunar
libration point. **Celestial Mechanics**, v. 7, n. 4, p. 458–473, 1973. ISSN
00088714. Available from: <https://doi.org/10.1007/BF01227511>. 164

FARRÉS, A.; JORBA, À. Station keeping of a solar sail around a Halo orbit.
Acta Astronautica, v. 94, n. 1, p. 527–539, 2014. ISSN 00945765. Available from:
<https://doi.org/10.1016/j.actaastro.2012.07.002>. 72, 164

FORWARD, R. Statite - a spacecraft that does not orbit. **Journal of Spacecraft
and Rockets**, v. 28, n. 5, p. 606, 1991. 71, 134, 164, 185

FUNASE, R.; SHIRASAWA, Y.; MIMASU, Y.; MORI, O.; TSUDA, Y.; SAIKI,
T.; KAWAGUCHI, J. On-orbit verification of fuel-free attitude control system for
spinning solar sail utilizing solar radiation pressure. **Advances in Space
Research**, v. 48, n. 11, p. 1740–1746, 2011. ISSN 02731177. Available from:
<https://doi.org/10.1016/j.asr.2011.02.022>. 169

GOEBEL, D. M.; KATZ, I. **Fundamentals of electric propulsion: ion and
hall thrusters**. [s.n.], 2008. 507 p. ISBN 9780470429273. Available from:
<https://doi.org/10.1002/9780470436448>. 72, 164

GOMEZ, G.; JORBA, A.; MASDEMONT, J.; SIMO, C. Study of the transfer from
the earth to a halo orbit around the equilibrium point l1. **Celestial Mechanics
and Dynamical Astronomy**, v. 56, n. 4, p. 541–562, 1993. 115, 116, 138

GOMEZ, G.; MASDEMONT, J.; SIMO, C. Quasi-halo orbits associated with libration points. **Journal of Astronautical Sciences**, v. 42, n. 2, p. 135–176, 1998. 115, 116, 138

HEILIGERS, J.; HIDDINK, S.; NOOMEN, R.; MCINNES, C. R. Solar sail Lyapunov and Halo orbits in the Earth-Moon three-body problem. **Acta Astronautica**, v. 116, p. 25–35, 2015. ISSN 00945765. Available from: <https://doi.org/10.1016/j.actaastro.2015.05.034>. 164

HOU, X.; TANG, J.; LIU, L. **Transfer to the Collinear Libration Point L3 in the Sun–Earth+Moon System**, Washington: NASA, 2007. (NASA Technical Report, 20080012700). 116, 138

HOWELL, K. C. Three-dimensional, periodic, 'halo' orbits. **Celestial Mechanics**, v. 32, n. 1, p. 53–71, 1984. ISSN 00088714. Available from: <https://doi.org/10.1007/BF01358403>. 164

HUA, T.; GONG, S.; MUA, J.; LI, J.; WANG, T.; QIAN, W. Switch programming of reflectivity control devices for the coupled dynamics of a solar sail. **Advances in Space Research**, v. 57, p. 1147–1158, 2016. 169

JANHUNEN, P. Electric sail for spacecraft propulsion. **Journal of Propulsion and Power**, v. 20, n. 4, p. 763, 2004. Available from: <https://doi.org/10.2514/1.8580>. 72, 164

JANHUNEN, P.; SANDROOS, A. Simulation study of solar wind push on a charged wire: Basis of solar wind electric sail propulsion. **Annales Geophysicae**, v. 25, n. 3, p. 755–767, 2007. ISSN 14320576. Available from: <https://doi.org/10.5194/angeo-25-755-2007>. 72, 164

JET PROPULSION LABORATORY. 2018. Available from: <https://ssd.jpl.nasa.gov/sbdb.cgi>. Access in: 18 Apr. 2018. xxii, xxiii, xxv, 149, 150, 152, 153, 159, 176

JEZEWSKI, D. An analytic solution for the j2 perturbed equatorial orbit. **Celestial Mechanics**, v. 30, p. 363, 1983. Available from: <https://doi.org/10.1007/BF01375506>. 27

JIANG, Y.; BAOYIN, H.; WANG, X.; YU, Y.; LI, H.; PENG, C.; ZHANG, Z. Order and chaos near equilibrium points in the potential of rotating highly irregular-shaped celestial bodies. **Nonlinear Dynamics**, v. 83, n. 1-2, p. 231–252,

2016. ISSN 1573269X. Available from:
<https://doi.org/10.1007/s11071-015-2322-8>. 137

JORBA, A.; MASDEMONT, J. Dynamics in the centre manifold of the collinear points of the restricted three body problem. **Physica D**, v. 132, p. 189–213, 1999. 115, 116, 138

KOON, W. S.; LO, M. W.; MARSDEN, J. E.; ROSS, S. D. Heteroclinic connections between periodic orbits and resonance transition in celestial mechanics. **Chaos**, v. 10, n. 2, p. 427–469, 2000. 115, 116, 138

LANDAU, L. D.; LIFSHITZ, E. M. **Mechanics**. 3. ed. Oxford, UK, and Burlington, MA, USA: Butterworth-Heinemann, 1976. 15

LARA, M. Simplified equations for computing science orbits around planetary satellites. **Journal of Guidance, Control, and Dynamics**, v. 31, n. 1, p. 172, 2008. Available from: <https://doi.org/10.2514/1.31107>. 42

_____. Equivalent delta-v per orbit of gravitational perturbations. **Journal of Guidance Control Dynamics**, v. 39, n. 9, p. 2157–2162, 2016. 11, 14, 27

LARA, M.; FERRER, S. Expanding the simple pendulum's rotation solution in action-angle variables. **European Journal of Physic**, v. 36, n. 5, p. 055040, 2015. Available from: <https://doi.org/10.1088/0143-0807/36/5/055040>. 43

_____. _____. **ArXiv e-prints**, arXiv:1503.03358 [nlin.SI], 2015. Available from: <https://arxiv.org/abs/1503.03358>. 43

LI, J.; POST, M. A.; VUKOVICH, G. Orbit and attitude stability criteria of solar sail on the displaced orbit. **Advances in the Astronautical Sciences**, v. 15, p. 604, 2015. 116

LLIBRE, J.; MARTINEZ, R.; SIMO, C. Transversality of the invariant manifolds associated to the lyapunov family of periodic orbits near l2 in the restricted three-body problem. **Journal of Differential Equations**, v. 58, n. 1, p. 104–156, 1985. 115, 116, 138

LUZUM, B.; CAPITAINE, N.; FIENGA, A.; FOLKNER, W.; FUKUSHIMA, T.; HILTON, J.; HOHENKERK, C.; KRASINSKY, G.; PETIT, G.; PITJEVA, E.; SOFFEL, M.; WALLACE, P. The IAU 2009 system of astronomical constants: the report of the IAU working group on numerical standards for fundamental astronomy. **Celestial Mechanics and Dynamical Astronomy**, v. 110, n. 4, p.

293–304, 2011. ISSN 09232958. Available from:
<https://doi.org/10.1007/s10569-011-9352-4>. 91, 148, 172, 176, 179

MATH INSIGHT. **Polar coordinates to cartesian coordinates**, 2018. Available
from: <http://mathinsight.org/image/polar_coordinates_cartesian>.
Access in: 30 July 2018. 29

MCINNES, C. Dynamics, stability, and control of displaced non-keplerian orbits.
Journal of Guidance, Control, and Dynamics, v. 21, n. 5, p. 799, 1998. 71

MCINNES, C. R. **Solar sailing technology, dynamics and mission
applications**. New York: Springer-Verlag Berlin Heidelberg, 2004. 4, 72, 76, 82,
118, 147, 148, 164, 169

_____. Space-based geoengineering: challenges and requirements. **Proceedings of
the Institution of Mechanical Engineers, Part C: Journal of Mechanical
Engineering Science**, v. 224, n. 3, p. 571, 2010. 116

MCINNES, C. R.; MCDONALD, a. J. C.; SIMMONS, J. F. L.; MACDONALD,
E. W. Solar sail parking in restricted 3-body systems. **Journal of Guidance
Control and Dynamics**, v. 17, n. 2, p. 399–406, 1994. ISSN 0731-5090. Available
from: <https://doi.org/10.2514/3.21211>. 164

MCINNES, C. R.; MCDONALD, A. J. C.; SIMMONS, J. F. L.; MACDONALD,
E. W. Solar sail parking in restricted three-body systems. **Journal of Guidance,
Control and Dynamics**, v. 17, n. 2, p. 399–406, 1994. 71, 116

MENGALI, G.; QUARTA, A. A. Non-Keplerian orbits for electric sails. **Celestial
Mechanics and Dynamical Astronomy**, v. 105, n. 1, p. 179–195, 2009. ISSN
09232958. Available from: <https://doi.org/10.1007/s10569-009-9200-y>.
72, 164

MORIMOTO, M. Y.; YAMAKAWA, H.; UESUGI, K. Artificial equilibrium points
in the low-thrust restricted three-body problem. **Journal of Guidance, Control
and Dynamics**, v. 30, n. 5, p. 1563–1567, 2007. 116

MORTARI, D.; GONZALES, M. E. A.; LEE, S. J2 propelled orbits and
constellations. **Journal of Guidance Control Dynamics**, v. 37, p. 1701–1706,
2014. 9

NAYFEH, A. H. **Perturbation methods**. Weinheim, Germany: Wiley-VCH
Verlag, 2004. 12, 18, 41

OLIVEIRA, T.; PRADO, A. Mapping orbits with low station keeping costs for con-stellations of satellites based on the integral over the time of the perturbing forces. **Acta Astronautica**, v. 104, p. 350, 2014. 11

OLIVEIRA, T.; PRADO, A.; MISRA, A. Determining orbits that can be controlled by natural forces. **Advances in the Astronautical Sciences**, v. 152, p. 3081, 2014. 11

OLIVEIRA, T. C.; PRADO, A. F. Mapping orbits with low station keeping costs for constellations of satellites based on the integral over the time of the perturbing forces. **Acta Astronautica**, v. 104, n. 1, p. 350, 2014. Available from: <https://doi.org/10.1016/j.actaastro.2014.06.035>. 32

PITJEVA, E. V.; STANDISH, E. M. Proposals for the masses of the three largest asteroids, the moon-earth mass ratio and the astronomical unit. **Celestial Mechanics and Dynamical Astronomy**, v. 103, n. 4, p. 365–372, 2009. ISSN 09232958. Available from: <https://doi.org/10.1007/s10569-009-9203-8>. 172

PRADO, A. Mapping orbits around the asteroid 2001sn263. **Advances in Space Research**, v. 53, p. 877, 2014. 11, 32

PRADO, A. F. B. A. Transfer orbits in the restricted problem. **Journal of Guidance, Control and Dynamics**, v. 18, n. 3, p. 593–598, 1995. 116, 138

PRADO, A. F. B. A. Searching for orbits with minimum fuel consumption for station-keeping maneuvers: an application to lunisolar perturbations. **Mathematical Problems in Engineering**, p. 1–11, 2013. Article ID: 415015. 10, 61

QIAN, Y. J.; ZHANG, W.; YANG, X. D.; YAO, M. H. Energy analysis and trajectory design for low-energy escaping orbit in earth moon system. **Nonlinear Dynamics**, v. 85, p. 463–478, 2016. 9

QUARTA, A. A.; MENGALI, G. New look to the constant radial acceleration problem. **Journal of Guidance, Control, and Dynamics**, v. 35, n. 3, 2012. 28, 35, 36

RANJANA, K.; KUMAR, V. On the artificial equilibrium points in a generalized restricted problem of three bodies. **International Journal of Astronomy and Astrophysics**, v. 3, p. 508–516, 2013. 71

RODRIGUEZ-SOLANO, C. J.; HUGENTOBLER, U.; STEIGENBERGER, P. Adjustable box-wing model for solar radiation pressure impacting gps satellites. **Advances in Space Research**, v. 49, p. 1113–1128, 2012. 169

ROMAGNOLI, D.; OEHLSCHLAGEL, T. High performance two degrees of freedom attitude control for solar sails. **Advances in Space Research**, v. 48, p. 1869–1879, 2011. 169

SALAZAR, F. J. T.; MCINNES, C. R.; WINTER, O. C. Intervening in earth's climate system through space-based solar reflectors. **Advances in Space Research**, v. 58, p. 17, 2016. 116

SAN-JUAN, J.; LOPEZ, L.; LARA., M. On bounded satellite motion under constant radial propulsive acceleration. **Mathematical Problems in Engineering**, v. 1, n. 12, 2012. Available from: <https://doi.org/10.1155/2012/680394>. 27

SANCHEZ, D.; PRADO, A.; YOKOYAMA, T. Gravitational capture and maintenance of a spacecraft around Pluto. In: AIAA/AAS ASTRODYNAMICS SPECIALIST CONFERENCE, 2014, San Diego. **Proceedings...** [S.l.], 2014. 11

SANCHEZ, D. M. On the use of mean motion resonances to explore the haumea system. In: AAS/AIAA ASTRODYNAMICS SPECIALIST CONFERENCE, 2017, Columbia River Gorge, Stevenson, WA. **Proceedings...** [S.l.], 2017. 61

SANCHEZ, D. M.; HOWELL, K. C.; PRADO, A. F. B. A. On the dynamics of a spacecraft in the irregular haumea-hi'iaka binary system. **Advances in the Astronautical Sciences**, v. 158, p. 3681, 2016. 9, 11

SANCHEZ, D. M.; PRADO, A.; YOKOYAMA, T. On the effects of each term of the geopotential perturbation along the time i: quasi-circular orbits. **Advances in Space Research**, v. 54, p. 1008, 2014. 11, 32

SANCHEZ, D. M.; PRADO, A. F. B. A. Perturbation maps for a spacecraft around the near-earth asteroid (153591) 2001 sn263. **Advances in the Astronautical Sciences**, AAS 18-320, 2018. 11, 32

SANTOS, J.; CARVALHO, J.; PRADO, A.; MORAES, R. Searching for less perturbed elliptical orbits around europa. **Journal of Physics Conference Series**, v. 641, p. 012011, 2015. Available from: <https://doi.org/10.1088/1742-6596/641/1/012011>. 11

SHORT, C.; HOWELL, K.; HAAPALA, A.; DICHMANN, D. Mode analysis for long-term behavior in a resonant earth–moon trajectory. **Journal of the Astronautical Sciences**, v. 64, n. 2, p. 156, 2017. Available from: <https://doi.org/10.1007/s40295-016-0098-9>. 32

SIMMONS, J.; MCDONALD, A.; BROWN, J. The restricted 3-body problem with radiation pressure. **Celestial Mechanics**, v. 35, p. 145, 1985. 71

SYMON, K. R. **Mechanics**. Philippines: Addison-Wesley, 1971. 74, 75, 117, 139

TANTARDINI, M.; FANTINO, E.; REN, Y.; PERGOLA, P.; GOMEZ, G.; MASDEMONT, J. Spacecraft trajectories to the l3 point of the sun-earth three-body problem. **Celestial Mechanics and Dynamical Astronomy**, v. 108, n. 3, p. 215–232, 2010. 115, 116, 137

TSANDER, K. **From a Scientific Heritage**, Washington: NASA, 1967. (NASA Technical Translation, TTF-541). 71

TSIEN, H. S. Take-off from satellite orbit. **Journal of the American Rocket Society**, v. 23, p. 233, 1953. 3, 27, 35

TSIOLKOVSKY, K. Extension of man into outer space. **Proceedings Symposium Jet Propulsion**, v. 2, 1936. 71

TSUDA, Y.; MORI, O.; FUNASE, R.; SAWADA, H.; YAMAMOTO, T.; SAIKI, T.; ENDO, T.; YONEKURA, K.; HOSHINO, H.; KAWAGUCHI, J. Achievement of ikaros - japanese deep space solar sail demonstration mission. **Acta Astronautica**, v. 82, n. 2, p. 183, 2013. 129, 173

UENO, K.; FUNAKI, I.; KIMURA, T.; HORISAWA, H.; YAMAKAWA, H. Thrust measurement of a pure magnetic sail using parallelogram-pendulum method. **Journal of Propulsion and Power**, v. 25, n. 2, p. 536–539, 2009. ISSN 0748-4658. Available from: <https://doi.org/10.2514/1.39211>. 72, 164

VENDITTI, F.; PRADO, A. Mapping orbits regarding perturbations due to the gravi-tational field of a cube. **Mathematical Problems in Engineering**, v. 2014, 2014. 11, 32

WATERS, T.; MCINNES, C. Periodic orbits above the ecliptic in the solar-sail restricted three-body problem. **Journal of Guidance, Control, and Dynamics**, v. 30, n. 3, p. 687, 2007. 72

WILLIAMS, K. E. Overcoming genesis mission design challenges. **Acta Astronautica**, v. 52, n. 2, p. 281, 2003. 130, 137, 138

YAMAKAWA, H.; FUNAKI, I.; NAKAYAMA, Y.; FUJITA, K.; OGAWA, H.; NONAKA, S.; KUNINAKA, H.; SAWAI, S.; NISHIDA, H.; ASAHI, R.; OTSU, H.; NAKASHIMA, H. Magneto-plasma sail: an engineering satellite concept and its application for outer planet missions. **Acta Astronautica**, v. 59, n. 8-11, p. 777–784, 2006. ISSN 00945765. Available from: <https://doi.org/10.1016/j.actaastro.2005.07.003>. 72, 164

ZUBRIN, R. M.; ANDREWS, D. G. Magnetic sails and interplanetary travel. **Journal of Spacecraft and Rockets**, v. 28, n. 2, p. 197–203, 1991. ISSN 0022-4650. Available from: <https://doi.org/10.2514/3.26230>. 72, 164